POLYETHERSULFONE/3-AMINOPROPYLTRIETHOXYSILANE-SILICA COMPOSITE HOLLOW FIBER MEMBRANE FOR SYNTHETIC OIL-IN-WATER EMULSION SEPARATION

TUNMISE AYODE OTITOJU

UNIVERSITI SAINS MALAYSIA

2019

POLYETHERSULFONE/3-AMINOPROPYLTRIETHOXYSILANE-SILICA COMPOSITE HOLLOW FIBER MEMBRANE FOR SYNTHETIC OIL-IN-WATER EMULSION SEPARATION

by

TUNMISE AYODE OTITOJU

Thesis submitted in fulfilment of the

requirements for the degree of

Doctor of Philosophy

February 2019

ACKNOWLEDGEMENT

My sincere gratitude goes to the greatest of all potters, who designed us in His image by setting the plastic clay rolling, so we can wonderfully be like Him. I appreciate Him for His mercies and protection over me, and for His grace and opportunity bestowed upon me for the successful completion of my thesis, and most importantly for granting me perfect health throughout the duration of my studies at Universiti Sains Malaysia.

Heartfelt gratitude goes to Prof Dr. Abdul Latif Ahmad (my main supervisor) for his unwavering support and invaluable advice. He has supported me during this course of study with patience, encouragement, constructive criticism, knowledge and deep intellectual insight. It also goes to Assoc. Prof Dr. Ooi Boon Seng (my co-supervisor) for his advice and assistance.

Sincere gratitude also goes to the Universiti Sains Malaysia for their financial support under the USM fellowship scheme and USM Membrane Science and Technology Cluster. I also wish to extend my profound appreciation to the laboratory technicians and administrative staff of the School of Chemical Engineering for their warm acceptance and support.

It is also with great joy to mention at this point, a part of my everyday progress: my parents, my wife and my siblings. Completing this study would not

have been possible without their love, prayers, endurance and support. Special thanks are also due to Prof Dr G.T. Olutunla, Prof Dr Lau Seng, Prof Dr Gabriel Tonga Noweg, Dr Shaun Welman, Dr P.U. Okoye, Dr Abdullateef Jimoh, Pang Sing Tyan, Chiadighikaobi Ikenna and all my friends for their encouragements throughout my study.

Lastly, appreciations are also due to those who have not been mentioned but had one way or another contributed directly or indirectly to this study.

Tunmise Ayode Otitoju

USM, Penang, February 2019

TABLE OF CONTENTS

CHAPTER THREE – METHODOLOGY

CHAPTER FOUR – RESULTS AND DISCUSSIONS

LIST OF PUBLICATIONS

LIST OF TABLES

LIST OF FIGURES

LIST OF ABBREVIATIONS

AFM	Atomic force microscopy
AG	Air gap
ANOVA	Analysis of variance
APTES	3-aminopropyltriethoxysilane
ATR	Attenuated total reflection
BF	Bore fluid
BFT	Bore fluid temperature
CA	Contact angle
CBT	Coagulation bath temperature
CCD	Central composite design
CP	Condensation polarization
CPr	Coagulation power
DCMD	Direct contact membrane distillation
DEF	Dope extrusion flowrate
DEP	Dope extrusion pressure
DI	Deionized
DLS	Dynamic light scattering
DMAC	N-N-dimethylacetamide
DMF	Dimethylformamide
DMSO	Dimethylsulfoxide
DOE	Design of experiment
DR	Draw ratio

EDX	Energy Dispersion X-Ray
EG	Ethylene glycol
FESEM	Field emission scanning electron microscopy
FRR	Flux recovery ratio
FTIR	Fourier transform infrared
HF	Hollow fiber
IE	Interfacial energy
LCST	Lower critical solution temperature
Md	Mean diameter
MMM	Mixed matrix membrane
MPS	Mean pore size
NPs	Nanoparticles
OPF	Oil permeate flux
OR	Oil rejection
PDA	Polydopamine
pdI	Polydispersity index
PEG	Polyethylene glycol
PES	Polyethersulfone
PSD	Pore size distributions
PVA	Polyvinyl alcohol
PWF	Pure water flux
RF	Relative flux
RFR	Relative flux reduction
RSM	Response surface methodology

RT	Residence time
SiO_2	Silica
TEM	Transmission electron microscopy
TEOS	Tetraethylorthosilicate
TGA	Thermogravimetric analysis
TMP	Transmembrane pressure
TS	Take-up speed
UF	Ultrafiltration
UV	Ultraviolet
WCA	Water contact angle

LIST OF SYMBOLS

$Js/_{Ji}$	Relative flux	-
Dh	Hydro-dynamic diameter	nm
P_c	Concentration of particles	nm
wgt_2	Weight of the petri dish containing dried particles	g
wgt_1	Weight of dried petri dish without particles	g
ɖ	Gravitational elongation	%
ε	Membrane porosity	%
FRR	Flux recovery ratio after hydraulic cleaning	%
Ji	Initial permeate flux	kg/m^2 h
Js	Permeate flux	kg/m^2 h
J_{wf1}	Initial pure water flux	kg/m^2 h
J_{wf2}	Pure water flux after back cleaning	kg/m^2 h
OR	Oil rejection	%
Ra	mean surface roughness	nm
υ	Permeate volume of water	kg
C_{pmt}	Content of oil in permeate	kg
C_{fd}	Content of oil in feed	kg
Δt	Time	h
A	Effective area of membrane	m^2
w	Weight of wet membrane	g
d	Weight of the dry membrane	g
ρp	Density of the PES polymer	kg/m^3

ρw	Density of H_2O	kg/m^3
Sr	Stokes radius of PEG	-
MW	Molecular weight of PEG	g/mol
Z	Zeta potential	mV
R	Rejection of PEG	%
μ_d	Geometric mean diameter of PEG	g/mol
S_d	Diameter of PEG	g/mol
σ_d	Geometric standard deviation about μ_d	nm
σ_p	Geometric standard deviation	nm
y	Intercept	-
m	Slope	-
μ_p	Effective mean pore size	nm
Rt	Total resistance	%
Rir	Irreversible resistance	%
Rr	Reversible resistance	%

POLIETERSULFONA/3-AMINOPROPILTRIETOKSILANA-SILIKA MEMBRAN KOMPOSIT SERAT BERONGGA UNTUK PEMISAHAN EMULSI MINYAK-DALAM-AIR

ABSTRAK

Kesan pengotoran membrane oleh minyak merupakan isu kritikal dalam aplikasi air kumbahan. Masalah permukaan kotor dapat dikurangkan dengan memfungsikan membran bagi mempertingkatkan sifat-sifat hidrophilik. Walaubagaimanapun, dapat disimpulkan daripada penyelidikan terdahulu bahawa dengan meningkatkan hidrofilik permukaan adalah mekanisme yang boleh dilaksanakan untuk mengurangkankan permukaan daripada pengotoran, parameter lain seperti kekasaran dan morfologi membran juga antara faktor penyumbang. Dalam kajian ini, zarah 3-aminopropyltriethoxysilane silika yang diubahsuai (APTES-SiO_2) telah disintesis melalui tindakbalas pengubah satu pot. Kaedah tindakbalas permukaan berdasarkan reka bentuk komposit pusat telah digunakan untuk menghasilkan membran HF komposit PES melalui proses pemutaran basah kering. Keputusan menunjukkan bahawa nisbah zarah bagi polietilena glikol terhadap zarah APTES-SiO_2 mestilah bersamaan dengan 1 atau lebih daripada campuran untuk memastikan penyebaran APTES-SiO_2 dalam matrik PES yang lebih baik serta mempertingkatkan prestasi. Formula larutan optimum yang diperolehi kemudiannya digunakan untuk membina membran komposit PES/APTES-SiO_2 dengan mengubah nisbah etanol yang membentuk komposisi bendalir liang. Dari segi komposisi bendalir liang, membran HF yang diputar dengan 25/75 wt.% etanol menunjukkan morfologi permukaan yang lebih baik dan mempertingkatkan ciri-ciri penelapan. Ciri-ciri membran dikaji dari

segi saiz liang, keliangan, kekasaran, hidrofilik, sifat mekanikal dan termal. Imej SEM bagi membran HF menunjukkan bahawa zarah telah berjaya dimasukkan dan disebarkan ke dalam matriks membran dengan baik. Kekasaran permukaan bagi semua membran komposit adalah lebih rendah berbanding dengan membran yang dikawal. Membran komposit PES/APTES-SiO_2 menunjukkan peningkatan hidrofilik, kebolehtelapan dan permukaan yang anti kotor apabila diuji untuk aplikasi air kumbahan. Prestasi penolakan membran komposit PES/APTES-SiO_2 semasa penapisan minyak sintetik dalam air menunjukkan bahawa penggabungan 2.5 wt.% APTES-SiO_2 mampu mengeluarkan 99.87 minyak berbanding hanya 97.23 untuk membran tulen. Membran komposit didapati mempunyai pengurangan fluks relatif yang rendah, nisbah pemulihan fluks yang unggul dan rintangan terhadap pengotoran yang lebih baik berbanding dengan yang kawalan yang digunakan iaitu disebabkan oleh pengurangan kekasaran permukaan, struktur liang dan penyebaran zarah APTES-SiO_2 yang baik di atas permukaan membran. Untuk mendapatkan butiran prestasi membran komposit yang lebih terperinci, keadaan operasi yang berbeza seperti tekanan transmembran, kepekatan suapan, dan kadar aliran suapan turut disiasat. Model blok perantaraan telah dikenalpasti sebagai faktor paling penting yang menyumbang kepada pengotoran membran. Kajian ini menunjukkan bahawa dengan memfungsikan permukaan SiO_2 dengan APTES, membran HF dengan kekasaran permukaan yang rendah dan sifat-sifat anti kotoran boleh dicapai untuk penyingkiran minyak daripada emulsi minyak-dalam-air sintetik yang berkesan.

POLYETHERSULFONE/3-AMINOPROPYLTRIETHOXYSILANE-SILICA COMPOSITE HOLLOW FIBER MEMBRANE FOR SYNTHETIC OIL-IN-WATER EMULSION SEPARATION

ABSTRACT

Membrane fouling effect by oil is a critical issue in wastewater applications. Fouling can be mitigated by functionalizing the membrane with enhanced hydrophilic properties. Although, previous research have concluded that an increase in surface hydrophilicity is a feasible mechanism for fouling mitigation, other parameters such as membrane roughness and morphology may contribute as well. In this work, 3-aminopropyltriethoxysilane modified silica (APTES-SiO_2) particle was synthesized via one pot reaction modification. Response surface methodology based on central composite design was used to prepare the PES composite HF membranes via dry-wet spinning process. The result shows that the ratio of polyethylene glycol to APTES-SiO_2 particles must be equal to 1 or more than unity to ensure better dispersion of APTES-SiO_2 in the PES matrix as well as improved performance. The optimum dope formulation obtained was subsequently used to develop PES/APTES-SiO_2 composite membrane by varying ethanol fraction the bore fluid composition. In terms of bore fluid composition, HF membrane spun with 25/75 wt.% of ethanol shows a better surface morphology and improved permeation properties. Membrane properties were studied in terms of pore size, porosity, roughness, hydrophilicity, mechanical and thermal properties. The SEM images of the HF membranes shows that the particles have been successfully incorporated in the membrane matrix and well dispersed. The surface roughness of all composite membranes were lower as

compared to the controlled membrane. The PES/APTES-SiO_2 composite membrane show an improved hydrophilicity, permeability and anti-fouling effects when tested for wastewater applications. The rejection performance of PES/APTES-SiO_2 composite membrane during filtration of synthetic oil in water shows that the incorporation of 2.5 wt.% of APTES-SiO_2 was able to remove 99.87 of oil as compared to only 97.23 for pristine membrane. It was found that the composite membranes had low relative flux reduction, superior flux recovery ratio and fouling resistance as compared to the controlled which can be as a result of the decrease in surface roughness, pore structure and well dispersed APTES-SiO_2 particles on the membrane surface. To get more details on the performance of the composite membrane, different operating conditions such as transmembrane pressure, feed concentration, and feed flow rates were also investigated. The intermediate block model was identified as the most critical factor that contributed to membrane fouling. This work demonstrated that by functionalizing SiO_2 surface with APTES, HF membranes with low surface roughness and anti-fouling properties can be achieved for effective removal of oil from synthetic oil-in-water emulsion.

CHAPTER ONE

INTRODUCTION

This chapter gives an overview of the current research project. At the beginning, ultrafiltration membranes for wastewater treatment followed by improvement of particle dispersion with mono-dispersed silica were introduced. The problem statement was highlighted and discussed based on the current development of monodispersed composite membrane. Subsequently, the research objectives and scopes of study as well as the organization of the thesis are also presented.

1.1 Ultrafiltration membranes for oily wastewater treatment applications

Oil contaminant in water is a significant global environmental problem currently faced by mankind, which puzzles the development and survival of human society (Ju et al., 2015). This oil contaminant are generated by mankind's living behaviours and production (Y. Zhu et al., 2014). Direct discharge of the contaminated oily wastewater might lead to either long-term worse influence on people's health and the environment in general or lead to huge pressure on vulnerable ecosystem (Zhu et al., 2015). It was estimated that by year 2030, the daily petroleum consumption will increase to 107 million barrels (Drioli et al., 2016) compared to the current demand of 97 million barrels (IEA, 2017). Oil spills make up about 12% of the oil that enters the ocean. The global wastewater production was estimated to increase from 314 million barrels per day in year 2014 to 441 million barrels per day in year 2020 (Gwi, 2017).

The generated water effluent often contains micrometer-sized oil droplets dispersed in water, forming a stable oil-in-water emulsion even without any stabilizer (Wang et al., 2015). Oil is an organic matter in wastewater and an important

contaminants in wastewater issues in the environment (Pulido, 2015). In general, oil from oily wastewater may be broadly classified, according to the sizes of the oil droplets, into three categories: free floating oil (>150 μm), dispersed oil (20 μm–150 μm), and emulsified oil (<20 μm) (Jamshidi Gohari et al., 2015). However, the importance of such separation is due to its toxic characteristics and severe environmental hazards (Karimnezhad et al., 2014) and moreover, this has become an important world-wide challenge in the area of industrial production, environment protection and energy conservation (Taylor et al., 2015). Therefore, it is necessary to purify wastewater so that they can be reused to save water resources as well as protect the environment (Kong et al., 2016).

Among membrane technology, ultrafiltration (UF) membranes which are operated based on the principle of size exclusion has been widely reported as an alternative solution to remove micron-sized oil emulsion due to it suitable pore size ranging from 0.002 to 0.05 μm, in comparison to the common oil droplet size in oily wastewater ranging from 0.1 to 10 μm (Jamshidi Gohari et al., 2014). It is able to remove emulsified oil droplet without any de-emulsification processes and at the same time offers high fluxes at a relatively low pressure. UF membrane technology can retain such small oil droplets without any de-emulsification process to meet the maximum total oil and grease discharge limit of 10 mg/L. This discharge limit was set in Malaysia Environmental Quality (Sewage and Industrial Effluents) Regulation, 1979 under Third Schedule of Environmental Quality Act, 1974 (EQA, 1974). At the same time, it also offers benefits in term of lower cost and energy requirement, no phase change involved, compact design and do not generate secondary pollution as compared to conventional treatment (Gohari et al., 2014).

Amongst all membrane materials, polyethersulfone (PES) has drawn great consideration in oil emulsion separation from researchers throughout the world owing to its high mechanical strength, chemical resistant, thermal stability, and outstanding oxidative characteristics (Abdel-Karim et al., 2017). It has also been widely applied in desalination, production of drinking water and wastewater recovery (Jimoh et al., 2018; Peydayesh et al., 2018; Son et al., 2017). However, its slight hydrophobic nature may lead to severe fouling problem in wastewater treatment which has become a major barrier for membrane application in water recovery process (Zheng et al., 2016). Hydrophobic interaction between oil emulsion and membrane surface play an important role in membrane fouling. Fouling reduces the membrane's life-span which lead to the increase in operational cost and make the process energy intensive (Huang et al., 2015). In order to effectively solve the fouling problem, membrane which is void of agglomeration with anti-fouling properties is required to prolong the life-span of the membrane and to ensure its optimum productivity.

1.2 Enhancement of membrane properties and performance

As discussed in section 1.1, membrane fouling usually lead to severe flux decline during oil in water emulsion separation. In the past, several approaches to mitigate this fouling phenomena have been proposed by researchers via altering the membrane hydrophilicity, morphology (porosity, roughness and pore size) and surface charges which are known as the key controlling factor for membrane fouling (Jiang et al., 2017).

Compared to hydrophobic membrane, hydrophilic membrane tends to exhibit high flux recovery and lower fouling during membrane applications. Thus, many approaches have been investigated to improve the membrane hydrophilicity including plasma modification, surface modification and blending with hydrophilic additives. However, in long term operation, once the membrane fouling begin to occur, surface modification is no longer effective in fouling prevention (Karimnezhad et al., 2014).

An approach of incorporating inorganic particles to prepare polymer-inorganic membranes have been favoured recently due to their attractive advantages such as simple preparation technology and operating process. Generally, two approaches are often used: (1) the particle is introduced in the dope solution, followed by phase inversion (Yin and Deng, 2015); (2) particles are coated on already prepared membrane surface via chemical bonding (Lu et al., 2016). Introducing the particle in the polymer matrix has proven to be a versatile approach in recent times. Generally, a common limitation of direct incorporation of particle is the high surface energy in the dope solution which often cause poor dispersion and distribution of particles through particle entrapment in the membrane matrix. The poor distribution is ascribed to the shearing of the dope solution or poor mixing and the low colloid stability; leading to low functional surface area, which is a conspicuous setback for practical applications. Typically, these particles can be subjected to shear force to enable their physical dispersion and can help reduce particle aggregations and agglomeration via sonicator. However, due to stiff interactions between particles, there is a limitation to break the intra-particles with using sonicator (Mukherjee and De, 2016; Safarpour et al., 2015). Therefore, for

feasible application, the preparation of size controlled, mono-dispersed particles is of great concern.

Stöber reaction based on sol gel synthesis method for preparing mono-dispersed spherical SiO_2 particles with sizes covering almost the whole colloidal range has been a favorable method in the past. Recently, few studies have been carried out via doping monodispersed silica particles (mostly at lower concentration) in polymer matrix (Jullok et al., 2016; Lin et al., 2016). Specifically, even at low particle concertation (≤ 1 wt.%), incorporating monodispersed silica in polymer matrix is still facing difficulty of surface aggregation. Therefore, a method to improve the dispersibility of the monodispersed silica in PES matrix is of great concern.

1.3 Problem Statement

In the past. several membrane fouling mitigation methods were investigated to mitigate the fouling including alteration of membrane hydrophilicity (via physical and chemical modification), surface charge, and morphology. Membrane surface modification is a time consuming and complicated process which poses difficulty to be scaled up at the present stage (Y. Zhu et al., 2014). This improvement is permanent and may however lead to the degradation of PES chains on the surface of membrane (Kang and Cao, 2014). Although composite blending is a facile method but due to their high surface energy, their dispersion is always a challenging task. It usually induces particle agglomeration due to colloidal instability in the polymer dopes solution as well as unwanted membrane surface roughness due to non-homogenous distribution. These are serious setbacks for their practical applications.

It is documented that by reducing particle size, membrane roughness can be reduced consequently improving membrane anti-fouling properties. Therefore, it is of great important to prepared SiO_2 particle (with particle size <100 nm) in order to reduce membrane roughness and fouling effects of the composite membranes is important. Is functionalizing the surface of SiO_2 with APTES enough to alter membrane structure and performance? To address this question and to explore the morphological relationships and performance of HF membranes that the incorporation of APTES modified SiO_2 in the membrane matrix is necessitated.

It has been well documented that HF membranes have wider use among other membrane configurations due to their high surface area to volume ratio as well as packing density (Sengur et al., 2015). On this basis, HF membrane is considered near to real application than the flat sheet membrane. Unfortunately, till date there has been no great deal of study that focuses on the simultaneous control of preparation and spinning conditions in order to reach a high performance ultrafiltration (UF) of synthetic oil in water emulsion. In addition, almost all of the previously published works have adopted the conventional methods, that involves the variation of the major parameter studied while the other parameters are maintained constant. However, such methods have disadvantages (such as much time consuming experimental runs while ignoring the interacting effects between the variables, which often times result to low process optimization efficiencies) which could be avoided with response surface methodology (RSM) which has successfully been introduced in works by Fouladitajar et al. (2015) and Ghandashtani et al. (2015). RSM was chosen due to its ability to represent a comprehensive and valid model for the optimization of effective parameters to reach a high level efficiency of an applied

process (Javadi et al., 2014). Thus, there is need to carry out an optimization study on the effects of preparation variables and the interaction of variables.

Compared to flat sheet membrane, hollow fiber (HF) membrane fabrication seems to be more complex and delicate because several parameters can influence membrane performance and properties. Over the years, the influence of these parameters on membrane performance and morphology have received considerable attention. Indeed, fabrication of HF membranes with both desirable morphology as well as separation performance is challenging. In the past, HF irregularities have always been attached to parameters such as dope speed, residence time, take-up speed, external coagulation bath. However, have not been related with bore fluid composition. Furthermore, the use of soft non-solvents such as ethanol in the coagulation bath has been well documented in the literature. However, their use as bore fluid and their influence on membrane irregularities, properties and performance remains controversial. When ethanol fraction is added into water bath, the surface tension of water tends to reduce and can also provide a high degree of hydrogen bonding effects during the phase inversion. Although, there is no dispute that ethanol alters membrane irregularities and properties, as assayed upon addition in coagulation bath composition, but are these effects similar to when ethanol fraction are used as bore fluid. Furthermore, are they enough to alter membrane structure and performance? To address this question and to explore the morphological relationships and performance of HF membranes that the role of varying ethanol concentration in the bore fluid is beneficial for optimization of the microstructure and performance of HF membranes for oily wastewater treatment is necessitated. In addition, the intrinsic correlation between ethanol of varied composition in the bore

fluid liquid will develop more understanding of their potential for industrial applications, which will be used as a guideline for membrane end users and also serve as a guide for membrane characterization in the future of membrane filtration.

Furthermore, the operating conditions namely operating pressure, feed flowrate and feed concentration are also crucial in affecting membrane fouling propensity which needed a systematic investigation. Furthermore, the fouling mechanisms is mathematically analysed.

1.4 Research objectives

The aim of this present work is to develop PES hollow fiber membrane embedded with well dispersed APTES-SiO_2 particles. On this note, the objectives of this present work include:

1. To synthesize and characterize APTES-SiO_2 particles prepared through one-pot modified Stober method.
2. To optimize the preparation parameters for the PES HF membranes by generating statistical model and understanding the interacting effects between parameters.
3. To evaluate the effect of bore fluid component on the structure and performance of PES/APTES-SiO_2 HF membrane for oil in water emulsion separation.
4. To synthesize and characterize PES/APTES-SiO_2 HF membrane prepared by varying only the loading of APTES-SiO_2 particles for oil in water emulsion separation.

5. To evaluate the effect of operating conditions on flux, oil rejection and flux recovery ratio.
6. To mathematically analyse the fouling mechanisms of the PES/APTES-SiO_2 composite membrane.

1.5 Scope of study

The first step of this research work is to synthesize the APTES-SiO_2 particles via one-pot Stober process by functionalizing the SiO_2 surface with 3-aminopropyltriethoxysilane (APTES). This is a crucial step to obtain a stable APTES-SiO_2 particle suspension. The functionalization is to ensure the homogenous distribution of APTES-SiO_2 particle on the membrane surface which could help to reduce membrane surface and thus reduce fouling phenomenon. The as-synthesized particle is then characterized via fourier transform infrared (FTIR), dynamic light scattering (DLS) and transmission electron microscopy (TEM) to confirm the existence of the APTES modified SiO_2 particles.

Next, design of experiment is used to investigate the optimized formulation of PES/APTES-SiO_2 HF membrane. The optimization study is done using the preparation parameters with the aim to achieve the highest pure water flux (PWF), oil permeate flux (OPF) and oil rejection. Four variables are chosen including PES (15 to 18 wt.%), PEG (0 to 5 wt.%), APTES-SiO_2 (0 to 5 wt.%) and coagulation bath temperature (0 to 60 ºC). A mathematical regression model is generated to represent the preparation process using central composite design. The interacting effects among variables are validated using statistical approach and the most influential parameters were identified. Optimization method is subjected to maximum PWF,

OPF and oil rejection. The optimized membrane is characterized using FESEM, CA, EDX, pore size, FTIR and performance testing for oil-in-water emulsion.

The optimized HF membrane is used to produce different kinds of membranes at different bore fluid composition (0%, 25%, 50%, 75% and 100%). The proper spinning conditions are selected based on the bore fluid component to produce membrane with fully circular inner contour. By utilizing the best bore fluid mixture, different PES/APTES-SiO_2 HF membranes are produced at various APTES-SiO_2 particles loading (0, 1.2, 2.5, 3.6 and 5 wt.%). The content of the particles were varied from low to high concentration while maintaining a fixed ratio for other preparation parameters which was not carried out using design of experiment.

Next, the study of the PES/APTES-SiO_2 HF membrane at different operating conditions including feed flowrate (0.15 L min^{-1}, 0.45 L min^{-1}, 0.75 L min^{-1}), transmembrane pressure (2.0 bar, 1.5 bar, 1.0 bar,) and feed concentration (100 mg/L, 250 mg/L, 500 mg/L) is discussed accordingly. Lastly, the behaviour of membrane permeate flux reduction is examined based on four different fouling mechanisms (cake filtration, intermediate blocking, standard blocking and complete blocking).

1.6 Organization of thesis

The thesis is divided into five chapters that provides specific information about this research project.

In chapter one, a brief introduction on this research was given. This chapter starts with the ultrafiltration membranes for wastewater application. This is followed by brief overview of the improvement in particle dispersion with mono-dispersed silica. Thereafter, the problem statements which gives the rationale and basis to justify the research direction in the present study are explained. Based on the problem statement, the specific objectives of the research followed by the research scope are presented clearly in this chapter.

In chapter two, literature review on the background of the present research project was outlined. This chapter provides the literature review on the oily wastewater and the limitations of ultrafiltration membranes in oil removal. Flux and hydrophilicity enhancement methods were introduced, and more details were given to the enhancement by blending/composite. Then, an overview on HF membrane configuration was presented under various HF membrane spinning conditions. The roles of hydrodynamic and operational conditions on the membrane fouling phenomena were also outlined. Finally, the chronological development of ultrafiltration PES HF composite membrane were introduced.

In chapter three, the information about the materials and methodology used in this research project was described. The first part of this chapter presents the list of all chemicals and materials used in the present research project. Subsequently, the experimental procedures for preparation method of pristine PES and HF composite membranes were outlined. The characterization methods, together with the analytical techniques were also given. The overview of the experimental work was summarized in a flow chart. The equations for all data analysis were also supplied.

In chapter four, the experimental results and discussion of the present project were outlined. This section is divided into several part. In the first part, the characterization of oil emulsion was presented in terms of oil droplet size and oil concentration. The second part focused on the characterization of synthesized APTES-SiO_2 particles. In the third part, an optimization study of membrane synthesis parameters was carried out using RSM to obtain higher response which consists of PWF, OPF and oil rejection. This is followed by the characterization and performance of optimum HF membrane for oil in water emulsion treatment. In the fourth part, an assessment study of the effect of bore fluid composition on the properties and performance of optimum HF membrane was done. This is subsequently followed by effects of different APTES-SiO_2 loadings on PES/APTES-SiO_2 membrane properties and performance. Furthermore, the fouling evaluation of optimized PES/APTES-SiO_2 membranes were investigated. In the last part, the influence of operating conditions on optimum membrane were investigated. This is followed by the stability of the PES HF membrane under six continuous cycles of water permeation.

Chapter five gives the summaries of the whole research findings of the present work. This findings were concluded point by point based on the research objectives. Furthermore, some reasonable recommendations for future research work to improve the performance of PES/APTES-SiO_2 HF membrane were also proposed.

CHAPTER TWO

LITERATURE REVIEW

This chapter highlights the significance of this work by summarizing the current development in membrane science and technology especially on the modification of PES membrane. Firstly, the discussion on the impact of oily wastewater to the environment and how the research works using various technology especially membrane technology to treat the oily wastewater are outlined. Subsequently, the information on the performance enhancement of PES membrane were discussed. This is followed by review on hollow fiber spinning systems. The role of operational conditions on the membrane fouling phenomena were also outlined and discussed. Lastly, the research gaps are highlighted.

2.1 Oily wastewater

The rate at which industries generate billions of gallons of wastewater containing a high concentration of organic matters is inevitable. This rate will continue to be persistent as more and more volumes of wastewater are produced during extractions, transport, in petrochemical plants, oil refineries, metal-working plants and specifically, in oil terminals during the washing of reserving tanks (Yusoff and Murray, 2011). The generated water effluent often contains micrometer-sized oil droplets dispersed in water, forming a stable oil-in-water emulsion even without any stabilizer (Fakhru'l-Razi et al., 2009). Oil is an organic matter in wastewater and an important contaminants in wastewater issues in the environment (Bayat et al., 2005). In general, oil from oily wastewater may be broadly classified, according to the sizes

of the oil droplets, into three categories: free floating oil (> 150 µm), dispersed oil (20 µm – 150 µm), and emulsified oil (< 20 µm) (Um et al., 2001).

As one of the major pollutants in the aquatic environment, their presence from oily wastewater possesses a serious threat to the environment and human health in general. The importance of such separation is due to its toxic characteristics and severe environmental hazards (Fakhru'l-Razi et al., 2009) and moreover, this has become an important worldwide challenge in the area of industrial production, environment protection and energy conservation (Kota et al., 2012). Therefore, it is of significant importance to purify this oily waste-water so that they can be reused to save water resources as well as protect the environment (Chen et al., 2003). As a result of this trends, considerable sustainable approach has been applied towards the removal of oil from this effluent using many kinds of conventional-adopted technologies, such as gravity separation and skimming, air flotation, coalescence, de-emulsification, centrifugation, flocculation, coagulation (Gobi et al., 2011; Hu et al., 2015; Kang et al., 2011; Stack et al., 2005; Wang et al., 2014; Yi et al., 2011; Yuliwati et al., 2012; Y. Zhu et al., 2014), and metal mesh (Jing et al., 2013). All this aforesaid methods have been widely employed for decades and are found to present several disadvantages such as high operation costs and problems, low efficiency, corrosion, huge production of sludge and recontamination problems (Ahmed, 2006; Fratila-Apachitei et al., 2001) which subsequently leads to inefficiency during the removal of emulsified oil droplets in micron and sub-micron sizes (Akbari and Mehrabadi, 2010).

These aforementioned approaches have been proven not capable and insufficient for removing 99% of oil from oily wastewater as well as considered ineffective in removing smaller oil droplets from emulsions with size ≤ 20 μm, especially when the oil droplets are finely dispersed with very low content (Chakrabarty et al., 2010). In addition, their performance efficiency cannot meet the minimum environment quality requirements due to the increasing awareness rate of environmental protection concerns at present. However, all of these respective limitations have prompted and promoted membrane separation (Meng et al., 2015).

Over the last few decades, membrane separation has become a desired and surpassing solution as it can efficiently and reversibly adhere to the dispersed oil droplets in the emulsion (Moslehyani et al., 2016; Zhao and Chen, 2015). It has also been widely applied in other various fields including water treatment (Ghosh et al., 2011), gas purification (Y. Zhang et al., 2013), food processing (Charcosset, 2009), antibiotic production (Zaviska et al., 2013), medical application (Stępnik and Malinowska, 2013), and environmental protection (Ebin et al., 2015). This technology is playing a more prominent role in the removal of oil from oily wastewater due to its intrinsic advantages: require no chemical additives or thermal input to break the emulsion, require no regeneration of spent media (Pendergast and Hoek, 2011), relatively lower energy requirements, quite compact and fully automated treatment facilities (Yan et al., 2009), recyclability of throughput material in crossflow membrane assemblies, ease of cleaning, highly pure permeates (Sukitpaneenit and Chung, 2011), scalability of modular, as well as high oil removal efficiencies (Jamshidi Gohari et al., 2014). In contrast with the conventional

separation methods, this process offers wider advantages. Table 2.1 shows the pros and cons of membrane separation and conventional filtration.

Table 2.1: Pros and cons of membrane and conventional filtration

Membrane separation	Conventional filtration
Efficient for treating free-floating oil	Efficient for dispersed and dissolved oil treatment
Extremely compact or compact footprint	Large land requirements
Pressure driven	Gravity driven with coarse filtration
Minimal chemical use	Chemical intensive
Low transmembrane flux	Efficient for treating
Fouling phenomenon	Often preceded by pre-oxidation, or oxidation takes place concurrently
Chemical incompatibilities with process solutions	typically followed by disinfection at full-scale
Cannot be easily staged	Cannot remove all the viruses and bacteria in the water
Do not scale up very well to avoid massive stream sizes	

2.2 Polymeric based membranes for oily wastewater separation

Most commercial membranes are made using polysulfone (PSf), polyethersulfone (PES), polyvinylidene fluoride (PVDF) due to their excellent physical and chemical stabilities, making them ideal in preparing asymmetric membranes with difference in pore size and surfaces (Rahimpour et al., 2012). The final membrane properties and performance is influenced by the composition (additives, solvent, content) and dope solution temperature, the mixture of non-solvents or the non-solvent, as well as the coagulation bath or surrounding environment (Barth et al., 2000). However, all the three are hydrophobic and susceptible to fouling caused as a result of oil deposition onto the membrane surface or inside membrane pores (Shi et al., 2007; Wang et al., 2009). This fouling phenomenon limits the flux and causes an increase in operating cost of the system. This is considered one of the most serious problems hindering their practical usage in

membrane technologies. Significant efforts has been reported to understand the fouling mechanisms and develop fouling control strategies, with aim towards reduction of membrane fouling (Mollahosseini et al., 2012).

The ability to select a proper materials for membrane formation along with choosing the best membrane preparation technique plays a very crucial role in the membrane performance. Although, this reasons may not be sufficient to reach the best performance. The most commonly used techniques for the preparation of membranes includes phase inversion, interfacial polymerization, electrospinning, stretching and track-etching. Among these techniques, phase inversion and electrospinning are the most commonly employed techniques for the preparation of membranes. Phase inversion process involves a controlled transformation of a thermodynamically stable or homogenous polymer solution from a liquid to a porous solid state. Such phase separation of a casting solution into a polymer lean and a polymer rich phase may be induced by: non-solvent induced phase separation, thermally induced phase inversion, evaporation-induced phase inversion and vapor-induced phase inversion (Binyam et al., 2009; Kochkodan, 2013). In the following subsequent section, a detailed review on the existing trends for the performance of polymeric based membrane for water and wastewater applications is given.

2.3 Performance enhancement of polymeric membranes

Performance of polymeric membranes can be characterized according to their permeability, rejection efficiency, and fouling resistance (Lee et al., 2001). More specifically, their performance during applications can be compromised due to pore

clogging via oil particle, preferential adsorption of oil which can result to fouling as well as the formation of cake layers on the membrane surface which generally result to a reduction in permeate flux. In addition, the separation efficiency of a membrane is primarily dependent on the membrane pore size (Kang and Cao, 2014). A membrane with small pore size is able to reject smaller size of oil droplets and vice versa. In the past few decades, numerous studies has been conducted and reported on the performance of unmodified polymeric membranes for oil rejection efficiency. Generally, these membranes are subjected to ruin and tends to result into severe fouling during oily wastewater separation. It is due to this limitation, that some modification (surface modifications and blending) attempts have been recently made in order to enhance its performance. Table 2.2 presents the distinctions between both methods.

Table 2.2: Distinctions between blending and surface modification

Blending	**Surface modification**
Leaching	Degradation of polymer chains
Formation of agglomerations	Non-uniformity
Incompatibility between polymer and surface/functional groups	Require lot of further processing such as additional chemistry, purification and isolation of modified materials.

2.3.1 Surface modification

Membrane surface modification is another frequently used and effective method to enhance performance of membrane. In surface modification, a hydrophilic layer is formed on the existing membrane surface which aids the prevention of contact between membrane and solute, thus reducing membrane fouling. Many surface modification methods have been adopted to reduce membrane fouling (Huang et al., 2016). The surface modification can be mainly classified into two

categories such as the physical modification and chemical modification. The physical modification signifies that the hydrophilic modifiers exist on membrane surface via physical interaction but not covalently bonded. In other words, the chemical composition of membrane remains unchanged although the chemical reaction may be required during the modification. The physical modification of membranes can be achieved by two ways: (a) the hydrophilic organic material is directly coated or deposited on membrane surface (further treatment is conducted sometimes) providing a strong binding force between hydrophilic coatings and substrates, (b) firstly, the membrane is coated by or immersed in a solution of chemically active monomers. Then, the monomers are immobilized onto the surface of the membrane by polymerization reaction or crosslinking without the membrane chemically participating.

2.3.1.1 Surface coating

Coating of membrane surface is an effective method for surface modification (Kang and Cao, 2014). It often does not involve the direct attachment of chemical groups or chemical alteration of the surface the way conventional chemical modification techniques does, but still alters the surfaces. In this process, factor such as preparation conditions plays a key effect on the performance of the membrane (Xu et al., 2013). For instance, Miller et al. (2014) coated the surface of PES ultrafiltration (UF) membranes with polydopamine (PDA). The deposition of PDA was found to increase the membrane hydrophilicity, even at 5 min which is the shortest deposition time. The hydrophilicity remained largely unchanged with increase in deposition time of PDA, indicating that even low levels of PDA

deposition is enough to alter surface hydrophilicity. The PDA modified membranes showed lower trans-membrane pressures as compared to the unmodified membranes of the same permeance. However, organic rejection of PDA-modified membranes was similar to the unmodified membranes of the same pure water permeance. Surface coating with hydrophilic polymers has been proven to be advantageous for enhancing the performance properties. Liu et al. (2016) reported a polyaniline coated PVDF membranes for effective separation of oil-in-water emulsions which was fabricated by a simple one-step dilute polymerization at low temperature. The PANI-modified PVDF membranes presents a water fluxes up to 3000 L/m^2 h under 0.6 bar. The water flux gradually decreases with separation time during one cycle treatment which was subsequently recovered to the initial flux after rinsing. In addition, the superhydrophilic membranes with PANI coatings demonstrated a high oil rejection, stable underwater superoleophobic properties after ultrasonic treatment and immersing in oils and various harsh conditions, and high and steady water permeation flux after several cycles.

Although, this approach tends to cause the decrease in water flux due to the increase in permeate resistance and membrane pores blockage, especially for membranes with smaller pore sizes. In addition, the interaction between the coated layer and membrane surface is relatively weak. The hydrophilicity of the modified membrane is probably lost during long-term operation due to the delamination of hydrophilic coating.

2.3.1.2 Surface adsorption and grafting

In this modification, the membrane surface is modified through covalent bonding interaction. In procedure, the polymer chains are firstly activated by chemical reaction or through a high-energy radiation, and thereafter followed by the grafting of hydrophilic additives. In this scenario, the surface properties of the membrane tends to improve while the membrane bulk is not significantly affected. Moreover, the covalent attachment of modifiers on membrane surface offers a long-term chemical stability, in contrast with physical surface coating.

Ju et al. (2015) prepared a PVDF membrane by non-solvent induced phase separation and then grafted the prepared membrane with polyethylene glycol diacrylate (PEGDA) via a low-pressure plasma-induced surface copolymerization at low-pressure plasma source with a radio frequency of 13.56 MHz. The result displayed oil rejection of about 97% with high permeate flux for crude oil in water, lubricating oil in water and soybean oil in water. Garcia-Ivars et al. (2016) presents a PES UF membranes modified using UV assisted irradiation in the presence of aluminium oxide (Al_2O_3) nanoparticles and polyethylene glycol (PEG). They observed a decrease in water permeability principally because both grafting and UV-induced modification would reduce the pore size. This was ascribed to the higher degree of modification obtained at high content of additives (PEG and Al_2O_3). In addition, superior anti-fouling property was observed for PES membranes modified with 0.5% Al_2O_3 and low time of irradiation (10 min). Bernstein et al. (2018) reported the graft polymerization of PES surface using ink-jet printing. In their study, a zwitterionic acrylate monomer was printed on a PES UF membrane with

subsequent UV-irradiation. The membrane permeability following modification was maintained even at high degree of grafting, and PEG rejection was only slightly affected. Adsorption measurements of protein confirmed that the modified membrane presents a low fouling properties. Furthermore, a large reduction in water permeability of 66% and 87% were observed for modified membranes irradiated for 10 and 20 min, respectively.

Zhu et al. (2015) prepared a pH induced membrane by grafting hyperbranched poly (ethylene imine) (PEI) onto PVDF/polyacrylic acid (PAA) acid grafted PVDF blend membrane via a simple amidation reaction for soybean oil in water separation. The membrane exhibits an ultralow oil adhesion and thus displays a superior anti-fouling performance in acidic condition. In the study, PVDF/PAA-g-PVDF was prepared via a non-solvent induced phase separation (NIPs). The oil retention of PEI-g-PVDF/PAA-g-PVDF membrane was 99.96% and 99.97% under neutral and acidic condition, respectively, which were much higher than the pristine membrane (96.3% and 96.9%) and PVDF/PAA-g-PVDF blend membrane (99.4% and 99.8%). Lin et al. (2018) presented the facial surface modification via grafting of poly(ethylenimine) (PEI) chains onto brominated tetramethyl PES (TM-PES) membranes (Figure 2.1). TM-PES was synthesized by tetramethyl bisphenol A (TMBPA) and bis(4-fluorophenyl) sulfone (FPS) in the presence of potassium carbonate (K_2CO_3) (Figure 2.2). The TM-PES membrane was found to be hydrophobic with CA of >90°. After grafting with PEI, the membranes becomes more hydrophilic due to enhanced hydrophilicity of grafted chains. The PEI-grafted TM-PES membranes show excellent anti-fouling ability with sufficient WF coupled with outstanding separation performance. Typically, the PEI grafted membrane with

bromination degree of 73% show a high WF of 72 L/m^2 h, BSA rejection of 91.4% and FRR of ~90%.

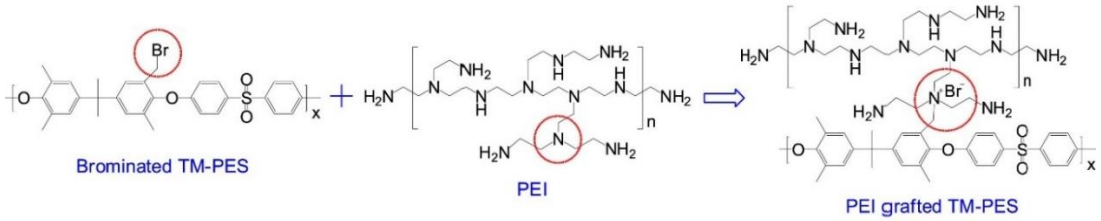

Figure 2.1: The reaction between brominated TM-PES and PEI (Lin et al., 2018).

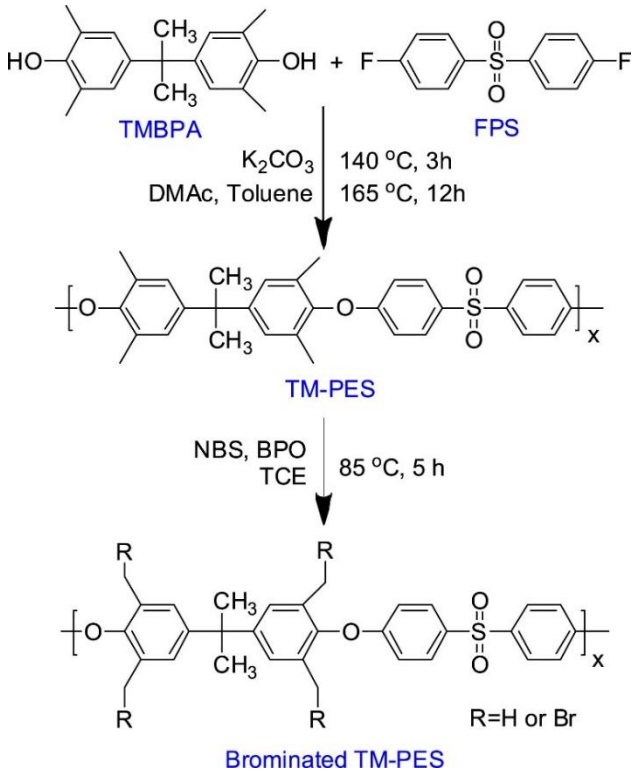

Figure 2.2: Synthesis process of brominated TM-PES (Lin et al., 2018).

As compared with the physical modification, the additives are covalently bonded with membrane surface in chemical modification. Therefore, such improvement of the surface hydrophilicity is permanent and may however lead to the

degradation of polymer chains on the surface of membrane (Kang and Cao, 2014). Generally, these methods usually require caustic chemicals and as a result limit its wide use for water and wastewater separation.

2.3.2 Improvement in preparation process of membrane

Membrane enhancement can be achieved during preparation process via blending, owing to its convenient operation under mild conditions (Yuliwati and Ismail, 2011). This introduction can be achieved by adding polymer material and inorganic nanofillers into the cast solutions.

2.3.2.1 Addition of polymer materials

In this approach, hydrophilic organic polymers are dissolved in dope solution. The materials commonly used includes polyvinyl pyrrolidone (PVP), polyethylene oxide (PEO), polyethylene glycol (PEG) derivatives due to their high compatibility with the backbone polymer-PES and their reasonable price (Rana and Matsuura, 2010). It has been well documented that addition of PVP proportionally increases membrane hydrophilicity due to its inherent hydrophilicity and high water solubility when small amounts of PVP are added (Basri et al., 2011). Abdel-Karim et al. (2017) observed an increase in the water flux from 2.2 L/m^2 h for pristine PES membrane to more than 40 L/m^2 h with the introduction of 3 wt.% PVP in the PES matrix. In addition, roughness and porosity increased significantly resulting in an increase in their fouling resistances, whereas rejection was low. These membranes showed 67% rejection of BSA as compared to ~90% for pristine PES membrane.

Kourde-hana et al. (2017) evaluated the influence of different PVP content in the PES matrix. The pure PES membrane displayed the lowest permeability (around 70 L/m^2 h) while the most permeable membrane was observed for membrane synthesized with 16% PVP content (135 L/m^2 h). Despite its hydrophilic nature, it was observed that higher content of PVP in the casting solution led to a decrease in the flux of membrane. In other words, flux did not exhibit a monotonous trend with the amount of PVP. This was attributed to the hydrophilic nature and pore forming ability of PVP (can either decrease or increase the pore size and is dependent on its amount). Interestingly, the initial PVP content did not seem to influence PEG rejection. Son et al. (2017) also studied the influence of different concentration on the performance of PES matrix for humic acid fouling. The addition of 1 wt.% PVP increased flux to 1,107 L/m^2 h from zero flux with > 90% humic acid rejection. The PWF of the membrane with 10 wt.% of PVP reached 2,439 L/ m^2 h as compared to lower PWF for pristine membrane. PWF decreased to around 1,000 L/m^2 h as PVP was increased to 20 wt.%. Membrane with 10 wt.% PVP displayed the best fouling resistivity.

2.3.2.2 Addition of amphiphilic co-polymers

One general issue of blending with polymer is the elution of this polymer and their poor compatibility with polymer matrix (Kang and Cao, 2014). To address this issue, some researchers have looked into the use of amphiphilic co-polymers as well as amphiphilic copolymers containing polymer chains with hydrophobic parts as modifiers. Amphiphilic modifier contains hydrophilic and hydrophobic properties which are able to interact with hydrophobic polymer, totally insoluble in water and

are also able to interact with hydrophobic polymer. The hydrophobic chains guarantees the compatibility with host polymer, while the hydrophilic chains is enriched onto the membrane pore during phase inversion due to segregation effect, thus, providing a high coverage of hydrated side chains anchored by a hydrophobic backbone that is entangled with the polymer bulk and water insoluble (Bushell, 2012). Moreso, by controlling the ratio of hydrophobicity and enhancing the hydrophilicity during the membrane casting, one can expect desirable membrane performance properties, such as a higher solute rejection, fouling resistance and permeability (Nunes and Car, 2013).

Liu et al. (2015) synthesized an amphiphilic modifier (MF-g-PEGn) by etherification of melamine formaldehyde (MF) pre-polymer with PEG, and blended in PES matrix. Figure 2.3 presents the synthetic route of MF-g-PEGn. The presence of MF-g-PEGn reduced the thermo-dynamic stability of the dope solution, thus endowing the membranes with higher porosity with evident influence on contact angle. The PWF of membranes were improved from 60.7 L/m^2 h for the PES control membrane to 164.7 L/m^2 h for PES/MF-g-PEG with no influence on rejection as all membranes possessed 100% rejection efficiency. Furthermore, flux recovery ratios (FRR) of the PES control membrane and PES/MF-g-PEG were 70.8 and 91.6%, respectively.

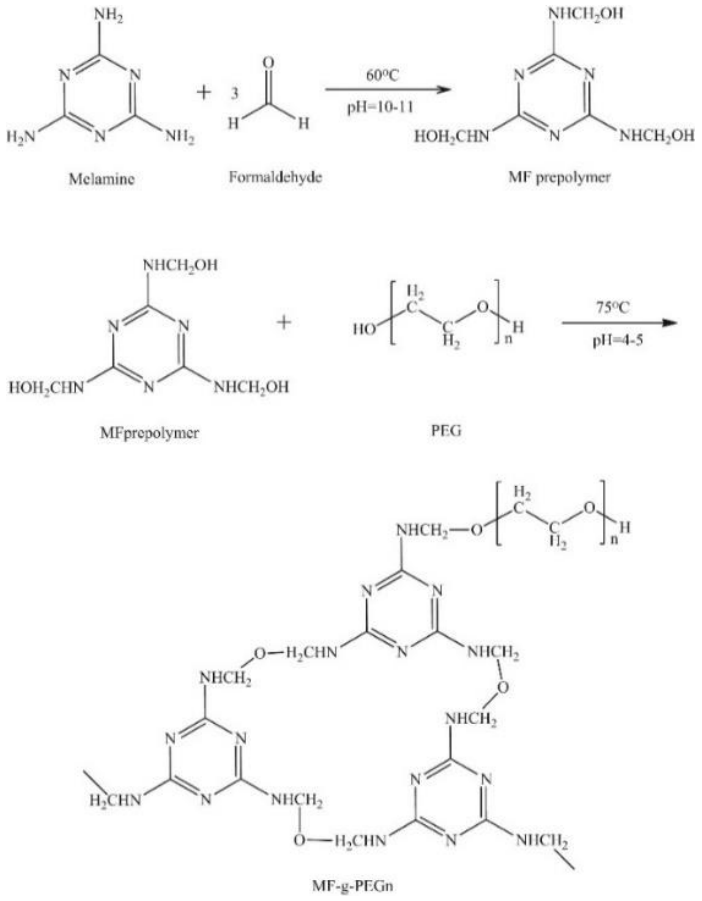

Figure 2.3: Synthetic route of MF-g-PEGn (Liu et al., 2015).

Su et al. (2015) synthesized an amphiphilic co-polymers bearing pluronic F127 and poly(methacrylic acid) (PMAA) segments (PMAAn–F127–PMAAn) and introduced as additive in PES dope solution. The water flux of blend membrane was in the range of 192.1 and 238.6 L/m^2 h as compared to pristine membrane with WF of 180.8 L/m^2 h. Jalali et al. (2016) synthesized an hydrophilic polysulfide-amide (PSA) co-polymer with thioether linkages, thiazole rings and nitro groups was synthesized via phosphorylation poly-condensation and incorporated into PES matrix. Figure 2.4 shows the schematic of synthesis of polysulfide amide co-polymer. By addition of the polyamide additive to the PES casting solution, the porosity is increased. The FRR of the bare membrane was observed better than the modified membrane.

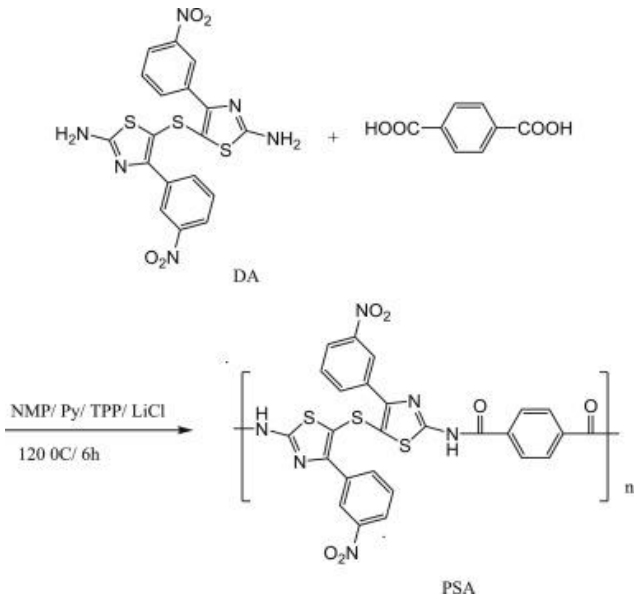

Figure 2.4: Schematic of synthesis of PSA co-polymer (Jalali et al., 2016).

Recently, some amphiphilic copolymers containing polymer chains as hydrophobic parts have also been applied with polymeric membranes. For instance, Zhao et al. (2016) introduced an amphilic co-polymer PES-block-poly(sulfobetaine methacrylate) (PES-b-PSBMA) into PES matrix. The triblock copolymer, PES-b-PSBMA was synthesized via the combination of quaternization and RAFT polymerization (Figure 2.5). After modification, the WCA for the PES-g-PSBMA membranes decreased significantly from 90 to 60º. Pure water flux increased from 45.6 to 115 L/m^2 h while rejection of BSA changed slightly with increase in the content of co-polymer. Compared with FRR of the PES membrane (49%), the FRRs for PSBMA-grafted PES membranes was effectively enhanced to 80%.

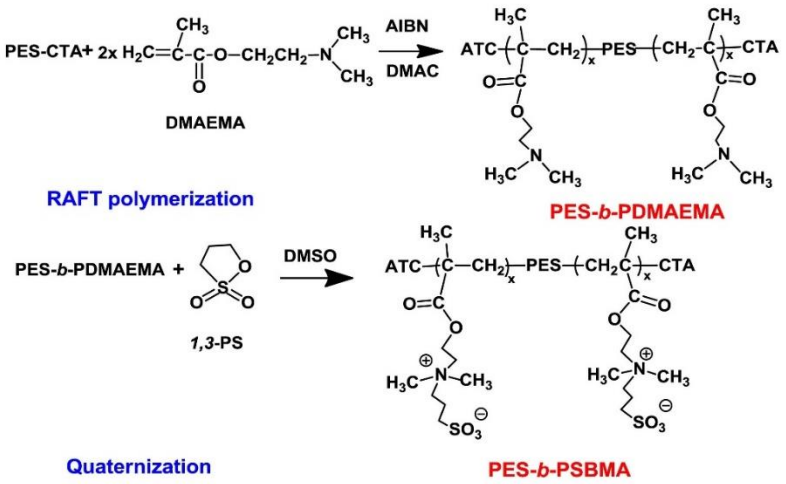

Figure 2.5: Schematic representation for the synthesis of PES-b-PDMAEMA and PES-b-PSBMA (Zhao et al., 2016).

Zhu et al. (2014) prepared a hollow fiber membrane using PVDF as the base material and a modified PVDF copolymer via a dry-wet spin phase inversion. In the study, P(VDF-co-CTFE) polymer was first grafted with tert-butyl methacrylate (tBMA) monomers via an atom transfer radical polymerization (ATRP) method. Then, the grafted PtBMA chains were hydrolyzed to poly (methacrylic acid) (PMAA) to produce the intermediate polymer of P(VDF-co-CTFE)-g-PMAA. Finally, P(VDF-co-CTFE)-g-PMAA was esterified with perfluoroalkyl polyethylene glycol (fPEG) or polyethylene glycol (PEG) to obtain an additive polymer of P(VDF-co-CTFE)-g-PMAA-g-fPEG which was blended with PVDF to prepare the dope solution. Figure 2.6 shows the structure of synthesized amphilic copolymers. The as-membrane were used to separate hexadecane in water separation, crude oil in water, and palm-oil in water which resulted to a rejection efficiency of 98%, 99% and 70%, respectively. Furthermore, the membranes exhibited much lower oil fouling effect and had much higher flux recovery rate during hexadecane-water separation. However, the study recommended hollow fiber membranes with smaller

pores by increasing the dope polymer concentration in order to achieve a complete removal of oil.

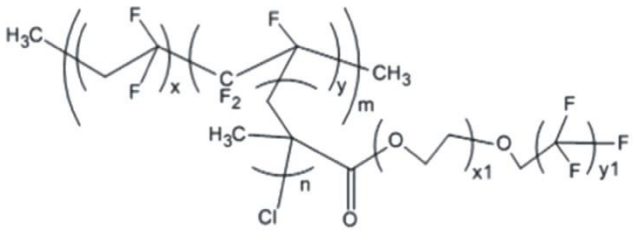

Figure 2.6: The structures of the synthesized additive polymers P(VDF-co-CTFE)-g-PMAA-g-fPEG (X. Zhu et al., 2014).

Generally, it has been well documented that these copolymers had better compatibility with polymer bulk, and could be used as modifiers to enhance the hydrophilicity, antifouling properties and performance of polymeric membranes (Wu et al., 2013).

2.3.2.3 Addition of inorganic materials

Apart from introducing polymer and co-polymers, the inorganic materials are another promising modifier. The addition of inorganic material with PES matrix has become an attractive approach for the fabrication of polymeric membranes and has capture much attention in recent times (Džunuzović et al., 2012). Much bulk of research has been carried out on the preparation of composite membranes by the addition of inorganic materials. For instance, the presence of the dispersed inorganic materials in the polymeric membrane matrix has been reported to improve the membrane performance and properties particularly by: (a) increase permeability due to the larger effective membrane surface area of NPs; (b) induce membrane with the functional properties of the nanomaterials (Zhang et al., 2018); (c) improving

membranes hydrophilicity as well as fouling resistance properties (Li et al., 2010); (d) improving the thermal and mechanical properties (Calebrese et al., 2011). Up till date, many types of inorganic materials have been incorporated as additives in polymer matrix, including titanium dioxide, silicon dioxide, carbon nanotubes, halloysite nanotubes, manganese oxide, cellulose nanocrystals, graphene oxide, silver, zirconia, zinc oxide, alumina, metal organic framework. However, there are two ways to introduce these materials into PES membrane during the preparation process: blending them in coagulation bath or in the polymer solution. Compared to the blending of these materials in coagulation bath, blending the inorganic material in the polymer solution has been the dominant method.

Tilahun et al. (2018) introduced TiO_2 in order to prepare PES/TiO_2 membrane. Upon introduction of 1 wt.% of NPs, membrane hydrophilicity was enhanced, permeability increases by 59%, with a negative effect on solute rejection which decreases from 97 to 94.9%. Ahmad et al. (2017) investigated the fouling behaviour of PES/ZnO HF membranes for humic acid removal. In their study, the FRR of HF-0, HF-0.5, HF-2, HF-3.62, and HF-5 were 97.01, 92.30, 75.93, 91.10, and 88.17%, respectively indicating that the addition of ZnO-NPs to PES did not help to reduce fouling effect. Nasrollahi et al. (2018) presented PES UF membranes blended with different CuO/ZnO (CZN) contents. When CuO-ZnO content was 0.2%, they observed about 32% improvement in pure water flux, BSA rejection flux increased from 92.5 to 117.7 L/m^2 h, and FRR increases from 44.6 to 50.1%. Pang et al. (2014) prepared ZrO_2/PES UF membranes and observed that both rejection of OVA as well as rejection of BSA decreased with increasing content of ZrO_2 in the dope solution. The water recovery rate of nanocomposite membrane was about 1.8

times higher than that of bare membrane and 1.7 times higher than that of bare membrane after surface fouling by ovalbumin (OVA) solution.

Ghaemi (2016) investigated the ability of Al_2O_3 NPs to improve heavy metals adsorption and for efficiency copper removal by PES membranes. Composite membrane demonstrated higher PWF up to NPs loading ≤ 1 wt.% due to the enhanced hydrophilicity and porosity Al_2O_3 NP. However, further increase in Al_2O_3-NPs wt.% >1 wt.% did not show any change in performance of the NC. Daraei et al. (2013) introduced Fe_3O_4 into the PES matrix and observed that the water flux was much lower, decreasing from 36 to 33 L/m^2 h. This might be attributed to pore blockage as a result of the NPs accumulation in membrane surface pores. Furthermore, the FRR value for the modified membrane was 68% as compared with pristine membrane (52%). In a study by Ananth et al. (2014), n-Ag was prepared by bacteria mediated biosynthesis method and then introduced to produced resulting composite membrane. At 1.5 wt.% of n-Ag in pristine PES, decrease in the rejection and enhancement in BSA flux were observed. The flux of PES/n-Ag composite membrane was higher while the BSA rejection decreases upon modification. Furthermore, the PES/n-Ag membrane shows the highest FRR of 79.4% against 53.5% for pristine membrane. (Scott Matteucci, Victor A. Kusuma, Scott D. Kelman, 2008) incorporated nano-sized MgO as the filler phase and poly(1-trimethylsilyl-1-propyne) (PTMSP) as the continuous phase to prepared the composite membrane. the gas permeability coefficients were 17–50 times (depending on the gas) higher than in an unfilled polymeric membrane under similar condition. More interestingly, gas permeability in a membrane containing 75 vol.% MgO slightly increased over time, solving the physical aging problem of PTMSP.

Abdel-Karim et al. (2018) prepared MMM by blending graphene oxide (GO) with PES and found that that the membrane hydrophilicity was significantly improved and porosity increased significantly from 26 to 83%. Flux increased from 2 to 13 L/m^2 h while the rejection of BSA from ~90 to 97%. Furthermore, the addition of GO increased the FRR to 62% when GO content was 0.3 wt.% as compared to 25% for pure PES. Aditya Kiran et al. (2016) reported GO flakes incorporated in PES MMMs. It was found that hydrophilicity, PWF were improved for GO/PES membrane. WF increases from 43 to 57 L/m^2 h. The tensile stress was significantly improved from 0.99 to 2.81 MPa. Furthermore, a maximum of 54% removal of color was observed for distillery spent wash effluent. Sengur et al. (2015) formed a nanocomposite polymer solutions by adding functionalized MWCNTs and PES and observed a maximum increase in stress which was 125% over pristine hollow fibers. Membranes with greater MWCNTs concentrations exhibited increase in permeation rates from ~180 to ~960 L/m^2 h. Wang et al. (2018) prepared an hybrid membrane. Prior to blending, MWCNTs was functionalized by non-covalent modification with sodium lignosulfonate (SLS). Filtration and protein adsorption tests indicated that the anti-fouling performances were dramatically increased, the amount of protein pollutants adsorbed by the hybrid membranes was significantly lower than the nascent membranes. PF increases from 170 to 460 L/m^2 h while BSA rejection was negatively affected as it declined from ~98 to 96%. Furthermore, the FRR of modified membrane (90%) was higher than the unmodified membrane (62%).

Gholami et al. (2018) reported a novel hydrophilic PES membrane was synthesized by blending with TMU-5 Metal-Organic frameworks (MOFs). They found that the addition of 0.1 wt.% MOF NPs led to an increase in PWF from 133.29

to 182.02 L/m^2 h. Furthermore, the FRR for the unfilled PES membrane (24.47%) was lower than the FRR for the membranes prepared with MOF nanofillers (98.74%). Low et al. (2014) introduced a two dimensional ZIF with leaf-shaped morphology (ZIF-L) into PES membranes. ZIF-L was synthesized in zinc salt and 2-methylimidazole aqueous solution at room temperature. The introduction of 0.5% ZIF-L nano-flakes resulted to increase in water flux from 215 to 378 L/m^2 h (75% increase) and increase in FRR from 72 to 82%. Furthermore, the membrane showed almost twice the fouling resistance improvement against BSA.

Numerous inorganic additives have been incorporated in polymeric matrix, each with its own characteristics and functionalities for specific application. The emerging aim of incorporating these inorganic additives is to produce membrane in a way that these additives are present on the surface of the membrane and internal surface pore, while significantly influencing membrane permeability for intended applications. The most crucial problem when using inorganic additive is their poor dissolution and dispersion of synthesized nanocomposites in various organic solvents as well as weak interaction with polymer matrix (Oueiny et al., 2014). These factors are important in the utilization of additive in the composite membranes. The additive concentration is another parameter, which when at relatively higher amount produce aggregations and as a consequence will cause pore blockage. This will also lead to non-uniformity in particle distribution in PES matrix which will lead to leaching out of the particles.

2.4 Silica based composite membranes

The addition of SiO_2 NPs have been investigated intensively and proven ideal as an additive for polymeric membranes due to properties such as fine suspendability in aqueous solution, relatively environmentally inert, thermally and chemically stable with large surface area (SA) and highly miscible (Tang et al., 2007). For example, Zhang et al. (2013), doped SiO_2 into PVDF to prepare SiO_2/PVDF composite membranes. Their result shows that an improvement of oil rejection for SiO_2/PVDF membrane from 86.0% (pristine membrane) to 91.2% at 45 mg/L oil in feed, TMP of 0.10 MPa, temperature of 25 ºC and pre-evaporation time of 15s. Similarly, Zhang et al. (2014) prepared a SiO_2/PVDF composite membrane by doping SiO_2 with PVDF via a phase inversion method for machine oil in water separation. In the study, result shows an improvement of oil rejection for SiO_2/PVDF membrane from 93.8% (pristine membrane) to 94.5% (modified membrane) at 45 mg/L oil in feed, TMP of 0.10 MPa, temperature of 25 ºC and pre-evaporation time of 15s. Moreover, the permeate flux increased from 160 to 198 L/m^2 h upon the addition of SiO_2 nanoparticles. In the study, it was observed that PVDF polymer chains did not interact well with SiO_2 particles and therefore, could not supply excellent anti-compaction capabilities to resist the outer impact forces. Their result also shows a downtrend of flux with increase in operating pressure above 0.10 MPa. This is similar to study by Zhang et al. (2015), who observed that the permeate flux of the composite membrane was better compared to the pristine membrane. Oil rejection of 88.13% was attained at 0.1 MPa, 25 ºC as compared to the pristine membrane of 77.33%. The result shows that the pore diameter of PVDF membrane increases upon doped with SiO_2 particles.

Boshrouyeh et al. (2015) observed an increase in permeate flux (PF) and hydrophilicity by introducing a low content of SiO_2 NPs (up to 0.7 wt.%) into PES matrix whereas at high content above this value resulted in PF reduction which might be attributed to particle agglomeration, resulting to pore blockage. In another study by Muhamad et al. (2015), SiO_2 nanoparticles of various loading (0 - 4 wt.%) was introduced to modify PES HF membrane. Results show that the addition of 2 wt.% SiO_2 in the PES matrix produced membrane with an improved the BSA rejection and WF, achieving 94% and 87.2 L/m^2 h, respectively. As a comparison, the unmodified PES membrane only exhibits rejection of 81% and WF of 44.2 L/m^2 h. Results further shows that the flux recovery ratio (FRR) of the unmodified membrane was improved from 82% to 93% for membrane embedded with 2 wt.% SiO_2.

One generally issue of doping with commercially available SiO_2 additives is due to problem of dispersibility of introduced SiO_2 in the membrane matrix is challenging, particularly when dealing with HF membrane matrix. The high surface energy of SiO_2 often results in agglomeration; leading to low surface area, membrane surface aggregation and high surface roughness, which is a serious setback for practical application.

2.4.1 Sol-gel synthesis route

The sol–gel method as a classical approach to organic–inorganic nanocomposites has been extensively studied since the 1980's. Through the controlled hydrolysis and condensation of the inorganic alkoxide precursors, accompanying the solidification of polymer chains, nano-sized inorganic particles are in situ generated within the polymer matrix (Laberty-Robert et al., 2011). The

molecular-level mixing of precursor, polymer and solvent in a sol–gel reaction system is beneficial to improving filler dispersion and polymer–filler contact (Laberty-Robert et al., 2011). Moreover, the viscous hybrid sol allows the straightforward preparation of composite membranes for diverse shapes of membrane modules.

Stöber reaction based on sol gel synthesis method for preparing mono-dispersed spherical SiO_2 particles with sizes covering almost the whole colloidal range has been a favorable method in the past. Stöber SiO_2 particles has been used as model colloids in large number of experimental investigations. Lin et al. (2016) introduced mono-dispersed SiO_2 as an additive in ultra-low ratio to synthesize inorganic–organic PES membranes and observed an improved hydrophilicity due to the high H_2O interaction of nano SiO_2, and hence resulted in a higher permeability and fouling property. They observed a decrease in permeability at high concentration of nano-SiO_2 (i.e., nano-SiO_2 > 0.3 wt.% ≤ 0.5 wt.%) due to macrovoids alteration in the membrane sub-layer and pore plugging. A good rejection of humic acid (~95.35 %) using doped PES at 0.5 wt.% nano-SiO_2, and a rejection of methylene blue of ~99.1% was obtained with 0.2 wt.% nano-SiO_2. They observed no visible agglomeration of nano-SiO_2 particles on membrane surface at low contents ranging from 0.10 to 0.30 wt.%. However, at higher amount ranging from 0.4% to 0.5%, there were several traces of NPs aggregation on membrane surface, which resulted to clusters being formed. Wu et al. (2014) developed a polysulfone (PSf)-based hybrid membranes developed by doping with SiO_2–GO nanohybrid. The rejection was lower as compared to the pristine membrane due to the incompatibility between two phases was not good enough resulting in the formation of non-selective voids while the PWF flux

increases significantly. The hybrid membrane presents a higher water flux than that of pure PSf membrane.

Wang et al. (2016) present a hybrid PVDF ultrafiltration membranes prepared using hollow silica microspheres ($HSiO_2$) with particle size of 500 nm. Their results showed that $HSiO_2$ microspheres had inner cavity structure, mesoporous wall, good dispersion and excellent hydrophilicity, and could be used to construct stepped permeable channels for decreasing the mass transfer resistance of water molecules in the porous support layer of PVDF membrane. The improved hydrophilicity and constructed channels of PVDF matrix by added $HSiO_2$ improved the separation and antifouling performance of hybrid PVDF membrane. The water flux of the modified PVDF UF membranes exhibited a rising trend with the rejection of 83% - 88%, which overcame the trade-off phenomenon of separation membrane. Abolhassan et al. (2018) also reported a chitosan/poly(vinyl alcohol)(PVA)/SiO_2 nanocomposite electrospun nanofibrous membranes (ENMs). They found that with the addition of 0.5 wt.% SiO_2, the Young's modulus of the prepared membranes almost doubled from 0.74 MPa for chitosan/PVA ENM to 1.69 for nanocomposite ENM. A marked increase in both water permeability and dye rejection was attained at 1.0 wt.% SiO_2. The optimized nanocomposite membrane provided 98% Direct Red 23 rejection and 1711 L/m^2 h flux under 0.4 bar transmembrane pressure.

The sol–gel method shows some apparent advantages over the physical blending method in many situations, while the range of available fillers is relatively narrow. Firstly, the center atoms of sol–gel precursors are limited to silicon as well as some metal. Secondly, it remains challenging to in situ synthesize fillers with

multi-scale structures and multiple functionalities. Although composite membranes containing mesoporous silica have been successfully prepared by the template-assisted sol– gel method, many tough works are still waiting to be accomplished, such as enlarging the range of available polymers, tailoring the particle size and in-situ modifying the filler surface.

2.4.2 Synthesis with silane coupling agents

Recently, silane coupling agents have been used in a wide range of applications because of their unique ability to bond polymers with silica. The bond thus formed has good initial strength as demonstrated by failure of the composite by polymer rupture, and the bond exhibits excellent retention of strength even after severe environmental aging. The siliceous matter or metal may be in the form of fibers, particulate fillers, or massive structures. For example, Xiang et al. (2015) reported the preparation of a thermally responsive PVDF membrane with underwater superoleophobicity and under oil superhydrophobicity properties. In their study, poly (N-isopropyl acrylamide) (PNIPAAm)–polyvinyl pyrrolidone (PVP)–vinyltriethoxysilane (VTES) micro-hydrogel were elaborately synthesized and incorporated into PVDF membrane. The PVDF membrane exhibited super-antiwetting, outstanding permeability, high separation efficiency (>99.90%), excellent antifouling property and reliability for long-term application. The membrane also exhibited much higher flux of 5487 and 11,774 L/m^2 h for oil/water, and water/oil micro-emulsion at 40 °C than 5070 and 4500 L/m^2 h at 20 °C respectively. Liu et al. (2016) also reported a superhydrophobic poly(vinylidene fluoride) membranes with controllable structure and tunable wettability prepared by one-step electrospinning. A tunable wettability from hydrophobic to

superhydrophobic or from superoleophilic to superamphiphobic was realized through modifying PVDF membranes with aqueous ammonia solution and incorporating 1H,1H,2H,2H-perfluorodecyltriethoxysilane (POTS). These superhydrophobic membranes also demonstrated excellent durability, anti-fouling property and oil water separation ability after dozens of cycles. Their result also shows the surface of the membrane was still without any contaminant residues after 30 cycles. Moreover, the superhydrophobic membranes modified with POTS and ammonia demonstrated excellent anti-fouling property and oil-water separation ability after dozens of cycles.

Martín et al. (2015) synthesized mesostructured silica functionalized with amino group [3-(2-aminoethylamino) propyl] trimethoxysilane (AEAPTMS) and carboxylic groups (3-aminopropyl) tri-methoxysilane (APTMS) and then incorporated in PES matrix which led to significant improvement explained by the combined effect of incorporation of hydrophilic fillers near the membrane surface and formation of higher surface pore. The water permeation flux was found to increased upon incorporating silica fillers from 180 to 315 L/m^2 h for membrane with no functional group and up to 631 L/m^2 h for membrane with amino group. In addition, the intrinsic resistance contribution for doped membranes was around 50% of the total resistance in comparison with the 38% observed for the pristine PES membrane. Jullok et al. (2016) also synthesized and introduced SiO_2 NPs into polyphenylsulfone (PPSU) matrix to fabricate SiO_2 modified PPSU-based membranes. Prior to blending, SiO_2 NPs were organically modified with hexamethyldisilazane to form trimethylsilyl groups. In their study, they observed NPs agglomeration on the top-layer of membrane. Ngang et al. (2017) reported a thermo-responsive polyvinylidene fluoride/silica-poly (N-isopropylacrylamide)

(PVDF/SiO_2-PNIPAM) mixed matrix membranes were synthesized using diffusion induced phase separation techniques via direct blending method. Thermo-responsive SiO_2-PNIPAM particles was synthesized through radical polymerization using SiO_2/3-methacryloxypropyl trimethoxysilane particles as core material to introduce C=C onto the SiO_2 particles surface. Compared with pristine PVDF membrane, the PVDF/SiO_2-PNIPAM membrane showed higher alternated thermal cleaning ratios (N=2.04) especially at 1 wt.% SiO_2-PNIPAM particle concentrations. The antifouling properties were negatively influenced as the unmodified membrane presents the best antifouling performance.

2.4.3 APTES functionalized surface

Aminosilanes are widely used coupling agents for silica-based materials because of their bifunctional nature. Nucleophilicity of $–NH_2$ groups in aminosilanes, for example, is taken advantage of in promoting adhesion in glass-resin composites (Plueddemann, 1991). In aqueous media of low to medium pH values, $–NH_3^+$ groups promote the attachment of negatively charged species, such as DNA (Kneuer et al., 2000; Roy et al., 2005) and nanoparticles (Chen et al., 2006; Enders et al., 2006). Whether the applications of aminosilanes are industrial, biological, or environmental, the hydrolytic stability of the aminosilane-derived layers is critical to the success of the derivatization reactions and the long-term stability of the conjugated systems.

3-aminopropyltriethoxysilane (APTES) is the most commonly used aminosilane. The popularity of this aminosilane is coupled with complexities in its

usage. One of the main issues lies in the fact that there are many possible ways for it to interact with surface silanol/silanolate groups, via hydrogen bonds, electrostatic attractions, and siloxane bonds (Figure 2.7) (Asenath Smith and Chen, 2008). Some of the conformations have been implicated in low silane grafting density (Figure 2.7b) (Sofian M. Kanan, William T Y Tze, 2002) and others result in weakly attached silane molecules (Figure 2.7 c-e). Secondly, APTES has three ethoxy groups per molecule and is capable of polymerizing in the presence of water, which can give rise to a number of possible surface structures: covalent attachment, two-dimensional self-assembly (horizontal polymerization), and multilayers (vertical polymerization) (Fadeev and McCarthy, 2000). Thirdly, excess water results in not only uncontrolled polymerization of silane molecules on surface, but also formation of oligomers and polymers of silanes in bulk/solution (Kinkel and Unger, 1984), which can also react with and attach to the surface. The extents of alkoxy hydrolysis and amine protonation in the silane layers also depend on the amount of water present (Caravajal et al., 1988). Additionally, the amine functionality can inter- and intra-molecularly catalyze silane attachment and formation of oligomers and polymers of silanes (Sofian M. Kanan, William T Y Tze, 2002). Some typical structural features in an APTES-derived layer are shown in Figure 2.8. The physiosorbed, hydrogen bonded (a) or electrostatically attached (b) silane molecules are not stable. Among the covalently attached silanes, some have reacted with only surface silanol groups (c) and others have bonded with neighbouring silane molecules in horizontal (d) and/or vertical directions (e). Some of the silanes shown are attached to the surface in oligomeric form (f), which introduces additional disorder in the silane layer.

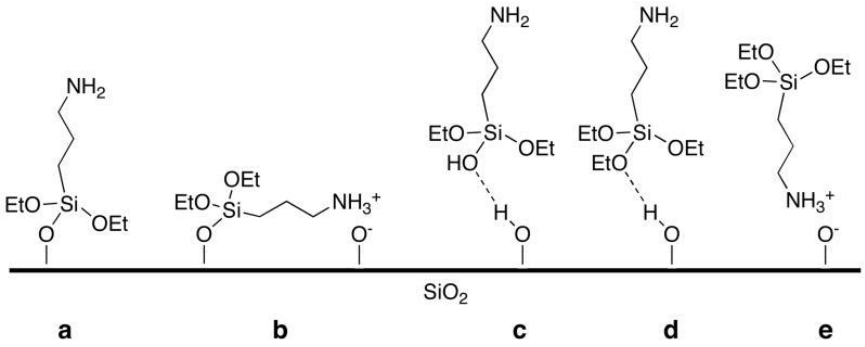

Figure 2.7: Different types of interactions between APTES molecules and silicon dioxide substrates: (a) a covalently attached APTES molecules with its amine group extending away from the interface, (b) a covalently attached APTEs molecule with its amine group interacting with a surface silanol group, and (c) weakly bounded APTES molecules (Zhu et al., 2012).

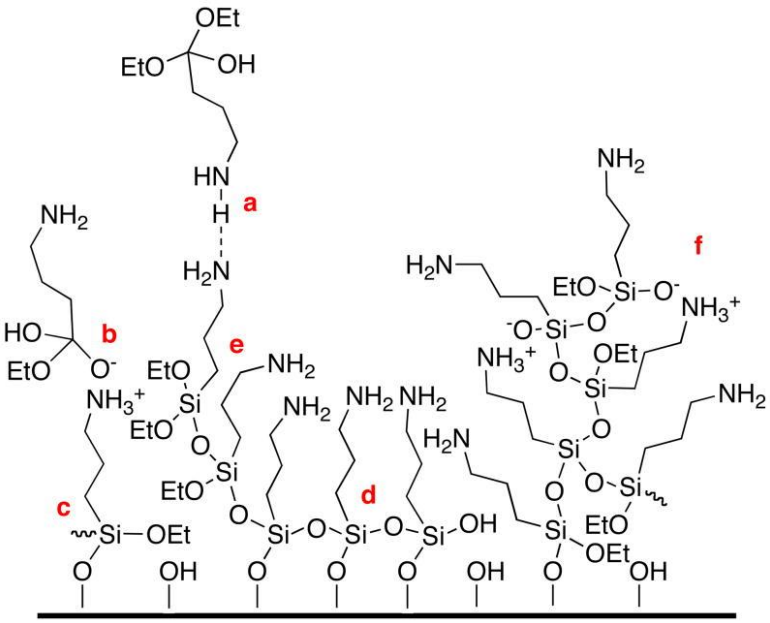

Figure 2.8: An APTES-derived layer with structural irregularities: individual silane molecules can be incorporated into the layer via a) hydrogen bonding, b) electrostatic attraction, c) covalent bonding with the substrate, d) horizontal and e) vertical polymerization with neighbouring silanes; f) oligomeric/polymeric silanes can also react/interact with functionalities present at the interface (Zhu et al., 2012).

The functionalization of a material or composite with APTES has found space in wide applications. In a study by (He et al., 2017), APTES-functionalized

graphene oxide (APTES-GO) was synthesized by one-step refluxing of GO with APTES for effective removal of Cr(VI) from aqueous solution. Their results showed that the Cr(VI) adsorption onto APTES-GO was highly pH dependent, and the maximum adsorption capacity reached up to 215.2 mg/g at 328 K. In another study by (Chen et al., 2016), 4-aminothiophenol and 3-aminopropyltriethoxysilane were firstly used to functionalize GO in order to promote the sorption efficiencies of methylene blue (MB) and copper (Cu^{2+}). Adsorption isotherm results showed that the maximum adsorption capacities of MB by 4-aminothiophenol modified GO (GO-SH) and 3-aminopropyltriethoxysilane modified GO (GO-N) were 763.30 and 676.22 mg/g, which was much higher than original GO 455.95 mg/g. For Cu^{2+} adsorption, the maximum adsorption capacities by GO-SH and GO-N were 99.17 and 103.28 mg/g, suggesting that the engineered GO exhibited greater Cu^{2+} sorption ability than original GO of 32.91 mg/g. Both MB and Cu^{2+} removal rates increased with pH and adsorbent dosage increased, while the sorption rates weakly reduced with increasing ionic strength. The modification with -SH and -NH_2 groups did not only increase the sorption sites, but also cause chelation with heavy metals, and thus improving the sorption capacities of MB and Cu^{2+}.

(Huang et al., 2010) developed a seeding-free preparation of dense LTA zeolite membranes by using APTES as covalent linker between zeolite membrane and porous Al_2O_3 support. In a first step, the ethoxy groups of the APTES reacted with surface hydroxy groups of the support. In a second step, the 3-aminopropylsilyl groups reacts with silanols of the zeolite crystals, leading to a “bridge” between the growing LTA zeolite membrane and the support being built to anchor the LTA zeolite layer onto the support. The LTA zeolite membrane displays good molecular

sieving performance. For binary mixtures at 20 °C, the separation factors of H_2/CH_4, H_2/N_2, H_2/O_2 and H_2/CO_2 are 3.6, 4.2, 4.4 and 5.5, respectively, which were higher than the corresponding value of Knudsen diffusion. (Sun et al., 2016) prepared a porous membrane adsorbent (PEI/SA) by immobilizing polyethyleneimine (PEI) with sodium alginate (SA), then further functionalized PEI/SA with APTES and tested its adsorption performance for removing Cu(II). The results show that the maximum adsorption capacity of Cu(II) onto the PEI/SA was approximately 329.8 mg/g, which was 7 times more than that of pristine SA porous membrane. The reusability experiments also show that the PEI/SA has excellent adsorption–desorption efficiencies.

(Mahmoud et al., 2016) functionalized nano-magnetic iron oxide with APTES [Nano-Fe_3O_4–SiO_2–NH_2] which was synthesized using a microwave-assisted procedure. The metal sorption properties of the magnetic nano-sorbent with four different divalent metal ions, viz. Pb(II), Cu(II), Cd(II) and Hg(II) were evaluated by heating the interacting metal ion solution in contact with the sorbent in a microwave oven for 5–30 s. Pb(II) was found the highest extracted metal ion and the capacity value was identified as 1250 μmol g^{-1} after heating for 5 s, while the equilibrium capacity value was obtained as 1300 μmol g^{-1} at 15 s. In a study by (A. Ahmad et al., 2017), CNTs was prepared using a chemical vapor deposition method with acetylene and synthesized mesoporous Ni-MCM41 as the carbon source and catalyst, respectively, and were then functionalized using APTES through the co-condensation method and loaded with commercial TiO_2. The functionalized-CNTs loaded TiO_2 was tested as an adsorbent for removal of methyl orange (MO) in

aqueous solution, and results show that 94% of MO is removed after 10 min of reaction, and 100% after 30 min.

(Ostwal et al., 2011) enhanced CO_2/N_2 selectivity of mesoporous silica membranes by surface modification using APTES. Mixed gas separation factors as high as 10 for CO_2 over N_2 were observed at 393 K and CO_2 partial pressures of 15 kPa; whereas for pure gases (CO_2 partial pressure of 303 kPa), no separation was seen. The permeance of CO_2 is highly non-linear, and increases with decreasing CO_2 partial pressure in the feed gas. In a study by (Ha et al., 2008), montmorillonite (MMT) was functionalized with APTES via surface modification. The analysis found that MMT functionalized APTES produces good dispersion of MMT in the epoxy and increases the intercalation effect. Fracture toughness was found to decrease up to 4 wt.% of MMT and increased at 6 wt.%, followed by another decrease at 10 wt.%. This occurs due to the nanocomposite's increased brittleness and increased debondings between MMT and epoxy, as well as voids.

2.5 Hollow fiber spinning system

The conversion of polymer into fiber is known as spinning. Hollow fiber (HF) spinning technologies involves the continuous production of single and multiple fiber via extrusion through the spinneret which then returned to the solid state (via solidification). This results into fibers with varying properties which are dependants on the parameters and process used. The methods involved in HF spinning can also be referred to as solution spinning and melt spinning. In this spinning process, the polymer flakes or pellets are heated and melted in an extruder

which subsequently pumps the liquid through a spinneret to form the liquid-spinning dope (Behavior and Lipscomb, 1994). This filament, which depends on the number of holes in the spinneret is drawn and cooled until it solidifies in a draw region. The final fiber velocity is fixed by the godet roller, which consists of one or more wheels, rotating at a constant rate. The nascent fiber then moves at the same linear velocity as the wheels due to contact frictional force. Like sewing thread, the fiber is finally wound on a spool for storage (Behavior and Lipscomb, 1994).

Unlike the melt spinning, the solution spinning method can be classified as either wet or dry-wet spinning. In wet spinning, the dope solution is extruded into an external bath containing a liquid which acts as non-solvent for the dope. The exchange between solvent from dope and coagulant (non-solvent) causes phase inversion leading to removal of solvent, solidification and precipitation of fiber. Solidification is the transfer of mass through the non-solvent-dope solution interface, which can cause defects including cross shape irregularities and voids (Gupta et al., 2007). However, by applying an AG (> 0) between the end of the coagulation bath and the spinneret, formation of defects can be reduced or prevented, and is referred to dry-wet spinning. In other word, the process of wet spinning occurs if the air gap is 0 whereas it is referred to as dry/wet spinning, if the air gap is > 0. In dry-wet spinning, the extrusion of the filaments is in presence of AG distance, which enables stress relaxation of polymer chains (Gupta et al., 2007). After a dope is extruded out of the spinneret, the nascent HF passes through the AG; then enters the coagulation bath; and finally goes through the godet rollers and is subsequently collected by the winding wheel (collection drum).

HF can be assembled as a single entity or as group in form of bundles of several fibers as shown in Figure 2.9. As compared with flat sheet membrane, the advantages of HF membranes are self-supporting properties with high productivity. High productivity comes from its large surface area and high packing density. Self-supporting property helps to reduce the complexity of the hardware fabrication of module in which it can be easily assembled into metal or plastic tube (Razmjou et al., 2012). In the case of flat sheet membranes module, their use in UF process requires more complex and additional hardware such as porous supports and spacers (Han et al., 2007).

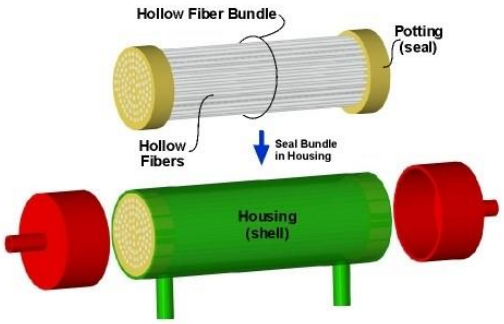

Figure 2.9: Hollow fiber modules containing several fibers.

Different types of instabilities in fiber which might occur during spinning of HF including break up, draw resonance, necking, and irregularity in fiber formation and cross section (Bonyadi et al., 2007). This aforementioned limitations can occur due to the amplifications of the various conditions of spinning which will be discussed in the subsequent sections.

2.5.1 Spinning parameters

As mention previously, several conditions are available in the preparation of hollow fibers (HF) membrane, which will adversely be of significant influence the kinetics of the phase inversion which will largely determine resultant membrane morphology and properties. In this section, the influence of conditions involved in producing HF membrane such as dope extrusion flowrate, air gap, bore fluid chemistry, travelling distance, extrusion temperature and pressure, residence time, external coagulation type and temperature, spinneret design and take-up speed are described. Table 2.3 presents the effect of the spinning parameters

Table 2.3. Parameters that affects the HF spinning process

Parameters	Effects
Bore fluid type	Prevents the collapse of nascent HFs.
Bore fluid temperature	Lower temperature will lead to slower de-mixing rate between solvent and polymer. The higher the temperature, the lower the cooling rate at the inner part of the HF.
Bore fluid flowrate	Controls the inner skin morphology.
Air gap distance	Larger AG means a longer RT of nascent HFs in air. Affected by DR and dope elasticity. Larger AG may produce defects due to elongational and gravity stress. Plays an important role in mass transfer in formation of nascent HFs. At a larger AG, the gravity induced and moisture induced partial phase inversion occurs simultaneously. At constant AG, a higher DR produces a stronger stress (tension) in the HF.
Dope extrusion flowrate	Determines the HF thickness after precipitation. A high extrusion flowrate may make the selective outer-layer defective or thicker while a low extrusion flowrate can produce a dense selective outer layer that is defective. A faster extrusion flowrate will produce larger outer diameter HFs.

Table 2.3 Continued.

Parameters	Effects
Dope extrusion pressure	Dependent on properties of dope, dope extrusion flowrate, geometry of extruder and matrix. Higher Dope extrusion pressure gives a less time for solvent/nonsolvent exchange at the interface between bore fluid and the HFs. A higher DEP may lead to the collapse of the outer layer. Detachment of the outer layer from the inner support layer.
Dope viscosity	Affects the kinetics of the coagulation. High viscosity will promote chain entanglement of nascent HF.
Take-up speed	Affects the formation of defect free dual layer HFs.
Spinneret design	Spinneret concentricity is a determining factor. The smaller the spinneret dimension, the smaller the dimension of fibers.
External coagulation type	To achieve complete phase inversion of the external layer of HF.
External coagulation temperature	Coagulant temperature affects the mass transfer between the non-solvent, solvent and polymer, as well as the HF morphology. Determines the crystallinity of nascent HFs. The higher the temperature, the faster the diffusion process of solvent and vice versa.
Residence time	RT is determined by the air gap, dope extrusion flowrate and take-up speed.
Traveling distance and coagulation bath depth	Determines the RT of nascent HFs in the external coagulation medium.

2.5.1.1 Residence time

The residence time (RT) of the nascent HF is a function of the length of the air gap (AG), the speed with which the polymer dope exit the spinneret or dope extrusion flowrate (DEF) and the take-up speed (TS) (Çulfaz et al., 2010). It can defined mathematically as:

$$\mathrm{Rt} = \frac{\mathrm{AG}}{(\mathrm{TS}+\mathrm{DEF})/2} \tag{2.1}$$

Variation of these variables will lead to changes in RT which will significantly affect the formation of resultant HF. Generally, when a nascent HF spends longer RT, the influence of die-well and shear forces may result in decreased in overall diameter of spun fibers (Wienk et al., 1995). In a study by Xu et al. (2014) shows that the shorter the air gap, the thinner the skin layer. Shukla et al. (2015) reported that a longer RT will enable water vapour to go into the fiber which will subsequently allow a slow phase separation to take place. In a study by Sengur et al. (2015) shows that fiber spun with longer RT result in the formation of sponge-like structures and suppression of macrovoids which as consequence decrease porosity and permeability to increase. Another study by Viguié et al. (2013) reported that under longer RT, the size of macrovoids close to the outer skin becomes shorter with barely no macrovoids close to the inner skin at shorter RT. The circularity of macrovoids near the outer skin increases regularly with RT whereas the relative length decreases (Figure 2.10). In their study, macrovoids were significantly more abundant beyond a critical RT in air which was estimated to be between 1 and 1.5 s.

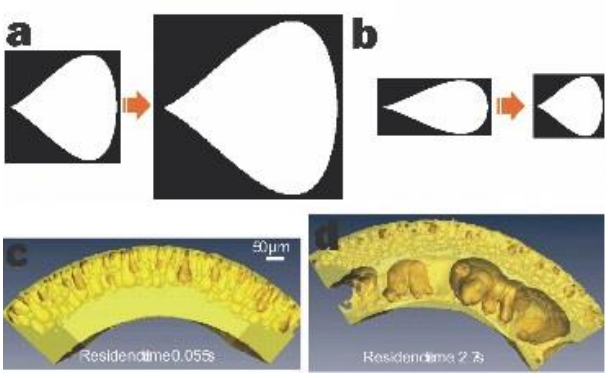

Figure 2.10: Qualitative evolution of the dimensions and shape of macrovoids when the RT varies from 0.055 s to 2.7 s for macrovoids (a) close to the inner skin and (b) close to the outer skin. (c) 3D segmented image of HF membranes made up with 0.055 s and (d) 2.7 s (Viguié et al., 2013).

2.5.1.2 Extrusion pressure and rate

Dope extrusion pressure (DEP) depends on the properties of dope, the dope extrusion flowrate and the geometry of the extruder and matrix. The relationship between the these properties and DEP is derived from the deformation energy that is needed to overcome the input area into the holes of the die as well as the friction on the wall inside the spinneret hole (John Benbow and John Bridgwater, 1993). High DEP will provide less time for the nonsolvent/solvent exchange on the inner interface between the bore fluid and the fiber before precipitation of HF precursor can be completed in the external coagulation bath (Shao et al., 2014). A higher DEP may lead to the collapse of the outer layer and the detachment of the outer layer from the inner support layer. For instance, Shao et al. (2014) shows that the fingerlike voids originating from the inner surface decreased in length with increase in DEP. In addition, when DEP was decreased from 0.20 to 0.10 MPa, pure water flux (PWF) was observed to increase substantially from 1568 to 5142 L/m^2 h while fiber bending strength decreased from 100 to 20 MPa. This is different from reports by Radjabian et al. (2013) who observed an increase in porosity of the outer layer with smaller nanopores which could not be assembled into regular hexagonal pattern when DEP was reduced.

The dope extrusion flowrate (DEF) also plays an critical role as it determines the fiber thickness after precipitation. The DEF can be controlled by a gear pump or with the aid of a controlled gas pressure of their combined system to enable the production of varying shear rates of dope inside the spinneret. In this case, the dope shear rate tends to increase with increase in DEF. A high DEF will produce a defective or thicker selective outer layer whereas a low DEF will produce a defective

dense selective outer layer. Li et al. (2017) have shown that at a high DEF, backpressure effects and the dye swelling tends to be more severe and as a consequence cause the formation of irregular surfaces.

2.5.1.3 External coagulation type and condition

By controlling the external coagulation bath conditions and chemistry, the external surface morphology of spun HF membrane can be designed. When a strong coagulant such as water is used as coagulant, a smooth outer surface and dense surface is formed. However, when a mixed solvent as ethanol (EthOH) or methanol (MetOH) is introduced, the outer surface pore is formed. Furthermore, when non-solvent (such as water) has a higher rate of diffusion in the outer layer in contrast to that in the inner layer, the outer layer tends to hold more water at the interface as well as expand to form large macrovoids. As a consequence, the accumulated water can impede the adhesion of the two layers, leading to delamination. If water has a slower rate of penetration through the outer layer dope than the inner layer dope, good adhesion of these two layers can be expected. In this case, since macrovoids can form the inner layer leading to the expansion of the inner layer, they can also become irregular and distorted (Setiawan et al., 2012). One of the effects of using weak coagulant is the delayed precipitation and de-mixing leading to a more porous outer skin. This effect probably dominates over crystallized structure and sponge-like cells evolved with using weak coagulant and characteristic of higher mass transfer resistance (Song and Jiang, 2013). In the past, external coagulant have been selected from different solvent such as water, isopropanol (IPA) (Bonyadi et al., 2007; Lu et al., 2016; Zuo et al., 2017), propylene glycol (PG) (Jeon et al., 2018), triethyl phosphate (TEP) (Chang et al., 2017), NMP (García-fernández et al., 2017), ethanol

(EthOH) (Feng et al., 2017; García-fernández et al., 2017; Song and Jiang, 2013), and DMAC (García-Fernández et al., 2017a).

The temperature of coagulation bath is an important parameter which helps to determine the crystallinity and membrane structure of HF membranes. The higher the temperature, the faster the diffusion process of solvent which will in turn affect the pore volume. The lower the temperature, the slower the rate of diffusion which will determine the regularity and uniformity of pore formation (Raharjo et al., 2017). At high external coagulation temperature, the composition path of the fiber tends to cross the gelation region, spinodal and binodal line instantaneously, start liquid-liquid de-mixing, and form poor polymer phase and high connected rich polymer phase. After polymer phase solidification, a high connected fibriform or leaf form network substrate morphology membrane can be formed (Wang et al., 2008). A low external coagulation bath temperature leads to sponge-like structures, whereas fingerlike structures can be formed at high temperature. Li et al. (2017) observed that fiber spun at high temperature (47 °C) result to irregularity of fiber and collapse microvoids as fiber is susceptible to shrinkage due to compression in the spin line guide zone or the outer layer phase separation. Furthermore, mechanical strength of HF decreases dramatically with increase in coagulation temperature.

2.5.1.4 Dope viscosity

The dope viscosity is a diffusional property of the dope which will influence the de-mixing rate of the solvent transport between phases and dope solution (Giwa et al., 2017). This crucial parameter can affect the kinetics of coagulation through its effects on the inter-diffusion between solvent and the nonsolvent (H. Zhang et al.,

2018). Spinning is not possible when the viscosity is below the threshold viscosity (H. Zhang et al., 2018), as the dope is the framework of the HF. Basically, a high viscosity of dope may hinder the growths of finger-like structures and macro-voids. Furthermore, a higher content of solid will lead to higher viscosity, which will reduce membrane porosity as well as promotes chain entanglement (Chang et al., 2008). Also, the addition of nonsolvent additives will increase the dope viscosity, thereby result in reduction in mutual diffusion between non-solvent in the external bath and solvent in the dope (kinetic effect) (Giwa et al., 2017). The solvent dissolves the polymer, producing a single-phase dope that is homogeneous. The solvent choice depends on the properties of the polymer, but solvents with higher boiling point including DMSO, NMP, DMF and DMAc are often desirable because of their miscibility with ethanol or water and strong dissolving power with polymer (Khan et al., 2018).

Numerous works have been reported on the influence of dope viscosity on membrane properties and performance. For instance, Chang et al. (2017) and Zhang et al. (2017) observed an hindrance on the solvent exchange rate which suppresses the formation of macrovoid in spun HF with higher dope viscosity. As the liquid-liquid de-mixing process is suppressed, the semi crystalline polymer tends to undergo the solid-liquid de-mixing, leading to the formation of spherical globules in the HFs. García-fernández et al. (2017) and Jeon et al. (2018) shows that an increase in dope viscosity will result to an increase in skin-layer thickness and diameters. Karkhanechi et al. (2016) observed a decrease in pore size, CA and porosity with increase in dope viscosity. Thong et al. (2018) reported a decrease in permeability

and MWCO with increase in dope viscosity. Jeon et al. (2018) observed an increase in mechanical properties of fibers with increasing dope viscosity.

2.5.1.5 Take-up speed

Take-up speed (TS) is another important parameter which can affect the formation of defect free dual-layer HF membrane in the process of spinning. When the TS is the similar with the free gravitational flow, the elongational stress is zero. In the wet spinning process, the spinning velocity is almost as that of the spinneret exit and there is no elongational stress. A little change in TS will cause a change in tensile stress, which may induce surface defects on HF. However, controlling the TS during wet speed is more important than in the dry-wet spinning process. Li et al. (2017) observed two effects of TS on HF spinning. First, the phase separation time of the HFs in the coagulation bath is decrease. Second, it might help to squeeze out the dope's solvent that speed up the phase separation process (Wang et al., 2004). The high TS, which is caused by gravity (elongation-induced alignment), may shortens the time of phase separation of HF in coagulant leading to buckling in the spin-line guide zone, soft HF and also lead to a more monodisperse interstitial chain spacing between the polymer molecules (Li et al., 2017; Min et al., 2017).

Researchers have shown that when TS is increased, the wall thickness, ID and OD of HF membranes decreases (Li et al., 2017; Thong et al., 2018; Válek et al., 2017; Zuo et al., 2017) as well as an increased the surface area to volume ratio (Sengur et al., 2015). Generally, the rigid elastic shell will have a smaller radius due to the orientation of the polymer molecules as explained by Chou and Yang (2005), who stated that the molecular chains in the HF would be more oriented when the TS

is increased. The free volume between the polymer chains will decrease, which will consequently result in HFs with smaller diameters and greater resistance to buckling. At low TS, the OD of the HF tends to be larger than that of the spinneret probably due to the die swell effect from the pressurized dope solution (Matsuyama et al., 2003). When the fiber wall thickness decreases due to increase in take up speed, this allows water to take a shorter path across the membrane as well as reduces the transport resistance (Thong et al., 2018).

An increment in TS can effectively produce membranes with narrower pore size distribution (PSD) and smaller pore size (Bildyukevich et al., 2017; Zhang et al., 2017). These observations may be due to the better alignment of polymer chains at higher TS (Praveen et al., 2015). When a higher TS is used, the polymer chains within the dope is susceptible to undergo elongation-induced alignment which will lead into a more monodisperse interstitial chain spacing between the polymer molecules (Min et al., 2017). And as result, the selective outer-layer of the HF membranes will encourage the formation of smaller pore sizes. Bildyukevich et al. (2017) observed a lower porosity with increase in TS due to higher external stresses during spinning. Sengur et al. (2015) reported that membranes formed at higher TS tended to demonstrate high tensile strength and stress resistance due to stretching. These tensile stresses can cause micro-pores. HF spun at higher TS have a consistent greater strain values before deformation than HF spun at lower TS. Zhang et al. (2017) and Zulhairun et al. (2014) have shown that an increase in TS results in decrease in surface roughness. A higher TS result in smoother outer surface (nodules become flatten) with less porous defects. In study by Min et al. (2017) and Thong et al. (2018) shows that increase in TS result in the reduction of PWP and MWCO due

to the formation of close-packing structure caused by shear-induced polymer chain orientation (Loh and Wang, 2014).

In industrial scale HF fabrication, a high TS is often employed in order to reduce production cost minimization and maximize productivity. Generally, when TS is increased, the diameter of HF membranes tend to decrease. An increase in TS usually lead to permeation flux reduction because a high TS induces varying precipitation paths as well as facilitates chain packing and orientation owing to elongational and gravitational forces.

2.5.1.6 Bore fluid chemistry

During spinning of HF membrane, the internal surface morphology of HF can be decided suitably by appropriate selection of the bore fluid (BF) from a wide number of materials such as water, ethylene glycol (EG), NMP, TEP, EthOH, IPA, DMAC, dimethylsulfoxide (DMSO), dimethylformamide (DMF), nitrogen, gamma-butyrolactone (GBL), polyvinylpyrrolidone (PVP) and hexane. The proper selection of the bore fluid will affect the rate of phase inversion, and thus prevent fiber from collapsing during dope extrusion. Table 2.4 presents the summary of the various solvents used as bore fluid.

Table 2.4: Various solvents used as bore fluid

Bore fluid	Conditions	Remarks	Ref
NMP	As NMP content increases	Increase oxygen permeation performance. Increase pore size, porosity decrease. Poor mechanical strength, probably due to the closer packing of sponge-like region.	(X. Zhang et al., 2015)
NMP	As NMP content increases	Increase pore size and porosity decrease. Slight decrease in gas permeance and wetting resistance. The inner surface becomes more porous due to the suppression of the solvent-out flux from the polymer solution phase to the coagulant phase.	(Rahbari-sisakht et al., 2012a)
NMP	As NMP content increases	Poor mechanical strength due to closer packing of sponge-like region.	(Li et al., 2017)
NMP	-	Poor mechanical strength.	(Loh and Wang, 2014)
NMP	As NMP increases	Lower pressure tolerance	(Le et al., 2016)
NMP	As NMP increases	Decrease in the number of corrugations. Reduction of CO_2 absorption. Enhancement in mechanical properties.	(Fashandi et al., 2016)
NMP	As NMP increases	High CO_2/N_2 selectivity. Decrease in gas permeance and wetting resistance.	(H. Zhu et al., 2017)
NMP	-	Skinless inner HF surface. High maximum lysozyme binding capacity.	(Lazar et al., 2015)
Glycerol	-	Dense skins with smaller pore size.	(Lazar et al., 2015)
DMAC	As DMAC content increases	Formation of a porous particulate morphology at the lumen-side. Enhancement of mechanical properties. Decrease in thickness of finger-like structure on the lumen side.	(García-Fernández et al., 2017b)

Table 2.4 Continued.

Bore fluid	Conditions	Remarks	Ref
DMAC	As DMAC content increases	Formation of a porous particulate morphology at the lumen-side. Transformation of finger-like to a sponge-like particulate morphology in the inner skin layer. Generate less macrovoids.	(Choi et al., 2010)
DMAC	As DMAC increases	Transformation from double skin to single skin.	(Zhang et al., 2011)
DMAC	As DMAC content increases	Formation of loosed skin on the inner surface. Enhancement of mechanical properties.	(Kumbharkar et al., 2011)
DMAC	As DMAC content increases	Decrease in thickness of finger-like structure on the lumen side. Generate less macrovoids.	(Xu et al., 2008)
DMAC	-	Membrane permeability and CO_2 flux significantly improved.	(Mansourizadeh et al., 2014)
EG	-	Produces fibers with a spongelike layer near the surfaces and finger-like bi-layered structure. Higher water permeance. Disfavors the formation of fingerlike macrovoids and hence decrease fiber porosity. High rejection of ~80% for myoglobin.	(Le and Nunes, 2017)
TEP	As TEP content decreases	Formation of macrovoid-free membrane structure. Improvement in Tensile stress by over 50%.	(J. Chang et al., 2017)
IPA	-	Strong effect on pore distribution on the surface of the HF membranes.	(Alsalhy et al., 2014)
DMSO	-	Elimination of thin spongelike layer at the inner region. Formation of fingerlike micro-channels.	(Lee et al., 2014)
DMF	As DMF decreases	Formation of macrovoids at the inner surface Elimination of macrovoids at the inner surface as DMF increases.	(Simone et al., 2010)
IPA	-	Reduction of macro-voids layer thickness due to delayed de-mixing.	(Bey et al., 2011)

Table 2.4 Continued.

Bore fluid	Conditions	Remarks	Ref
PVP	As PVP content increases	The region between the lumen and sponge membrane matrix with macrovoids becomes larger, causing macrovoids to shift toward the fiber periphery. Increase in hydrophilicity and rejection coefficient. Decrease in PWF.	(Bildyukevich et al., 2017)

Note:

IPA: isopropanol; PG: propylene glycol; TEP: triethyl phosphate; DMAC: dimethylacetamide; PVP: polyvinylpyrrolidone; GBL: gamma-butyrolactone; NMP: N-Methyl-2-pyrrolidone; MetOH: methanol; EtOH: ethanol; DMF: dimethylformamide; EG: ethylene glycol; DMSO: dimethylsulfoxide.

When a strong bore fluid (BF) such as water is employed, a smooth and dense surface tends to be formed, whereas when a weak BF such as DMSO, NMP, DMAC and DMF or their mixtures with water is employed, a relatively rough and porous surface is formed. The presence of an alcohol or a solvent with longer organic chain in the BF will cause a delayed liquid liquid de-mixing and, hence, a reduction or elimination of macrovoids. However, when using strong coagulants (i.e 15% NMP), faster coagulation causes the development of finger-like macrovoids, as evidenced in Figure 9. On the contrary, when using softer coagulants, such as 30% IPA or 45% NMP, macrovoids are replaced by spongy structures. The high water content in the BF would cause early phase separation through the AG and quickly solidify the inner surface of HFM, which would trigger the formation of defective skin layer (H. Zhu et al., 2017). When the content of solvent increases, the flexural rigidity of inner elastic shell decreases and the inner HF became less viscous (Bonyadi et al., 2007).

When NMP is introduced in the BF composition, the porous layer on the lumen side disappears. Consequently, the bulk diffusion path becomes delayed while the two surface exchange reaction steps on the lumen side pores are eliminated (Tan et al., 2011), leading to formation of a more porous skin and suppression of finger-like structure (Darvishmanesh et al., 2011; Naim et al., 2013). The presence of ethylene glycol (EG) with its high viscosity in BF and weak non-solvent property can lead to improve permeability and high porosity. When an immiscible and inert fluid such as hexane is used as BF, two thin-layers of spongelike structures are formed at the outer and inner regions, sandwiching a layer of finger-like voids.

By using a mixture of water and varying proportions of solvents as the BF, rates of de-mixing of dope solution can be adjusted to yield a more porous sub-layer in the HF wall to reduce the total transmembrane resistance and a more open surface structure in the HF inner surface layer (Yan and Lau, 1998). The rate of polymer de-mixing can be related to the difference in polymer and solubility parameter of BF. In this case, the difference can serve as a scale to indicate the coagulation power (CP) of the BF. At low CP, HF with a more open structure in the HF wall and its inner surface could be made which will produce higher flux due to the lower transmembrane resistance in the fiber (Yan and Lau, 1998). Low content of solvent in BF can facilitate the solvent diffusion of the BF into the dope and results in a large ID of the HF. At high content of solvent, the nonsolvent/solvent exchange rate in the HF bore-side is slow and tends to cause the fibers to break easily (Li et al., 2017).

When the bore fluid temperature (BFT) is high, the cooling rate in the inner part of HF tends to be low, which will allow more time for spherulites to form and

grow which will result in higher porosity and mean pore size (Cui et al., 2013). However, a lower BF temperature will cause slower demixing rate between the solvent and polymer. For instance, Abdullah et al. (2016) studied the effect of BFT on mechanical properties of membrane and found that the mechanical strength significantly increased when BFT was increased from 10 to 50 °C. This is different from report by Cui et al. (2013) who observed a decrease in mechanical properties with increase in porosity, MPS, and water permeability when the BFT is increased. Tang et al. (2012) observed that the increase in BFT (45–75 °C) results in HF with larger outer and inner diameter as well as smaller thickness. This was ascribed due to the increase in vapor pressure of BF as the temperature is raised, which is supposed to expand the HF lumen dimension. Additionally, the rise in BFT result in the enlargement of average pore size and decreasing porosity, which led to a maximum membrane distillation flux at 55–65 °C.

2.5.1.7 Air gap

The air gap (AG) distance determines the time the fiber is exposed to air during spinning process (Clausi and Koros, 2000). A higher AG means a longer RT of HF in air which tends to promotes the formation of a thicker skin-layer. However, the AG is decided by many factors, including DR and dope elasticity. Moreover, a larger AG may also generate defects due to elongational and gravitational stress (Khan et al., 2018). HF spun with longer AG have tighter molecular packing and greater molecular orientation. This effect is less stronger at the inner surface and stronger at the outer surface. Generally, in the process of wet spinning, the die swell is expected to cause instantaneous coagulation when in contact with external

coagulant and the orientation induced within the spinneret may be rapidly frozen into the solidified outer skin of the wet spun HF (Hamid et al., 2011). This will result in HF with the largest diameter when spun at zero AG as compared to those fabricated by dry-wet spinning process. A medium stress may induce molecular orientation and reduce the free volume or porosity of membrane whereas a high elongational stress may pull phase-separated domains or molecular chains apart in the early stage of phase inversion and create porosity.

Also at high AG distance, wall thickness, ID and OD diameter of fibers tends to decrease (Ahmad et al., 2017; Raharjo et al., 2017). This can be related to the die swell effect of polymer macromolecules when extruding from the spinneret due to the dope's visco-elastic properties (Khayet, 2003) and elongation stretch on HF caused by gravity while travelling through the air–gap (Korminouri et al., 2015). If the surroundings are humid air, the situation becomes more complicated. Firstly, the external surface gets in contact with air and then passes through a humid-induced phase inversion process and the condensed moisture changes the surface tension. Consequently, the elongational stress may induce orientation and reduce the porosity of membrane at the selective or inner skin, and pulls apart the molecular chains at the outer humid-induced phase inversion or loose-skin at the early stage of phase inversion and creates free volume (Chung et al., 1999).

During dry-wet spinning process, the nascent fiber tends to experience a convective internal coagulation in the lumen and a non-convective external coagulation in the AG region. Then, rapid solvent exchange at external surface in

non-solvent coagulation batch; in the AG region, the moisture-induced phase separation much slower than in coagulation batch slowed the speed of polymer chain contracting and provided a needed time to contracting polymer chains for conformation rearrangement (Chung and Hu, 1997).

2.5.1.8 Spinneret design and travelling distance

The spinneret is a device used to extrude a dope solution to form nascent HFs (Norman et al., 2009). The streams of viscous polymer exit out from the spinneret into air or liquid leading to a phase separation which allows the solidification of the polymer. The individual polymer chains tend to align in the fiber because of viscous flow (Cao et al., 2004). The design of spinneret and the flow angle in the spinneret is also important in spinning process. For instance, when a spinning solution exit from the spinneret, it undergoes some external stress which tend to affects its macromolecular chain packing and orientation. Spinneret concentricity is critical for the fabrication of sandwich-structured HF. Generally, spinneret dimensions differs depending on the requirement and goals of the specific HF formation. Basically, a spinneret with smaller dimension will produce smaller HFs that can withstand high pressure during application. Peng and Chung (2008) studied the influence of varying the dimension of spinneret. They found that HF spun from a small spinneret dimension possesses a higher degree of chain packing and a thicker outer-skin portion. Moreover, spinneret with thinner flow channel tends to induce a higher shear stress under similar condition of spinning. They came up with the conclusion that; (a) upon increase in spinneret dimension, a higher elongation draw ratio (DR) was required to produce defect-free HF membranes with thinner the dense-selective

layer; (b) the bigger the spinneret dimension, the higher the permeance and selectivity. Fu et al. (2015) modified a 3 capillary needle to produce an ultra-thin outer and middle layers, in order to solve the morphological problems of fibers such as uneven layers, inconsistency in fiber thickness, irregularity in membrane shape, delamination and middle-layer discontinuous. In their study, spinnerets with a tight accuracy control were fabricated in the press-fit mode which can reach a concentricity as low as 5 μm and obtained regular round-shape fibers. Generally, without proper alignment, the resultant HF membranes would result into different kinds of defects in the outer, middle and inner layers irrespective of the spinneret designs and dimensions.

2.5.1.9 Travelling distance and external coagulation bath depth

Among other spinning parameters, the travelling parameter and coagulation bath depth is another important parameter as it is the distance covered by the nascent fiber in external coagulation bath when extruded out of the spinneret. The coagulation bath depth determines the residence time (RT) of nascent HFs as it passes through the external coagulation medium. A deeper external coagulation bath will help to form the porous structure and skin layer of HFs as the fibers have longer RT in the external coagulation bath. The external coagulation bath medium, the height, and the temperature must be carefully adjusted to allow a complete phase inversion so that HFs are not squeezed by guide-roll to form an oval structure (Khan et al., 2018). For instance, Li et al. (2017) have shown that a sufficiently long distance of external bath is necessary for HF to solidify and resist fiber deformation. As travelling distance of HF in the water bath was reduced to 1.5 m, an oval-shaped cross-section was produced.

2.6 Roles of Operating Conditions on Membrane Fouling

Fouling mechanisms can be associated to the feed stream conditions, membrane properties and operating conditions. During membrane performance, mitigating fouling can be achieved by altering the operating conditions. By altering the operating conditions including feed concentration, transmembrane pressure and feed flowrate will result to different membrane fouling profile which will significantly affect membrane performance.

2.6.1 Transmembrane Pressure (TMP)

Transmembrane pressure (TMP) is one of the driven force during the application of membrane in pressure driven membrane processes. Arnot et al. (2000) reported that different pore blocking mechanisms can be promoted by change in TMP. At fixed feed flow rate, an increase in TMP tends to enhance the rate of fouling due to a high force applied on the foulants, allowing its partial penetration in the pores of the membrane. Generally, this phenomenon is true for particles such as oil emulsion that can be sequenced easily out of the membrane pores at high operating pressure. Chakrabarty et al. (2010) shows that membrane operated at high operating pressure tends to indirectly lead to poor selectivity. This is because at higher pressure, the small droplet size of oil is permeated through the pore structure of the membrane. A lower pressure will promote the formation of loosed cake layer that will result to lowering the rate of flux decline. At a higher pressure which is above the critical TMP, the exerted force will lead to the compression and thickening of the cake layer, and as a consequence result to flux reduction (Zhu et al., 2016).

Rezaei et al. (2011) reported that the rate of fouling is dependent upon the applied TMP. In their study, a higher rate of flux decline was observed under high operating pressure. Basically, membrane operated at pressure (above optimum pressure) will result to aggregation and denaturation of foulant which is induced by compaction and compression which forms the gel layer and as a result will cause severe flux decline.

2.6.2 Feed Flowrate

By increasing the feed flow rate, the irreversible fouling of membrane can be reduced. An increase in feed flow rate will increase the mass transfer coefficient and thus decrease the concentration polarization (mass boundary layer). In comparison to operating pressure, the effect of feed flow rate on the reduction of flux is inconspicuous, most especially as the separation process commences. The deposition of foulant on the surface of membrane during cross-flow process is made up of two phenomena such as foulant deposition transported with flux as well as removal of foulant from membrane surface via cross-flow shear. Rezaei et al. (2011) stated that the two competitive phenomena tends to be at equilibrium when the flux attains the pseudo steady state.

In a study by Chakrabarty et al. (2010), the flow rate was observed to have a significant influence on permeate flux in respective of the membrane type. The concentration polarization and oil deposition build-up on the surface of membrane was observed to have reduced at higher feed flow rate, which induced a higher shear rate and turbulence near the surface of membrane. The permeate flux decreased from

223.0 to 77.0 L/m^2 h when the feed flowrate decreases at a constant TMP of 1.724 bar. This was ascribed due to the decrease in total resistance at higher flowrate, which prevented the formation of thicker cake layer. In another study by Alpatova et al. (2014) also shows that an increase in feed flowrate will reduce the turbidity of permeated water and suspended particles. This was similar to the observation by Zuo and Wang (2013) who showed that under high flow rate, the occurrence of fouling is minimal as a result of high shear rate, causing the oil on the membrane surface to be easily flushed away. In another study by Tanudjaja et al. (2017), the critical flux was observed to increase with increase in feed flow rate which was as a result of pore plugging mitigation at lower concentration of oil. Furthermore, oil droplets on the surface of the membrane was observed to disappear at high flowrate because of increase in shear stress on membrane surface.

2.6.3 Feed Concentration

The concentration of the feed is another important parameter during membrane separation processes (Das et al., 2009). Pal et al. (2008) reported that membrane performance could be highly influenced by the concentration of the feed. They observed reduction of permeate flux of ~60% with increase in solute concentration from 0.1 % – 0.4 % at constant feed flowrate and TMP. This was ascribed due to the existence of more solute at higher concentration, which influenced the surface deposition of the solute on the membrane surface.

Das et al. (2009) also observed the concentration polarization near the surface of the membrane tends to increase at high concentration of feed. By decreasing feed

concentration from 400 mg/L to 100 mg/L, the initial permeate flux at 1min was observed to increase by ~43%. However, the final permeate at 30 min was ~53% higher for lower feed concentration (100 mg/L) as compared to higher feed concentration (400 mg/L). This reason was explained due to the effect of lowered CP near the surface of the membrane. This is similar to observation made by Chakrabarty et al. (2008) who reported the formation of thicker oil layer on the surface of membrane at higher feed concentration, and as such resulted to flux reduction.

2.7 Membrane Fouling and Its Mechanisms

Numerous studies had demonstrated that oil emulsion is a major foulant in membrane application that resulted in performance deterioration, increase of membrane replacement costs and higher energy consumption (Tanudjaja et al., 2017; Tummons et al., 2016; X. Zhu et al., 2017). Chen et al. (2009) reported that rapid flux decline was observed at the initial stage of oil separation process due to the oil droplets adsorption and deposition. The deposited oil droplets (cake layer formation) had exerted higher membrane resistance resulting in dramatically flux reduction. Similar observation was reported by Zhu et al. (2017) who found that the initial membrane fouling by emulsified oil drops is dominated by cake layer formation based on their experimental results and theoretical calculation. They also reported that in the later stage, the oil droplet starts to wet the membrane surface and forming gel layer once the critical pressure drop was achieved thus leads to irreversible membrane fouling. These reported fouling behaviors were quantified based on the indirect evidence through the measured values of permeation flux and rejection efficiency.

The oil droplet and its behavior at the membrane surface was monitored using real-time visualization to provide better understanding of membrane fouling during oil emulsion separation (Tanudjaja et al., 2017; Tummons et al., 2016). For instance, Tummons et al. (2016) conducted a direct observation on MF membrane fouling by oil emulsion in the presence of crossflow. In their study, they observed that membrane fouling by oil emulsion at the membrane surface can be categorized into three characteristic stages; first stage is the oil droplet attachment and clustering followed by oil droplet deforming and lastly is the oil droplet coalescence.

Apart from practical experiments, numerical and theoretical models were also investigated for better understanding and prediction of membrane fouling during oil emulsion separation. For example, Mohammadi et al. (2005) had developed a mathematical model to predict the flux reduction in UF process for oil emulsion separation. In their works, they found out that the initial flux reduction was due to pore blocking followed by cake layer formation on the membrane surface. In addition, concentration polarization in crossflow ultrafiltration of oil emulsion was also investigated by Asadi Tashvigh et al. (2015) using computational fluid dynamics modelling. It was reported that the thickness of the concentration polarization (CP) layer grew with a sharp rate from the entrance of the feed solution to about 40 % of the membrane's length. However, the CP layer growth rate showed approximately constant after 40 % of membrane's length. The growth rate estimation was important in designing the optimum module length. The growth rate of the CP layer was further predicted at different operating condition such as effect of oil droplet size, oil concentration as well as crossflow velocity. It was reported that the experimental data trend observed show good agreement with the CP model predictions.

Therefore, membrane fouling in oil emulsion separation was mainly caused by CP, cake layer formation as well as gel layer mechanisms with the condition that membrane pore size is smaller than oil droplet size. In contrast, membrane with larger pore is susceptible to pore blocking or adsorption of oil droplet inside the membrane pore walls which exerted higher difficulties in membrane cleaning process. In recent years, many investigations on fouling mechanism have been carried out to explain the permeation flux reduction over time during membrane separation process (Saleem et al., 2017; Vincent Vela et al., 2009). Therefore, it is crucial to understand the underlying fundamental of membrane fouling mechanisms to have a precise prediction of the membrane maximum volumetric capacity ($Vmax$) (Zydney and Ho, 2002).

2.7.1 Classical Filtration Models

Membrane fouling mechanisms can be determined through blocking filtration law. Hermia's model is the most common model use to identify and understand the membrane fouling mechanisms. Hermia demonstrated a blocking model for explaining various blocking behaviour in UF process. The blocking models is defined as:

$$\frac{dJ}{dt} = -K(J - J_{ss})J^{2-n} \tag{2.2}$$

where t refers to filtration time, J_{ss} refers to steady state permeation flux, J refers to permeate volume collected per unit of membrane area, K and n is the blocking

models function, which refer to the resistance coefficient and blocking index, respectively (Hermia, 1982).

The blocking models can be divided into four types of membrane fouling mechanisms namely cake filtration (n=0), intermediate blocking (n=1), standard blocking (n=1.5) as well as complete blocking (n=2) which are categorized based on different blockage phenomenon (Vincent Vela et al., 2009). The foulant size and shape in relation to the membrane mean pore size were analyzed to identify the fouling mechanisms. All the fouling mechanisms contribute to the reduction in permeate flow are illustrated in Figure 2.11.

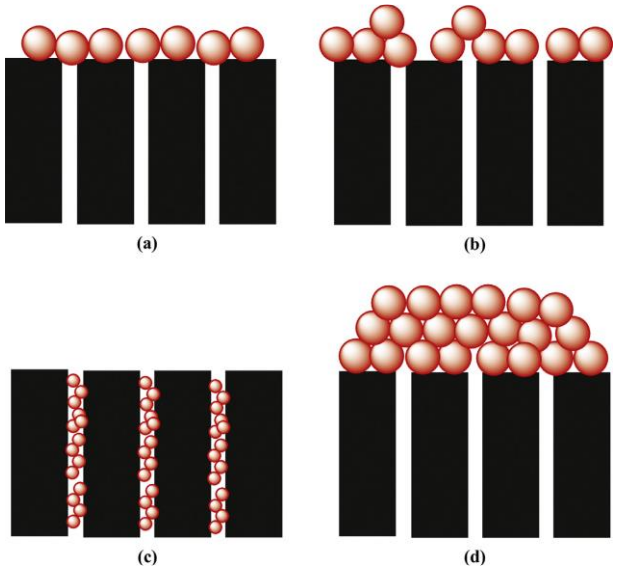

Figure 2.11: Illustration of the membrane fouling mechanisms: (a) complete pore blocking, (b) intermediate pore blocking, (c) standard pore blocking, (d) cake filtration/formation (Ng et al., 2014) .

The blocking models for fouling mechanisms identification was further developed by Bolton et al. (2006) based on the Darcy's law for constants TMP operation as defined as:

$$Q = \frac{PA}{R_m \mu} \tag{2.3}$$

where Q refer to the flowrate, A refer to the membrane area, P refer to the transmembrane pressure, μ refer to solution viscosity and Rm refer to the resistance of the membrane. These four membrane fouling mechanisms relate the amount of permeated volume collected through specific membrane area as a function of time as shown in Table 2.5. Kc, Ki, Ks, and Kb are the pore blocking coefficients, J represents the accumulated permeate volume through specific membrane dimension (m^3/m^2), Jo refer to the initial flux (m^3/m^2s), and t represents the time (s) (Bolton et al., 2006).

Table 2.5: Summary of the classical filtration models at constant pressure (Bolton et al., 2006).

Fouling mechanism	N	Equations	Pore blocking coefficients
Cake filtration	0	$J = J_o/\sqrt{1 + (2K_c{J_o}^2 t)}$	K_c (s/m^2)
Intermediate blocking	1	$J = J_o/(1 + K_i J_o t)$	K_i (m^{-1})
Standard blocking	1.5	$J = J_o/(1 + \frac{K_s {J_o}^{\frac{1}{2}}}{2}\ t)^2$	K_s (m^{-1})
Complete blocking	2	$J = J_o \exp(-K_b t)$	K_b (s^{-1})

2.8 Gap in knowledge

It has been shown in literatures that the surface modification of PES membranes is indispensable to alleviate fouling in membrane. The incorporation of hydrophilic modifiers does not only enhance membrane resistance to fouling, but also improved permeability. Basically, an increasing in the concentration of organic polymer (pore former) will negatively influence mechanical properties and result in producing membrane with bigger pore structure. This will consequently affect oil rejection as well as membrane resistance towards fouling. Furthermore, various authors have reported that the concentration of organic additives tends to decrease during specific applications. Recent advances in nanotechnology have greatly expanded the avenues of membrane modification by introducing NPs in the fabrication of various types of nanocomposite membranes in improving their synergistic effects on wastewater treatment and water purification (Kim and Van der Bruggen, 2010).

Among the different inorganic particles, SiO_2 emerged as a highly promising candidate as hydrophilic additive due to its outstanding physical and chemical characteristics, and has been a subject of intensive research from both practical application and fundamental research perspective (Nandanwar et al., 2015). Furthermore, SiO_2 composite membrane have shown to have more negative charge on selective top layer giving them the ability to prevent oil adsorption on the surface of membrane. Generally, two approaches are often used to incorporate SiO_2 into the membrane matrix: (1) the NPs is introduced in the dope solution, followed by phase inversion (Razmjou et al., 2011); (2) SiO_2 are coated on already prepared membrane

surface via chemical bonding (Basri et al., 2012). However, agglomeration (due to poor mixing and stability of colloids) is a troublesome problem during physical blending as it aggravates phase separation between polymer and SiO_2, as a consequence affects their dispersion and distribution in membrane matrix which is worse in HF membrane. Furthermore, the agglomerated particles in most cases could settle in dope tank prior to spinning causing spinneret nozzle plugging.

Stöber reaction based on sol gel synthesis method for preparing mono-dispersed spherical SiO_2 particles with sizes covering almost the whole colloidal range has been a favorable method in the recent. There is no doubt of its benefits to improve particle dispersion and polymer filler contact due to molecular level mixing of precursor. From previous literatures, a rather low concentration of nano SiO_2 ($\leq$1 wt.%) were reportedly doped in the dope solution (Jullok et al., 2016; Lin et al., 2016; Ngang et al., 2017), still with challenges of high surface roughness and mean particle size (particle size <100 nm). However, even at lower ratio of monodispersed silica, it still remains a great challenge to produce a HF membrane with low surface roughness without sacrificing its performance properties. Therefore, for feasible application, it is crucial to obtain ultrafine and stable nano-dispersions for the production of highly functional HF membranes with low surface roughness and high mechanical properties, even with a much higher concentration of nanosilica (>1 wt.%). Thus, by combining both hydrophilic, good particle distribution and mechanical properties of the composite membrane, it is expected that the production of composite HF membrane is feasible for oil-in-water separation.

3-aminopropyltriethoxysilane (APTES) are widely used aminosilane for surface functionalization as it contains amino groups which is hydrophilic. Their application to modify SiO_2 synthesis for HF composite membrane has not be studied. The presence of APTES to modify SiO_2 is thought to establish covalent bonding and compatibility between polymer and silica dispersed phase. NH_2 group from APTES can enhance membrane homogeneity, thermal stability and flexibility due to compatibility with OH groups. Thus, the incorporation of APTES functionalized SiO_2 can help to produce membrane with well distributed particles, low surface roughness, higher mechanical properties and permeability with low fouling effects.

The preparation parameters for PES membrane fabricated by variety of modification strategy, methods and conventional techniques were also well documented in literatures. Nevertheless, there has been no great deal of study that focuses on the simultaneous control of HF membrane preparation and spinning conditions in order to reach a high performance ultrafiltration (UF) of synthetic oil in water emulsion. In addition, almost all the previously published works have adopted the conventional methods, that involves the variation of the major parameter studied while the other parameters are maintained constant. However, such methods have dis-advantages (such as much time consuming experimental runs while ignoring the interacting effects between the variables, which often times result to low process optimization efficiencies) which could be avoided with RSM which has successfully been introduced in some similar works by Fouladitajar et al. (2015) and Ghandashtani et al. (2015). RSM is a statistical behaviour-prediction process that involves the responses to a limited amount of experimental runs which are designed by factors varying over a wide range (Boshrouyeh et al., 2015). RSM is able to

represent a comprehensive and valid model for the optimization of effective parameters to reach a high level efficiency of an applied process (Javadi et al., 2014). Thus, the optimization and preparation of hollow fiber membranes from the selected materials formulation and spinning condition is very crucial in the development of such types of membranes with enhance performance.

CHAPTER THREE

METHODOLOGY

This chapter highlights the materials, chemicals and equipment applied in this research work. The overall experimental flowchart, experimental methods and procedures are also highlighted. The properties of chemicals and materials used are provided at the beginning of this chapter followed by the flowchart of the overall experimental work. Subsequently, the detailed fabrication, characterizations and performance of PES/APTES-SiO_2 composite HF membranes are outlined. The last part ends with the effect of operating conditions on membrane performance.

3.1 Chemicals and materials

The chemicals and reagents used in this research for membrane fabrication, characterization and performance test are presented in Table 3.1.

Table 3.1: List of chemicals and materials.

Reagent/Chemical	Grade/ Purity	Density (g/cm^3)	Boiling point (°C)	Supplier	Purpose
Polyethersulfone Ultrason E6020P	-	1.37	-	BASF	Polymer
Dimethylacetamide (DMAc)	99.5%	0.94	165	Merck, Malaysia	Solvent
Glycerol	99%	1.26	290	Merck, Malaysia	Membrane preservative
Ethanol	99%	0.789	78.37	Merck, Malaysia	Module preservative, Solvent for silica synthesis
Tween 80	-	1.07	>100	Sigma Aldrich (USA)	Surfactant for model solution
Crude oil	-		-	Petronas, Malaysia	Model foulant
Tetraethyl orthosilicate (TEOS)	≥99.99%	0.94	169	Merck, Malaysia	Precursor for silica synthesis

Table 3.1 Continued.

Reagent/Chemical	Grade/ Purity	Density (g/cm^3)	Boiling point (°C)	Supplier	Purpose
3-aminopropyltriethoxysilane (APTES)	98 %	0.946	217	Sigma Aldrich (USA)	Silane for SiO_2 surface modification
NH_4OH		0.88	24.7	Merck, Malaysia	Catalyst
Tungstophosphoric acid hydrate		0.96	-	Merck, Malaysia	As staining agent for TEM imaging
PEG 4000Da	99.5%	1.125	>250	Sigma Aldrich (USA)	MWCO measurement
PEG 10000Da	99.5%	1.125	>250	Sigma Aldrich (USA)	MWCO measurement, pore former additive
PEG 20000Da	99.5%	1.125	>250	Sigma Aldrich (USA)	MWCO measurement
PEG 35000Da	99.5%	1.125	>250	Sigma Aldrich (USA)	MWCO measurement
Nitrogen gas	-	0.0012504	-195.8	Wellgas, Malaysia	To compress dope solution
Liquid nitrogen	-	0.807	-195.8	Wellgas, Malaysia	Fracturing of membrane

3.2 Flowchart of the Overall Experimental Works

The overall experiments carried out in the study are summarized in Figure 3.1.

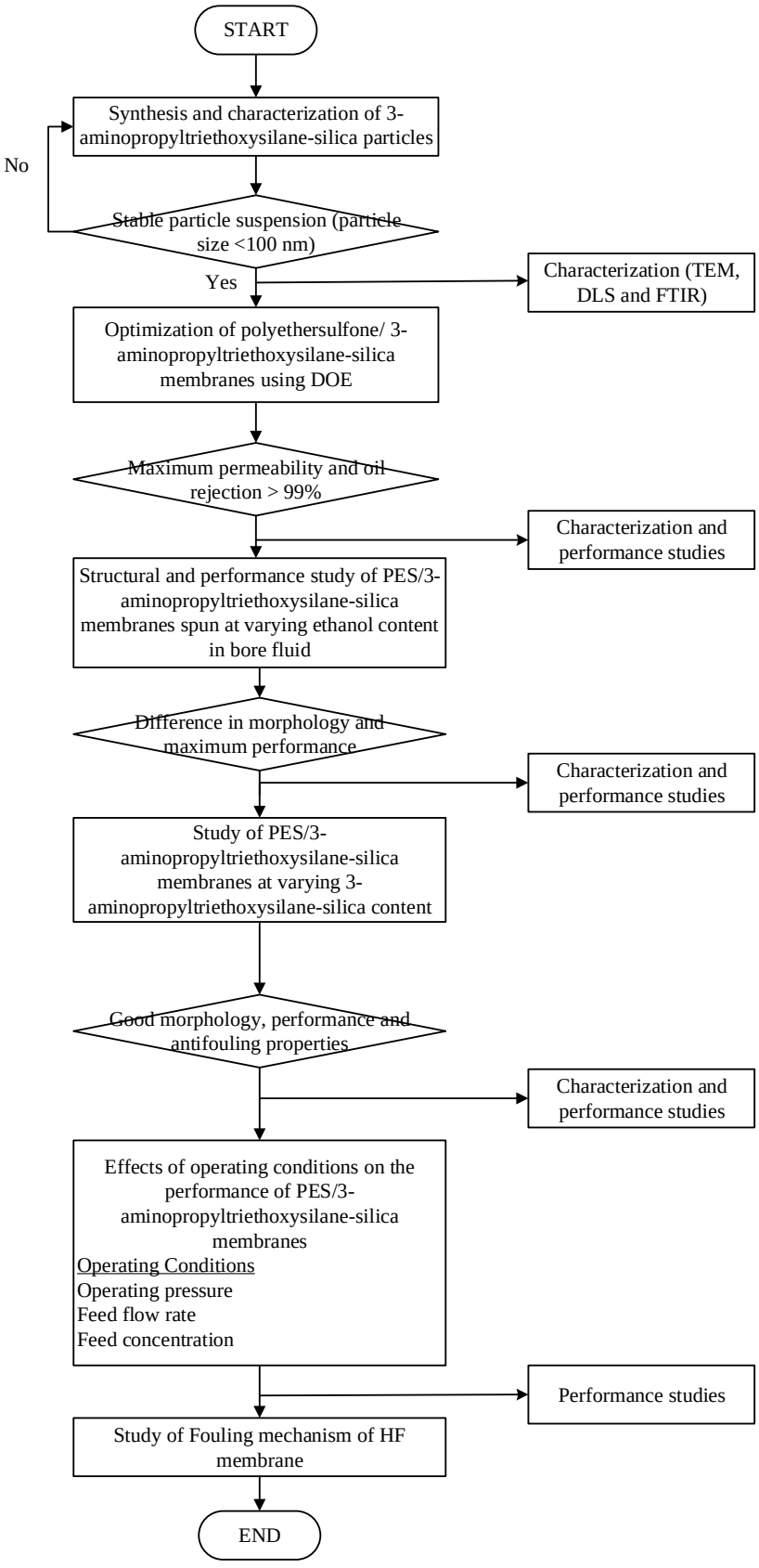

Figure 3.1: Flowchart of the preparation, characterization and performance of PES/APTES-SiO_2 composite hollow fiber membrane.

3.3 Synthesis of PES/APTES-SiO_2 composite HF membrane

This section discusses the synthesis of APTES modified SiO_2 particles and PES/APTES-SiO_2 composite HF membrane. It also describes the process of membrane optimization and statistical analysis.

3.3.1 Synthesis of APTES modified SiO_2 particles

The 3-aminopropyltriethoxysilane (APTES) modified SiO_2 (APTES-SiO_2) particles were prepared according to a APTES one pot reaction modification (He et al., 2010). In this method, APTES containing $–NH_2$ groups was added and reacted with the Si-OH groups on the surface of the silica by hydrolysis to produce SiO_2 particles with $–NH_2$ functionalized surface. In detail, a mixture of 12 mL of NH_4OH, 22 mL of deionized water (DI) and 200 mL of ethanol was added into 500 mL glass flask and then subjected to heating at a stirring speed of 300 rpm and a temperature of 30 ºC. 12 mL of TEOS was added drop-wise into the mixture and continuously stirred for 24 h. Subsequently, 3 mL of APTES solution containing a mixture of 1.5 mL of ethanol and 1.5 mL of APTES was introduced into the mixture at 0.2 mL/min. The reaction was continued with vigorous stirring for another 24 h. The SiO_2-APTES suspension was then heated up to 75 ºC for 2 h to enable covalent bonding (Hua and Helmut, 2015). Thereafter, four cycles of centrifugation (Heraeus Mega-fuge 40 Centrifuge) was carried out at a force of 10,000 x g for 15 min and re-suspended in ethanol to remove the unreacted APTES residuals. This is followed by re-dispersed in deionized (DI) water under sonication (Model 8510, Branson). Lastly, the APTES-SiO_2 particles were re-dispersed in DMAc under two cycles of centrifugation at a force of 10,000 x g for 15 min, in order to fully exchange the existing DI water with

the DMAc solvent. The SiO_2-APTES particles suspension was keep in desiccator prior to use to avoid moisture from being trapped.

The gravimetric method was carried out by drying 25 ml particle suspension in predetermined DMAc in the transparent glass petri dish. Prior to this process, a transparent petri dish was heated up to 105 ºC using hotplate stirrer for 10 minutes in order to remove the moisture content. The petri dish was later transferred to the desiccator to prevent moisture absorption as well as to cool down. Immediately, the weight of the void petri dish (wgt_1) was recorded. After measurement, the APTES-SiO_2 particles suspension was placed in the petri dish and heated up to 180 ºC (which is above boiling point of DMAc) for 2 h. The petri dish was later transferred again to desiccator and the weight (wgt_2) was also recorded. These procedures were severally repeated until the constant weight was realized. The concentration of APTES-SiO_2 particles (P_c) in grams was determined using below equation:

$$P_c = \frac{wgt_2 - wgt_1}{Vl} \tag{3.1}$$

where wgt_2 is the weight of the petri dish containing dried particles (gram), wgt_1 is the weight of dried petri dish without particles (gram) and Vl is the volume of particles suspension added for measurement (ml). The total particle concentration (P_c) was given to be 0.01624 mg/ml (Appendix A1).

3.3.2 Optimization of PES/APTES-SiO_2 HF membrane using design of expert (DOE)

Based on literatures and preliminary works, four independent variables were chosen. The influence of these four independent variables (obtained by selecting three preparation conditions and one spinning parameter) on membrane performance was analysed using design of experiments (DOE). The independent variables includes PES, PEG, APTES-SiO_2, and coagulation bath temperature (CBT). 30 sets of experiments were designed according to response surface methodology (RSM) based on central composite design (CCD) to prepare the PES/PEG/APTES-SiO_2 HF membrane using NIPS. RSM is a combination of experimental strategy, mathematical and statistical methods to investigate the influence of considered controllable factors on response variables. The RSM was a full factorial design. The CCD consisted of 5 levels, including 6 central points, 16 factorial points and 8 axial points. Level selection of independent variables were made based on preliminary experiments and observations. The experiments were constructed for the inspection of the cross products, quadratic and linearity of the preparation variables. The levels and range of preparation (independent) variables that were investigated can be found in Table 3.2. Each of the variables used at 5 levels are coded as +α, –α, 0, -1, and +1. Every variables at zero level belongs to the centre points whereas the combinations of each individual variables at +α level or -α level with other variables at zero level belongs to axial points. The midpoint for each factor was repeated six times to estimate the experimental error. The value of α depends on variables number (m), where m = 4, $\alpha = \sqrt{m} = 2$.

Table 3.2: Actual and coded values of variables

Variable	Codes	Units	Levels				
			–α	-1	0	+1	+α
PES	A	wt.%	15	15.75	16.5	17.25	18
APTES-SiO_2	B	wt.%	0	1.25	2.5	3.75	5
PEG	C	wt.%	0	1.25	2.5	3.75	5
CBT	D	° C	0	15	30	45	60

3.3.3 Statistical Analysis

Analysis of variance (ANOVA) and regression analysis were carried out using the Design-Expert software version 7.0.0 (Stat-Ease, Inc., Minneapolis). Responses including PWF, OPF, and OR were analyzed via response surface methodology with the quadratic equation. Regression method that is applied for the model can be deemed useful when one or more experimental factors are quantitative (Mendonza et al., 2006). Regression analysis was performed to describe the obtained response, where an actual response was based on the functional relationship between one or more input variable and the predicted response. The regression model of 4 factor factorial experiment can be written as:

$$y = \beta_0 + \beta_1 X_1 + \beta_2 X_2 + \beta_3 X_3 + \beta_4 X_4 + \beta_{11} X_1^2 + \beta_{22} X_2^2 + \beta_{33} X_3^2 + \beta_{44} X_4^2 + \beta_{12} X_1 X_2 + \beta_{13} X_1 X_3 + \beta_{14} X_1 X_4 + \beta_{23} X_2 X_3 + \beta_{24} X_2 X_4 + \beta_{34} X_3 X_4 \quad (3.2)$$

where y signifies the response, the βs are parameters whose values will be determined later, X_4 denotes factor D, X_3 denotes factor C, X_2 denotes factor B, X_1 denotes factor A, X_2X_4, X_1X_2, X_2X_3, X_3X_4, X_1X_3 and X_1X_4 denotes the interacting effect between the variables. Since there are 4 manipulated variables used in this

study, it is easier to make use of the 2nd order terms instead of 3rd order terms to develop the regression model.

The last step in RSM study was to determine the optimum membrane that will produce membranes with highest PWF, OPF, and OR with the optimization conditions. Finally, the actual responses were compared with the predicted responses to determine the experimental error which can be calculated using the following equation:

$$Experimental\ error\ (\%) = \frac{AcV - PdV}{AcV} * 100 \quad (3.3)$$

where AcV is the actual value and PdV is the predicted value.

3.3.4 Preparation of PES/APTES modified SiO_2 membrane

Membranes were synthesized from different PES dope solutions. PES pellets were oven dried for 3 h at 75 °C prior to use so as to remove moisture. A pre-determined amount of PEG and PES were dispersed in DMAc for 30 min using ultrasonic (Appendix A2). Subsequently, pre-determined amount of APTES-SiO_2 particles was added to the PES/PEG solution. The pre-determined amount of materials used were determined according to the experimental designs as presented in Table 3.2. The mixture was stirred continuously for 15 h at 60 °C until it attains a

clear homogenous mix. The solution was left in ultrasonic bath for 3 h for de-aeration. The bubble free dope was later transferred into a dope tank.

The HF membranes were fabricated using the dry-wet spinning process and the process parameters are presented in Table 3.3. The produced membranes were kept in water for 48 h while the water was concurrently changed in order to fully eliminate the left over solvent. Subsequently, membranes were placed in a 50:50 solution of glycerol and water for a day in order to prevent the collapse of porous membrane and then dried at room temperature.

Table 3.3: Spinning conditions for the preparation of PES HF membranes

Spinning parameters	**Values**
Bore fluid flow rate (ml/min)	1.8
External coagulant	H_2O
Spinneret external diameter (cm)	0.1
Air gap (cm)	25.5
Take up speed (cm/s)	30
Spinneret internal diameter (cm)	0.05
Bore fluid	Water
Draw ratio	1.25
Dope speed (cm/s)	24
Room temperature (°C)	21-22
Relative humidity (%)	62-68

3.4 Structural and performance study of PES/APTES-SiO_2 HF membrane using varying content ethanol as bore fluid

As previously mentioned, HF membranes were fabricated using the dry wet spinning process. In this session, the composition of the bore fluid will be varied while the other parameters will be kept constant. For commercial production of HF membrane, one of the most important issues is to produce HF membrane with fully circular internal perimeter to prevent the reduction of mechanical strength of fiber. Bore fluid composition is one important parameter that can affect the morphology and performance of the produced HF membrane. There is a strong relation between the bore fluid composition on fiber formation. In this study, the bore liquid compositions were varied as shown in Table 3.4 while other spinning parameters were left constant throughout the whole fabrication processes.

Table 3.4: Membrane samples according to bore fluid composition

Membrane	Ethanol (wt.%)	Water (wt.%)
E1-3.6	100	0
E2-3.6	75	25
E3-3.6	50	50
E4-3.6	25	75
E5-3.6	0	100

3.5 Study of PES/APTES-SiO_2 HF membrane at different APTES-SiO_2 concentration

Different concentration of APTES-SiO_2 including 0 wt.%, 1.2 wt.%, 2.5 wt.%, 3.6 wt.%, and 5 wt.% were added to 17.25 wt.% of PES concentration with

pre-determined amount of DMAc at 60 ºC under continuous stirring speed of 550 rpm for a duration of 14 h (Table 3.5).

Table 3.5: Preparation parameters for PES membranes at different APTES-SiO_2 concentration

Membrane	PES (wt.%)	PEG (wt.%)	APTES-SiO_2 (wt.%)	DMAc (wt.%)	Bore fluid	
					Ethanol (%)	Water (%)
E0`	17.25	3.72	0	79.03	0	100
E4-0	17.25	3.72	0	79.03	25	75
E4-1.2	17.25	3.72	1.2	77.83	25	75
E4-2.5	17.25	3.72	2.5	76.53	25	75
E4-3.6	17.25	3.72	3.6	75.43	25	75
E4-5	17.25	3.72	5	74.03	25	75

3.6 Characterization of APTES-SiO_2 particles

This section gives the characterization process of synthesized APTES-SiO_2 particles to reveal its particle size, morphology and functional groups.

3.6.1 Transmission electron microscope (TEM)

Transmission electron microscope (TEM), equipped with DOCO v3.2 image was used to inspect the shape and core size of APTES-SiO_2 particles. For TEM, 0.1 g/L APTES-SiO_2 suspension was added to ethanol solution for fast drying process, and subsequently kept for suspension after sonication. Precipitation was allowed to take place and a drop of the upper layer solution was pipetted out and dropped on a 3 mm diameter, 400-mesh copper grid. The droplet was allowed to dry at room temperature and then viewed under varying magnification.

3.6.2 Fourier transform infrared (FTIR)

Fourier transform infrared (FTIR) spectra of SiO_2 and APTES-SiO_2 particles were obtained to investigate the possible functional groups and chemical bonding which appeared on the particle surface. FTIR spectroscopy (Nicolet Nexus 670, US), equipped with OMNI-sample attenuated reflection (ATR) smart accessory and coupled to a diamond crystal operated at incidence angle of 45°. Each spectrum recorded at an average of 32 scans with a resolution of 4 cm^{-1} was collected over a number range of 4000 – 500 cm^{-1}.

3.6.3 Zeta potential and Dynamic light scattering (DLS)

The suspension stability was evaluated based on the zeta potential and particle size distribution (apparent hydrodynamic size) of APTES-SiO_2 particles using Malvern Zetasizer Nano ZS90 coupled with a He-Ne laser (at a wavelength of 633 nm). The Dh measurement of APTES-SiO_2 particles were performed using disposable sizing cuvette at 25 °C. About 10 mg/L (low concentration to avoid interaction of particles and multiple scattering) of APTES-SiO_2 suspension was used for DLS measurement. The shape of all APTES-SiO_2 particles were assumed to be spherical.

3.7 Characterization of PES/APTES-SiO_2 HF membranes

This section presents the physical and chemical analysis of the hollow fiber membranes.

3.7.1 Rheological property of dope solution

Rheological properties of the prepared dope solution was analyzed by viscosity measurement with the aid of the Brookfielf digital Rheometer (Model DV-III, USA) at 25 °C and under a shear-rate of 10 s^{-1}. Thereafter, the average of five samples together with standard error were reported.

3.7.2 Field emission scanning electron microscopy

Prior to SEM analysis, the membrane pieces were thoroughly rinsed with distilled water, transferred to a glycerol/water (50/50) solution and then dried at room temperature. For the SEM morphological cross-sections analysis, the membrane samples were fractured via immersion in liquid nitrogen. In the case of the membrane surface, the samples were cut into small piece and affix horizontally on a double-sided adhesive foil which serves as the membrane sample holder. Before SEM imaging, sputter coating (Quorum – SC7620) was applied on the surface and cross sectional area of the samples to prevent from electrostatic discharge. Membrane cross-section and surfaces were observed via the Supra TM 35vp Zesis and HITACHI Table-top microscopy instrument (TM-3000, Japan).

3.7.3 Mechanical properties

To investigate the influence of adding different ratio of silica sol on the mechanical property of PES HF membranes, break strain (%), maximum strain (%) and maximum stress (MPa) of HF membranes were determined with the Instron 3366 (USA) at room temperature, with a load cell of 10 kN. Prior to the

measurement, membrane sample were cut into 10 cm (relative humidity of 67%, temperature of 25 °C), vertically attached to two clamps and stretched in tension with a strain rate of 5 mm/min. Their response were documented until failure. For each membrane, the average of five times measurements were determined for accuracy.

3.7.4 Contact angle measurement

The water contact angle (WCA) was used to determine the surface hydrophilicity using a goniometer (Rame-Hart 250-F1, USA). The membranes were placed horizontally on a glass slide using double sided tape. Prior to water droplet, the HF membrane was flattened with the aid of a microscopic slide. A water droplet (0.2 µL) is placed on the dried membrane surface at room temperature. In order to reduce experimental error, five readings were taken at different locations on the membrane surface and their average WCA value were calculated. The change in WCA with time was also obtained with the aid of the stopwatch.

3.7.5 Thermo gravimetric analysis

Thermo gravimetric analysis (TGA) were used to evaluate the heat stability and degradation of membranes with TGA 7 Analyzer (Perkin Elmer, USA). Aluminium open pans were used as sample holders. A membrane sample were placed on a pan by means of a plastic syringe in order to keep the sample mass and shape as uniform as possible. The sample mass weighing approximately 5 to 7 mg was used. Degradation temperatures were determined by heating the HF membrane sample under air atmosphere at a heating rate of 20 °C/min from 30 to 850 °C. Heating was stopped when the temperature reached 850 °C and the profile of

significant weight loss was observed. The APTES-SiO_2 concentration on membrane surface was estimated from the residual weight.

3.7.6 Atomic force microscopy

The atomic force microscopy (AFM) images were obtained using Park System (Park Scientific-XE100, Korea). The measurement was carried out at atmospheric pressure and the membranes were dried at room temperature prior to surface analysis. In detail, small size of prepared membranes (1 cm^2) were glued on glass substrate and imaged in a scan size of 20 µm x 20 µm, using a non-contact cantilever (Item no: 610-1081, Item: SSS-NCH 10M). The surface roughness was expressed in term of the mean roughness (R_a).

3.7.7 Porosity

Membrane porosity can be defined as volume occupied by water, which can be calculated using the following equation:

$$\boldsymbol{\varepsilon} = \frac{\frac{w-d}{\rho w}}{\frac{w-d}{\rho w}+\frac{d}{\rho p}} \text{x } 100 \qquad (3.4)$$

where $\boldsymbol{\varepsilon}$ is porosity of membrane (%), d is the weight of the membrane after drying (g), w is weight of wet membrane (g), ρp is the density of polymer (PES) at 1.37 g/cm^{-3}, and ρw is the density of H_2O at 998 kg/m^3. For the preparation the wet membranes, seven hollow fibers having a length of 15 cm were kept in isopropanol

for 72 h and finally in deionized H_2O for 72 h. Prior to weighing the membranes, the left over water on the surface of individual membrane were removed via airflow. In order to determine the weight of dry membranes, wet HFs were oven dried at 50 °C for 10 h. In order to avoid experimental error, five measurements were recorded and the average value of individual membrane porosity value were taken.

3.7.8 Pore size distribution

The mean pore size (MPS) and the pore size distributions (PSD) of the HF membranes were determined using from solute transport information. The concentrations of the solute (PEG) were obtained using total organic carbon (TOC) analyzer (TOC-VCPH total organic carbon analyzer-SHIMADZU). The Stokes radii (Sr) of solute was calculated using the below equation:

$$Sr = 16.73 \times 10^{-12} \times MW^{0.557} \quad (3.5)$$

where Sr is the stokes radius of solute and MW is the molecular weight of solute (g/mol). Solute rejection can then be expressed as log-normal probability function according to solute size (Michaels, 1980), as illustrated below:

$$R = erf(y) = \frac{1}{\sqrt{2\pi}} \int_{-\infty}^{y} e^{-u^2/2} du, \quad \text{where } y = \frac{InS_d - In\mu_d}{In\sigma_d} \quad (3.6)$$

where R, μ_d, S_d, σ_d are PEG rejection in %, geometric mean diameter of PEG at R = 50%, PEG diameter, geometric standard deviation about μ_d (the ratio of S_d at rejection = 84.13% and 50%), respectively.

PEG Rejection at different MWs, including 35000 Da, 20000 Da, 10000 Da, 4000 Da and 1500 Da were plotted against the Einstein-Stokes diameters of PEG on a scale of lognormal probability. Thereafter, the results were fitted on a linear line using the below equation:

$$F(R) = y + m\,(In\,S_d) \tag{3.7}$$

where m is slope and y is the intercept. By ignoring the hydro-dynamic effect and steric interactions effect between PEG and pore, the effective mean pore size (μ_p) and the geometric standard deviation (σ_p) can be assumed the same value as (μ_d) and (σ_d) (Michaels, 1980; Yang et al., 2007). With respect to μ_p and σ_p, the PSD (d_p) can be expressed using probability density function as shown below:

$$\frac{dR\,(d_p)}{dd_p} = \frac{1}{d_p In\sigma_p\sqrt{2\pi}} exp\left[-\frac{(Ind_p - In\,\mu_p)^2}{2(In\sigma_p)^2}\right] \tag{3.8}$$

Using the values of μ_p and σ_p for HFs, the probability density function and the cumulative PSD curves can be realized.

3.7.9 Fourier transform infrared (FTIR)

The chemical composition of all HF membranes were characterized using FTIR spectroscopy (FTIR Nicolet Nexus 670, USA) over a wave number range of 4000 - 500 cm^{-1}. The procedure was similar to the method as described in section 3.4.3.

3.7.10 Energy Dispersion X-Ray Spectroscopy

The existence of APTES-SiO_2 on the membrane surface was accessed by FESEM equipped with EDX spectroscopy (EDAX Inc., USA).

3.8 Preparation and Characterization of synthetic oil-in-water emulsion

This section describes the preparation and characterization of synthetic oil in water emulsion.

3.8.1 Preparation of synthetic oil-in-water emulsion

Crude oil (with no purification) was used to prepare the synthetic oil-in-water emulsion. In brief, the oil-in-water emulsion was prepared by dissolving pre-determined amount of crude oil and Tween 80 (as a stabilizer) in 1 L of distilled water under continuous stirring condition. The solution was dispersed for 5 min with a blender (Khind BL-1515, 300 W) at room temperature (Chakrabarty et al., 2010). In order to remove any trapped air bubbles during dispersion, the resulting solution was sonicated for 5 min. The pre-determined amount of crude oil and surfactant at constant ratio were added to the distilled water to produce different concentrations of oil-in-water emulsion as tabulated in Table 3.6.

Table 3.6: Composition of oil emulsion used in this experimental work

Oil concentration (mg/L)	Crude oil (mL)	Tween 80 (mL)	DI water (mL)
10	0.014	0.003	999.983
20	0.028	0.006	999.966
50	0.070	0.015	999.915
100	0.140	0.030	999.830
250	0.350	0.075	999.575
500	0.700	0.150	999.150

Note: Crude Oil density = 0.71429 g/cm^3.

3.8.2 Preparation of Calibration Curve

The content of oil in feed was determined using UV-visible spectrophotometer (Pharo 300) in order to enable the construction of calibration curve to obtain absorbance with oil emulsion concentration (Chakrabarty et al., 2010). Based on the absorbance spectrum in Appendix B1, wavelength of 225 nm was chosen due to the maximum light absorbance for the oil emulsion. The preparation of oil emulsion concentrations ranging from 0 to 100 mg/L follows a similar procedure as presented in section 3.6.1. Calibration curve of absorbance versus oil concentration was constructed and displayed in Appendix B1.2 and B1.3.

3.8.3 Particle Size Distribution of Oil Emulsion

The intensity based hydro-dynamic diameter (Dh) distribution of synthetic oil-in-water emulsion was determined using the Malvern Zeta-sizer Nano ZS90 (Malvern Instruments Ltd., U.K) (Ong et al., 2015; Sadeghi et al., 2013). The synthetic oil-in-water emulsion was observed stable with constant size over the duration of experiment (please refer to Appendix B3 for the oil emulsion stability over 4 h duration).

3.9 Performance evaluation of PES/APTES-SiO_2 composite HF membrane

This section describes the membrane filtration setup, module fabrication and the performance of HF membranes.

3.9.1 Permeation System

The HF membrane permeability and separation performance of the prepared HF membranes were measured using crossflow permeation setup, as shown in Appendix C. The filtration rig consists of crossflow cell, pressure gauge, control valve, peristatic pump, and feed tank. The systematic diagram of the crossflow filtration rig is shown in Figure 3.2. All experiments were performed at 22 ± 1 ºC.

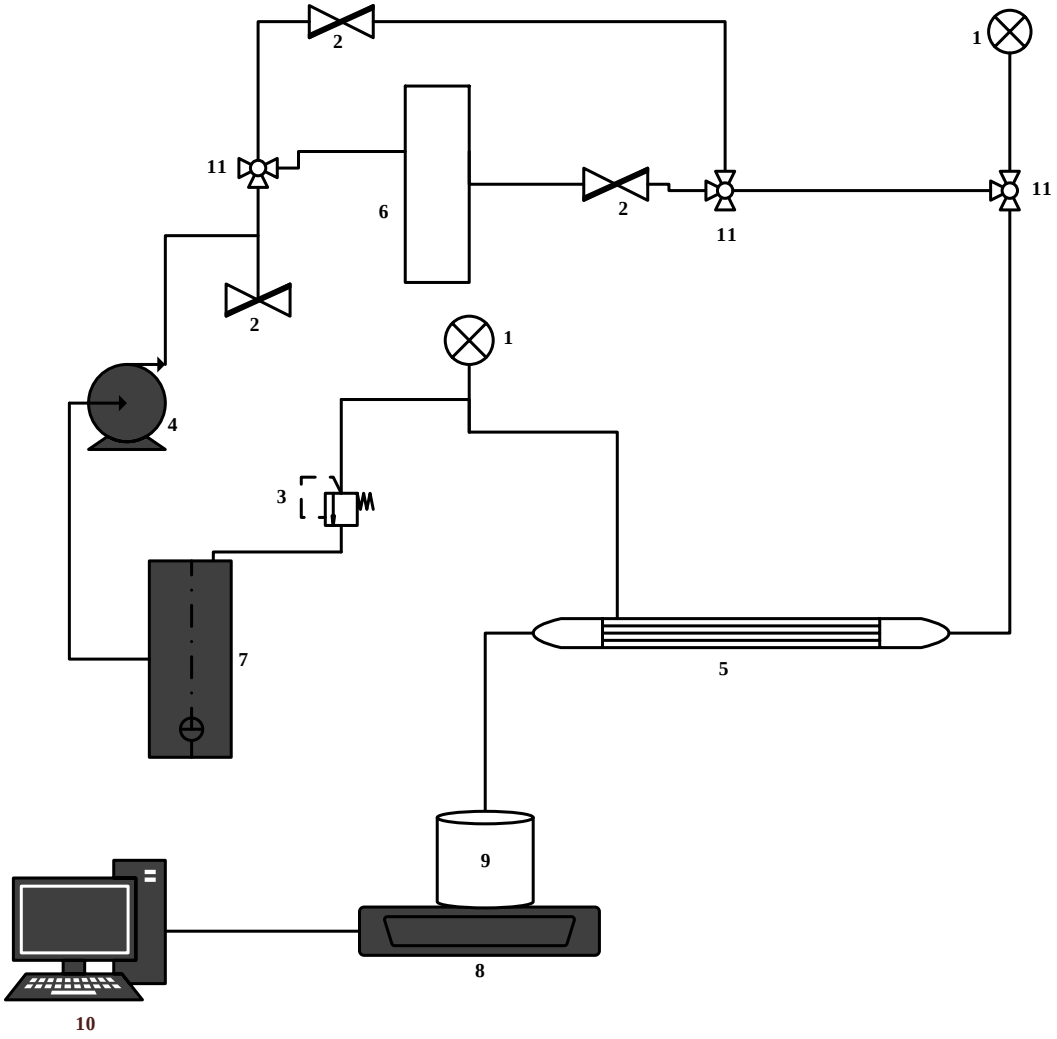

Figure 3.2: Systematic diagram of the cross-flow membrane filtration test rig: (1) UNIJIN pressure gauge, (2) control valve, (3) pressure relief, (4) COLE-PARMER peristatic pump (, (5) hollow fiber cross-flow, (6) flat sheet cross-flow, (7) feed tank, (8) A&D digital balance (FX-3000i), (9) permeate container, (10) computer, and (11) three way valve.

3.9.2 Ultrafiltration test for synthetic oil-in-water emulsion separation

Each module consists of 0.95 cm metal tube and two swagelok stainless steel male runtees. Eight HFs with an effective membrane length of 45 cm were then loaded into the module and sealed with epoxy at both ends of the male runtees (the preparation detail can be found in Appendix D). It is important to note that the effective membrane areas of all membranes vary due to difference in fibers' effective

diameters. However, the membrane effective area of the optimum membrane is presented in Appendix F. The prepared module were soaked in ethanol for at least 3 h and then kept in distilled water for 2 days. It is noteworthy to mention that the effective membrane area varies base on the outer diameter of spun fibers. Furthermore, the average of three experiments were conducted for all membranes.

Membrane compression test were carried out for all membranes with distilled water at 2.25 bar for 1 h. All experiments were carried out at temperature, TMP, stirring speed, filtration time and flow rate of 22 °C, 1.5 bar, 350 rpm, 3 h and 0.45 L/min, respectively. The pure water flux (PWF) measurement were performed using de-ionized water and are determined using the below equation:

$$J_{wf1} = \frac{\upsilon}{A * \Delta t} \tag{3.9}$$

where J_{wf1} is the initial PWF (kg/m^2 h), υ refers to the permeate volume of water (kg), A is effective area of membrane (m^2) and Δt is time (h). After the PWF experimental run, the pure water (PW) feed was switched with the synthetic oil-in-water emulsion. The oil permeate flux in kg/m^2 h for oil/water emulsion was also measured using Eq. (3.9) and is denoted as J_s. The content of oil in permeate (C_{pmt}) and feed (C_{fd}) were determined using UV-visible spectrophotometer (UV mini-1240, Shimadzu). The oil rejection of all membranes was determined using the following equation:

$$Rejection\ (\%) = \left(1 - \frac{C_{pmt}}{C_{fd}}\right) X\ 100 \tag{3.10}$$

3.9.3 Membrane fouling test

After 3 h of ultrafiltration test of oil-in-water emulsion, back-washing was carried out in the same cross-flow mode using fresh distilled water for 45 min. A new pure water flux was calculated using equation 3.10 and denoted as J_{wf2}. This was to examine whether the flux can be recovered as much as possible using the physical cleaning process. In order to calculate the anti-fouling property and the membrane cleaning efficiency, the flux recovery ratio (FRR) and the relative flux reduction (RFR) were calculated based on the following equations:

$$FRR = \left(\frac{J_{wf2}}{J_{wf1}}\right) X100 \tag{3.11}$$

$$RFR = \left(1 - \frac{J_s}{J_{wf1}}\right) X100 \tag{3.12}$$

where J_{wf2} is pure water flux after back-washing with de-ionized H_2O (kg/m^2 h) and J_{wf1} is initial pure water flux (kg/m^2 h), RFR is the relative flux reduction, J_s is oil permeate flux (kg/m^2 h) and J_{wf1} is initial pure water flux (kg/m^2 h). The higher the FRR and lower the RFR, the better the anti-fouling ability.

Fouling resistance of all HFs were estimated using the following equations:

$$Rt = \left(\frac{J_{wf1} - Js}{J_{wf1}}\right) X100 \quad (3.13)$$

$$Rr = \left(\frac{J_{wf2} - Js}{J_{wf1}}\right) X100 \quad (3.14)$$

$$Rir = \left(\frac{J_{wf1} - J_{wf2}}{J_{wf1}}\right) X100 \quad (3.15)$$

where Rr, Rt, Rir and are reversible resistance, total resistance and irreversible resistance, respectively.

3.10 Effect of operating conditions on membrane performance

PES/APTES-SiO_2 composite HF membrane was further assessed at different operating condition namely feed flowrate, operating pressure and feed concentration. Furthermore, their antifouling ability were also evaluated as well.

3.10.1 Effect of operating pressure

Separation of synthetic produced water was carried out at three different operating pressure including 1.0 bar, 1.5 bar and 2.0 bar with feed flowrate and feed concentration were fixed at 0.45 L/min and 250 mg/L, respectively. The membrane was subjected to compression at 2.25 bar prior to every filtration experiments.

3.10.2 Effect of feed flowrate

Oil in water emulsion concentration (250 mg/L) and operating pressure of 1.5 bar were fixed to study the role of feed flowrate. The composite membrane was

evaluated at three different feed flowrates varied as 0.15 L/min, 0.45 L/min and 0.75 L/min. The membrane was subjected to compression at 2.25 bar prior to every filtration experiment.

3.10.3 Effect of feed concentration

Three different synthetic produced water concentrations namely 100 mg/L, 250 mg/L, and 500 mg/L were prepared to evaluate the effect of feed concentration. The operating pressure and feed flowrate were maintained at 1.5 bar and 0.45 L/min, respectively. The membrane was subjected to compression at 2.25 bar prior to every filtration experiment.

CHAPTER FOUR

RESULTS AND DISCUSSSION

The main goal of this present research is the development of PES/APTES-SiO_2 composite membrane with high mechanical properties, high performance and stability for synthetic oil in water separation. This chapter discusses the results of the current research in respect to the objectives as stated in Section 1.4. It has been well documented that the development of a high performance HF membrane depends on the manipulation of several factors including polymer content, additive content and as well as the hollow fiber spinning conditions. The chapter begins with the characterization of APTES modified silica particles followed by structural and performance study of PES/APTES-SiO_2 HF membrane at varying bore liquid composition were performed. Subsequently, the effect of APTES-SiO_2 on membrane morphology and performance were evaluated. It also presents the performance evaluation of the HF membrane at different operating conditions towards synthetic oil in water emulsion separation.

4.1 Characterization of APTES-SiO_2 particles

This section described the characterization of synthesized APTES-SiO_2 particles.

4.1.1 TEM and DLS of APTES-SiO_2 Particles

The particle size distribution of APTES-SiO_2 which was determined using DLS is presented in Figure 4.1. The mean diameter (Md) of APTES-SiO_2 particle was calculated as 92.55 ± 5.48 nm with poly-dispersity index (PdI) value of 0.0035.

In order to determine the micro-structure of the particle, APTES-SiO_2 particles were further inspected using TEM (Figure 4.2 and Figure 4.3), which showed that particles have well-defined size with nearly perfect spherical shape.

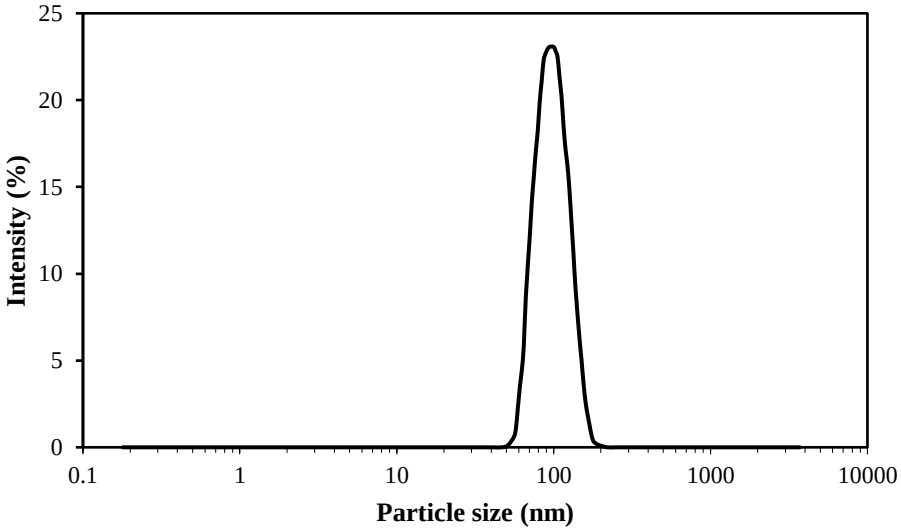

Figure 4.1: Hydro-dynamic size distributions of APTES-SiO_2 particles using DLS measurement.

Table 4.1 presents the size of particles obtained from DLS and TEM analysis. As seen, the mean particle diameter for the APTES-SiO_2 particles was 92.55 ± 5.48 nm and 88.20 ± 4.32 nm for DLS and TEM analysis, respectively. The values were slightly different from each other. For instance, the mean particle diameter for DLS analysis was slightly bigger than the value obtained for TEM, which can be as a result of inclusion of the hydration layer in the prediction using DLS (Chernyshev et al., 2015; Fissan et al., 2014). Furthermore, upon dispersion in deionized (DI) water, APTES-SiO_2 particles showed a high negative surface charge with zeta potential (ζ) of -42.6 ± 0.796 mV, showing that a stable particle suspension was obtained as a

result of the strong electro-static force of repulsion which prevented APTES-SiO_2 particles from agglomerating.

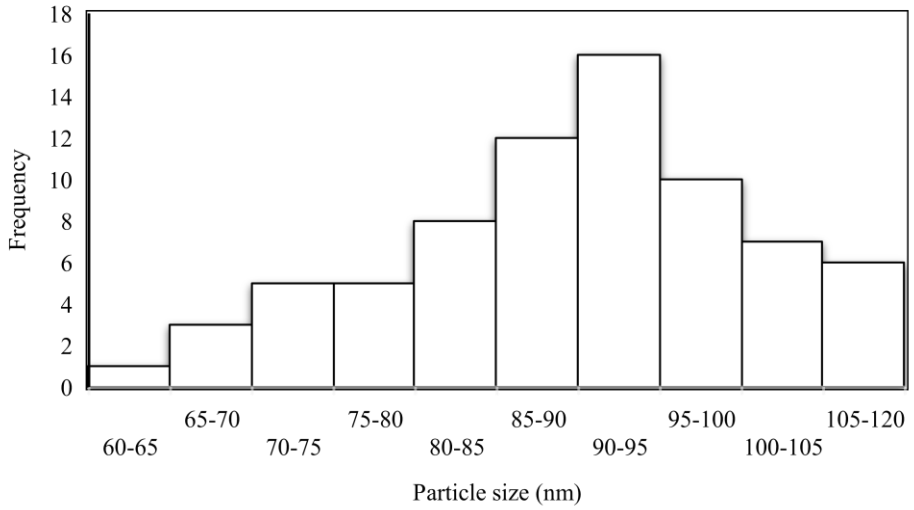

Figure 4.2: TEM frequency of particle size for APTES-SiO_2 particles.

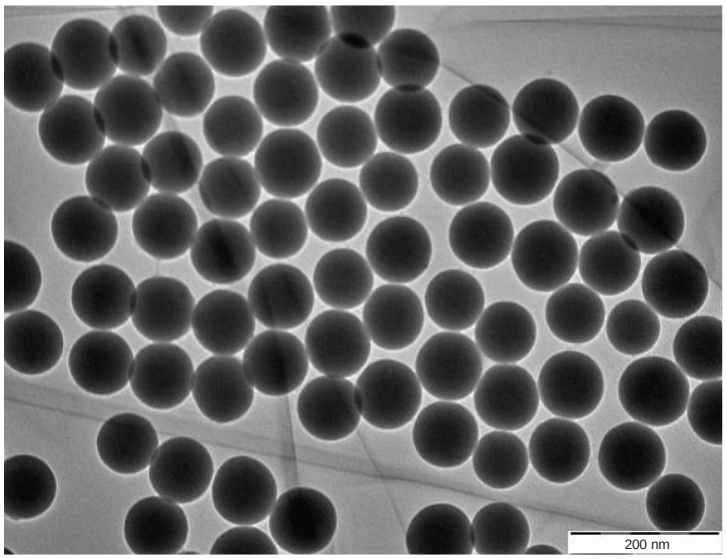

Figure 4.3: TEM image for APTES-SiO_2 particles.

Table 4.1: Summary of the sizing results from DLS and TEM analysis.

	APTES-SiO_2		
	Mean diameter (nm)	Standard deviation (nm)	PdI
DLS Analysis	92.55	5.48	0.0035
TEM Analysis	88.20	4.32	0.0024

$$\text{Standard deviation} = \sqrt{PdI} \times mean\ diameter \quad (4.1)$$

$$\text{PdI} = \left(\frac{Standard\ deviation}{Mean\ deviation}\right)^2 \quad (4.2)$$

PdI for DLS analysis is auto generated by DLS.

4.1.2 Absorption spectra of APTES-SiO_2 particles

Figure 4.4 shows the FTIR spectra of the SiO_2 and APTES-SiO_2 particles. The characteristic peaks at 1064 cm^{-1} and 801 cm^{-1} corresponds to the symmetric stretching and asymmetrical stretching of Si-O groups in SiO_2 particles (Yakun et al., 2007). The three adsorption peaks at 698 cm^{-1}, 1590 cm^{-1} and 1640 cm^{-1} corresponds N-H bending of terminal primary amine group (Miao et al., 2016). The two small shoulder peaks at 3344 cm^{-1} and 3266 cm^{-1} corresponds to the N-H asymmetric stretching of the terminal primary amine H-bonds, indicating a possible interaction of NH_2 toward PES surface (Aneja et al., 2015; Wang et al., 2013).

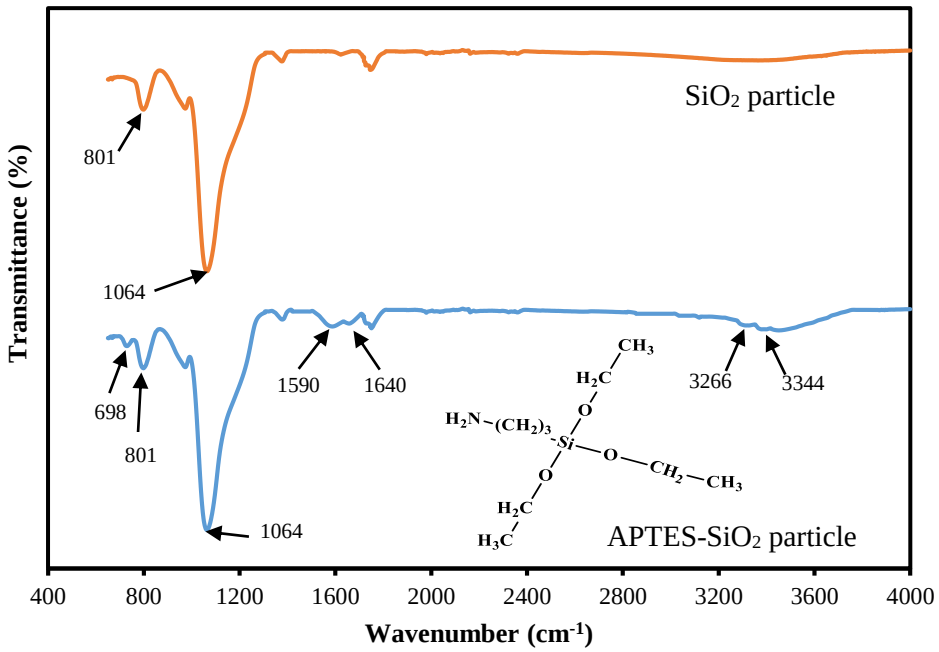

Figure 4.4: The FTIR spectra of SiO_2 and APTES-SiO_2 particles.

4.2 Optimization of PES/APTES-SiO_2 HF membrane using design of experiment

It has been generally accepted that the kinetic and thermo-dynamic properties of the dope solution vary based on the composition and contents of dope solution. In the case where different additives are embedded into the dope solution, the solution tends to be more complex as it does not only alter the kinetic and thermo-dynamic properties, but also the compatibility and dispersion rate. Design of experiment (DOE) using response surface methodology (RSM) was applied to investigate the major parameters in the synthesis of PES/APTES-SiO_2 HF membrane. The major aims includes (i) formulating the preparation parameters for enhanced performance, (ii) to study the interaction between chosen parameters such as PES (A) in wt.%, APTES-SiO_2 (B) in wt.%, PEG (C) in wt.%, and coagulation bath temperature, D (CBT) in ºC. Table 4.2 presents the parameters, experiments and their responses. As

observed, pure water flux ranges between 13.18 kg/m^{2}h (Run 14) to 539.72 kg/m^{2}h (Run 19), oil permeate flux range from 11.43 kg/m^{2}h (Run 14) to 230.4 kg/m^{2}h (Run 7) while oil rejection range between 89.5% (Run 17) to 99.6% (Run 24). Experimental error was observed using the responses from the centre points (run no. 2, 8 – 10, 15 and 16).

Table 4.2: The experimental conditions and the responses using central composite design

Std	Run	Type	PES (wt.%)	APTES-SiO_2 (wt.%)	PEG (wt.%)	CBT (^{o} C)	PWF (kg/m^2 h)	OPF (kg/m^2 h)	OR (%)
17	1	Axial	15	2.5	2.5	30	346	165.6	95.77
29	2	Center	16.5	2.5	2.5	30	184	124.8	95.2
23	3	Axial	16.5	2.5	2.5	0	153.05	122.4	99.45
7	4	Fact	15.75	3.75	3.75	15	308	158.4	96.23
24	5	Axial	16.5	2.5	2.5	60	209.05	160.29	97.7
20	6	Axial	16.5	5.0	2.5	30	161.72	150.21	92.98
15	7	Fact	15.75	3.75	3.75	45	248	230.4	95.77
27	8	Center	16.5	2.5	2.5	30	171.4	150.48	94
26	9	Center	16.5	2.5	2.5	30	100	89.6	94.5
28	10	Center	16.5	2.5	2.5	30	124	100.8	96.08
8	11	Fact	17.25	3.75	3.75	15	200	95.04	99.48
1	12	Fact	15.75	1.25	1.25	15	150	86.4	96.16
13	13	Fact	15.75	1.25	3.75	45	360	223.2	96.5
21	14	Axial	16.5	2.5	0	30	13.19	11.43	97.63
25	15	Center	16.5	2.5	2.5	30	184	126.72	96.08
30	16	Center	16.5	2.5	2.5	30	186	128.16	96.5
19	17	Axial	16.5	0	2.5	30	250	172.8	89.5
18	18	Axial	18	2.5	2.5	30	40	31.88	98.25
22	19	Axial	16.5	2.5	5.0	30	539.72	208.8	95.15
14	20	Fact	17.25	1.25	3.75	45	47	42	95.77
12	21	Fact	17.25	3.75	1.25	45	34.28	29	95.15
2	22	Fact	17.25	1.25	1.25	15	23	20.05	97
10	23	Fact	17.25	1.25	1.25	45	45.83	39.404	97.32
11	24	Fact	15.75	3.75	1.25	45	75	65.4	99.6
6	25	Fact	17.25	1.25	3.75	15	295	201.6	95.05
9	26	Fact	15.75	1.25	1.25	45	240	144	98.7
3	27	Fact	15.75	3.75	1.25	15	85.71	79.2	99.3
16	28	Fact	17.25	3.75	3.75	45	295.55	165.6	98.87

Table 4.2 Continued.

Std	Run	Type	PES (wt.%)	APTES-SiO_2 (wt.%)	PEG (wt.%)	CBT (° C)	PWF (kg/m^2 h)	OPF (kg/m^2 h)	OR (%)
4	29	Fact	17.25	3.75	1.25	15	26	22	95.77
5	30	Fact	15.75	1.25	3.75	15	320	175.68	94.53

The 1st and the 2nd order model were used to fit the actual results, which are presented in Table 4.3. Furthermore, the R^2 of responses, actual and coded significant terms of parameters ate also presented in the table. As seen from the Table 4.3, the R^2 square of all models were slightly lower (although > 0.7) which could be associated due to other varied condition in the membrane synthesis which cannot be controlled like bore fluid temperature. As a result, the temperature of the bore fluids was not constant in each membrane preparation. Thus, these variations is thought to affect the performances of the membranes. Studies by Alobaidy et al. (2017) have shown that by varying the temperature of internal coagulation bath with affect membrane pore size will as a result affects membrane performance. The details of all analysis of variance (ANOVA) for individual responses are presented in Appendix E1-3. The insignificant model parameters such as (parameter B) in Appendix E1, (A, C and D) in Appendix E3 was not removed so as to maintain model's hierarchy. The p-value for every used models were observed significant (p-value is less than 0.05), while an insignificant value (p is greater than 0.05) was observed for the lack of fit. For PWF, the parameter that show significant influence include PEG (parameter C), PES (parameter A) and interacting effect of APTES-SiO_2 and PES (parameter B*A). For oil permeate flux, the parameters that shows significant influence are PES (parameter A) and PEG (parameter C). The system behaviour was explained in which the regression model in terms of coded factors for pure water flux, oil permeate flux and oil rejection is as follows:

$$PWF = 2691.70 - 162.61 * PES - 560.95 * APTES - SiO_2 + 81.56 * PEG + 33.22 * PES * APTES - SiO_2 \quad (4.3)$$

$$OPF = 764.75 - 45.30 * PES + 40.04 * PEG \quad (4.4)$$

$$OPF = 423.33 - 37.22 * PES + 3.25 * APTES - SiO_2 - 17.93 * PEG - 0.261 * CBT + 0.98 * PES * PEG + 1.06 * (PES)^2 - 0.54 * (APTES - SiO_2)^2 + 0.28 * (PEG)^2 + 0.00438 * (CBT)^2 \quad (4.5)$$

Table 4.3: ANOVA results of three response

Resp.	R^2	Sign. Terms (actual)	Sign Terms (coded)
PWF	0.7915	PES, PEG, PES * APTES-SiO_2	A, C, A * B
OPF	0.7284	PES, PEG	A, C
OR	0.7119	APTES-SiO_2, (PES*PEG), $(PES)^2$, $(APTES\text{-}SiO_2)^2$, $(CBT)^2$	B, A*C, A^2, B^2, D^2

For oil rejection, Factor B (APTES-SiO_2) displayed a 1st order effect on OR. The parameters that show a quadratic effect on OR includes PES (A), APTES-SiO_2 (B) and CBT (D). Furthermore, the interaction of PES with PEG (A*C) also presents significant model term. Although in all three responses, CBT show insignificant effects in the first order term in all three responses but its quadratic effect show significant effect on OR response. The predicted values were compared with the actual (experimental) values for all responses and are presented in Figure 4.5 to 4.7. As observed, the actual values of all responses were satisfactory fitted using equations 4.3 to 4.5.

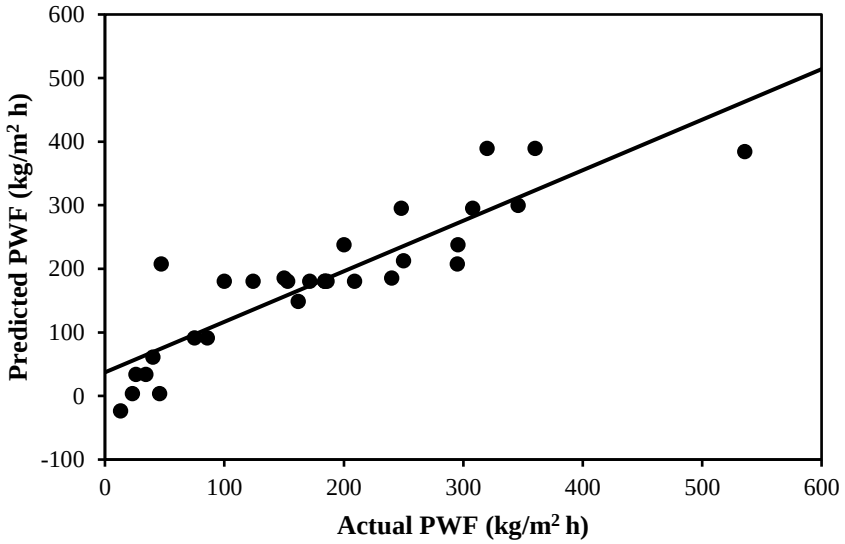

Figure 4.5: Predicted vs actual (experimental) values of pure water flux.

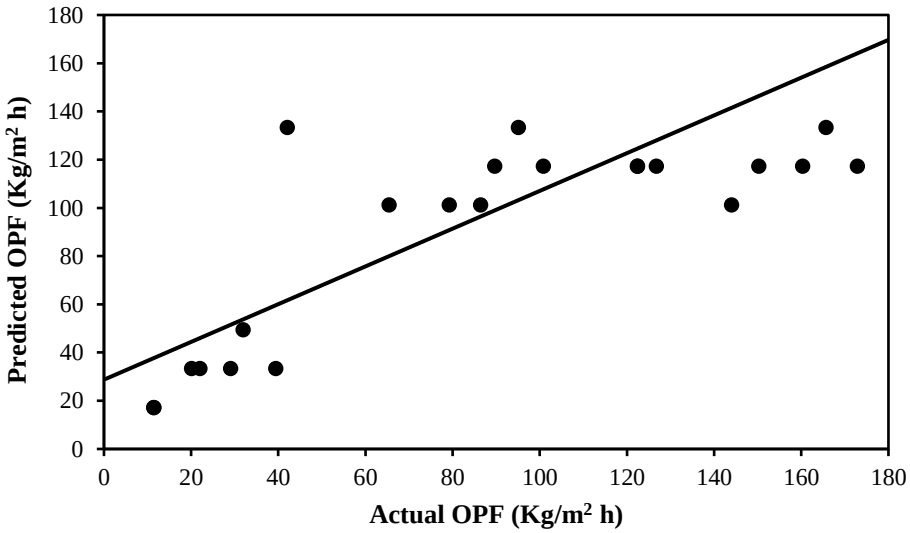

Figure 4.6: Predicted vs actual (experimental) values of oil permeate flux.

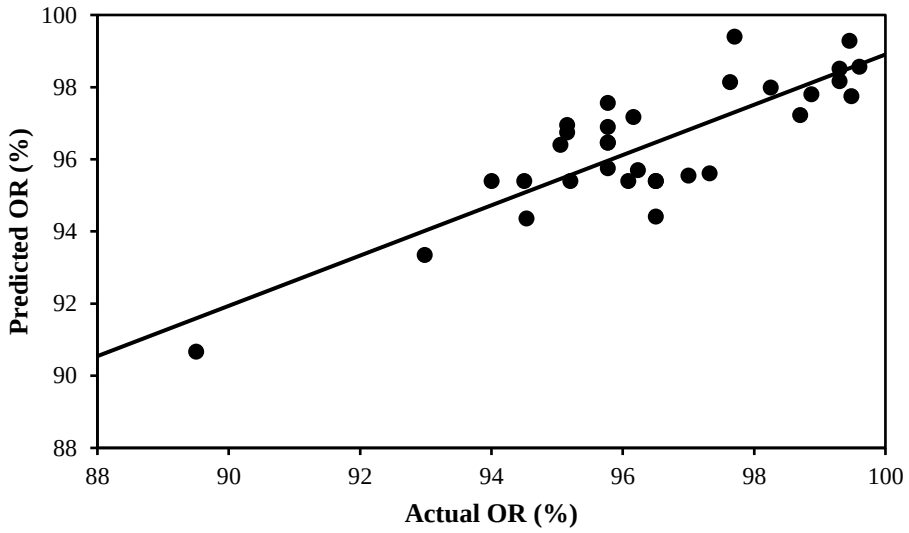

Figure 4.7: Predicted vs actual (experimental) values of oil rejection.

4.2.1 ANOVA Results for PWF and OPF

In this work, it is of paramount importance to investigate the effect of the two additives namely APTES-SiO_2 and PEG. In this case, the SEM micrographs of run no. 14 and 17 are presented in Figure 4.8. Run no 17 and 14 are dope solution without ATES-SiO_2 and PEG, respectively. For run 17, a highly porous, big macrovoid in sub-layer with relatively porous skin layer was observed (Figure 4.8a and 4.8b). Whereas run 14 show a less surface pores with clusters of APTES-SiO_2 on the surface.

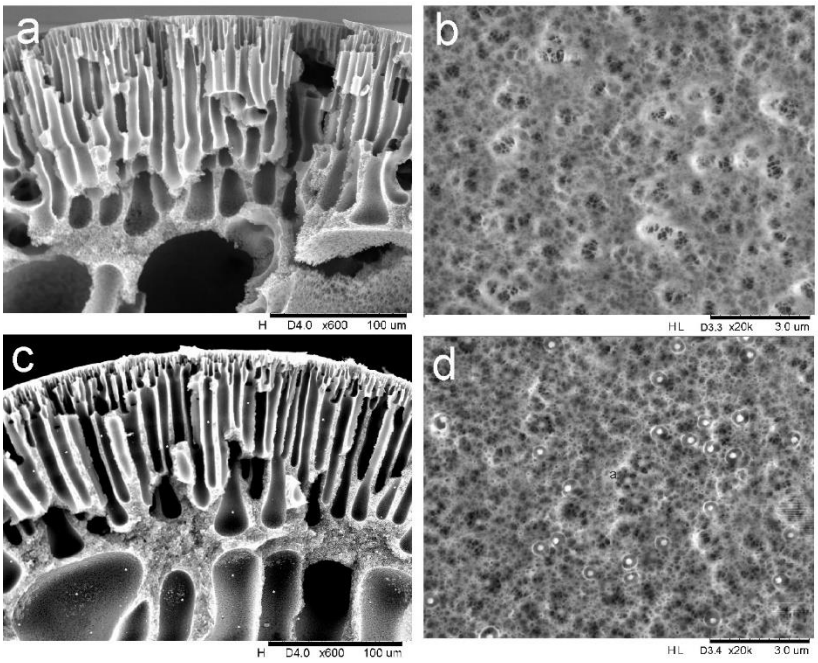

Figure 4.8: SEM micrographs of run 17 (16.5 wt.% of PES; 0 wt.% APTES-SiO_2; 2.5 wt.% PEG; 30 ºC CBT) (a-cross section, b-surface); run 14 (16.5 wt.% of PES; 2.5 wt.% APTES-SiO_2; 0 wt.% PEG; 30 ºC CBT) (c-cross section, d-surface).

In Figure 4.9 and 4.10, the characteristics of the OPF and PWF in a 3D surface plot were presented where CBT and APTES-SiO_2 were fixed at 30 ºC and 2.5 wt.%, respectively. As seen, when PES decrease with increasing PEG, both OPF and PWF increases linearly. Furthermore, when PES increases with decrease in PEG, both OPF and PWF decreases linearly. This can be as a result of the presence of APTES-SiO_2 and PEG which can enhance membrane hydrophilicity and this increase the water uptake. Other than that, the presence of PEG in the casting solution will enhance the demixing rate and thus accelerate the phase inversion in the casted solution (Basri et al., 2010). Besides, the addition of PEG in the cast solution can contributes to the enlargement of pores rather than suppression of macrovoid

structure in the prepared membranes which will subsequently result in increase in hydrophilicity and increase in permeability (Al Malek et al., 2012).

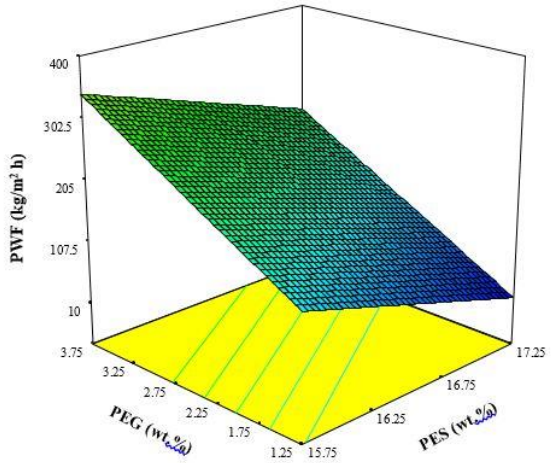

Figure 4.9: Surface plot of PWF at different PEG and PES content (2.5 wt.% APTES-SiO_2 and 30 ºC CBT).

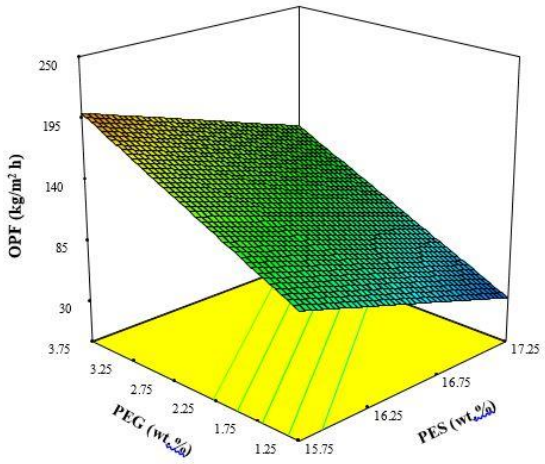

Figure 4.10: Surface plot of OPF at different PEG and PES content (2.5 wt.% APTES-SiO_2 and 30 ºC CBT).

Some studies have shown a similar trend that as the polymer concentration increases, the water permeability decreases (Lishun et al., 2010; Ma et al., 2014; Vatsha et al., 2014) due to decrease in pore size. In order to investigate the effect of

PEG on the surface morphology of membrane, Figure 4.11 presents the SEM micrographs of membranes of run 12 (15.75 wt.% of PES, 1.25 wt.% APTES-SiO_2, 1.25 wt.% PEG and 15 ºC CBT) and run 30 (15.75 wt.% of PES, 1.25 wt.% APTES-SiO_2, 3.75 wt.% PEG and 15 ºC CBT). The difference in both runs were the difference in amount of PEG content. As observed from Table 4.4, when PEG content increases from 1.25 to 3.75 wt.%, the pore size becomes larger. This can be attributed due to the property of PEG, basically to enhance the formation of pores (Liu et al., 2003). This can also lead to an improved surface hydrophilicity which will be more attractive to the molecules of water although on most occasions, the PEG is susceptible to be leached out during testing. Aside from the ability to enhance the formation of pores, PEG was embedded to enhance APTES-SiO_2 dispersion as well as improve compatibility between the APTES-SiO_2 and PES (Zhao et al., 2015). When the dispersion rate of APTES-SiO_2 is strengthened, membrane hydrophilicity is improved which will result in the increase in PWF and OPF as that is the case with PEG increase from 1.25 to 3.75 wt.%.

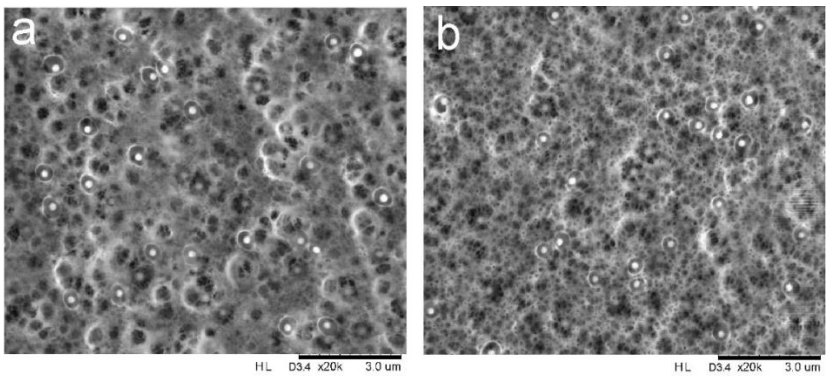

Figure 4.11: Surface micrographs of (a) run 30 - (15.75 wt.% of PES, 1.25 wt.% APTES-SiO_2, 3.75 wt.% PEG and 15 ºC CBT), and (b) run 12 - (15.75 wt.% PES, 1.25 wt.% APTES-SiO_2, 1.25 wt.% PEG and 15 ºC CBT).

Table 4.4: Pore size of run 12 and 30 membranes

Run	PES	APTES-SiO_2	PEG	CBT	Pore size (nm)
12	15.75	1.25	1.25	15	47.23
30	15.75	1.25	3.75	15	49.02

APTES-SiO_2 was impregnated in PES matrix in the presence of PEG to improve surface hydrophilicity which subsequently led to an improvement in OPF and PWF. In this case, the increase of membrane flux can be associated due to improved membrane pore formation, hydrophilic effect and better dispersibility of APTES-SiO_2 particles. The interacting effect between APTES-SiO_2 and PES toward PWF that their interaction is presented in Figure 4.12. As observed, there exist a rapid decrease in PWF from 271.84 to 90.22 kg/m^2 h at low APTES-SiO_2 content with increase in PES content. However, at high APTES-SiO_2 content, PWF decreases slightly from 177.48 to 120.43 kg/m^2 h as PES content increases. Accordingly, researches have shown that the addition of nanoparticles resulted in viscosity increase (Shen et al., 2012a). In order to confirm the influence of nanoparticles on viscosity that the viscosity (at 15.75 and 17.25 wt.% PES) against APTES-SiO_2 content are presented in Figure 4.13. Under varying content of PES, the viscosity were significantly increased with increase in APTES-SiO_2 content. At 1.25 wt.% APTES-SiO_2, the difference in dope viscosities (at 17.25 and 15.75 wt.%) reached their maximum limit. Furthermore, it can be concluded that the variation in viscosity of dope at 1.25 wt.% APTES- SiO_2 affected the PWF more significantly as the PWF rapidly decline with increase in PES content. Another important issue is that, at the low APTES-SiO_2 content, PEG/APTES-SiO_2 ratio is more than unity. At this ratio, the dispersion of APTES-SiO_2 tends to be better than at a ratio of PEG/APTES-SiO_2 less than unity. Therefore, the change in PWF might be ascribed

to both the change in viscosity and improved dispersion of APTES-SiO_2 as a result of increase in the ratio of PEG/APTES-SiO_2.

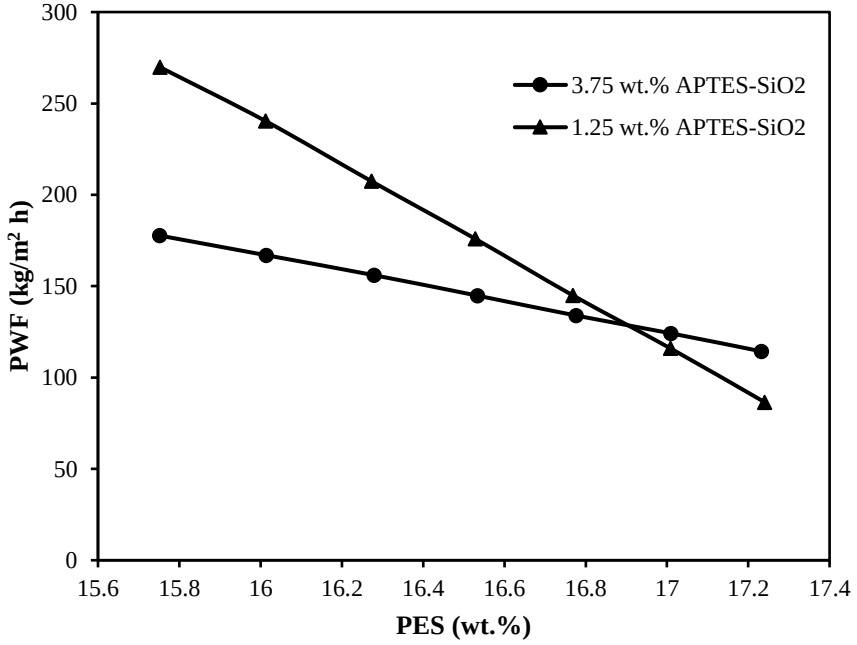

Figure 4.12: Interacting effect between APTES-SiO_2 and PES (at 3.75 wt.% PEG) on PWF.

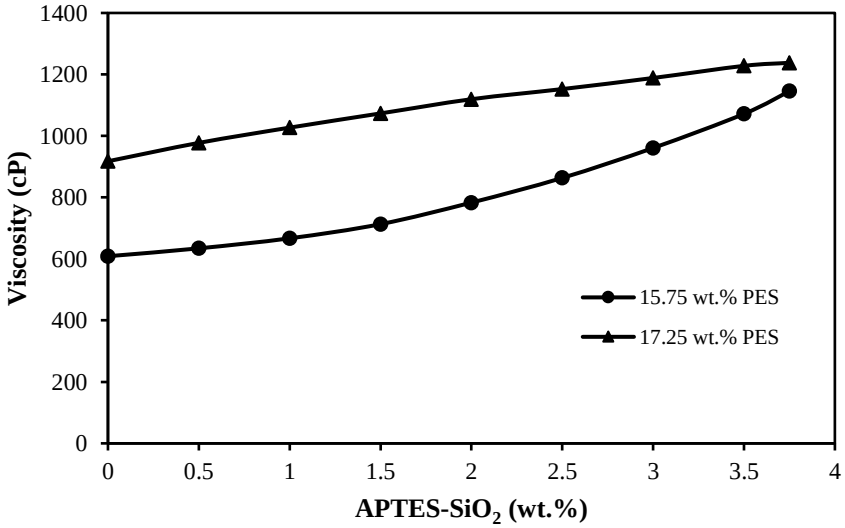

Figure 4.13: Difference in viscosity with increase in APTES-SiO_2 content at two PES content (at 15.75 and 17.25 wt.%).

4.2.2 ANOVA result for oil rejection

The 2nd order of coagulation bath temperature, CBT (D^2) exhibited the most significant parameter in OR model (Appendix E3). In order to investigate the effect of this CBT, the surface micrographs of two similar membranes, which contain different CBT value (run no. 30 and 13) were selected and are shown in Figure 4.14. As observed, the size of pores becomes bigger with increase in coagulation bath temperature from 15 ºC to 45 ºC (Table 4.5 and Figure 4.14). This can be as a result of the instantaneous liquid–liquid demixing which took place at higher temperature, which will as a consequence result in the formation of highly porous surface (Woo et al., 2015).

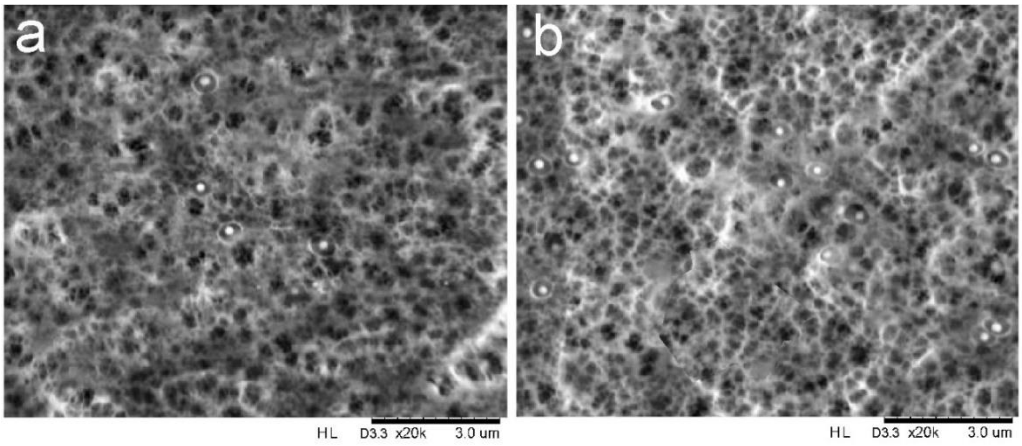

Figure 4.14: SEM micrographs of (a) run 13 - 15.75 wt.% of PES, 1.25 wt.% APTES-SiO_2, 3.75 wt.% PEG, 45 ºC CBT and (b) run 30 - 15.75 wt.% of PES, 1.25 wt.% APTES-SiO_2, 3.75 wt.% PEG, 15 ºC CBT.

Table 4.5: Pore size of run 13 and 30 membranes

Run	PES	APTES-SiO_2	PEG	CBT	Pore size (nm)
13	15.75	1.25	3.75	45	51.28
30	15.75	1.25	3.75	15	49.02

In order to examine the interacting effect between PEG and PES on OR, Figure 4.15 presents their interaction at the central levels of 30 ºC CBT and 2.5 wt.% APTES-SiO_2. As observed, increasing the PES content at low PEG of 1.25 wt.% causes oil rejection to decrease whereas increasing PES content at a high PEG content of 3.75 wt.% increases oil rejection. What this implies is that at a certain point when the ratio of PEG to APTES-SiO_2 < 1 (i.e. 1.25 wt.% PEG and 2.5 wt.% APTES-SiO_2), APTES-SiO_2 compatibility with PES tends to be poor and as a consequence will negatively influence the oil rejection. Whereas, when the ratio of PEG to APTES-SiO_2 > 1 (i.e. 3.75 wt.% PEG and 2.5 wt.% APTES-SiO_2), APTES-SiO_2 dispersion with PES tends to be better leading to improvement in oil rejection.

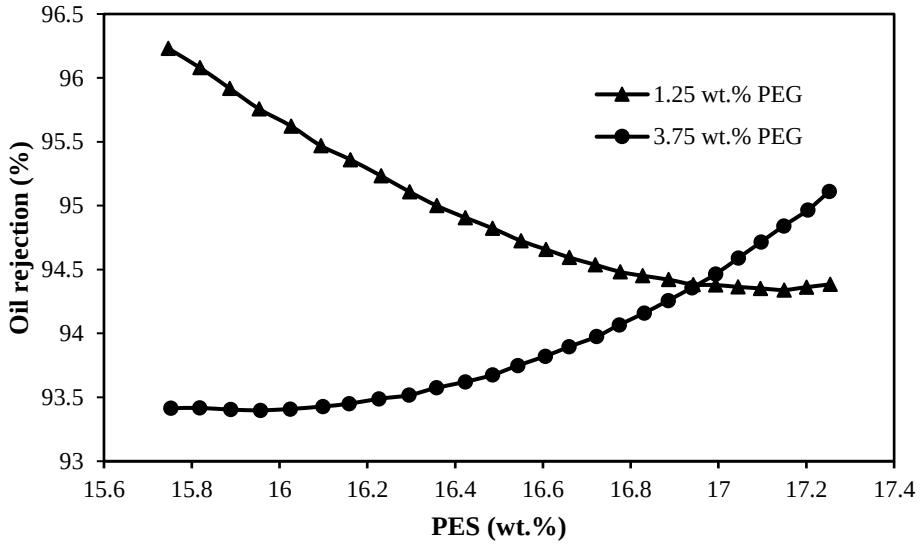

Figure 4.15: Interacting effect between PEG and PES (A*C) for OR (at 30 ºC CBT and 2.5 wt.% APTES-SiO_2).

In order to examine APTES-SiO_2 dispersion at different content of PEG on the surface of membrane, surface micrographs of run 24 and 7 are presented in Figure 4.16. From the two images, APTES-SiO_2 distribution was improved at 3.75

wt.% PEG (Figure 4.16b). The presence of high content of PEG (3.75 wt.%) not only helped to strengthen the pores but also enhance the distribution of APTES-SiO_2 in PES matrix. As a consequence led to improvement in both PWF and OPF.

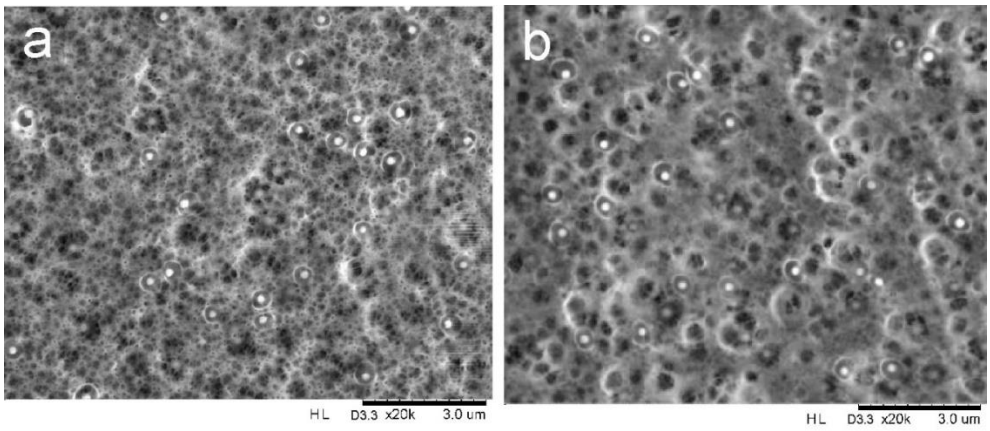

Figure 4.16: SEM micrographs of (a) run 24 – 15.75 wt.% of PES, 3.75 wt.% APTES-SiO_2, 1.25 wt.% PEG, 45 ºC CBT and (b) run 7 – 15.75 wt.% of PES, 3.75 wt.% APTES-SiO_2, 3.75 wt.% PEG, 45 ºC CBT.

Figure 4.17 presents the influence of APTES-SiO_2 and PES content on oil rejection (OR) at the central level of PEG and CBT. As observed, OR varies slightly with PES content and increase with increase with APTES-SiO_2. By introducing APTES-SiO_2 into the membrane caused the oil rejection to significantly improve. In order to further confirm the influence of APTES-SiO_2, Figure 4.18 presents the PSD of run no. 17 (0 wt.% APTES-SiO_2) and 16 (2.5 wt.% APTES-SiO_2). As observed, the pore structure becomes slightly tighter when APTES-SiO_2 content was 2.5 wt.%, hence the reason for the increased oil rejection.

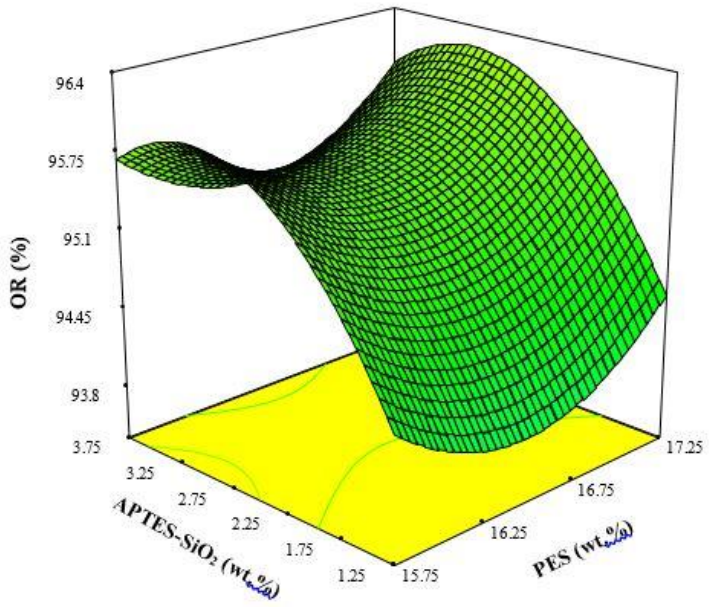

Figure 4.17: The surface plot of OR at varying APTES-SiO_2 and PES content (at 2.5 wt.% PEG and 30 ºC CBT).

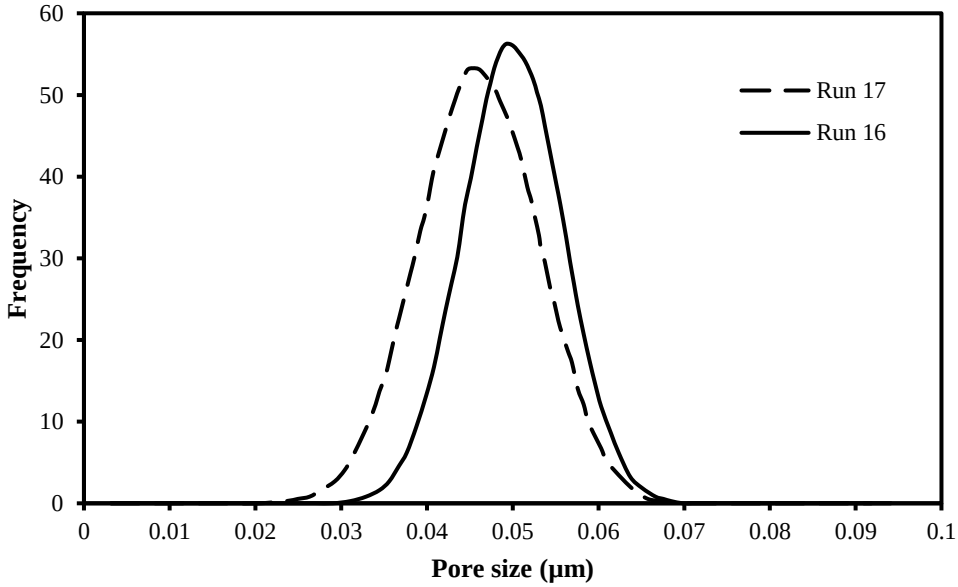

Figure 4.18: PSD of run 17 (16.5 wt.% of PES, 0 wt.% APTES-SiO_2, 2.5 wt.% PEG, 30 ºC CBT) and run no 16 (16.5 wt.% of PES, 2.5 wt.% APTES-SiO_2, 2.5 wt.% PEG, 30 ºC CBT).

From the observations, it was found that OPF and PWF were significantly affected by PEG and PES. In the case of OR, it was significantly affected by the 2^{nd} order terms of CBT and APTES-SiO_2. Also, the interacting effect of PES and PEG (A*C) significantly increased OR and PWF when the ratio of PEG to APTES-SiO_2 was greater than 1. However, in order to maximize the performance of membrane, there will be a limited amount of PEG that should be incorporated into the matrix. Furthermore, due to the conclusion drawn from Figure 4.15, it is believed that optimal membrane with best performance will result from membrane with PEG/APTES-SiO_2 ratios equal to or greater than unity.

4.2.3 Validation of predictive model

A numerical optimization technique was applied to find the optimal conditions to reach a high efficient membrane in UF of oil-in-water emulsion based on four controllable factors. In order to clearly investigate the importance of combining the preparation and spinning conditions on the morphology and subsequently on the performance of fabricated membranes, a case with goal of maximizing the pure water flux, permeate flux and oil rejection were considered which is represented in Table 4.6. The obtained optimal case was experimentally checked by performing the confirmation runs. As it was expected, under desirability of 0.920, a high value of PWF, OPF and OR was achieved at PES, APTES-SiO_2, PEG, and CBT of 17.25 wt.%, 3.6 wt.%, 3.72 wt.% and 15 ^oC, respectively. The corresponding pure water flux, oil permeate flux and oil rejection of these conditions were 233.645 kg/m^2 h, 132.251 kg/m^2 h, and 97.825%, respectively. Table 4.6 shows that the experimental data are in a reasonable agreement with predicted values,

confirming the validity of the suggested model. Furthermore, as it was earlier confirmed that the ratio of PEG to APTES-SiO_2 will be equal to or greater than unity, therefore this assumption proves to be valid. However, in order to determine the error percentage (i.e., the reflection between predicted and the actual value), these values were compared with experimental observations which was repeated by taking cognisance of the average of 5 experimental runs for the optimal membrane (Table 4.6).

Table 4.6: Predicted and actual values of the initial PWF (J_{wf1}), oil permeate flux (J_s), and oil rejection (Operating conditions: time: 3 h, TMP: 1.5 bar, flow rate: 0.45 L/min, feed concentration = 250 mg/L)

	PWF (kg/m^2 h)	**OPF (kg/m^2 h)**	**OR (%)**
Predicted	233.645	132.251	97.825
Test 1	239.75	169	98.42
Test 2	223.12	154	99.52
Test 3	219.00	165	99.79
Test 4	247.67	158	99.5
Test 5	246.45	153	98.94
Average	235.20 ± 13.33	159.8 ± 6.98	99.23 ± 0.55
Error (%)	0.673	17.248	1.421

4.2.4 Characterizations of optimum membrane

Figure 4.19 presents the micrographs of optimum membrane (represented as E5-3.6) and pristine membranes (represented as E0). As observed from the surface, the APTES-SiO_2 particles are well-dispersed on the surface of the membrane. The introduction of APTES-SiO_2 created low surface porosity which might induce a lesser membrane surface area for the adsorption of oil to take place which will subsequently promote low adsorption, particular when dealing with high concentration of oil. As shown in the figure, a typical asymmetric structure can be seen in the cross-section of both membranes which are made up of porous finger-like

sub-layer, fully developed macrovoids at the bottom-layer and thin dense top layer. As seen, the macrovoids of the pristine membranes are larger than the optimum membrane which can be ascribed due to the increase in dope viscosity upon addition of APTES-SiO_2 particles. Additionally, the wall thickness, inner diameter (ID) and outer diameter (OD) of the optimum and pristine membrane were also measured and presented in Table 4.7.

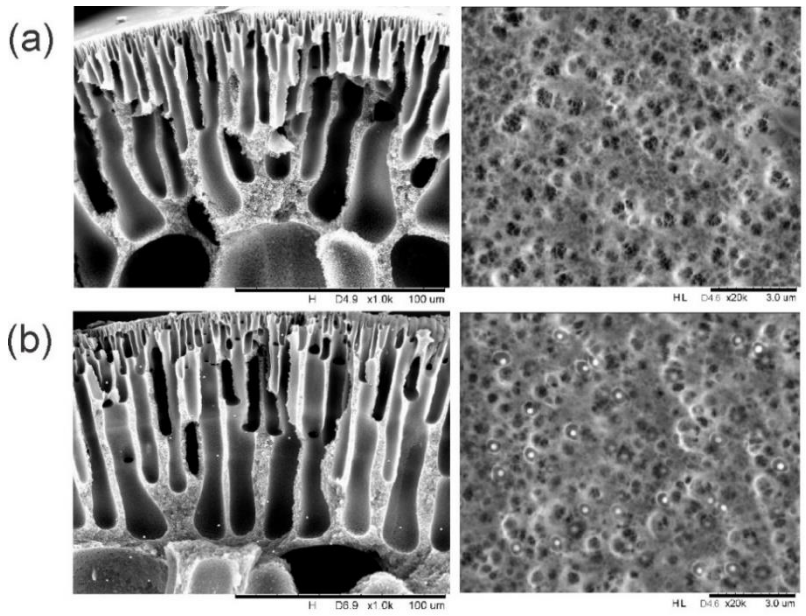

Figure 4.19: FESEM images of membrane cross-section (left) and surface (right) for (a) E0 membrane (b) E5-3.6 membrane.

Table 4.7: Wall thickness, inner and outer diameter of E5-3.6 and E0 membrane

Membrane	Inner skin layer (nm)	Outer skin layer (nm)	ID (mm)	OD (mm)
E0	223.10 ± 26.91	493.3 ± 40.52	0.427 ± 0.08	0.853 ± 0.03
E5-3.6	363.6 ± 81.24	515.8 ± 57.20	0.432 ± 0.04	0.859 ± 0.05

In Figure 4.20, the 3D image of the surface topology revealed that the pristine membrane displayed a higher surface roughness (Ra) in comparison with optimum

membrane. For pristine membrane, the surface roughness was 93.174 nm and was decreased to 74.408 nm for optimum membrane. The decrease in the roughness can be due to the surface enrichment of PES by well dispersed APTES-SiO_2. The reduced surface structure could be as a result of the interaction between APTES-SiO_2 particles in the casting solution and the phase inversion kinetics. The incorporation of APTES-SiO_2 particles in the PES casting solution will reduce the activity of polymer and DMAc, increase thermodynamic stability, thereby decreasing the driving force for DMAc outflow of fiber precipitation in external coagulation bath and accordingly produce membrane with smoother surface roughness. This result is in tandem with observation by Vatanpour et al. (2012) who found that the mean roughness decreases with increase in TiO_2 coated CNTs. This is different from the result by Dutreilh-Colas et al. (2008) who found that the roughness parameters of an hybrid silica film increases due to the presence of small drops of silica on the surface. Yang et al. (2015) also reported that the roughness of acrylate polyurethane film increases when coated with SiO_2 film. High roughness might translate to high porosity (see Table 4.8) and the nano-structured architecture of membrane (Zhang and Wang, 2014). Thus, in this work, the decrease in roughness of composite membrane may be associated due to the impregnation of well dispersed APTES-SiO_2 in PES matrix.

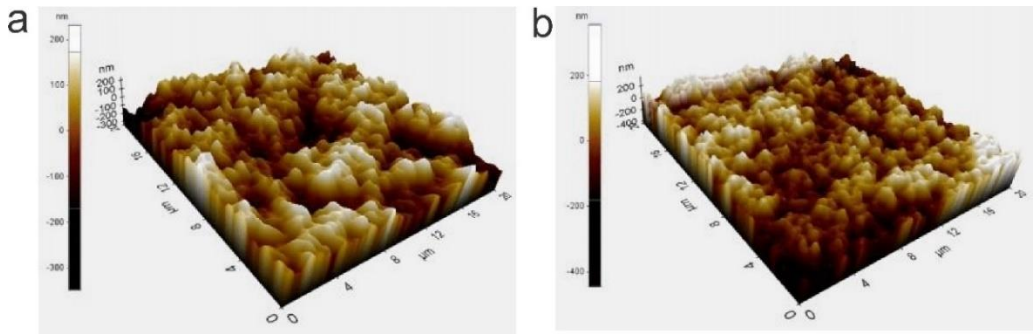

Figure 4.20: AFM images of E0 membrane (left) and E5-3.6 membrane (right).

APTES-SiO_2 is well known for its hydrophilic properties when introduced in membrane matrix. Therefore, the presence of APTES-SiO_2 in the dope solution is expected to result in improvement of hydrophilicity. In order to investigate the influence of APTES-SiO_2 on membrane hydrophilicity, the dynamic water contact (variation of WCA with time) was measured and presented in Figure 4.21. As observed, the WCA of the pristine membrane was higher than the optimum membrane. Furthermore, the decline rate of optimum membrane was faster as compared to the pristine membrane. This signifies an improvement in hydrophilicity upon incorporation of APTES-SiO_2 particles. This is similar with observation by Vatanpour et al. (2012) who found that the surface hydrophilicity increases when TiO_2 coated CNTs was incorporated in the PES membrane matrix.

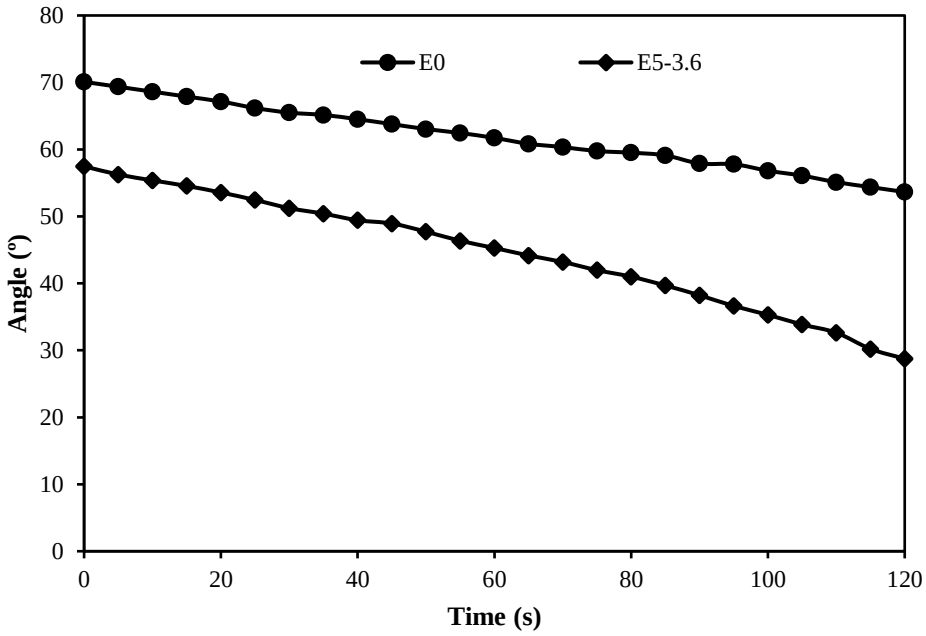

Figure 4.21: Dynamic contact angle of E0 and E5-3.6 membrane.

The ability of water to pass through membrane surface could also be influenced by the pore size. In order to investigate the influence of pore size on the

membrane hydrophilicity, Figure 4.22 presents the PSD curve. As observed, there is difference in slope of both membranes, an indication of a slightly different PSD upon introduction of APTES-SiO_2 particles. The MPS were further calculated and presented in Table 4.8.

Table 4.8: Mean pore size and porosity (£) of E0 and E5-3.6 membranes.

Membrane	**Mean pore size (nm)**	**Porosity (£)**
E0	39.98 ± 0.18	82.91 ± 3.6
E5-3.6	43.29 ± 0.11	78.27 ± 1.4

From the figure, the PSD of E0 membrane was slightly broader as compared to the optimum membrane (E5-3.6). The mean pore size was increased by ~8.3% upon introduction of 3.6 wt.% APTES-SiO_2 particles and as a consequence will bring about reduction in capillary force and thereby result in decrease in water contact angle. This difference can be ascribed due to introduced particles which produced slightly bigger pore size at some certain locations.

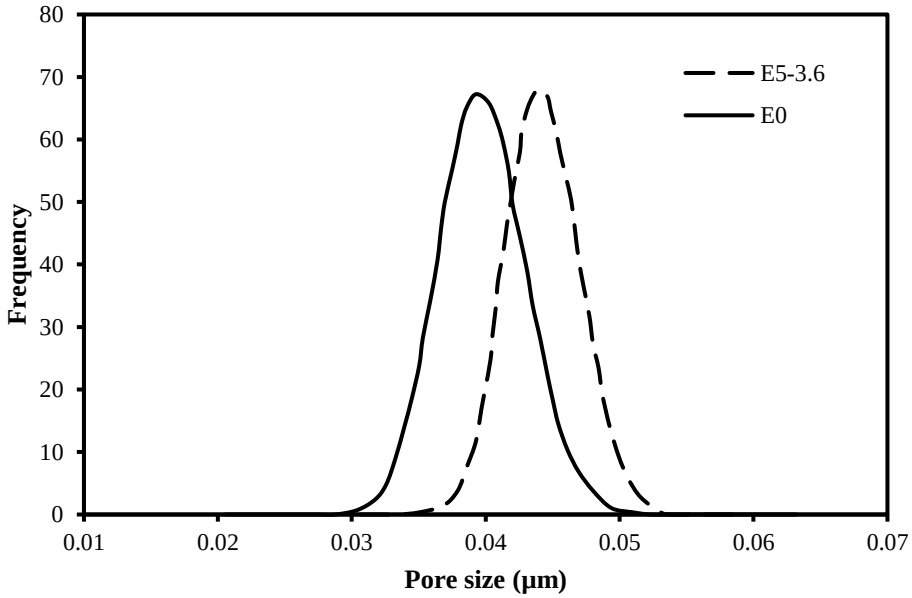

Figure 4.22: Pore size distribution of E0 and E5-3.6 membranes.

The porosity and mean pore size are displayed in Table 4.8 indicated that the porosity of E5-3.6 membrane was also affected upon addition of APTES-SiO_2 particles in the membrane matrix, where porosity decreased from 82.91 to 78.27%. This can be as a result of an increase in the content of solid or APTES-SiO_2 contents in the membrane matrix. A high APTES-SiO_2 particles in the casting solution will yield smaller porosity and thus increases the mass transfer resistance through the HF membrane (Shen et al., 2014). Similar observation have been reported by Li et al. (2009) during the preparation of PES-TiO_2 membrane where membrane porosity was found to decrease with increase in TiO_2 contents.

To obtain useful information regarding the functional groups and molecular structures, FTIR spectroscopy was carried out. Figure 4.23 presents the FTIR spectra of the E0 and E5-3.6 membranes. The broad adsorption peak at 944 cm^{-1} correspond

to the Si-OH stretching while the broad peak of 817 cm^{-1} corresponds to the symmetric vibration stretching of Si-O (Muhamad et al., 2015b; Yu et al., 2015). The presence of amino groups associated with 3-aminopropyltriethoxysilane was also observed. Two small shoulder peaks at 3347 and 3290 cm^{-1} corresponds to the N-H asymmetric stretching of the amine H-bonds, indicating a possible interaction of NH_2 toward PES surface (Aneja et al., 2015; Wang et al., 2013). The presence of an additional new N-H vibration peak, observed at around 1668 cm^{-1} results from the existence of free $–NH_2$ group (Miao et al., 2016). By going from E0 to E5-3.6 HF membrane, the strength of –OH stretching peaks at 3438 cm^{-1} was enhanced. These functional groups are responsible for improving surface hydrophilicity as well as fouling mitigation.

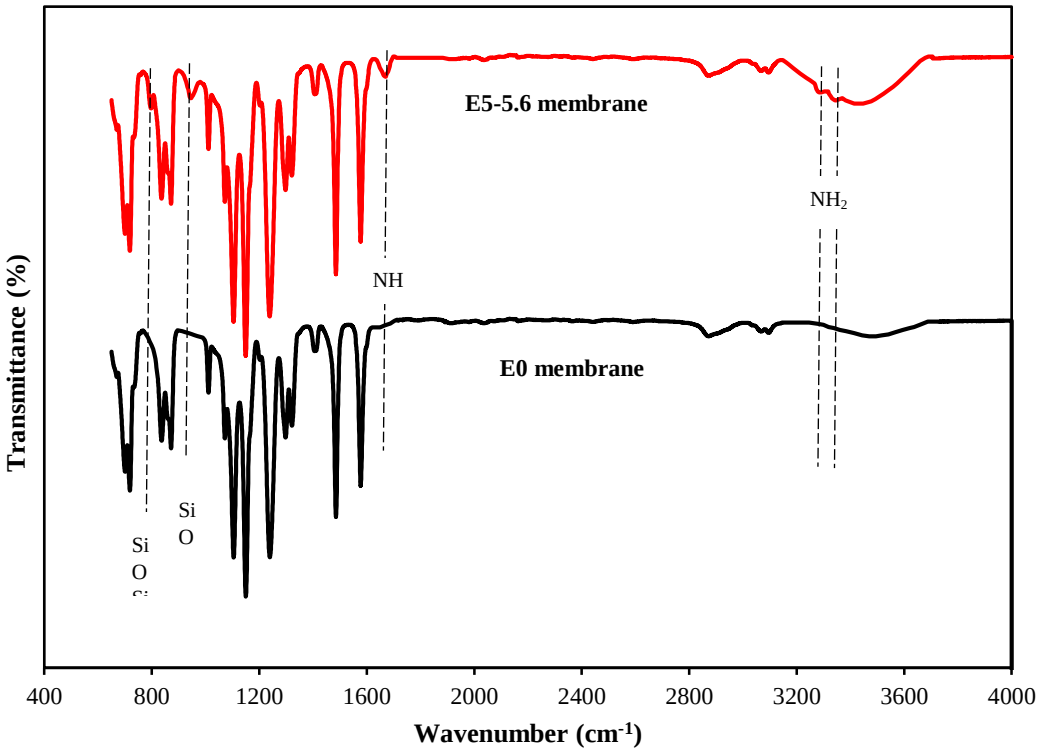

Figure 4.23: FTIR spectra of E0 membrane and E5-3.6 membrane.

4.2.5 Performance evaluations of E5-3.6 HF membrane

This section evaluates the performance of the optimum membrane in terms of pure water flux (PWF), oil permeate flux (OPF) and oil rejection. Furthermore, it reported the results of the fouling test using synthetic oily wastewater solution. The experimental values of the optimum membrane were further compared with the pristine membrane and are presented in Table 4.9. As observed, the PWF increased from 214.28 ± 12.71 kg/m^2 h to 235.20 ± 13.33 kg/m^2 h when APTES-SiO_2 concentration was 3.6 wt.%. Some studies have shown that the increase in PWF can be attributed due to several factors such as pore size, hydrophilicity and skin layer thickness (Li et al., 2015; Saedi et al., 2014). The decrease in water CA values from 71.1 to 57.5° was due the addition APTES-SiO_2 particles and the amount of hydrophilic groups. Lots of hydrogen bonds can be formed between -OH groups and H_2O molecules on the surface and channels of E5-3.6 membranes, allowing H_2O molecules to easily pass through the composite membrane. Simultaneously, this effect facilitated the sorption of H_2O on the surface of membrane, causing improvement in H_2O flux. Studies have shown that the ability to resist water flow by membranes depends on membrane skin layer. When the skin layer becomes thinner, the affinity of water molecules to flow becomes greater and vice versa when the situation is otherwise. As seen from Table 4.7, the inner skin layer thickness of E5-3.6 was higher than E0 whereas there was no significant change in outer skin layer for both membranes. However, a decrease in either the outer or inner skin layer thickness will result to PWF enhancement. For the case of E0, the small inner layer thickness did not influence PWF improvement. Thus, it can be concluded that the slight increase in pore size and presence of hydrophilic APTES-SiO_2 particles

(containing -NH_2 and -OH moieties) are the major factors which cause the PWF of E5-3.6 to increase.

Table 4.9: J_{wf1}, J_s, and oil rejection of E0 and E5-3.6 membranes (Operating conditions: time: 3 h, TMP: 1.5 bar, flow rate: 0.45 L/min, feed concentration = 250 mg/L).

Membrane	J_{wf1} (kg/m^2 h)	J_s (kg/m^2 h)	Rejection (%)
E0	214.28±12.71	129.41±9.01	97.97±1.54
E5-3.6	235.20±13.33	159.80±6.98	99.23±0.55

The permeate flux of E5-3.6 membrane exhibits higher value of 159.80 ± 6.98 kg/m^2 h than E0 membrane of 129.41 ± 9.01 kg/m^2 h. It is noteworthy to mention that hydroxyl group which occurs at the E5-3.6 membrane surface can influence membrane surface to becoming hydrophilic which will physically allows membrane surface to absorb molecules of H_2O (Krysztafkiewicz et al., 2002; Parida et al., 2006). In Table 4.9, the rejection of oil for E5-3.6 membrane was observed to be higher (99.23 ± 0.55%) as compared to E0 membrane (97.97 ± 1.54%). This indicate that E5-3.6 membrane has a better separation performance.

4.2.6 Fouling evaluation of PES/APTES-SiO_2 HF Membrane

The performance result of E5-3.6 membrane in the previous section have shown superiority over pristine membrane in respect to PF and rejection of oil. It is noteworthy to mention that the preparation of an efficient membrane does not depend on oil retention and permeate flux alone, but depends on other significant factors such as the regeneration of membrane due to the occurrence of adsorption of oil

molecules on the surface of membrane. To evaluate the anti-fouling behavior of the membranes, the FRR were introduced and their values are presented in Table 4.10. Generally, a higher FRR value signifies an improved antifouling property and that oil droplets deposited on membrane surface could be easily cleaned by washing. As observed, the FRR value of E5-3.6 membrane was apparently higher than the E0 membrane. This reason can be attributed due to an enhanced hydrophilicity and decrease in surface roughness upon introduction of 3.6 wt.% APTES-SiO_2 particles. This observation was in agreement with study by Vatanpour et al. (2012) who found that the FRR of PES/TiO_2-MWCNTs was enhanced when exposed to protein solution. Generally, membranes with higher surface roughness are more susceptible to fouling due to the availability of many adsorption sites for oil attachments (Ngang et al., 2012).

Table 4.10: Membrane fluxes due to different fouling mechanisms, RFR, and FRR of pristine and optimum membrane (Operating conditions: time: 3 h, TMP: 1.5 bar, flow rate: 0.45 L/min, feed concentration = 250 mg/L).

Membrane	J_{wf2} (kg/m^2 h)	J_{wf1} (kg/m^2 h)	FRR
E0	166.87±12.51	214.28±12.71	77.87±4.45
E5-3.6	212.76±14.77	235.20±13.33	90.46±7.27

Furthermore, the relative flux was calculated and displayed in Figure 4.24. As observed, the relative flux of both membranes declined with time. The possible reason is liable to be caused by the rapid build-up of a layer of the rejected oil particle near the membrane surface which acts as the secondary filtration element and as such will limit the passage of water from the active membrane layer (Khamforoush et al., 2015). This formed layer undergoes compaction with increasing operation time, so the flux drop was caused by the increased resistance offered by the

compressed secondary layer. For pristine membrane, the relative flux rapidly declined while there was a gradual decline of flux for optimum membrane. Although, both achieved a slightly similar steady-state flux towards the end of the test which could be as a result of the slight difference in pore size.

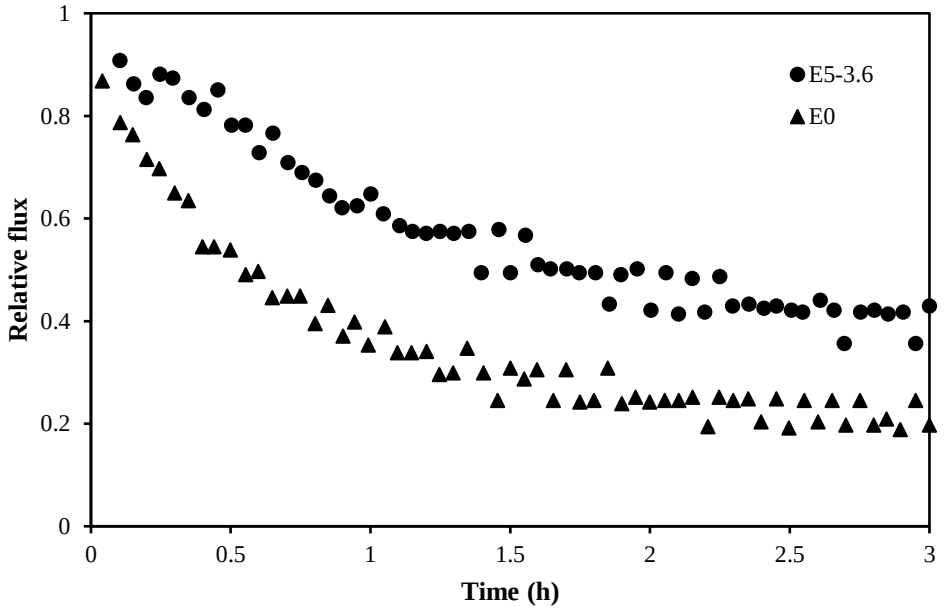

Figure 4.24: Relative flux of E0 membrane and E5-3.6 membrane.

For further anti-fouling behaviour, the fouling resistances of E0 and E5-3.6 HF membranes were presented in Figure 4.25. The total fouling resistance of the optimum membrane was lower as compared to controlled membrane. For E5-3.6, the irreversible resistance (Rir), and Rt were significantly lower than the E0 membrane while the reversible resistance (Rr) of E5-3.6 HF membrane was found to be higher. The surface of APTES-SiO_2 embedded membrane becomes more hydrophilic as compared to the pristine membrane which can be as a result of higher affinity of metal oxide to water as well as the increase in SiO_2 chain density on the membrane surface. The slightly narrower pore size of the optimized membranes also contributes

to lower irreversible resistance. Many recent researches have shown that the influence of NPs loadings on fouling resistance are expected to vary. This result confirms that the anti-fouling performance of the APTES-SiO_2 modified PES UF membrane has been successfully improved.

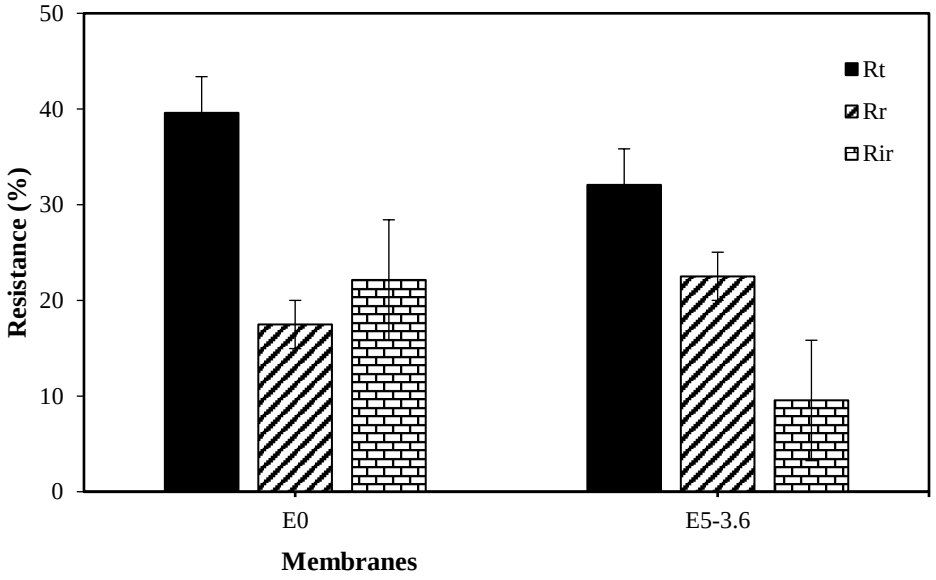

Figure 4.25: Fouling resistances of E0 and E5-3.6 HF membranes.

4.3 Assessing the effect of bore fluid composition on membrane properties

In hollow fiber spinning, one common type of instability produced is the formation of irregular cross–section in spun fiber. This type of irregularity can be influenced by the take up-speed, dope speed and draw ratio during hollow fiber spinning. The manipulation of the bore fluid can also lead to membrane with regular shape as well as fiber without distortion. For this reason, all other preparation conditions were fixed except the bore fluid composition which was varied. Therefore, the change in morphology and performance can be mainly attributed to the variation of the bore fluid composition.

Figure 4.26 shows the cross-sectional FESEM images of PES HF membrane using the ethanol-water mixtures with different ethanol contents as the bore fluid. As shown, all spun membranes displayed fingerlike structure in their cross-sectional morphology. Indeed, the most evident effect of the increasing ethanol concentration in the bore fluid is a gradual transformation of the circular inner layer morphology into a corrugated-like morphology, while there were no evident changes in the outer layer. The high water content in the bore fluid would cause early phase separation through the air gap and quickly solidify the inner surface of spun hollow fiber. As ethanol is added in the bore fluid, macrovoids formation on the membrane decreases. This can be attributed due to the delay in the rate of precipitation at the inner layer of the nascent membrane, which causes suppression in the formation of macro-voids pores (Saghafi et al., 2014). It has been well-known that the macrovoids formation can be avoided if the phase separation process undergoes a slower precipitation rate (Shieh and Chung, 1998). Thus if the coagulating power of the bore fluid is reduced by increasing the solvent concentration, it would reduce the solubility parameter difference between the bulk of HF and the bore fluid (Kumbharkar et al., 2011). As a consequence will slow down the phase inversion by the delayed liquid–liquid demixing process at the inner side of the fibre and is also consistent with literatures. Dong et al. (2010) reported similar observation for Matrimid® fibres. They reported that by increasing the content of solvent in bore fluid from 40–80%, macrovoids in the fibre were successively reduced in quantity and then vanished completely with further increase.

As seen from the cross-section, the number of corrugations or grooves diminishes with decreasing ethanol content in the bore fluid. This phenomenon can

be best explained regarding the time delay between precipitation of inner and outer layers of HF. Specifically, after ejecting from the spinneret, the dope solution is brought into direct contact with the bore fluid and solvent/non-solvent exchange starts and proceeds during passing through the AG. This favors the formation of inner layer of HFs which are composed of polymer-rich phases. Elastic moduli of polymer-rich phases will increase as time elapses and precipitation goes on. Inside the external coagulation bath, the outer layer of HFs also begins to precipitate into the polymer-rich phases. Obviously, at a given time after ejecting the solution from the spinneret, the elastic modulus of the HF inner layer will become higher than that of the outer layer due to the existence of air gap along which the solvent/nonsolvent exchange takes place only through the inner layer of HF. Stretching the spinning jet inside the coagulation bath will produce inward compressive radial forces; however, the elastic modulus of HF inner layer becomes too high to adapt the imposed changes and hence the inner layer is buckled. Therefore, the faster precipitation of the outer layer compared to that of the inner layer can reasonably explain why the inner layer of produced HFs has corrugated shape while the outer layer does not.

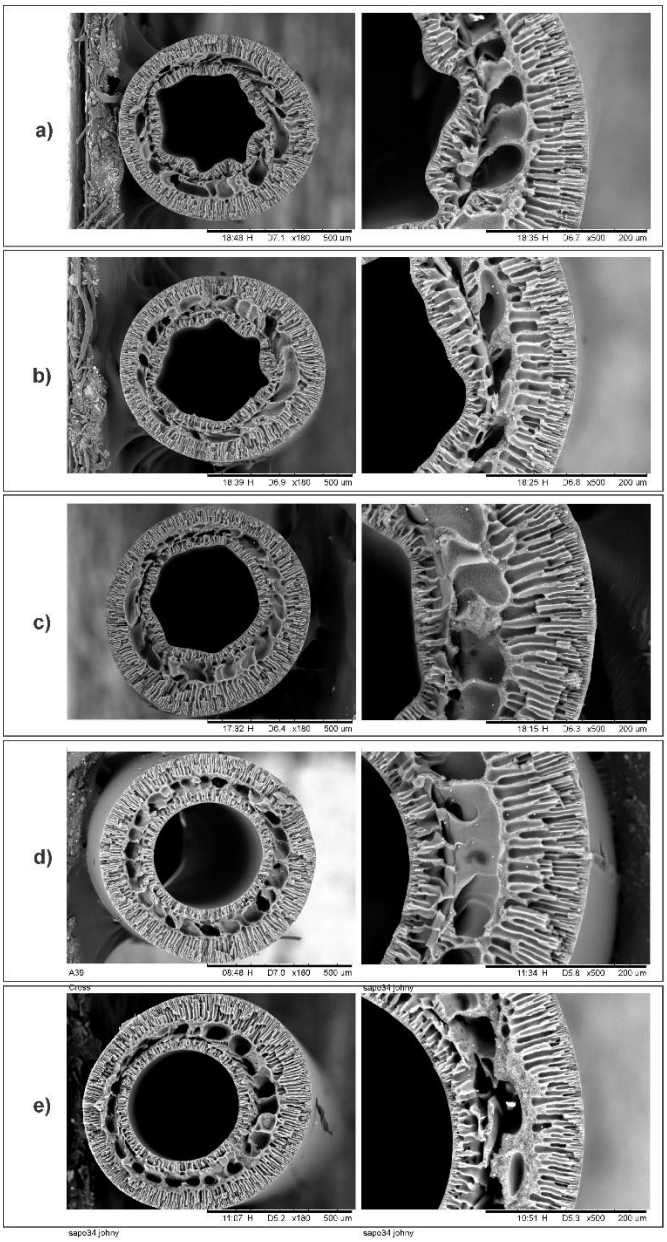

Figure 4.26: Effect of bore fluid composition on membrane morphology: cross-section at 180 x (left) and cross-section at 500 x (right). (a) 100% ethanol; (b) 75% ethanol; (c) 50% ethanol; (d) 25% ethanol; (e) 0% ethanol.

Table 4.11 presents the porosity and the mean pore size data of the prepared membranes. As observed, porosity is between 78.27 to 83.25%. The porosity of membrane increases significantly with increase in ethanol in bore fluid component.

In this case, the reduction in macrovoid density could account for the increased porosity with increasing ethanol contents in the bore fluid. The reduction of macrovoid density using coagulants of high solvent content has been also reported by Rahbari-sisakht et al. (2012). The maximum porosity of 83.25% was obtained for spun HF membrane with 100% ethanol as bore fluid.

Table 4.11: Effect of bore fluid composition on membrane physical properties

Membrane code	Ethanol content	Porosity (%)	Maximum stress (MPa)	Inner wall thickness (nm)	Pore size (nm)
E1-3.6	100%	83.25	3.641 ± 0.213	339.40 ± 0.6	59.43
E2-3.6	75%	82.71	3.739 ± 0.265	345.23 ± 0.4	55.65
E3-3.6	50%	81.39	4.067 ± 0.246	351.31 ± 0.8	51.83
E4-3.6	25%	79.64	4.103 ± 0.134	356.13 ± 0.12	45.18
E5-3.6	0%	78.27	4.176 ± 0.154	363.72 ± 0.10	43.29

As observed from Table 4.11, it is noteworthy that the internal coagulant composition also has influence on the inner wall thickness of prepared hollow fibre membranes. The increase of ethanol content in the internal coagulant results in thinner inner wall thickness. The higher water content in the bore fluid will cause an early phase inversion through the AG and thus quickly solidifies the inner surface of HF, which will quickly triggers the formation of inner wall thickness (H. Zhu et al., 2017). The membranes show inner wall thickness of 363.72 µm and 339.40 µm when water and 100% ethanol were used as the bore fluid, respectively. This is caused by the decreasing coagulant power and thus retarded phase inversion with the addition of ethanol. In this case, the nascent wet hollow fibre membrane can be stretched more easily by the elongational force and gravity induced by the take-up unit, resulting in thinner inner wall membrane thickness.

As also shown in Table 4.11, the hollow fibres spun using 25% ethanol and pure water as the internal coagulant demonstrated the highest maximum stress in the range of 4.103 and 4.176 MPa. As the ethanol content in the bore liquid is increased above 25%, the mechanical strength of the hollow fibre membranes decreases noticeably. As we know, the mechanical strength of hollow fibre membrane is determined not only by the material properties but also by the change in membrane structure and porosity as observed in Figure 4.26 and Table 4.11. Basically, hollow fiber membrane with lower porosity are reasonable expected to have higher mechanical properties, as previously demonstrated in Table 4.11.

The pore size slightly increases when the content of ethanol increases, and the change became a little more obvious when mixture of 75% ethanol–25% water and 100% ethanol were used as the bore fluid (Figure 4.27). This may be caused by the stretching of HF during spinning process under the action of elongational force and gravity induced by the take up unit (Zhang et al., 2015). This phenomenon was also observed by Zhang et al. (2015) in the preparation of porous yttria-stabilized zirconia HF membranes using NMP/water mixtures. Zhang et al. (2011) also observed a porous inner surface structures of PVB hollow fibers, when high DMAC amounts were added in the internal coagulants.

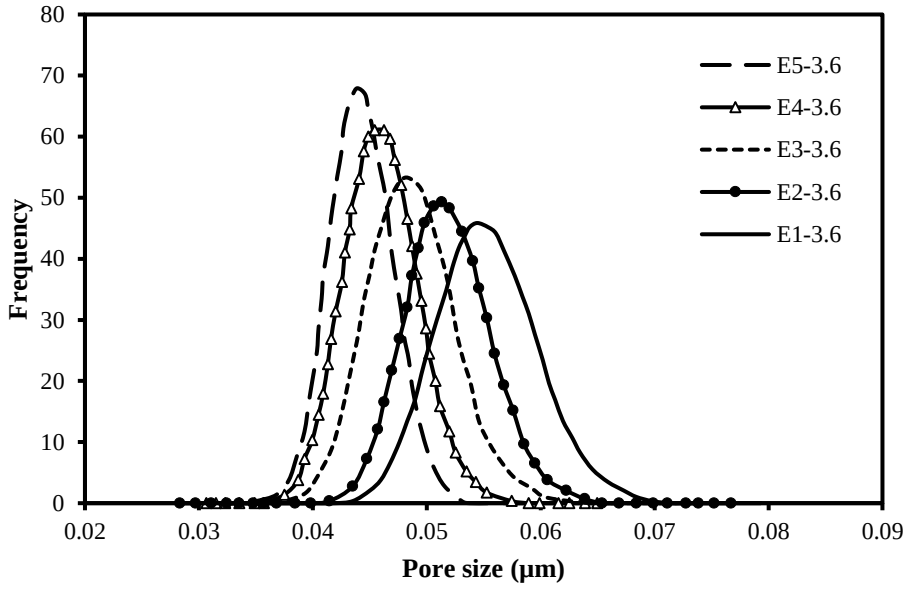

Figure 4.27: Pore size distribution of PES HF membranes at different bore fluid composition.

As can be seen, the PSD of the membranes can also be obviously influenced by the ethanol content in the bore fluid. A similar effect was observed by Zhang et al. (2015) for the yttria-stabilized zirconia (YSZ) fibers pore size distributions when NMP/water mixtures with higher amount of solvent were used as internal coagulants. The narrowest PSD corresponds to membrane prepared with pure water as bore fluid. Nevertheless, the PSD becomes much wider when more than 100% ethanol was used. This was also observed in this study for PVDF-HFP hollow fibers. An increase in ethanol content will result to reduction in the coagulating power. Due to the decrease in coagulating power, the draw rate will increase, causing the distance between organic particles to become larger and as a consequence producing membrane with larger pore size and higher porosity. The mean pore size of the aforementioned YSZ membranes and the PSf hollow fibers prepared by Rahbari-sisakht et al. (2012) also increased with increasing the NMP content in the bore

liquid. These results further confirm that the exchange rate between the water and ethanol mixtures are much slower than that between the 100% water as bore fluid.

Table 4.12 presents the permeate flux of the prepared hollow fibre membranes. As can be seen, the pure water permeability increases with the increase in ethanol content in the bore fluid. The hollow fibre membranes prepared with pure water as bore fluid shows a pure water permeability of 159.8 kg/m^2 h. When ethanol content was 25%, the membrane shows a slight increase in flux of to 163.59 kg/m^2 h, being increased by ~2.4% compared to HF membrane prepared without ethanol in the bore fluid. When ethanol content further increase to 75%, the membrane shows a relative higher flux of 175.17 kg/m^2 h, being increased by 9.6% as compared to HF membrane prepared without ethanol in the bore fluid. The pure water permeability further increases to 181.63 kg/m^2 h when ethanol content was 100%. This behaviour can be related to the variation in pore sizes which can aid the membranes to absorb water molecules with thinner wall thickness and high porosity of the prepared HF membranes.

Table 4.12: Permeate flux of the hollow fibre membranes as a function of ethanol content in the bore fluid.

Membrane code	Ethanol content	Permeate flux (kg/m^2 h)	Rejection (%)
E1-3.6	100%	181.63 ± 6.45	92.85 ± 0.85
E2-3.6	75%	175.17 ± 5.12	95.01 ± 0.91
E3-3.6	50%	166.97 ± 5.59	97.48 ± 0.54
E4-3.6	25%	163.59 ± 5.12	99.84 ± 0.12
E5-3.6	0%	159.80 ± 6.98	99.23 ± 0.55

Operating condition: TMP = 1.5 bar, flow rate = 0.4 L/min, temperature = 25 °C, oil concentration = 250 mg/L, ultrafiltration time = 3 h.

The oil rejection rate of the hollow fibre membranes prepared with different ethanol contents in the bore fluid is also presented in Table 4.12. It can be seen that the oil rejection rate increases with decrease in ethanol content and then reaches a relatively higher value of 99.84% when the ethanol content was 25%. This membrane also shows a moderate pore size coupled with high permeability. Judging from its permeate flux and rejection of the prepared hollow fiber membranes, membrane with a bore fluid concentration of 25% w/w of ethanol in water was chosen for further study (i.e. E4-3.6).

4.4 Characterization and performance of PES/APTES-SiO_2 HF membranes at different APTES-SiO_2 loading

In the previous section, the optimum membrane was prepared according to the desirability obtained from response surface methodology and bore fluid evaluation. From the reported results, it is established that APTES-SiO_2 has the ability to enhance the physical and performance properties of the resultant membrane. The introduction of 3.6 wt.% of APTES-SiO_2 was found to decrease the membrane roughness as well as decrease the irreversible resistance. However, it is possible that decreasing and increasing the content of APTES-SiO_2 could produce membrane with more significant improvement in membrane properties which will as a result improve the membrane performance. For this reason, APTES-SiO_2 particles were incorporated into the matrix at contents less than optimum (0, 1.2 and 2.5 wt.%), at the optimum (3.6 wt.%) and above the optimum content (5 wt.%).

4.4.1 Characterization of membranes at different APTES-SiO_2 content

4.4.1.1 SEM micrograph of PES HF membranes

SEM images of the cross-section of PES/APTES-SiO_2 HF membranes are presented in Figure 4.28 to evaluate the changes induced on the membranes. The cross-sectional micrographs shows that all membranes possesses similar finger-like structure. As observed, a distinct change in all membrane surfaces were found, confirming the existence of APTES-SiO_2 particles cluster, which increases with increase in APTES-SiO_2 loading. Furthermore, no visible aggregates of APTES-SiO_2 particles were observed on the surface micrographs of all polymer-inorganic membranes which means that APTES-SiO_2 particles were dispersed homogeneously with a ring-like gap (cavity) around them within PES membrane matrix. By addition of varying APTES-SiO_2 content, a dope solution with a high viscosity is produced which could affect the mechanism involved in the formation of the membrane in the quenching bath and membrane compactness (Wang et al., 2006). In addition, the finger-like becomes longer with addition of APTES-SiO_2 particles and it becomes wider with further addition (Table 4.13). This reason can be as a result of the kinetic effect on the rate of nonsolvent-solvent exchange during the process of phase inversion (Yuliwati et al., 2011).

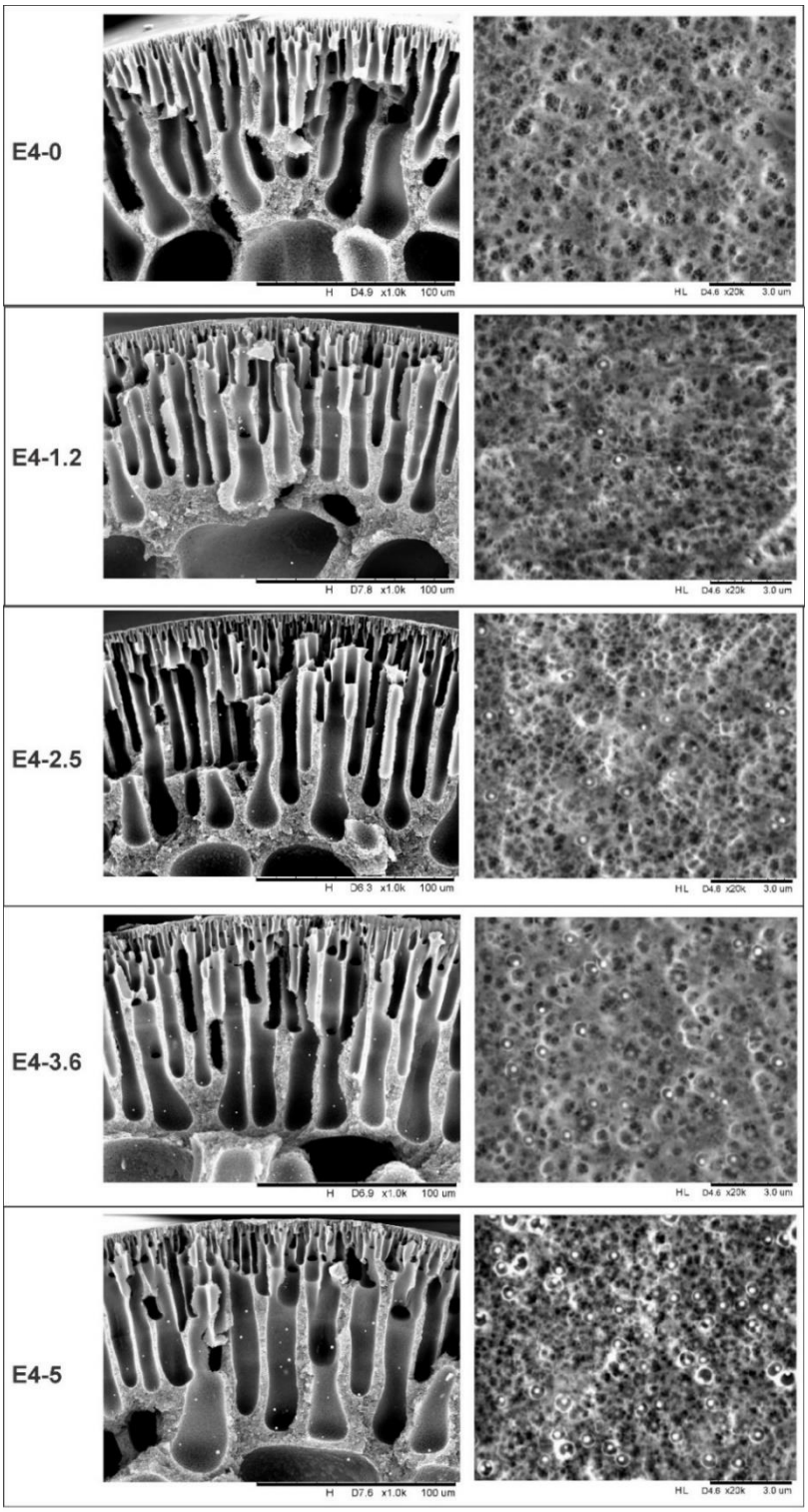

Figure 4.28: SEM micrographs of membranes (i) cross-section 1,000 x (left), (ii) surface at 20,000 x (right).

When fibers are spun with materials with different dope content or viscosities, there tends to be subjected to difference in elongation by stretch and the solution demixing. At higher dope viscosity, demixing rate will be delayed which will produce fibers with thicker inner skin (Wang et al., 2006). For this reason, the outer and inner skin thickness, which are responsible for the membrane separation are measured and presented in Table 4.13. For E4-1.2 and E4-2.5 membrane, the outer skin thickness decreases significantly. Whereas for the inner skin, there was no significant change in the thickness. For E4-3.6 and E4-5 membrane, the decrease in their inner skin layer thickness as well as the increase in outer skin layer thickness were not in linear proportion with increase in the APTES-SiO_2 particles which might be as a result of factors such as gravity elongation. Therefore, addition results involving elongation due to gravity is important.

Table 4.13: Finger-like thickness, outer and inner skin layer thickness of PES/APTES-SiO_2 HF membranes at different APTES-SiO_2 loadings

Membrane	Finger-like thickness (mm)	Inner skin layer (nm)	Outer skin layer (nm)
E4-0	0.0713	224.01 ± 25.71	483.92 ± 36.52
E4-1.2	0.0851	308.73 ± 47.43	315.57 ± 16.17
E4-2.5	0.0892	354.57 ± 38.03	279.05 ±34.50
E4-3.6	0.0913	356.75 ± 79.24	452.57 ± 35.02
E4-5	0.0908	269.33 ± 35.01	545.73 ± 36. 76

Gravitational elongation (ɖ) is expected when fibers are spun with same conditions with different dope viscosities and can be calculated using equation 4.6:

$$ɖ = \frac{(Outer\ diameter^2 - Inner\ diameter^2)_{Spinneret}}{(Outer\ diameter^2 - Inner\ diameter^2)_{Spun\ fiber}} \quad (4.6)$$

The values of gravity elongation of all membranes were measured and presented in Figure 4.29. As observed, there was a significant decrease in the gravitational elongation when the content of APTES-SiO_2 was above 2.5 wt.%. Thus, it can be concluded that the non-linear decrease in outer skin thickness and increase in their inner skin layer thickness for E4-3.6 and E4-5 might be associated due to the significant decrease in elongation due to gravity (Obaid et al., 2015).

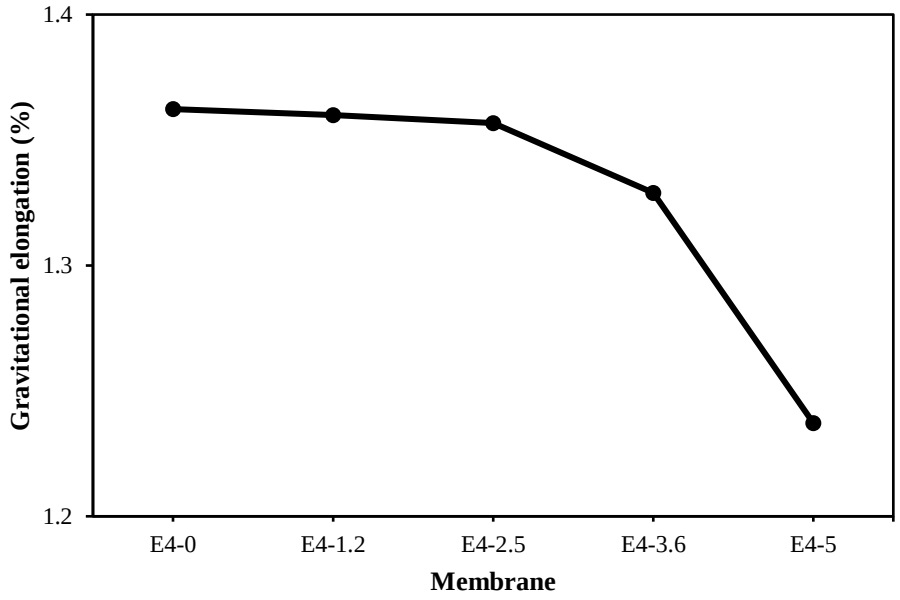

Figure 4.29: Gravitational elongation of PES/APTES-SiO_2 HF membranes at different APTES-SiO_2 loadings

4.4.1.2 Energy dispersion X-ray (EDX) analysis of PES HF membranes

EDX analysis was carried out to estimate the amounts of elements and the APTES-SiO_2 distributions. Each individual membrane sample were measured at three random points and their mean were calculated and presented in Table 4.14. EDX analysis confirmed the existence of APTES-SiO_2 in membrane matrix due to the presence of Si element peak. The quantity of SiO_2 in the composite membranes

increased with increasing SiO_2 loading in the membrane. The higher the concentration of APTES-SiO_2 added into PES membrane, the greater the percentage of Si element detected.

Table 4.14: Elementary analysis of PES/APTES-SiO_2 HF membranes at different APTES-SiO_2 loadings

Membrane	C (wt.%)	O (wt.%)	Si (wt.%)	S (wt.%)
E4-0	40.467 ± 0.389	32.472 ± 0.141	-	27.061 ± 0.731
E4-1.2	38.029 ± 0.41	32.718 ± 0.052	6.543 ± 0.041	28.710 ± 0.43
E4-2.5	37.365 ± 1.14	30.060 ± 0.269	8.623 ± 0.043	23.952 ± 0.823
E4-3.6	36.675 ± 0.328	28.535 ± 0.058	12.596 ± 1.16	22.194 ± 0.647
E4-5	34.536 ± 0.647	28.866 ± 0.253	15.611 ± 1.318	20.987 ± 0.418

Figure 4.30 presents the APTES-SiO_2 distribution of PES/APTES-SiO_2 HF membranes at different APTES-SiO_2 loadings which was carried out at three random points. From the image, APTES-SiO_2 density was found to increase with increase in particles loading. It can be concluded from the EDX analysis that APTES-SiO_2 particles were homogenously dispersed and well distributed in the matrix. Furthermore, in order to investigate the dispersion quality of APTES-SiO_2 nanoparticles, the EDX line mapping was performed on the active layer of the PES composite HF membrane incorporated with APTES-SiO_2 particles. From the figure, it is seen that the APTES-SiO_2 nanoparticles are distributed with little or no agglomeration across the cross-section since clusters of colours are not observed. The greater intensity of the coloration seen in E4-5 denotes an increase in concentration from 1.2 to 5 wt.% APTES-SiO_2 particles.

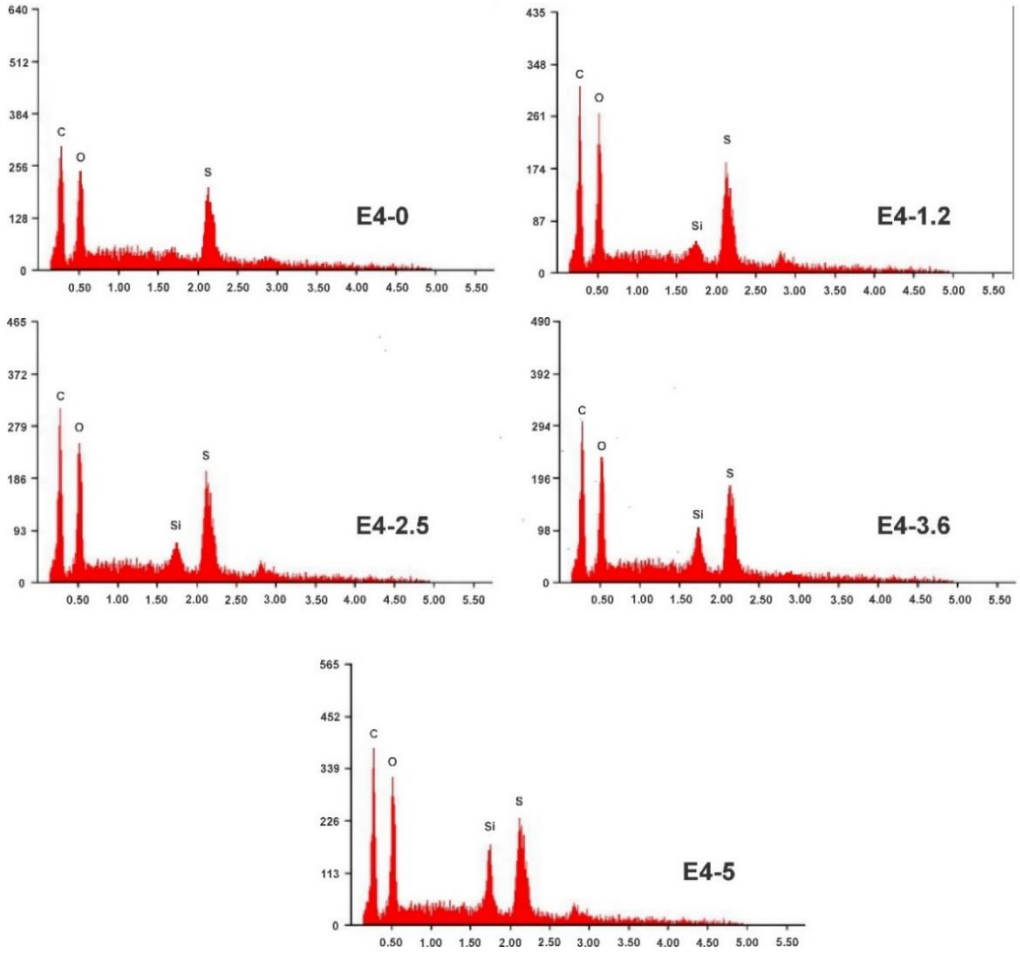

Figure 4.30: EDX distribution of APTES-SiO_2 on membrane surface.

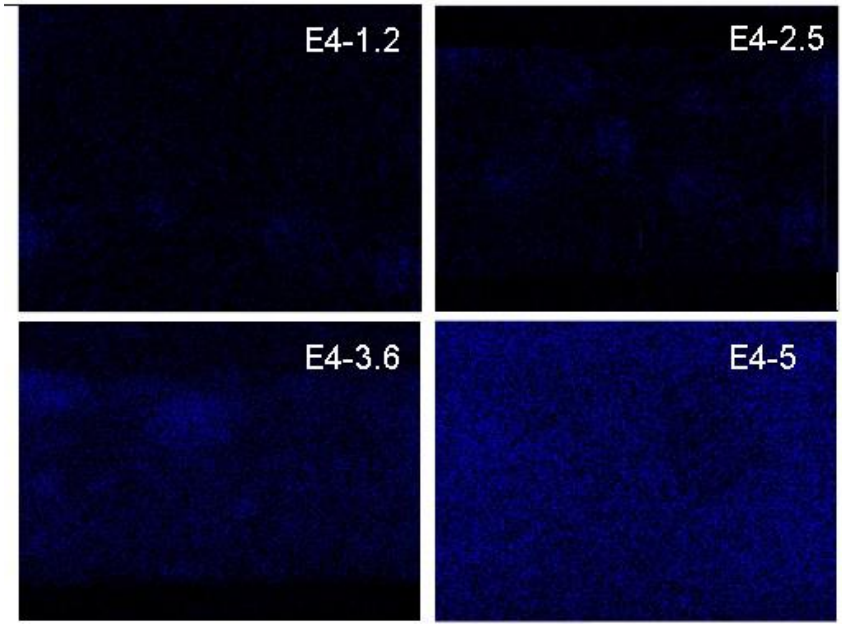

Figure 4.31: Silicon (Si) mapping of PES/APTES-SiO_2 composite HF membranes cross-sections.

4.4.1.3 Thermal stability of PES HF membranes

For more accurate reports on the amount of APTES-SiO_2 in the matrix, TGA was carried out under air atmosphere at a temperature between 30 ºC to 850 ºC. The theoretical and actual content of APTES-SiO_2 are presented in Table 4.15. As observed, the difference between the estimated and theoretical APTES-SiO_2 content are less which makes their difference accepted.

Table 4.15: Estimated and theoretical values for APTES-SiO_2 content in PES HF membrane

Membrane	**PES (wt.%)**	**PEG (wt.%)**	**APTES-SiO_2 (wt.%)**	**Calculated APTES-SiO_2* (wt.%)**	**Estimated APTES-SiO_2** (wt.%)**
E4-0	17.25	3.72	0	-	-
E4-1.2	17.25	3.72	1.2	3.9	4.056 ± 1.25
E4-2.5	17.25	3.72	2.5	8.9	8.883 ± 2.146
E4-3.6	17.25	3.72	3.6	13	12.856 ± 2.151
E4-5	17.25	3.72	5	17.5	16.972 ± 1.128

*The calculated amounts of APTES-SiO_2 in membranes were performed on the basis that there is no PEG left in the matrix after vitrification of membrane.

**Estimated amount of APTES-SiO_2 from TGA (Average of two analysis).

The thermal stability of all membranes under nitrogen were investigated and their results are presented in Figure 4.32. The first degradation of membrane took place below 100 ºC while the weight loss at around 175 ºC was caused by evaporating solvent (boiling point of DMAc). In the third stage at around 400 ºC, all membrane experienced a similar weight loss which might be due to decomposition of polymer main chains.

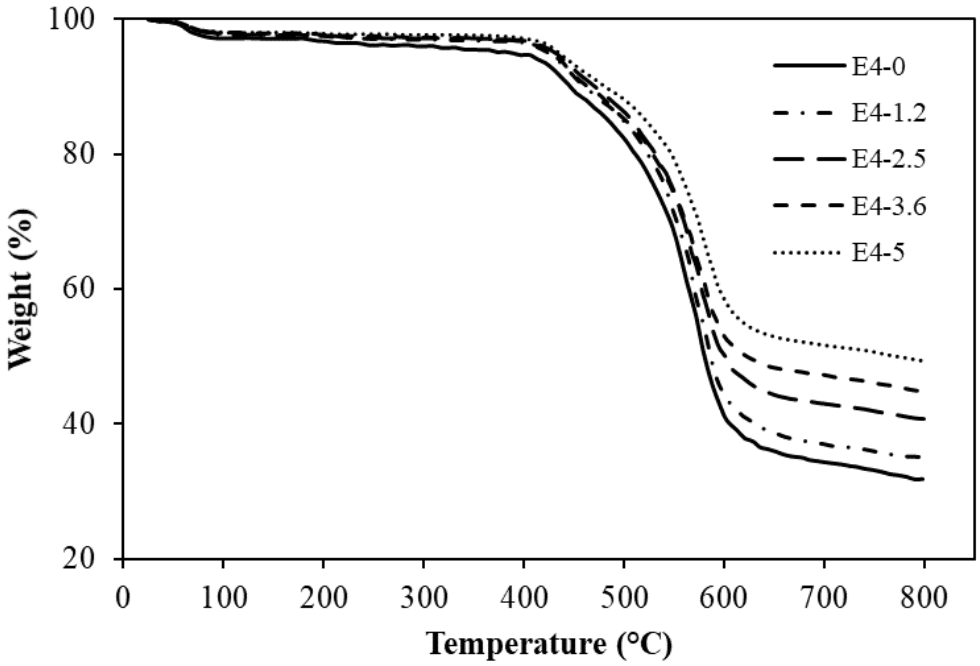

Figure 4.32: TGA curves under nitrogen atmosphere for membranes.

The decomposition temperature at 3% weight loss of the membranes are displayed in Table 4.16. As observed, the composite membrane displayed a higher decomposition temperature as compared to membrane without APTES-SiO_2 particles

which indicate the composite membranes possesses a higher thermal stability. The decomposition temperatures became higher at higher loading of APTES-SiO_2 particles with a temperature of 409 ºC as compared to 187 ºC of the pristine membrane. This result is in tandem with works by Shen et al. (2012) and Wei et al. (2011) who observed an increase in decomposition temperature with increase in NPs content. This improvement in thermal stability of the composite membranes can be ascribed due to the immobilization of APTES-SiO_2 in the PES matrix through in-situ APTES-SiO_2 cages.

Table 4.16: Decomposition temperature and the ratio of residue difference divided by APTES-SiO_2 of HF membranes

Membrane	Decomposition temperature (ºC) at 3% weight loss	$\frac{\boldsymbol{R_{composite} - R_{pristine}}}{\boldsymbol{APTES - SiO_2}\ (\boldsymbol{wt.}\%)}$
E4-0	187	-
E4-1.2	283	3.250 ± 0.393
E4-2.5	387	3.560 ± 0.232
E4-3.6	372	3.611 ± 0.319
E4-5	409	3.500 ± 0.030

*$\boldsymbol{R_{composite}}$ refers to the residue for composite membranes

*$\boldsymbol{R_{pristine}}$ refers to the residue for controlled membrane

From Figure 4.32, it is clear that the pristine membrane residue was about 31.9%. If the residue of the pristine PES membrane is subtracted from the residue of each composite membranes and the product is divided by the corresponding value of APTES-SiO_2 particles, then the ratio will be approximately similar for all composite HF membranes. From Table 4.16, it can be observed that the ratio of these values were approximately similar with increasing APTES-SiO_2 contents. Thus, it can be concluded from the TGA that the addition of APTES-SiO_2 led to the improvement in thermal stability of the composite membranes.

4.4.1.4 Surface roughness of PES HF membranes

The surface roughness of all membranes were analyzed by AFM and presented in Figure 4.33 (3D images with a size of 20 um x 20 um) and Table 4.17. Surface roughness of membrane is dependent on several factors including solvent type, type and ratio of additive, porosity as well as the type and content of polymer. As seen from the figure, the darkest region and brightest area signifies the valleys and highest point on membrane surface, respectively. As observed, the roughness value of E4-0 HF membrane decreases from 93.672 nm to 65.451 nm and 63.272 nm for 1.2 wt.% and 2.5 wt.% APTES-SiO_2 blended HF membranes, respectively, and then increased to 74.538 nm and 85.924 nm for 3.6 wt.% and 5 wt.% APTES-SiO_2 blended HF membranes, respectively. The smoother surface roughness of the composite HF membranes may be as a result of the strong interactions between APTES-SiO_2 particles in the casting solution and phase inversion kinetics. Blending of APTES-SiO_2 particles in the PES casting solution will reduce the activity of polymer and DMAc, increase thermodynamic stability, thereby decreasing the driving force for DMAc outflow of fiber precipitation in external coagulation bath and accordingly producing membrane with smoother surface roughness. In the low concentration of APTES-SiO_2 particles, because of low electrostatic interactions among the particles, they are regularly collocated, and as a consequence decreases the surface roughness (Hoon et al., 2017). However, when the content of APTEs-SiO_2 particle increases, the combination effect of adsorption and hydrophilicity of APTES-SiO_2 accelerated the exchange between the non-solvent and solvent during the phase inversion. Furthermore, due to the increase in surface pore and higher content of solid content on membrane, membrane surface roughness was increased. This result is in tandem with observation by Vatanpour et al. (2012) who found that

the mean roughness decreases with increase in TiO_2 coated MWCNTs. This is different from observation by Ong and co-workers who found that the nodular shape of TiO_2 NPs resulted in the formation of ridge and valley structure and as a consequence increase the surface roughness (Ong et al., 2015). Basically, an increase in surface roughness signifies that air is not being trapped in the surface pores of the modified membrane (Obaid et al., 2015). Sotto et al. (2012) attributed an increase in the surface roughness of PES/TiO_2 membrane to the formed cluster size on the surface of membrane as a result of particle agglomerations. However, some studies have reported the decrease in surface roughness with increase in NPs loading (Madaeni et al., 2012; Vatanpour et al., 2011; Zinadini et al., 2014). Overall, it can be concluded that the addition of APTES-SiO_2 decreased the surface roughness of the membrane due to improved particle dispersion and distribution in the membrane matrix.

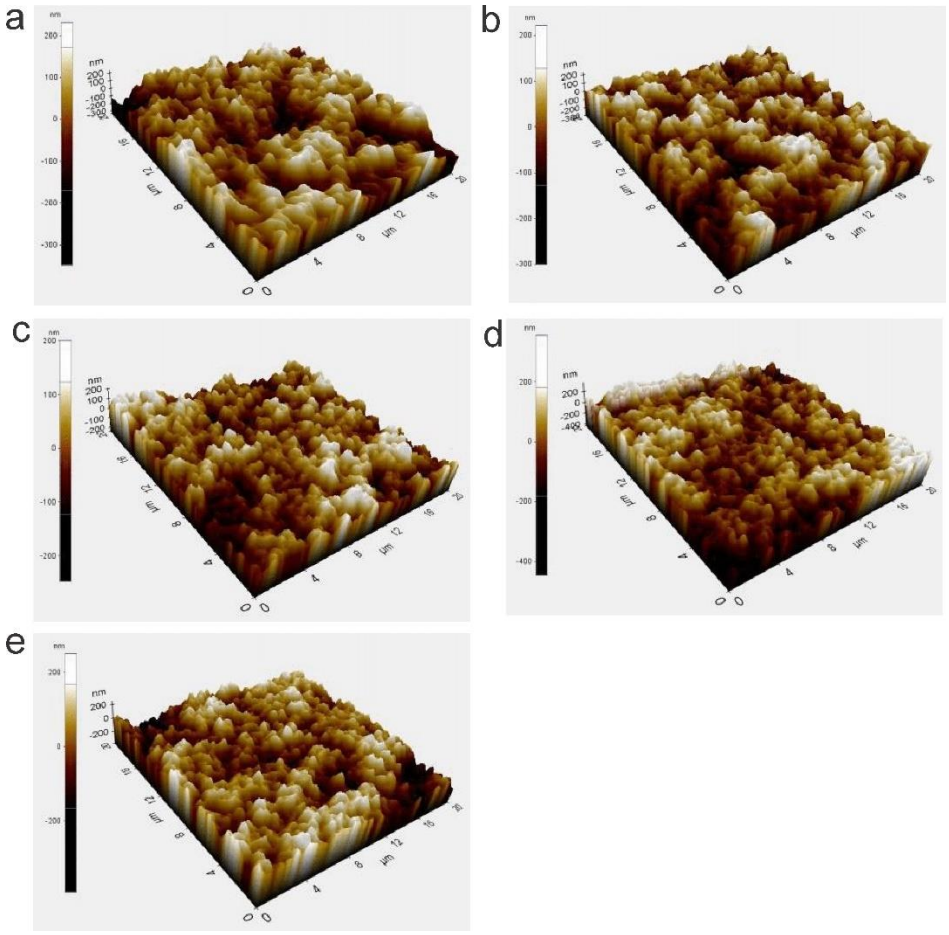

Figure 4.33: AFM 3D surface for (a) E4-0 (b) E4-1.2 (c) E4-2.5 (d) E4-3.6 and (e) E4-5 membrane.

4.4.1.5 Hydrophilicity of PES HF membranes

Contact angle (CA) is ineffective to estimate the surface hydrophilicity as contact angle is also dependent on porosity which is driven by capillary action (Yip et al., 2010). Basically, water CA is a clear indicator of interfacial energy (IE) between the water droplet and membrane surface. The higher the IE, the lower the CA, which will lead to high hydrophilicity. The hydrophilicity of all HFs were determined by water CA. As seen in Figure 4.34, all modified membranes show an improvement in surface hydrophilicity which can be ascribed due to the growth of APTES-SiO_2. The initial contact angle of the pristine membrane was 70.1º whereas

their initial values of the modified membrane ranges from 56.5 to 63.8º. Among all the membranes, E4-1.2 membrane presents a faster decrease in contact angle as well as the lowest contact angle which can be associated due to the existence of hydrophilic APTES-SiO_2 particles. This membrane also displayed the highest pore size among all membranes. Basically, hydrophilic improvement can be due to the effect of APTES-SiO_2 particles generated in the membrane matrix. As such, the molecules of water within the membrane matrix is directed and attracted to absorb into the hydrophilic pores of the membrane (Yin et al., 2012), and this will encourage the permeability of water to improve (Yang et al., 2007).

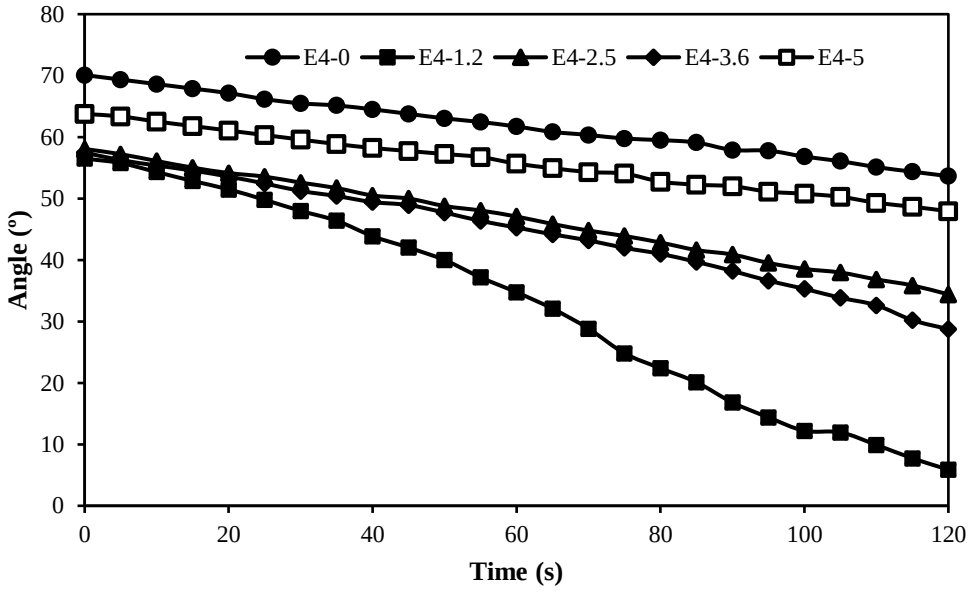

Figure 4.34: Dynamic contact angle of E4-0, E4-1.2, E4-2.5, E4-3.6 and E4-5 HF membranes.

Some studies have shown that the decay rate of nanocomposite membrane can be governed by factors including roughness, hydrophilicity, wettability of inner pore channels and pore size (Li et al., 2009; Zhang and Wang, 2014). From the

result, E4-1.2 membrane presents a better hydrophilicity and as such is thought to give a better resistance against fouling during wastewater filtration.

4.4.1.6 Pore size, porosity and pore size distribution of PES HF membranes

Another factor which could also influence the surface hydrophilicity is the pore size and porosity. For this reason, the membrane porosity and the pore size were determined and presented in Table 4.17. By contrast, data shows that all modified membrane displayed higher porosity than controlled membrane. It has been generally reported that the addition of NPs could increase porosity of membrane. However, an increase in porosity with increase in APTES-SiO_2 content in membrane matrix was insignificant as all membranes displayed reasonably higher porosity (between 79.64 and 83.45%). In a similar study by Lishun et al. (2010) who shows that porosity was not significantly influenced by varying particle content. It is thus believed that the presence of PEG which is hydrophilic and of high MW contributed immensely to the high porosity among all membranes. The presence of PEG might induce solution de-mixing during phase inversion, improve phase separation which will cause macro-pores to be enlarged and as a consequence lead to high porosity.

Table 4.17: Pore size (μ_p), porosity and roughness (Ra) of E4-0, E4-1.2, E4-2.5, E4-3.6 and E4-5 membranes.

Membrane	μ_p (nm)	Porosity (%)	Ra (nm)
E4-0	41.61±0.82	82.67±2.46	93.672
E4-1.2	51.63±0.25	81.55±3.14	65.451
E4-2.5	43.21±0.76	83.45±2.58	63.272
E4-3.6	45.18±0.11	79.64±2.84	74.538
E4-5	42.51±0.14	80.62±3.63	85.924

Pore size of PES/APTES-SiO_2 HF membrane was found to be higher upon addition of APTES-SiO_2 up to 1.2 wt.%, but decreases with further particle dosage. The rapid increase in pore size obtained for E4-1.2 HF membrane could be due to the rapid solvent exchange that took place during phase inversion which might have resulted in leaching of a small number of APTES-SiO_2 particles or incompatibility between polymer chains and particles, causing the formation of bigger pores. The reduction in pore size at higher particle concentration might be due to the slow exchange rate or diffusion of DMAc and water during gelation process, which forms a smaller pore on membrane surface. Among all membranes, the lowest pore size was recorded for E4-0 membrane. The pore size of E4-5 and E4-2.5 were observed to be nearly similar. Among all membranes, the narrowest pore size distribution was observed for E4-2.5 membrane (Figure 4.35). The pore size of E4-0 and E4-5 HF membranes were also found to be nearly similar. Several authors have also reported that an increase in pore size will significantly influence the surface properties of membrane. Alsalhy et al. (2013) observed that the pore size of membrane increases at low concentration of ZnO. They concluded that such increase led to an increase in surface roughness.

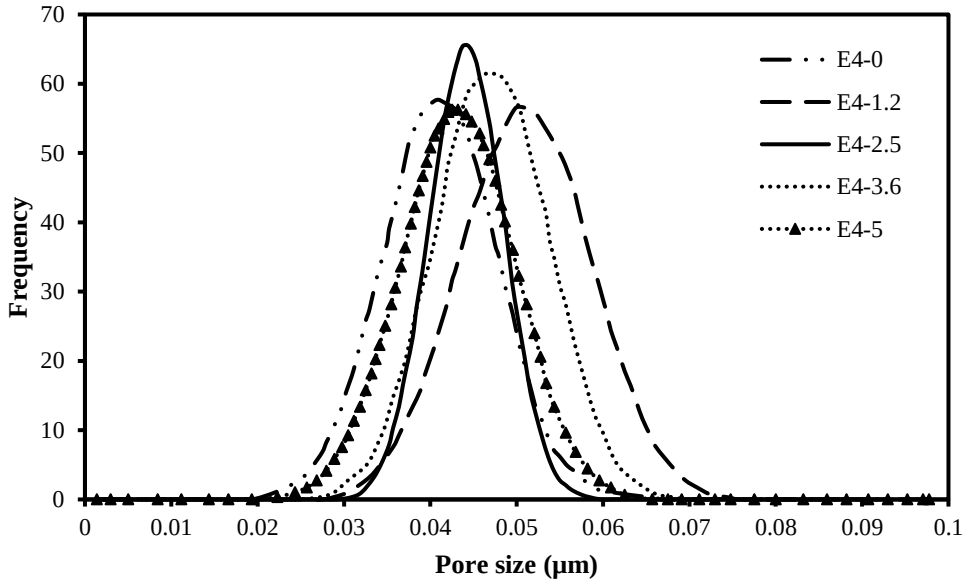

Figure 4.35: Pore size distributions of E4-0, E4-1.2, E4-2.5, E4-3.6 and E4-5 HF membranes.

With reference to Figure 4.34, it was observed that the dynamic contact angle of E4-5 HF membrane was not significantly different with that of the controlled membrane. This signifies that the membrane displayed no significant change in the dynamic contact angle. Therefore, the low tendency of E4-5 HF membrane to attract water molecules can be ascribed due to the effects of its narrower pore size distributions and smaller pore size.

4.4.1.7 FTIR Spectra of PES HF membranes

The purpose of FTIR spectroscopy analysis for composite membrane is to provide useful information that relates to the functional groups and molecular structures of the as-prepared membrane. Attenuated total reflection fourier transform infrared spectroscopy was employed and the spectra are presented in Figure 4.36.

The broad adsorption peak at 944 cm^{-1} correspond to the Si-OH stretching while the broad peak of 817 cm^{-1} corresponds to the symmetric vibration stretching of Si-O (Muhamad et al., 2015b; Yu et al., 2015). The presence of amino groups associated with 3-aminopropyltriethoxysilane was also observed. Two small shoulder peaks at 3347 cm^{-1} and 3290 cm^{-1} corresponds to the N-H asymmetric stretching of the amine H-bonds, indicating a possible interaction of NH_2 toward PES surface (Aneja et al., 2015; Wang et al., 2013). The presence of an additional new N-H vibration peak, observed at around 1668 cm^{-1} results from the existence of free $–NH_2$ group (Miao et al., 2016). By going from E4-0 to E4-5 HF membrane, the strength of –OH stretching peaks at 3438 cm^{-1} is enhanced which signifies that more hydrogen bonding is formed by introducing APTES-SiO_2 particles into PES membrane matrix (Muhamad et al., 2015b). These functional groups are responsible for improving surface hydrophilicity as well as fouling mitigation.

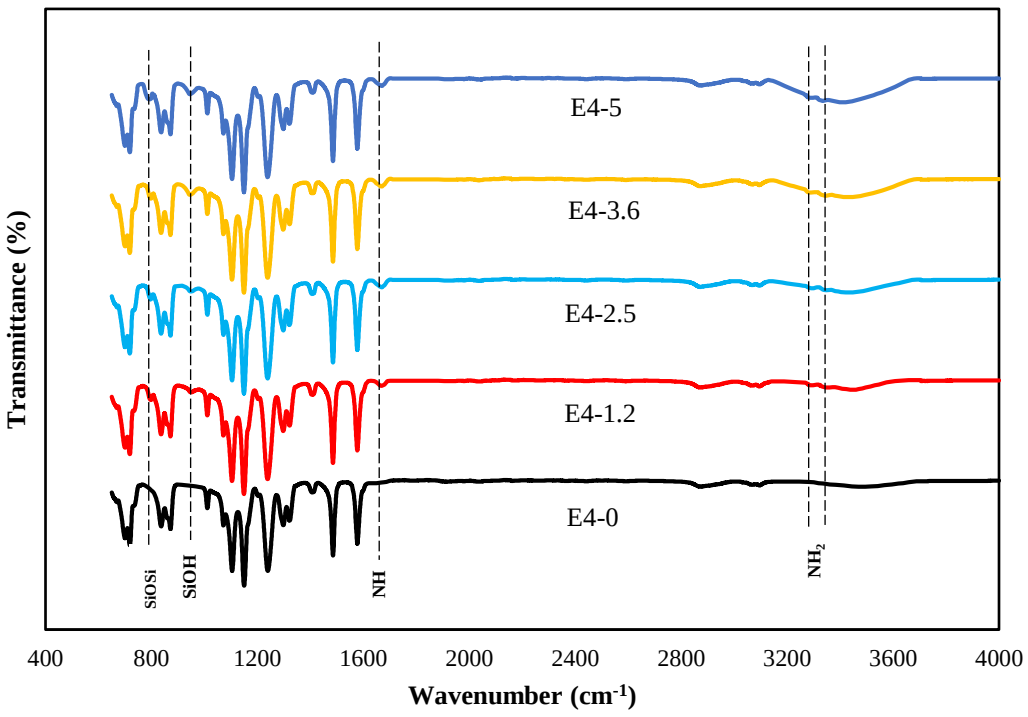

Figure 4.36: FTIR spectra of E4-0, E4-1.2, E4-2.5, E4-3.6 and E4-5 HF membranes.

4.4.1.8 Mechanical properties of PES HF membranes

The mechanical properties of the membrane which are of significant importance for wastewater applications. The break strain, maximum strain and maximum stress of PES membranes are shown in Table 4.18. As observed, all modified membrane displayed high maximum stress in the range of 3.757 to 4.103 MPa as compared to pristine membrane (3.814 MPa). The first reason for the improved mechanical properties is that SiO_2 itself has intrinsic and desirable good mechanical strength, which can alter the conditions of the process (Ju et al., 2015; Mazzoccoli et al., 2010). As indicated, the break strain, maximum strain and maximum stress of all membranes were all increased when APTES-SiO_2 were embedded in the matrix. The mechanical properties increases with increase in APTES-SiO_2 content up to 3.6 wt.% and decreased with further increase in APTES-SiO_2. The reasons for this phenomenon might be thought as follows. As APTES-SiO_2 particles were evenly dispersed and distributed in PES matrix and thus, PES chain could strongly interacts well with the particles via bonding with hydrogen (Roh et al., 2010; Yano et al., 1998) and as a consequence, the chains were entrapped between the precipitate of silica. Additionally, the improvement in mechanical properties could be as a result of the ability of APTES-SiO_2 to act as cross-linked point which can enhance the rigidity of PES chain. Meanwhile, when the ratio of APTES-SiO_2 particles was > 3.6 wt.%, the resultant APTES-SiO_2 particles in PES matrix caused the membrane rigidity to increase, causing the mechanical properties to decrease. Excessive increase in APTES-SiO_2 particles ratio can lead to a significant decrease in the dispersion of the APTES-SiO_2 particles, leading to defects formation and membrane stress convergence points under the force of loading and as a consequence will deteriorate the mechanical properties of the membrane.

Table 4.18: Break strain, maximum strain and maximum stress of PES blend membranes

Membrane	Maximum stress (MPa)	Break strain (%)	Maximum strain (%)
E4-0	3.814 ± 0.265	21.307 ± 2.417	20.325 ± 2.548
E4-1.2	3.906 ± 0.213	23.202 ± 1.831	20.409 ± 3.417
E4-2.5	4.035 ± 0.156	31.518 ± 2.775	28.913 ± 3.298
E4-3.6	4.103 ± 0.154	32.223 ± 2.447	28.712 ± 2.858
E4-5	3.757 ± 0.156	19.101 ± 2.775	15.830 ± 3.298

In conclusion, various characterization have shown that APTES-SiO_2 have been successfully incorporated in PES matrix. SEM micrographs show well distributed APTES-SiO_2 clusters on the surface of the membranes. Result also indicated that the skin-layer thickness were governed by gravitational elongation. The lowest outer skin layer thickness was obtained from membranes with 1.2 wt.% and 2.5 wt.% APTES-SiO_2 particles. The incorporation of varying content of APTES-SiO_2 particles led to decrease in surface roughness. In terms of hydrophilicity, the lowest WCA and highest decay rate was obtained for membranes with 1.2 wt.% APTES-SiO_2 particles.

4.4.2 Performance evaluations of PES/APTES-SiO_2 HF Membranes at different APTES-SiO_2 loading

This section evaluates the performance such as permeate flux and oil rejection of PES/APTES-SiO_2 membrane at different APTES-SiO_2 loading. The experimental results are presented in Table 4.19. As observed, the highest permeate flux was achieved for membrane with 1.2 wt.% APTES-SiO_2 particles, while the lowest flux was achieved for membrane with 5 wt.% APTES-SiO_2 particles. As observed from Table 4.19, the permeate flux (PF) of PES membrane increases from 134.63 to 168.14 kg/m^2 h with increase in concentration of APTES-SiO_2 from 0 to

1.2 wt.%, signifying ~ 24.9% improvement in permeability. This flux decreases when APTES-SiO_2 content increased further above 1.2 wt.%, and their permeate fluxes value were higher than the controlled membrane except for E4-5 HF membrane. This significant improvement can be attributed due to the improved surface hydrophilicity as observed in Figure 4.34, in addition to increased dimension of pores upon the introduction of APTES-SiO_2 particles. An increase in APTES-SiO_2 particles > 1.2 wt.% caused decline in PF which might be as a result of decrease in pore size. A decrease in membrane PS at higher APTES-SiO_2 can be a result to excess loading of the APTES-SiO_2 particles (as can be observed in Figure 4.35). Similar observations have been reported by other researchers who have stated that when particles are excessively loaded, they tend to influence the properties of membranes due to the non-uniformity in the dispersion of nanoparticles (Damodar et al., 2009; Yu et al., 2009; Yuliwati et al., 2011).

Table 4.19: PF and OR of E4-0, E4-1.2, E4-2.5, E4-3.6 and E4-5 membranes.

Membrane	PF ($kg/m^2 h$)	Oil rejection (%)
E4-0	134.630±6.078	97.23 ± 0.010
E4-1.2	168.140±9.565	98.79 ± 0.035
E4-2.5	159.880±7.318	99.87 ± 0.026
E4-3.6	163.590±5.122	99.84 ± 0.062
E4-5	129.430±6.966	99.91 ± 0.061

The improvement in the PF could also be as a result of the skin-layer thickness and porosity which were discussed earlier where it was observed that the outer skin-layer thickness of E4-1.2, E4-2.5 and E4-3.6 HF membranes were thinner, coupled with higher porosity as compared to other membranes. Thus, the combination of these factors might enhance the attraction of molecules of water inside the membrane matrix, and as such will cause water to penetrate easily through

the membrane. Similar observation was reported by Shen et al. (2012b) works by who found that a maximum permeability was obtained for PES/ZnO membrane with highest porosity.

As observed from Table 4.19, all composite membranes exhibited a high oil rejection as compared to the controlled membrane. The rejection of all modified membrane shows no significant changes occurred for all membrane in respect to varying content of APTES-SiO_2 particles. However, the oil rejection decreased in the order of E4-5>E4-2.5>E4-3.6>E4-1.2>E4-0. The highest oil rejection was obtained for E4-5 membrane which was as high as 99.91% as compared to the controlled membrane of 97.23%. Among all membranes, E4-1.2 shows the highest permeate flux but show the lowest oil rejection among all modified membrane. The relatively increase in permeate flux and oil rejection of all composite membranes can be attributed to the incorporation of APTES-SiO_2 in the membrane matrix and the enhanced hydrophilicity of the membrane.

4.4.3 Fouling evaluations of PES/APTES-SiO_2 HF Membranes

Fouling is a complex phenomenon which can be best evaluated by monitoring the relative flux decline with time during solute (oil) separation (Li et al., 2009). Figure 4.37 presents the relative flux with time for all PES HF membranes.

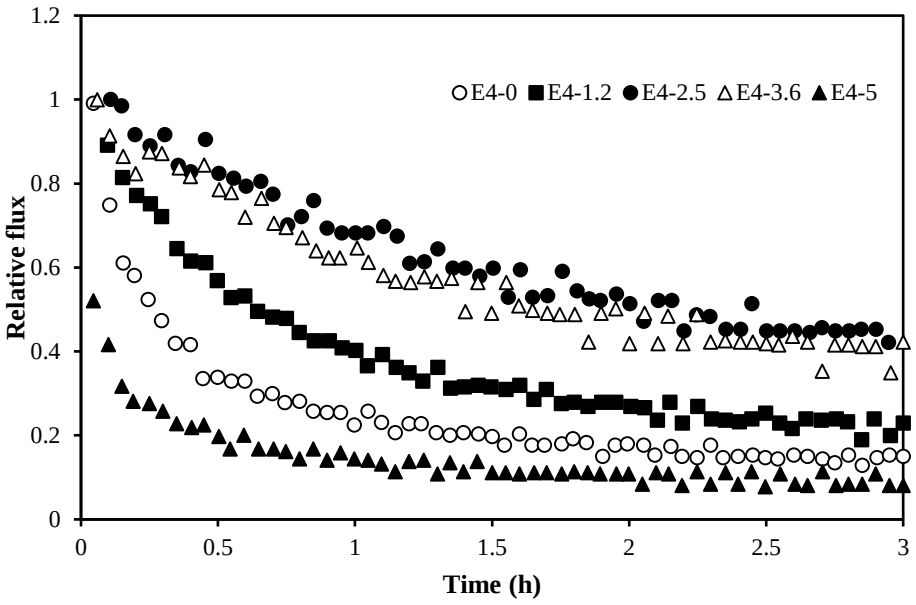

Figure 4.37: Relative flux of E4-0, E4-1.2, E4-2.5, E4-3.6, and E4-5 HF membranes (operating conditions: feed flow rate = 0.45 L/min, TMP = 1.5 bar, time = 3 h, feed concentration = 250 mg/L of oil-in-water emulsion.

The relative flux reduction was observed immediately after the oil-in-water emulsion was introduced into the filtration due to the adsorption and deposition of the oil droplet onto the surface of the membrane. Basically, the decline phenomenon in relative flux of all membranes is common as the existence of oil molecules in the feed solution might rapidly build up on the surface of membrane, which creates an additional water transport resistance to permeate and as a consequence lead to decline in relative flux due to increased resistance as a result of increased compression of additional layer (Khamforoush et al., 2015). As shown in Figure 4.37, membrane prepared with 5 wt.% APTES-SiO_2 (E4-5) demonstrated the highest relative flux decline followed by E4-0, E4-1.2, E4-3.6, E4-2.5 in descending order of E4-2.5< E4-3.6< E4-1.2< E4-0< E4-5. As observed, membrane prepared with 2.5 wt.% APTES-SiO_2 (E4-2.5) demonstrated the lowest relative flux declination. The

lower relative flux declination experienced by E4-2.5 membrane can be as a result of the enhanced hydrophilicity with its narrowest pore size distribution and moderate pore size.

The anti-fouling behavior of the membranes in terms of relative flux recovery (RFR) and flux recovery ratio (FRR) were introduced and their values are displayed in Table 4.20. Generally, a lower RFR and a higher FRR value signifies a better anti-fouling property and that oil droplets deposited on membrane surface could be easily cleaned by back-flushing. As observed, the RFR value of 38.636±3.763%, 33.308±2.579%, 29.723±1.273%, 31.730±0.589%, and 39.062±2.757% were obtained for E4-0, E4-1.2, E4-2.5, E4-3.6 and E4-5 membranes, respectively. E4-5 membrane possessed the highest RFR value among all modified membranes whereas the RFR of E4-2.5 membrane was apparently having the lowest RFR. Other membranes show no significant differences in RFR values. This result indicate that the anti-fouling capability of the membrane has been enhanced upon doping with 2.5 wt.% APTES-SiO_2 content.

Table 4.20: FRR, RFR and membrane fluxes of E4-0, E4-1.2, E4-2.5, E4-3.6 and E4-5 membranes.

Memb.	$Jwf1$ (kg/m^2 h)	J_{wf2} (kg/m^2 h)	J_s (kg/m^2 h)	FRR (%)	RFR (%)
E4-0	219.397±8.49	177.29±7.79	134.630±6.078	80.808±1.683	38.636±3.763
E4-1.2	252.115±10.70	223.704±11.72	168.140±9.565	88.731±1.486	33.308±2.579
E4-2.5	227.500±11.37	212.251±8.82	159.880±7.318	93.464±1.347	29.723±1.273
E4-3.6	239.622±9.31	209.680±12.68	163.590±5.122	87.505±2.207	31.730±0.589
E4-5	212.397±11.93	167.249±6.23	129.430±6.966	78.744±4.660	39.062±2.757

In addition, the FRR value of 80.808±1.683%, 88.731±1.486%, 93.464±1.347%, 87.505±2.207% and 78.744±4.660% were achieved for E4-0, E4-1.2, E4-2.5, E4-3.6 and E4-5 membranes, respectively. The highest FRR was achieved with E4-2.5 HF membrane, and the lowest FRR was obtained at 5 wt.% of APTES-SiO_2 (E4-5). The reason for the highest FRR obtained for E4-2.5 HF membrane can be ascribed due to the decrease in surface roughness. Basically, a decrease in surface roughness signifies that the membranes are less susceptible to fouling due to the availability of less adsorption sites for oil attachments.

Figure 4.38 presents the total resistances, reversible and irreversible resistance of all membranes. Irreversible and reversible resistance are also important parameters to evaluate membrane fouling. Basically, reversible fouling can be recovered by simple washing whereas irreversible fouling can only be cleaned by chemical treatment. A higher Rr signifies an enhanced self cleaning ability whereas a lower Rir signifies a higher antifouling effect (Zhao et al., 2013). For PES/APTES-SiO_2 HF membrane, the Rr of membrane with 2.5 wt.% APTES-SiO_2 particles was significantly higher than other composite membrane and E4-0 membrane, while the Rir of all composite membrane (except membrane with 5 wt.% APTES-SiO_2 particles) for the pristine was lower in comparison with the pristine membranes which indicates that the fouling resistance upon incorporation of APTES-SiO_2 particles in the PES HF membrane was significantly influenced. For E4-1.2, E4-2.5 and E4-3.6 HF composite membrane, the dominant resistance is reversible and cleaning procedure is more efficient whereas for the E4-5 HF composite membrane, the fouling mechanism may have a higher contribution of pore plugging which could be more difficult to remove using simple physical cleaning. Coupled with the best

performance in terms of permeate flux, rejection, FRR and RFR, E4-2.5 HF membrane demonstrated the best membrane resistance among all other composite membranes. However, by taking cognizance of the permeate flux and rejection, it can be concluded that PES composite membrane (E4-2.5) was found to be best membrane, as it achieved less flux reduction, high permeate flux and excellent oil rejection. This can be ascribed due to the enhanced hydrophilicity and the moderate pore size and narrowest PSD as well as abundant APTES-SiO_2 particles on the membrane, which affects oil sorption on membrane surface.

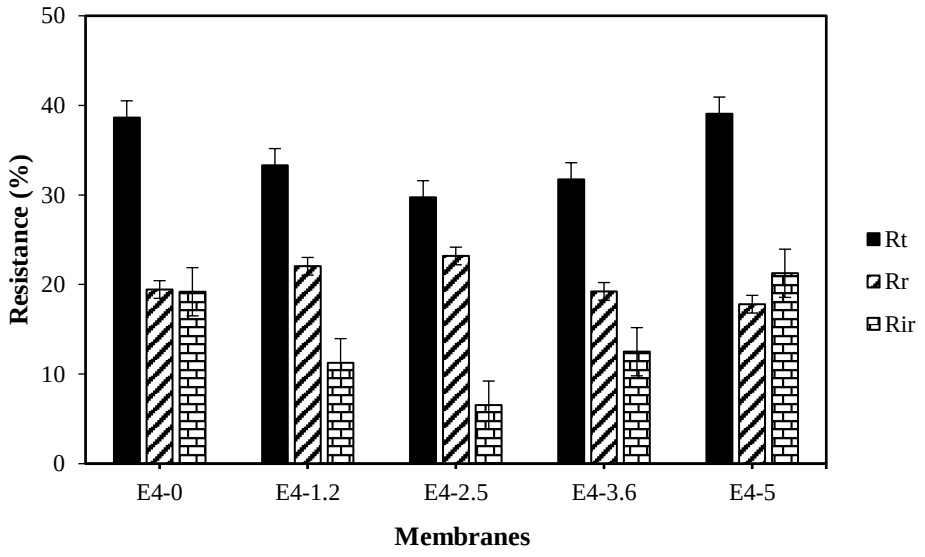

Figure 4.38: Results of fouling resistance of E4-0, E4-1.2, E4-2.5, E4-3.6 and E4-5 HF membranes.

In this section, it has been shown that the incorporation of well dispersed APTES-SiO_2 helped to improve membrane hydrophilicity which subsequently produce membrane with better performance and fouling resistance. Based on the performance of the composite membrane, E4-2.5 HF membrane has been chosen for further subsequent analysis which will be discussed in the following sections.

4.5 Influence of Operating Conditions on Membrane Performance

The influence of operating conditions including oil concentration, transmembrane pressure and feed flow rate during UF are very crucial issues during practical applications. This section evaluates the performance of the PES/APTES-SiO_2 membrane (E4-2.5) in term of oil rejection and PWF at those varying conditions. The oil concentration varies from 100 to 500 mg/L, TMP varied from 1.0 to 2 bar, and the feed flow rate varies from 0.15 to 0.75 L/min.

4.5.1 Effect of transmembrane pressure

The membrane was tested at different transmembrane pressure (TMP) include 1.0, 1.5, 2.0 bar while other operating conditions such as feed flow rate and concentration were set at fixed value of 0.45 L/min and 250 mg/L, respectively. Table 4.21 presents the initial PWF at different TMPs from 1.0 to 2.0 bar. As observed, the initial PWF value of 124.10 ± 6.89 kg/m^2 h, 227.500 ± 11.37 kg/m^2 h and 328.87 ± 11.58 kg/m^2 h were observed under TMP of 1.0 bar, 1.5 bar and 2.0 bar, respectively. This shows that the PWF increases with increase in TMP which can be due to the increase in driving force exerted on membrane which causes an increase in the passage of water.

Table 4.21: Effect of TMP on initial PWF of composite membrane

TMP (bar)	Initial PWF (kg/m^2 h)
1.0	124.10 ± 6.89
1.5	227.50 ± 11.37
2.0	328.87 ± 11.58

Figure 4.39 presents the effect of TMP on relative flux during oil emulsion filtration. As seen, the relative flux (RF) declination were observed at all TMP which can be due to the deposition of oil droplet on the surface of the membrane. This relative flux reduces significantly with increase in TMP. The condensation polarization (CP) and cake gel tends to be formed immediately after the process commenced. For TMP of 1.0 bar and as compared to other TMP (1.5 and 2.0 bar), the RF displayed a much slower rate of declination at the beginning of the process which can be as a result of lower fouling effect at low pressure. However, with increase in TMP, RF declination at the initial stage increases. Meanwhile, RF reduction rate was observed to be higher at higher TMP which can be due to layer compression of oil and the increase in rate of fouling, which tends to block the pores of the membrane (Chakrabarty et al., 2010; Yi et al., 2012).

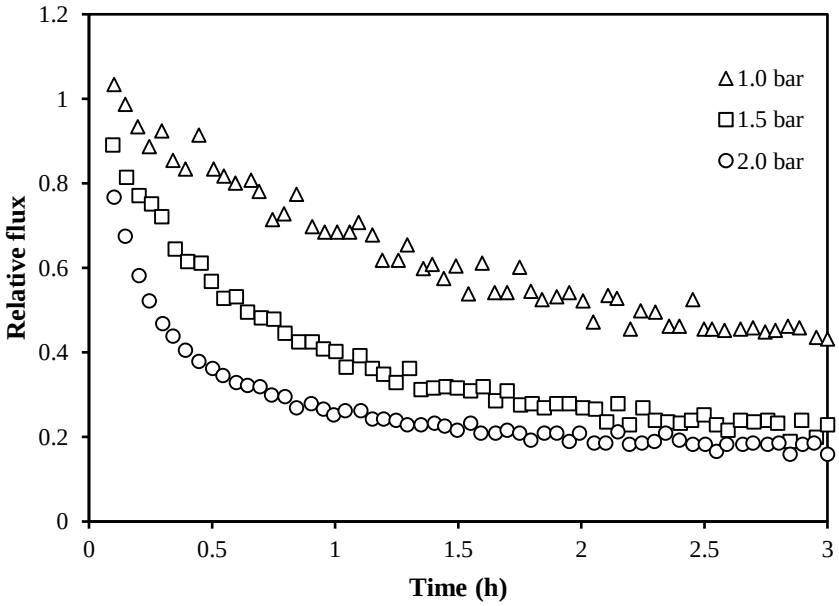

Figure 4.39: Effect of TMP on relative flux with time during oil emulsion filtration (at 0.45 L/min and 250 mg/L).

At a point in the process, the flux at all TMP attained a steady state due to the slow growth of compacted oil deposit (Van den Berg and Smolders, 1990). However, the relative flux decreased in the order of 2.0 bar > 1.5 bar > 1.0 bar. At the end of the filtration, the RF dropped down to 0.159, 0.229 and 0.432 for 2.0 bar, 1.5 bar and 1.0 bar, respectively. The nature of membrane fouling such as cake layer or pore blocking at elevated TMP is important. Under pore blocking phenomenon, the value of FRR will be relatively low as a consequence of irreversible fouling effect. Figure 4.40 displays the influence of TMP on oil rejection and FRR during oil-in-water emulsion filtration. The rejection of oil was observed to slightly increase at lower TMP, in which the value of 99.47%, 99.87% and 100% were obtained for 2.0 bar, 1.5 bar and 1.0 bar respectively. At high TMP, there tends to be a deformation in the structure of oil emulsion which will cause oil droplet to be squeezed out of the membrane, and as a consequence lead to reduction in oil removal efficiency (Saadati and Pakizeh, 2017). To avoid irreversible pore blockage, an operating pressure that is not more than 1.5 bar is therefore suggested in order to reduce the functionality of the membrane. After oil emulsion filtration, the membrane was subjected to cleaning with deionized water and the FRR were calculated and presented in Figure 4.40. As observed, the FRR value of 79.22 %, 93.46 % and 99.37 % were achieved under TMP of 2.0 bar, 1.5 bar and 1.0 bar, respectively. The FRR value of membrane operated at higher TMP were much lower than when operated at lower TMP. At elevated TMP, there was an occurrence of pore blocking which can be difficult to control and cleaned using simple physical cleaning method.

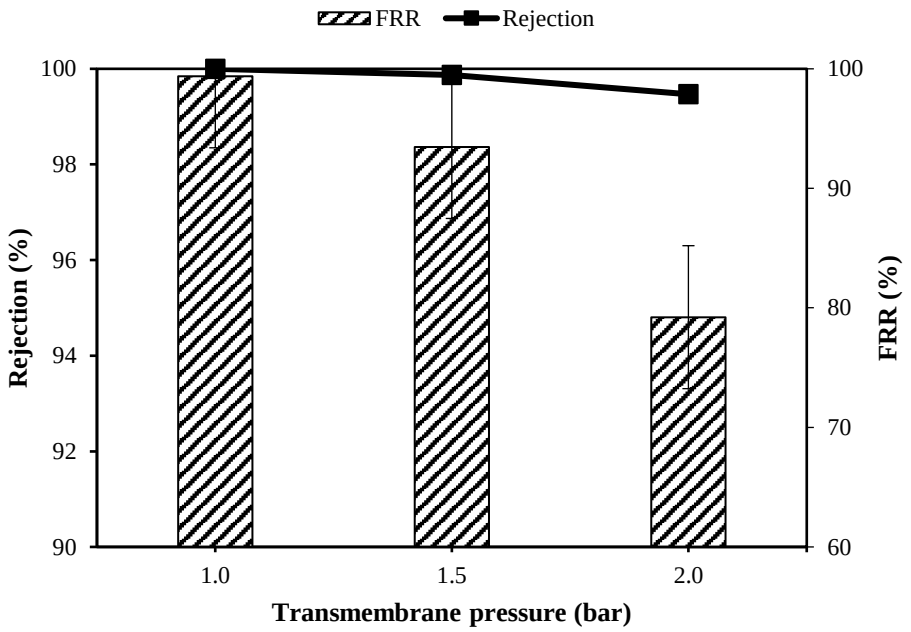

Figure 4.40: Effect of TMP on oil rejection and FRR during oil emulsion filtration (at 0.45 L/min and 250 mg/L).

4.5.2 Effect of Feed Flowrate

The influence of varying feed flow rate (FFR) is also an important parameters was also evaluated. The FFR including 0.15 L/min, 0.45 L/min and 0.75 L/min while other operating conditions such as feed concentration and TMP were set at fixed value of 250 mg/L and 1.5 bar, respectively. Figure 4.41 presents the effect of FFR on relative flux during oil emulsion filtration. As observed, the relative flux slightly increases with increase in feed flow rates from 0.15 L/min to 0.75 L/min. This behaviour is almost similar to that of the TMP. The relative flux improvement at high flow rate is likely due to the generation of circulation flow in the ultrafiltration system, which limits the oil absorbed onto the surface of the membrane. This shows that at the higher feed flow rate (0.75 L/min), the oil droplet can be easily swept away while preventing the further build-up of cake layer on the surface of membrane.

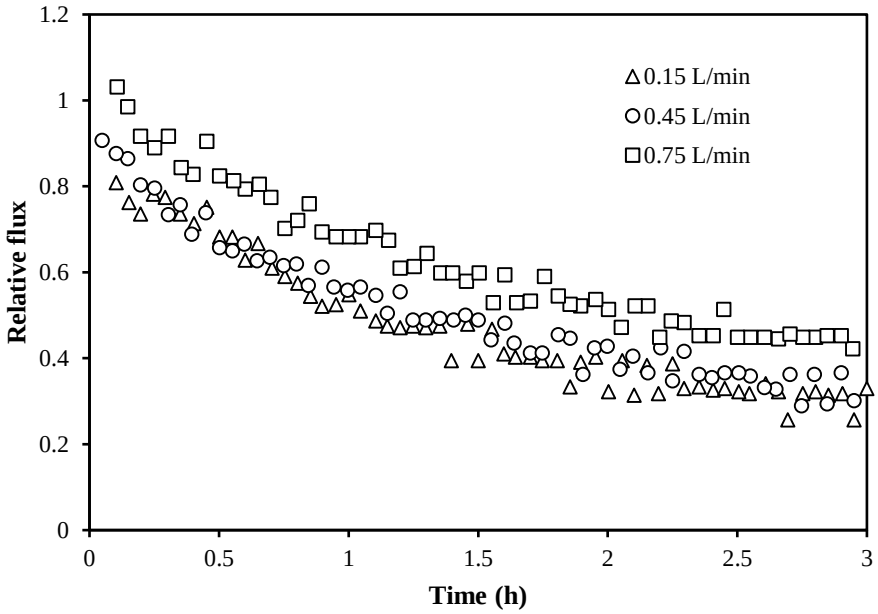

Figure 4.41: Effect of FFR on relative flux with time during oil emulsion filtration (at 1.5 bar and 250 mg/L).

Figure 4.42 displayed the influence of FFR on oil rejection and FRR during oil emulsion filtration. As observed, oil rejections of the membrane at varying FFR were all found to be above 99 %. In terms of FRR measurement after washing with deionized water, it was found that the membrane achieved above 90% for all flow rate which signifies that the FFR has less influence on FRR.

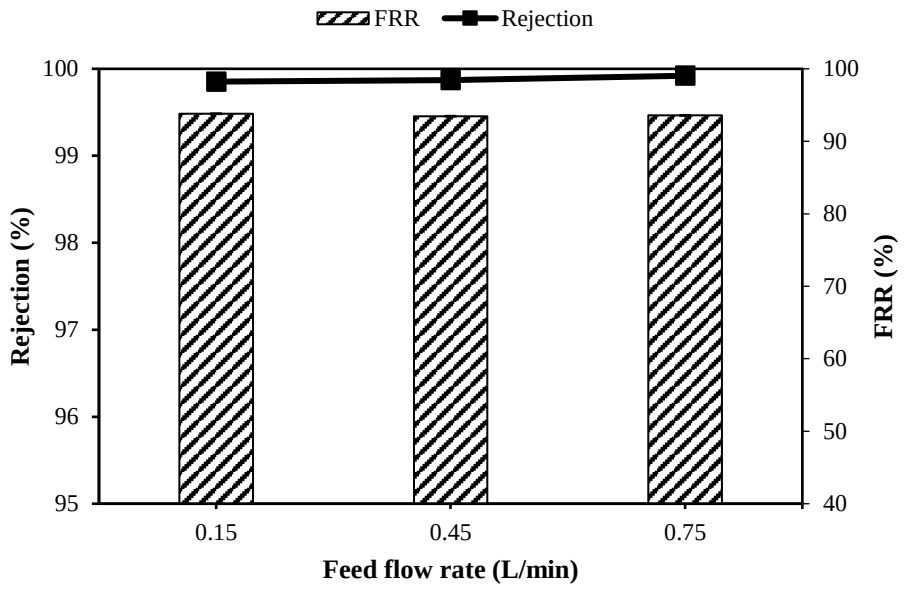

Figure 4.42: Effect of TMP on oil rejection and FRR during oil emulsion filtration (at 1.5 bar and 250 mg/L).

4.5.3 Effect of Feed Concentration

The feed concentration (FC) of oil emulsion including 100 mg/L, 250 mg/L and 500 mg/L while other operating conditions such as feed flow rate and TMP were set at fixed value of 0.45 L/min and 1.5 bar, respectively according to previous result. Figure 4.43 presents the effect of FC on relative flux during oil emulsion filtration. At the end of the filtration, the RF dropped down to 0.139, 0.421 and 0.906 for 500 mg/L, 250 mg/L and 100 mg/L, respectively. Similar observation was reported in a work by Ong et al. (2015) who showed that upon higher concentration of solute, there is a higher chance of flux decline which was associated due to the higher droplet of oil which induced the formation of thicker layer of oil. The build-up of thicker droplet of oil will increase the membrane resistance and as such lead to flux reduction (Yi et al., 2011). Two contributing factor for flux reduction in this observation can be related due to formation of thicker cake layer and increased

osmotic pressure. At higher concentration of oil, there is a high chance of excessive deposition of cake layer on the gel layer, leading to increased transport resistance.

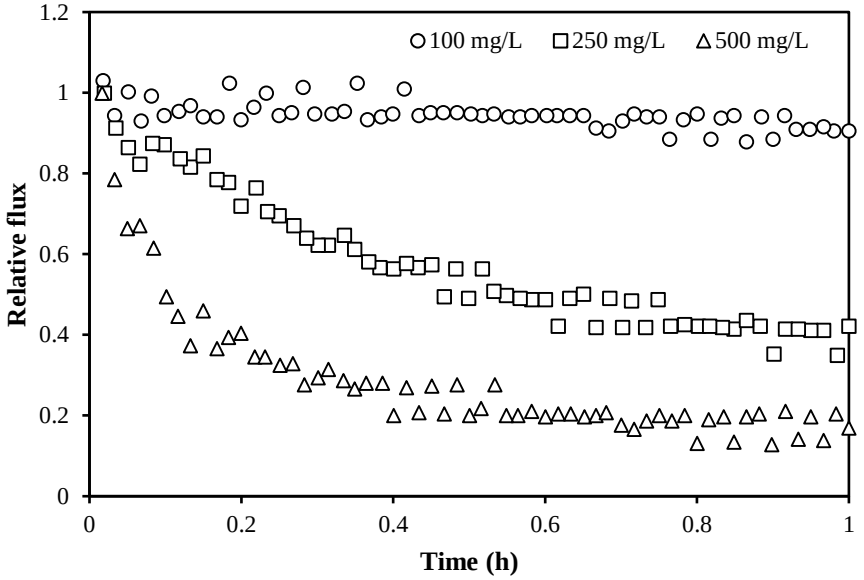

Figure 4.43: Effect of feed concentration on relative flux with time during oil emulsion filtration (at 1.5 bar and 0.45 L/min).

Figure 4.44 displayed the influence of FC on oil rejection during oil emulsion filtration. As observed, the oil rejection value of up to 91.58%, 99.87% and 100% was achieved under FC of 500 mg/L, 250 mg/L and 100 mg/L, respectively. The reason for the slight change in rejection could be due to bigger mean droplet to pore size ratio. When the concentration is high, the driving force (concentration gradient) will drive the feed to diffuse through the membrane. But due to the smaller pore size, the steric effect tends to be hindered. All membrane were still able to maintain a higher rejection value of ~90% at different oil concentration.

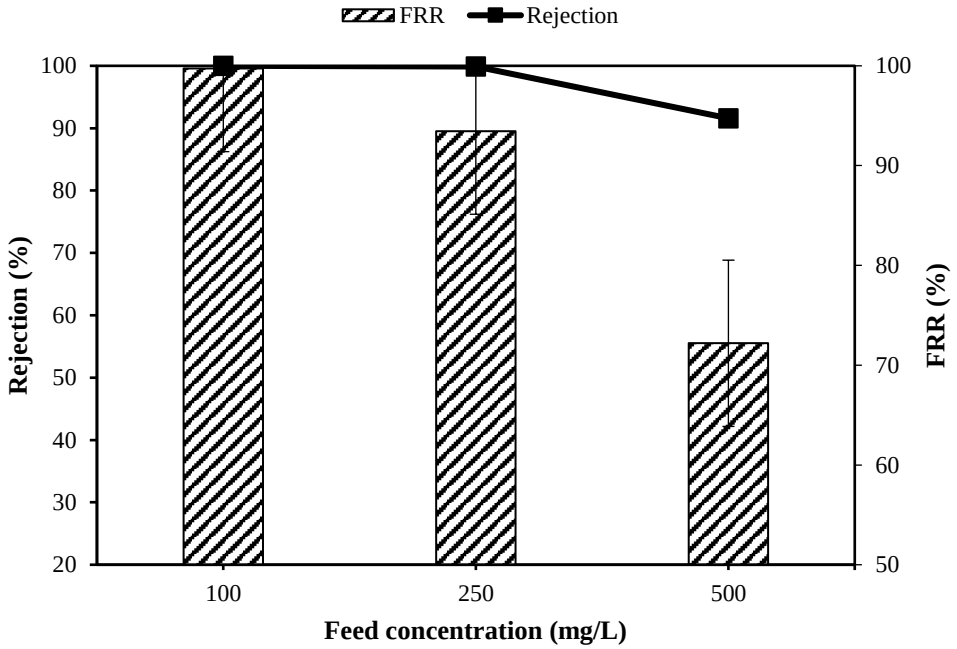

Figure 4.44: Effect of FC on oil rejection and FRR during oil emulsion filtration (at 1.5 bar and 0.45 L/min).

Figure 4.44 displays the influence of FFR on oil rejection and FRR during oil emulsion filtration. As observed, the FRR value of 72.19 %, 93.46 % and 99.73% were achieved under FFR of 500 mg/L, 250 mg/L and 100 mg/L, respectively. The lowest FRR values was achieved under the highest oil concentration (500 mg/L) which can be as a result of deposition of thicker layer of oil on the membrane surface which had been earlier explained and as such makes it difficult to be cleaned by simple washing method.

4.6 Fouling mechanism of E4-2.5 HF membrane

The convective flux through the membrane will lead to the formation of fouling layer on membrane surface and subsequently caused flux decline (Todisco et

al., 1996). The composite membrane (E4-2.5) was subjected to filtration at 1.5 bar of operating pressure, 0.45 L/min of feed flowrate, oil emulsion concentration was fixed at 250 mg/L and filtration time of 3 h. Figure 4.45 presents the experimental permeate flux decline tested during the UF of synthetic oil-in-water emulsion.

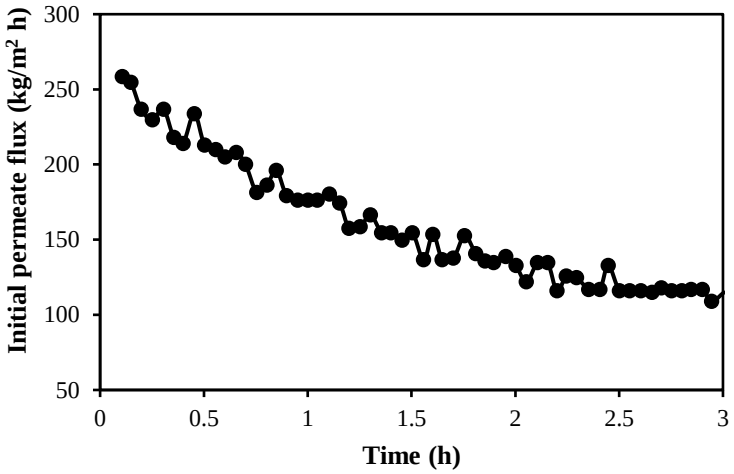

Figure 4.45: Initial permeate flux of PES/APTES-SiO_2 (E4-2.5) HF membrane.

The flux reduction in Figure 4.45 can be described by using the pore blocking models. As mentioned earlier, various mathematical expressions have been developed to describe the membrane flux under fouling conditions. For this reason, the fouling mechanisms of the synthesized PES/APTES-SiO_2 composite membrane was predicted and analyzed through classical blocking models. Curve-fit of the experimental permeation data to the classical filtration models (Table 2.5) is a simple way to predict the membrane fouling mechanisms. The fouling mechanisms of the composite membrane was represented by the best fitted fouling mechanisms with a maximum coefficient.

Figure 4.46 (a-d) show the plot of accumulated permeate volume versus the filtration time for experimental data and predicted data from different fouling mechanisms model. Furthermore, the calculated R^2 values were also represented in Table 4.22. When R^2 values obtained for four models are compared, it can be said that the higher R^2 value corresponds to a better fit of the model. However, as shown in Table 4.22, the classical intermediate blocking fouling mechanism fit the experimental data up to the greatest accuracy with the highest coefficient of 0.97346 making the intermediate blocking mechanism the dominant fouling mechanism. The intermediate blocking was followed by cake filtration, standard blocking and complete blocking, in descending order. Complete blocking showed the least severe fouling (with the smallest value of the model parameter).

This result proved that the gradual reduction of the permeate flux over time in this work has a good correlation with the intermediate pore blocking model (n = 1) which is demonstrated by the best-fitted line based on correlation coefficient (R^2). Intermediate blocking is a surface phenomenon showing that particle size/oil droplet is bigger than the pore size and it is basically contributed by both cake layer and complete blocking which is very much represented by the characteristic of the gel layer.

Table 4.22: Models fitting accuracy for the ultrafiltration of oil-in-water emulsion at 25 °C, 1.5 bar and 0.45 L/min: values of R^2 and coefficients.

Model	R^2	k
Cake filtration (n=0)	0.96928	1.04777E-5
Intermediate pore blocking (n=1)	**0.97346**	0.00194
Standard pore blocking (n=1.5)	0.95597	0.02635
Complete pore blocking(n=2)	0.92192	0.35285

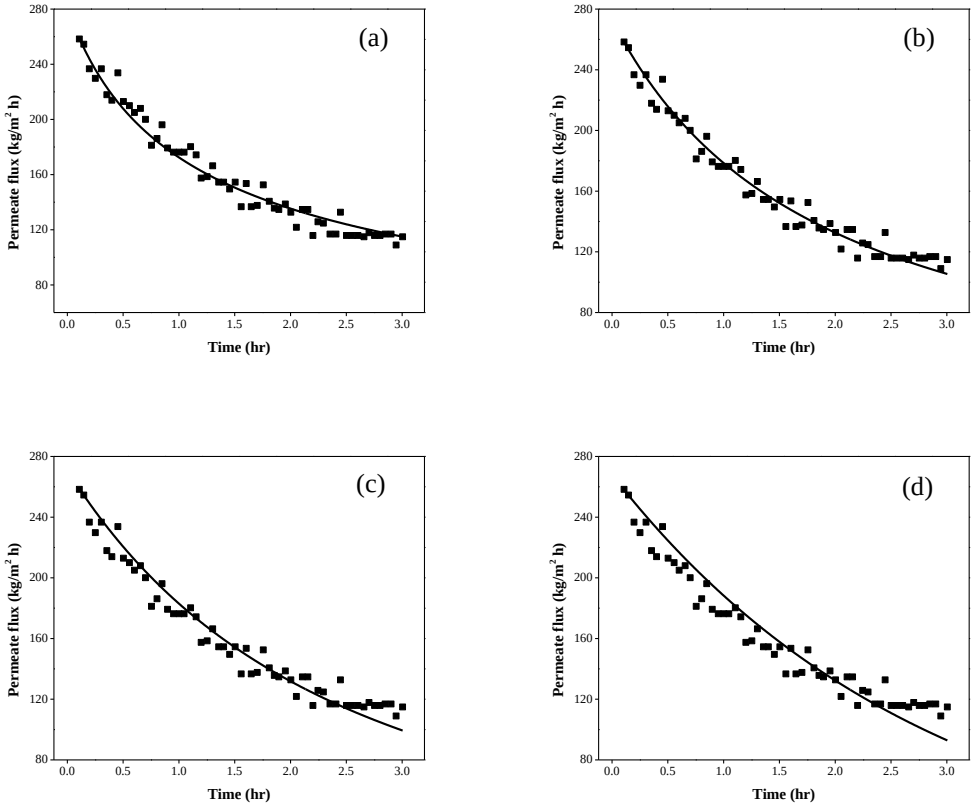

Figure 4.46: Actual and predicted membrane filtration profile by the classical models for (a) cake filtration, (b) intermediate blocking, (c) standard blocking, and (d) complete blocking during oil emulsion separation.

Based on the membrane fouling mechanisms study, the intermediate blocking mechanism was identified as the most crucial factor which contributes to the oil fouling on PES/APTES-SiO_2 composite membrane. Therefore, the intermediate pore blocking model provides a better agreement with the experimental data than the complete pore blocking model, as expected. The hypothesis of intermediate pore blocking and standard blocking models can be expected to take place for the experimental conditions tested in this work since solute particles/oil droplets were not completely retained by the membrane. Moreover, as the intermediate pore blocking model describes more accurately a real UF process than the complete pore

blocking model, better predictions are expected by the intermediate pore blocking and standard pore blocking models tested in this work. However, as observed the better permeate flux predictions can be obtained using the intermediate pore blocking model.

CHAPTER FIVE

CONCLUSIONS AND RECOMMENDATION

5.1 Conclusions

In this work, a stable APTES-SiO_2 particle was synthesized via one pot reaction modification. The mean particle diameter for the APTES-SiO_2 particles was found to be 92.55 ± 5.48 nm and 88.20 ± 4.32 nm for DLS and TEM analysis, respectively. Additionally, it was found that the synthesized APTES-SiO_2 particles showed a high negative surface charge with zeta potential (ζ) of -42.6 ± 0.796 mV, which signifies that a stable particle suspension was obtained as a result of the strong electro-static force of repulsion which prevented APTES-SiO_2 particles from agglomerating.

Response surface methodology based on the central composite design were used for statistical analysis, optimization and modeling of the PES membrane. PES and PEG (wt.%) were found to have a significant effect on PWF and OPF responses. PWF and OPF were found to increase with PEG content due to increase in both pore size and surface hydrophilicity (as a result of improved APTES-SiO_2 dispersion rate). The significant terms that affects PWF was observed to be PES, PEG and the interacting effects between PES and APTES-SiO_2 in which, the viscosity of dope was found to be a dominant factor especially with low APTES-SiO_2 loading. The most significant terms that affects OPF was observed to be PES and PEG. The significant terms for OR were observed to be the quadratic effects of PES, APTES-SiO_2, coagulation bath temperature as well as the interactions between PES and PEG.

The optimum conditions for PES, APTES-SiO_2, PEG and CBT were found to be 17.25 wt.%, 3.6 wt.%, 3.72 wt.% and 15 ºC, respectively with PWF, OPF and OR maintained at 235.2 kg/m^2 h, 159.8 kg/m^2 h and 99.23%, respectively.

The structure and properties of APTES-SiO_2 HF membranes can be adjusted by changing the composition of the bore fluid in the spinning process. Ethanol was selected due to its soft non-solvent ability and their influence on HFs properties and performance remains controversial. Obviously, the increase in ethanol content caused an increase in HFs porosity and pore size, which resulted to an increase in permeability but decreases the oil rejection except for HF membrane spun with 25/75 wt.% ethanol/water which maintained a relatively higher rejection. An increase in ethanol contents above 25% increases causes the number of fiber corrugations to increase. Furthermore, HF membrane spun with 25/75 wt.% ethanol/water resulted to an improved properties and performance as compared to other HF membranes.

The influence of varying APTES-SiO_2 loadings on membrane physicochemical properties towards their fouling propensity and performance were studied. The physicochemical properties of the membranes were varied based the dosage of APTES-SiO_2 particles. SEM analysis shows no existence of particle aggregation on the membrane surface and the particles were well distributed in the membrane matrix. Even at high loading, the prepared membrane presents a uniform dispersion of particles on the membrane surface. The AFM results confirms a decrease in surface roughness upon introduction of APTES-SiO_2 particles. The TGA analysis proved that the thermal properties of the composite membrane was

significantly improved upon introduction of APTES-SiO_2 particles. The EDX analysis shows that the distribution of APTES-SiO_2 particles of all composite membranes were good. The best performance was obtained when the APTES-SiO_2 content was 2.5 wt.%. In this case, the PWF rose from 219.397±8.49 to 227.500±11.37 kg/m^2 h, permeate flux increase from 134.630±6.078 to 159.880±7.318 kg/m^2 h and oil removal rose from 97.23 ± 0.10 to 99.87 ± 0.26%. It also presents the highest FRR of 93.464±1.347% and the lowest flux reduction rate of 29.723±1.273%.

The effect of flow rate, feed concentration and TMP on membrane performance were further investigated. The oil concentration varies from 100 to 500 mg/L, TMP varied from 1.0 to 2 bar, and the feed flow rate varies from 0.15 to 0.75 L/min. The PWF increases with increase in TMP which can be due to the increase in driving force exerted on membrane which causes an increase in the passage of water. The decrease in oil rejection was in proportional with the increase in transmembrane pressure and feed concentration, respectively. Feed flow rate has less influence on FRR. RF reduction rate was higher at higher TMP.

The fouling behaviour of membrane fouling mechanism was analysed using four typical fouling model. The variables on membrane fouling was determined and the results indicated that intermediate pore blocking model is the main cause of the flux decline during UF of synthetic oil-in-water emulsion.

5.2 Recommendation

For future development, the following recommendations are suggested:

1- The incorporation of APTES-SiO_2 particles into PES matrix did change the physicochemical and performance properties of the membrane for oil in water emulsion separation. However, it is suggested that the particle size of APTES-SiO_2 can be minimized to < 50 nm to minimize the effects of fouling. Small filer size will have advantages in decreasing membrane thickness. By utilizing smaller particle size, the particle density will be enhanced and membrane wall thickness is reduced so that the anti-fouling effect and cleaning efficiency of the composite membrane can be more significant.

2- It is recommended to synthesize the PES/APTES-SiO_2 HF membrane using the proposed method by varying the different spinning conditions such as resident time, draw ratio, take up speed and dope speed.

3- More characterization on the long-term stability as well as analytical study on membrane fouling mechanism on the optimum membrane should be further investigated.

4- Adsorption-desorption study of oil in water emulsion towards PES/APTES-SiO_2 HF membrane is important.

5- Study on the effects of various pH (alkaline and acidic medium) values on the performance of PES/APTES-SiO_2 HF membrane.

REFERENCES

Abdel-Karim, A., Gad-Allah, T.A., El-Kalliny, A.S., Ahmed, S.I.A., Souaya, E.R., Badawy, M.I., Ulbricht, M., 2017. Fabrication of modified polyethersulfone membranes for wastewater treatment by submerged membrane bioreactor. Sep. Purif. Technol. 175, 36–46. https://doi.org/10.1016/j.seppur.2016.10.060

Abdel-Karim, A., Leaper, S., Alberto, M., Vijayaraghavan, A., Fan, X., Holmes, S.M., Souaya, E.R., Badawy, M.I., Gorgojo, P., 2018. High flux and fouling resistant flat sheet polyethersulfone membranes incorporated with graphene oxide for ultrafiltration applications. Chem. Eng. J. 334, 789–799. https://doi.org/10.1016/j.cej.2017.10.069

Abdullah, N., Rahman, M.A., Othman, M.H.D., Ismail, A.F., Jaafar, J., Aziz, A.A., 2016. Preparation and characterization of self-cleaning alumina hollow fiber membrane using the phase inversion and sintering technique. Ceram. Int. 42, 12312–12322. https://doi.org/10.1016/j.ceramint.2016.05.003

Abolhassan, S., Vossoughi, M., 2018. Efficient dye removal from aqueous solution by high-performance electrospun nano fibrous membranes through incorporation of SiO2 nanoparticles. J. Clean. Prod. 183, 1197–1206. https://doi.org/10.1016/j.jclepro.2018.02.168

Aditya Kiran, S., Lukka Thuyavan, Y., Arthanareeswaran, G., Matsuura, T., Ismail, A.F., 2016. Impact of graphene oxide embedded polyethersulfone membranes for the effective treatment of distillery effluent. Chem. Eng. J. 286, 528–537. https://doi.org/10.1016/j.cej.2015.10.091

Ahmad, A., Razali, M.H., Mamat, M., Mehamod, F.S.B., Anuar Mat Amin, K., 2017. Adsorption of methyl orange by synthesized and functionalized-CNTs with 3-aminopropyltriethoxysilane loaded TiO2 nanocomposites. Chemosphere 168, 474–482. https://doi.org/https://doi.org/10.1016/j.chemosphere.2016.11.028

Ahmad, A.L., Abdulkarim, A.A., Mohd Shafie, Z.M.H., Ooi, B.S., 2017. Fouling evaluation of PES/ZnO mixed matrix hollow fiber membrane. Desalination 403, 53–63. https://doi.org/10.1016/j.desal.2016.10.008

Ahmad, A.L., Mohamad, Z., Mohd, H., 2017. Effect of Air Gap Distance on PES / PVA Hollow Fibre Membrane ' s Morphology and Performance. J. Phys. Sci. 28, 185–199.

Ahmed, F., 2006. Arsenic Mitigation Technologies in South and East Asia. East Asia 44.

Akbari, H.R., Mehrabadi, A.R.& T., 2010. Determination Of Nanofiltration Efficency In Arsenic Removal From Drinking Water. Iran. J. Environ. Heal. Sci. Eng. 7, 273–278.

Al Malek, S.A., Abu Seman, M.N., Johnson, D., Hilal, N., 2012. Formation and characterization of polyethersulfone membranes using different concentrations of polyvinylpyrrolidone. Desalination 288, 31–39. https://doi.org/10.1016/j.desal.2011.12.006

Alobaidy, A.A., Sherhan, B.Y., Barood, A.D., Alsalhy, Q.F., 2017. Effect of bore

fluid flow rate on formation and properties of hollow fibers. Appl. Water Sci. 7, 4387–4398. https://doi.org/10.1007/s13201-017-0584-7

Alpatova, A., Kim, E.-S., Dong, S., Sun, N., Chelme-Ayala, P., Gamal El-Din, M., 2014. Treatment of oil sands process-affected water with ceramic ultrafiltration membrane: Effects of operating conditions on membrane performance. Sep. Purif. Technol. 122, 170–182. https://doi.org/https://doi.org/10.1016/j.seppur.2013.11.005

Alsalhy, Q.F., Ali, J.M., Abbas, A.A., Rashed, A., Bruggen, B. Van der, Balta, S., 2013. Enhancement of poly(phenyl sulfone) membranes with ZnO nanoparticles. Desalin. Water Treat. 51, 6070–6081. https://doi.org/10.1080/19443994.2013.764487

Alsalhy, Q.F., Salih, H.A., Simone, S., Zablouk, M., Drioli, E., Figoli, A., 2014. Poly(ether sulfone) (PES) hollow-fiber membranes prepared from various spinning parameters. Desalination 345, 21–35. https://doi.org/10.1016/j.desal.2014.04.029

Ananth, A., Arthanareeswaran, G., Ismail, A.F., Mok, Y.S., Matsuura, T., 2014. Effect of bio-mediated route synthesized silver nanoparticles for modification of polyethersulfone membranes. Colloids Surfaces A Physicochem. Eng. Asp. 451, 151–160. https://doi.org/10.1016/j.colsurfa.2014.03.024

Aneja, K.S., Bohm, S., Khanna, A.S., Bohm, H.L.M., 2015. Graphene based anticorrosive coatings for Cr(vi) replacement. Nanoscale 7, 17879–17888. https://doi.org/10.1039/C5NR04702A

Arnot, T.C., Field, R.W., Koltuniewicz, A.B., 2000. Cross-flow and dead-end microfiltration of oily-water emulsions: Part II. Mechanisms and modelling of flux decline. J. Memb. Sci. 169, 1–15. https://doi.org/https://doi.org/10.1016/S0376-7388(99)00321-X

Asadi Tashvigh, A., Fouladitajar, A., Zokaee Ashtiani, F., 2015. Modeling concentration polarization in crossflow microfiltration of oil-in-water emulsion using shear-induced diffusion; CFD and experimental studies. Desalination 357, 225–232. https://doi.org/https://doi.org/10.1016/j.desal.2014.12.001

Asenath Smith, E., Chen, W., 2008. How To Prevent the Loss of Surface Functionality Derived from Aminosilanes. Langmuir 24, 12405–12409. https://doi.org/10.1021/la802234x

Barth, C., Gonçalves, M.C., Pires, A.T.N., Roeder, J., Wolf, B.A., 2000. Asymmetric polysulfone and polyethersulfone membranes: effects of thermodynamic conditions during formation on their performance. J. Memb. Sci. 169, 287–299. https://doi.org/10.1016/S0376-7388(99)00344-0

Basri, H., Ismail, A.F., Aziz, M., 2012. Microstructure and anti-adhesion properties of PES/TAP/Ag hybrid ultrafiltration membrane. Desalination 287, 71–77. https://doi.org/https://doi.org/10.1016/j.desal.2011.09.031

Basri, H., Ismail, A.F., Aziz, M., 2011. Polyethersulfone (PES)-silver composite UF membrane: Effect of silver loading and PVP molecular weight on membrane morphology and antibacterial activity. Desalination 273, 72–80. https://doi.org/10.1016/j.desal.2010.11.010

Basri, H., Ismail, A.F., Aziz, M., Nagai, K., Matsuura, T., Abdullah, M.S., Ng, B.C., 2010. Silver-filled polyethersulfone membranes for antibacterial applications - effect of PVP and TAP addition on silver dispersion. Desalination 261, 264–271. https://doi.org/10.1016/j.desal.2010.05.009

Bayat, A., Aghamiri, S.F., Moheb, A., Vakili-Nezhaad, G.R., 2005. Oil spill cleanup from sea water by sorbent materials. Chem. Eng. Technol. 28, 1525–1528. https://doi.org/10.1002/ceat.200407083

Behavior, P.S., Lipscomb, G.G., 1994. The Melt Hollow Fiber Spinning Process: Steady-state Behavior, Sensitivity and Stability 5, 745–758.

Bernstein, R., Singer, C.E., Singh, S.P., Mao, C., Arnusch, C.J., 2018. UV initiated surface grafting on polyethersulfone ultrafiltration membranes via ink-jet printing-assisted modification. J. Memb. Sci. 548, 73–80. https://doi.org/10.1016/j.memsci.2017.10.069

Bey, S., Criscuoli, A., Simone, S., Figoli, A., Benamor, M., Drioli, E., 2011. Hydrophilic PEEK-WC hollow fi bre membrane contactors for chromium (Vi) removal. DES 283, 16–24. https://doi.org/10.1016/j.desal.2011.04.038

Bildyukevich, A. V., Plisko, T. V., Liubimova, A.S., Volkov, V. V., Ususky, V. V., 2017. Hydrophilization of polysulfone hollow fiber membranes via addition of polyvinylpyrrolidone to the bore fluid. J. Memb. Sci. 524, 537–549. https://doi.org/10.1016/j.memsci.2016.11.042

Binyam, S., Mukhtar, H., Leong, L.K., 2009. Flux and Rejection of Monoethanolamine (Mea) in Wastewater Using Membrane Technology 139–151.

Bolton, G., LaCasse, D., Kuriyel, R., 2006. Combined models of membrane fouling: Development and application to microfiltration and ultrafiltration of biological fluids. J. Memb. Sci. 277, 75–84. https://doi.org/https://doi.org/10.1016/j.memsci.2004.12.053

Bonyadi, S., Chung, T.S., Krantz, W.B., 2007. Investigation of corrugation phenomenon in the inner contour of hollow fibers during the non-solvent induced phase-separation process. J. Memb. Sci. 299, 200–210. https://doi.org/http://dx.doi.org/10.1016/j.memsci.2007.04.045

Boshrouyeh, M., Zokaee, F., Karimi, M., 2015. A novel approach to fabricate high performance nano-SiO2 embedded PES membranes for microfiltration of oil-in-water emulsion. Appl. Surf. Sci. 349, 393–402. https://doi.org/10.1016/j.apsusc.2015.05.037

Bushell, A., 2012. Mixed Matrix Membranes of a Polymer of Intrinsic Microporosity with Crystalline Porous Solids. https://doi.org/10.1111/1467-8462.00273

Calebrese, C., Hui, L., Schadler, L.S., Nelson, J.K., 2011. A review on the importance of nanocomposite processing to enhance electrical insulation. IEEE Trans. Dielectr. Electr. Insul. 18, 938–945. https://doi.org/10.1109/TDEI.2011.5976079

Cao, C., Chung, T.-S., Chen, S.B., Dong, Z., 2004. The study of elongation and shear rates in spinning process and its effect on gas separation performance of

Poly(ether sulfone) (PES) hollow fiber membranes. Chem. Eng. Sci. 59, 1053–1062. https://doi.org/https://doi.org/10.1016/j.ces.2003.10.023

Caravajal, G.S., Leyden, D.E., Quinting, G.R., Maciel, G.E., 1988. Structural characterization of (3-aminopropyl)triethoxysilane-modified silicas by silicon-29 and carbon-13 nuclear magnetic resonance. Anal. Chem. 60, 1776–1786. https://doi.org/10.1021/ac00168a027

Chakrabarty, B., Ghoshal, A.K., Purkait, M.K., 2010. Cross-flow ultrafiltration of stable oil-in-water emulsion using polysulfone membranes. Chem. Eng. J. 165, 447–456. https://doi.org/10.1016/j.cej.2010.09.031

Chakrabarty, B., Ghoshal, A.K., Purkait, M.K., 2008. Ultrafiltration of stable oil-in-water emulsion by polysulfone membrane. J. Memb. Sci. 325, 427–437. https://doi.org/10.1016/j.memsci.2008.08.007

Chang, J., Zuo, J., Zhang, L., O'Brien, G.S., Chung, T.S., 2017. Using green solvent, triethyl phosphate (TEP), to fabricate highly porous PVDF hollow fiber membranes for membrane distillation. J. Memb. Sci. 539, 295–304. https://doi.org/10.1016/j.memsci.2017.06.002

Chang, Y., Li, Y., Wang, J., Wang, C., 2017. Novel wettability of Cu3SnS4 (CTS) surface for superamphiphilic or hydrophobicity-superlipophilic. Mater. Lett. 187, 162–165. https://doi.org/10.1016/j.matlet.2016.10.091

Chang, Y., Shih, Y.-J., Ruaan, R.-C., Higuchi, A., Chen, W.-Y., Lai, J.-Y., 2008. Preparation of poly(vinylidene fluoride) microfiltration membrane with uniform surface-copolymerized poly(ethylene glycol) methacrylate and improvement of blood compatibility. J. Memb. Sci. 309, 165–174. https://doi.org/https://doi.org/10.1016/j.memsci.2007.10.024

Charcosset, C., 2009. Preparation of emulsions and particles by membrane emulsification for the food processing industry. J. Food Eng. 92, 241–249. https://doi.org/10.1016/j.jfoodeng.2008.11.017

Chen, C.-F., Tzeng, S.-D., Lin, M.-H., Gwo, S., 2006. Electrostatic Assembly of Gold Colloidal Nanoparticles on Organosilane Monolayers Patterned by Microcontact Electrochemical Conversion. Langmuir 22, 7819–7824. https://doi.org/10.1021/la060656r

Chen, D., Zhang, H., Yang, K., Wang, H., 2016. Functionalization of 4-aminothiophenol and 3-aminopropyltriethoxysilane with graphene oxide for potential dye and copper removal. J. Hazard. Mater. 310, 179–187. https://doi.org/https://doi.org/10.1016/j.jhazmat.2016.02.040

Chen, W., Peng, J., Su, Y., Zheng, L., Wang, L., Jiang, Z., 2009. Separation of oil/water emulsion using Pluronic F127 modified polyethersulfone ultrafiltration membranes. Sep. Purif. Technol. 66, 591–597. https://doi.org/10.1016/j.seppur.2009.01.009

Chen, Z., Huang, G.H., Li, J.B., 2003. A GIS-based modeling system for petroleum waste management. Water Sci. Technol. 47, 309–317.

Chernyshev, V.S., Rachamadugu, R., Tseng, Y.H., Belnap, D.M., Jia, Y., Branch, K.J., Butterfield, A.E., Pease, L.F., Bernard, P.S., Skliar, M., 2015. Size and

shape characterization of hydrated and desiccated exosomes. Anal. Bioanal. Chem. 407, 3285–3301. https://doi.org/10.1007/s00216-015-8535-3

Choi, S., Tasselli, F., Jansen, J.C., Barbieri, G., Drioli, E., 2010. Effect of the preparation conditions on the formation of asymmetric poly (vinylidene fluoride) hollow fibre membranes with a dense skin. Eur. Polym. J. 46, 1713–1725. https://doi.org/10.1016/j.eurpolymj.2010.06.001

Chou, W.-L., Yang, M.-C., 2005. Effect of take-up speed on physical properties and permeation performance of cellulose acetate hollow fibers. J. Memb. Sci. 250, 259–267. https://doi.org/https://doi.org/10.1016/j.memsci.2004.10.030

Chung, T.-S., Hu, X., 1997. Effect of air-gap distance on the morphology and thermal properties of polyethersulfone hollow fibers. J. Appl. Polym. Sci. 66, 1067–1077. https://doi.org/10.1002/(SICI)1097-4628(19971107)66:6<1067::AID-APP7>3.0.CO;2-G

Chung, T.-S., Xu, Z.-L., Lin, W., 1999. Fundamental understanding of the effect of air-gap distance on the fabrication of hollow fiber membranes. J. Appl. Polym. Sci. 72, 379–395. https://doi.org/10.1002/(SICI)1097-4628(19990418)72:3<379::AID-APP8>3.0.CO;2-B

Clausi, D.T., Koros, W.J., 2000. Formation of defect-free polyimide hollow fiber membranes for gas separations. J. Memb. Sci. 167, 79–89. https://doi.org/https://doi.org/10.1016/S0376-7388(99)00276-8

Cui, Z., Tavajohi, N., Young, S., Myung, J., Taek, K., Sanguineti, A., Arcella, V., Moo, Y., Drioli, E., 2013. Poly (vinylidene fl uoride) membrane preparation with an environmental diluent via thermally induced phase separation. J. Memb. Sci. 444, 223–236. https://doi.org/10.1016/j.memsci.2013.05.031

Çulfaz, P.Z., Rolevink, E., van Rijn, C., Lammertink, R.G.H., Wessling, M., 2010. Microstructured hollow fibers for ultrafiltration. J. Memb. Sci. 347, 32–41. https://doi.org/10.1016/j.memsci.2009.10.003

Damodar, R.A., You, S.J., Chou, H.H., 2009. Study the self cleaning, antibacterial and photocatalytic properties of TiO2 entrapped PVDF membranes. J. Hazard. Mater. 172, 1321–1328. https://doi.org/10.1016/j.jhazmat.2009.07.139

Daraei, P., Madaeni, S.S., Ghaemi, N., Khadivi, M.A., Astinchap, B., Moradian, R., 2013. Fouling resistant mixed matrix polyethersulfone membranes blended with magnetic nanoparticles: Study of magnetic field induced casting. Sep. Purif. Technol. 109, 111–121. https://doi.org/10.1016/j.seppur.2013.02.035

Darvishmanesh, S., Tasselli, F., Jansen, J.C., Tocci, E., Bazzarelli, F., Bernardo, P., Luis, P., Degrève, J., Drioli, E., Bruggen, B. Van Der, 2011. Preparation of solvent stable polyphenylsulfone hollow fiber nanofiltration membranes. J. Memb. Sci. 384, 89–96. https://doi.org/10.1016/j.memsci.2011.09.003

Das, R., Bhattacherjee, C., Ghosh, S., 2009. Effects of operating parameters and nature of fouling behavior in ultrafiltration of sesame protein hydrolysate. Desalination 237, 268–276. https://doi.org/https://doi.org/10.1016/j.desal.2008.01.020

Dong, G., Li, H., Chen, V., 2010. Factors affect defect-free Matrimid® hollow fiber

gas separation performance in natural gas purification. J. Memb. Sci. 353, 17–27. https://doi.org/https://doi.org/10.1016/j.memsci.2010.02.012

Drioli, E., Ali, A., Lee, Y.M., Al-Sharif, S.F., Al-Beirutty, M., Macedonio, F., 2016. Membrane operations for produced water treatment. Desalin. Water Treat. 57, 14317–14335. https://doi.org/10.1080/19443994.2015.1072585

Dutreilh-Colas, M., Yan, M., Labrot, P., Delorme, N., Gibaud, A., Bardeau, J.-F., 2008. AFM evidence of perpendicular orientation of cylindrical craters on hybrid silica thin film templated by triblock copolymer. Surf. Sci. 602, 829–833. https://doi.org/http://dx.doi.org/10.1016/j.susc.2007.11.028

Džunuzović, E.S., Džunuzović, J. V, Marinković, A.D., Marinović-Cincović, M.T., Jeremić, K.B., Nedeljković, J.M., 2012. Influence of surface modified TiO2 nanoparticles by gallates on the properties of PMMA/TiO2 nanocomposites. Eur. Polym. J. 48, 1385–1393. https://doi.org/http://dx.doi.org/10.1016/j.eurpolymj.2012.05.017

Ebin, B., Lindbergh, G., Gürmen, S., 2015. Preparation and electrochemical properties of nanocrystalline LiBxMn2−xO4 cathode particles for Li-ion batteries by ultrasonic spray pyrolysis method. J. Alloys Compd. 620, 399–406. https://doi.org/10.1016/j.jallcom.2014.09.098

Enders, D., Nagao, T., Pucci, A., Nakayama, T., 2006. Reversible adsorption of Au nanoparticles on SiO2/Si: An in situ ATR-IR study. Surf. Sci. 600, L71–L75. https://doi.org/https://doi.org/10.1016/j.susc.2006.01.019

EQA, 1974. Environmental Quality (Sewage and Industrial Effluents) Regulations, 1979. Available from http//www.water-treatment.com.cn/resources/discharge-standards/malaysia.htm.

Fadeev, A.Y., McCarthy, T.J., 2000. Self-Assembly Is Not the Only Reaction Possible between Alkyltrichlorosilanes and Surfaces: Monomolecular and Oligomeric Covalently Attached Layers of Dichloro- and Trichloroalkylsilanes on Silicon. Langmuir 16, 7268–7274. https://doi.org/10.1021/la000471z

Fakhru'l-Razi, A., Pendashteh, A., Abdullah, L.C., Biak, D.R.A., Madaeni, S.S., Abidin, Z.Z., 2009. Review of technologies for oil and gas produced water treatment. J. Hazard. Mater. 170, 530–51. https://doi.org/10.1016/j.jhazmat.2009.05.044

Fashandi, H., Zarrebini, M., Ghodsi, A., Saghafi, R., 2016. Designing the inner surface corrugations of hollow fibers to enhance CO 2 absorption efficiency. J. Colloid Interface Sci. 476, 35–46. https://doi.org/10.1016/j.jcis.2016.05.004

Feng, X., Ying, L., Matsuura, T., Wu, P., 2017. Fabrication of hydrophobic / hydrophilic composite hollow fi bers for DCMD : In fl uence of dope formulation and external coagulant 401, 53–63. https://doi.org/10.1016/j.desal.2016.07.026

Fissan, H., Ristig, S., Kaminski, H., Asbach, C., Epple, M., 2014. Comparison of different characterization methods for nanoparticle dispersions before and after aerosolization. Anal. Methods 6, 7324–7334. https://doi.org/10.1039/C4AY01203H

Fouladitajar, A., Zokaee Ashtiani, F., Dabir, B., Rezaei, H., Valizadeh, B., 2015. Response surface methodology for the modeling and optimization of oil-in-water emulsion separation using gas sparging assisted microfiltration. Environ. Sci. Pollut. Res. 22, 2311–2327. https://doi.org/10.1007/s11356-014-3511-6

Fratila-Apachitei, L.E., Kennedy, M.D., Linton, J.D., Blume, I., Schippers, J.C., 2001. Influence of membrane morphology on the flux decline during dead-end ultrafiltration of refinery and petrochemical waste water. J. Memb. Sci. 182, 151–159. https://doi.org/10.1016/S0376-7388(00)00557-3

Fu, F., Zhang, S., Chung, T., 2015. Sandwich-structured hollow fi ber membranes for osmotic power generation. DES 376, 73–81. https://doi.org/10.1016/j.desal.2015.08.018

García-Fernández, L., García-Payo, M.C., Khayet, M., 2017a. Mechanism of formation of hollow fiber membranes for membrane distillation: 2. Outer coagulation power effect on morphological characteristics. J. Memb. Sci. 542, 469–481. https://doi.org/10.1016/j.memsci.2017.03.038

García-Fernández, L., García-Payo, M.C., Khayet, M., 2017b. Mechanism of formation of hollow fiber membranes for membrane distillation: 1. Inner coagulation power effect on morphological characteristics. J. Memb. Sci. 542, 456–468. https://doi.org/10.1016/j.memsci.2017.03.036

García-fernández, L., Wang, B., García-payo, M.C., Li, K., Khayet, M., 2017. Morphological design of alumina hollow fi ber membranes for desalination by air gap membrane distillation 420, 226–240. https://doi.org/10.1016/j.desal.2017.07.021

Garcia-Ivars, J., Iborra-Clar, M.-I., Alcaina-Miranda, M.-I., Mendoza-Roca, J.-A., Pastor-Alcañiz, L., 2016. Surface photomodification of flat-sheet PES membranes with improved antifouling properties by varying UV irradiation time and additive solution pH. Chem. Eng. J. 283, 231–242. https://doi.org/10.1016/j.cej.2015.07.078

Ghaemi, N., 2016. A new approach to copper ion removal from water by polymeric nanocomposite membrane embedded with γ-alumina nanoparticles. Appl. Surf. Sci. 364, 221–228. https://doi.org/https://doi.org/10.1016/j.apsusc.2015.12.109

Gholami, F., Zinadini, S., Zinatizadeh, A.A., Abbasi, A.R., 2018. TMU-5 metal-organic frameworks (MOFs) as a novel nanofiller for flux increment and fouling mitigation in PES ultrafiltration membrane. Sep. Purif. Technol. 194, 272–280. https://doi.org/10.1016/j.seppur.2017.11.054

Ghosh, a K., Bindal, R.C., Prabhakar, S., Tewari, P.K., 2011. Composite Polyamide Reverse Osmosis (RO) Membranes – Recent Developments and Future Directions 43–51.

Giwa, A., Chakraborty, S., Mavukkandy, M.O., Arafat, H.A., 2017. Separation and Puri fi cation Technology Nanoporous hollow fi ber polyethersulfone membranes for the removal of residual contaminants from treated wastewater e ffl uent : Functional and molecular implications. Sep. Purif. Technol. 189, 20–31. https://doi.org/10.1016/j.seppur.2017.07.058

Gobi, K., Mashitah, M.D., Vadivelu, V.M., 2011. Adsorptive removal of Methylene

Blue using novel adsorbent from palm oil mill effluent waste activated sludge: Equilibrium, thermodynamics and kinetic studies. Chem. Eng. J. 171, 1246–1252. https://doi.org/10.1016/j.cej.2011.05.036

Gohari, R.J., Halakoo, E., Lau, W.J., Kassim, M.A., Matsuura, T., 2014. RSC Advances improved anti-fouling properties for oily 17587–17596. https://doi.org/10.1039/c4ra00032c

Gupta, B., Revagade, N., Hilborn, J., 2007. Poly(lactic acid) fiber: An overview. Prog. Polym. Sci. 32, 455–482. https://doi.org/https://doi.org/10.1016/j.progpolymsci.2007.01.005

Gwi, 2017. GWI Research: Water for Onshore Oil & Gas - Conventional production.

Ha, S.R., Rhee, K.Y., Kim, H.C., Kim, J.T., 2008. Fracture performance of clay/epoxy nanocomposites with clay surface-modified using 3-aminopropyltriethoxysilane. Colloids Surfaces A Physicochem. Eng. Asp. 313–314, 112–115. https://doi.org/https://doi.org/10.1016/j.colsurfa.2007.04.082

Hamid, N.A.A., Ismail, A.F., Matsuura, T., Zularisam, A.W., Lau, W.J., Yuliwati, E., Abdullah, M.S., 2011. Morphological and separation performance study of polysulfone/titanium dioxide (PSF/TiO2) ultrafiltration membranes for humic acid removal. Desalination 273, 85–92. https://doi.org/https://doi.org/10.1016/j.desal.2010.12.052

Han, W., Liu, C., Bai, R., 2007. A novel method to prepare high chitosan content blend hollow fiber membranes using a non-acidic dope solvent for highly enhanced adsorptive performance. J. Memb. Sci. 302, 150–159. https://doi.org/https://doi.org/10.1016/j.memsci.2007.06.039

He, C., Yang, Z., Ding, J., Chen, Y., Tong, X., Li, Y., 2017. Effective removal of Cr(VI) from aqueous solution by 3-aminopropyltriethoxysilane-functionalized graphene oxide. Colloids Surfaces A Physicochem. Eng. Asp. 520, 448–458. https://doi.org/https://doi.org/10.1016/j.colsurfa.2017.01.086

He, H., Fu, G., Wang, Y., Chai, Z., Jiang, Y., Chen, Z., 2010. Imprinting of protein over silica nanoparticles via surface graft copolymerization using low monomer concentration. Biosens. Bioelectron. 26, 760–765. https://doi.org/https://doi.org/10.1016/j.bios.2010.06.043

Hermia, J., 1982. Constant pressure blocking filtration law application to powder-law non-Newtonian fluid. Trans. Inst. Chem. Eng. 183–187.

Hoon, K., Huang, Y., Yu, M., Heo, J., Flora, J.R. V, Jang, A., Jang, M., Jung, C., Min, C., Kim, D., Yoon, Y., 2017. Evaluation of graphene oxide-coated ultrafiltration membranes for humic acid removal at different pH and conductivity conditions. Sep. Purif. Technol. 181, 139–147. https://doi.org/10.1016/j.seppur.2017.03.026

Hu, D., Li, X., Li, L., Yang, C., 2015. Designing high-caliber nonwoven filter mats for coalescence filtration of oil / water emulsions. Sep. Purif. Technol. 149, 65–73. https://doi.org/10.1016/j.seppur.2015.05.014

Hua, Z., Helmut, S., 2015. Thermoresponsive PNIPAM/silica nanoparticles by direct photopolymerization in aqueous media. J. Polym. Sci. Part A Polym. Chem. 53,

1260–1267. https://doi.org/10.1002/pola.27593

Huang, A., Liang, F., Steinbach, F., Caro, J., 2010. Preparation and separation properties of LTA membranes by using 3-aminopropyltriethoxysilane as covalent linker. J. Memb. Sci. 350, 5–9. https://doi.org/https://doi.org/10.1016/j.memsci.2009.12.029

Huang, X., Wang, W., Liu, Y., Wang, H., Zhang, Z., Fan, W., Li, L., 2015. Treatment of oily waste water by PVP grafted PVDF ultrafiltration membranes. Chem. Eng. J. 273, 421–429. https://doi.org/10.1016/j.cej.2015.03.086

Huang, X., Wang, W., Zheng, Z., Fan, W., Mao, C., Shi, J., Li, L., 2016. Surface monofunctionalized polymethyl pentene hollow fiber membranes by plasma treatment and hemocompatibility modification for membrane oxygenators. Appl. Surf. Sci. 362, 355–363. https://doi.org/10.1016/j.apsusc.2015.11.236

IEA, 2017. International Energy Agency: Oil market report.

Jalali, A., Shockravi, A., Vatanpour, V., Hajibeygi, M., 2016. Preparation and characterization of novel microporous ultrafiltration PES membranes using synthesized hydrophilic polysulfide-amide copolymer as an additive in the casting solution. Microporous Mesoporous Mater. 228, 1–13. https://doi.org/10.1016/j.micromeso.2016.03.024

Jamshidi Gohari, R., Halakoo, E., Lau, W.J., Kassim, M.A., Matsuura, T., Ismail, A.F., 2014. Novel polyethersulfone (PES)/hydrous manganese dioxide (HMO) mixed matrix membranes with improved anti-fouling properties for oily wastewater treatment process. RSC Adv. 4, 17587–17596. https://doi.org/10.1039/C4RA00032C

Jamshidi Gohari, R., Korminouri, F., Lau, W.J., Ismail, A.F., Matsuura, T., Chowdhury, M.N.K., Halakoo, E., Jamshidi Gohari, M.S., 2015. A novel super-hydrophilic PSf/HAO nanocomposite ultrafiltration membrane for efficient separation of oil/water emulsion. Sep. Purif. Technol. 150, 13–20. https://doi.org/10.1016/j.seppur.2015.06.031

Javadi, N., Zokaee Ashtiani, F., Fouladitajar, A., Moosavi Zenooz, A., 2014. Experimental studies and statistical analysis of membrane fouling behavior and performance in microfiltration of microalgae by a gas sparging assisted process. Bioresour. Technol. 162, 350–357. https://doi.org/10.1016/j.biortech.2014.03.160

Jeon, S., Karkhanechi, H., Fang, L., Cheng, L., Ono, T., 2018. Novel preparation and fundamental characterization of polyamide 6 self-supporting hollow fiber membranes via thermally induced phase separation (TIPS). J. Memb. Sci. 546, 1–14. https://doi.org/10.1016/j.memsci.2017.10.008

Jiang, B.B., Sun, X.F., Wang, L., Wang, S.Y., Liu, R.D., Wang, S.G., 2017. Polyethersulfone membranes modified with D-tyrosine for biofouling mitigation: Synergistic effect of surface hydrophility and anti-microbial properties. Chem. Eng. J. 311, 135–142. https://doi.org/10.1016/j.cej.2016.11.088

Jimoh, O.A., Okoye, P.U., Otitoju, T.A., Shah Ariffin, K., 2018. Aragonite precipitated calcium carbonate from magnesium rich carbonate rock for

polyethersulfone hollow fibre membrane application. J. Clean. Prod. 195, 79–92. https://doi.org/https://doi.org/10.1016/j.jclepro.2018.05.192

Jing, B., Wang, H., Lin, K., Mcginn, P.J., Na, C., Zhu, Y., 2013. A facile method to functionalize engineering solid membrane supports for rapid and ef fi cient oil e water separation. Polymer (Guildf). 54, 5771–5778. https://doi.org/10.1016/j.polymer.2013.08.030

John Benbow and John Bridgwater, 1993. Paste Flow and Extrusion. Oxford University Press.

Ju, J., Wang, T., Wang, Q., 2015. Colloids and Surfaces A : Physicochemical and Engineering Aspects Superhydrophilic and underwater superoleophobic PVDF membranes via plasma-induced surface PEGDA for effective separation of oil-in-water emulsions. Colloids Surfaces A Physicochem. Eng. Asp. 481, 151–157. https://doi.org/10.1016/j.colsurfa.2015.01.041

Jullok, N., Van Hooghten, R., Luis, P., Volodin, A., Van Haesendonck, C., Vermant, J., Van der Bruggen, B., 2016. Effect of silica nanoparticles in mixed matrix membranes for pervaporation dehydration of acetic acid aqueous solution: plant-inspired dewatering systems. J. Clean. Prod. 112, 4879–4889. https://doi.org/https://doi.org/10.1016/j.jclepro.2015.09.019

Kang, G. dong, Cao, Y. ming, 2014. Application and modification of poly(vinylidene fluoride) (PVDF) membranes - A review. J. Memb. Sci. 463, 145–165. https://doi.org/10.1016/j.memsci.2014.03.055

Kang, J., Lu, L., Zhan, W., Li, B., Li, D., Ren, Y., Liu, D., 2011. Photocatalytic pretreatment of oily wastewater from the restaurant by a vacuum ultraviolet/TiO2 system. J. Hazard. Mater. 186, 849–54. https://doi.org/10.1016/j.jhazmat.2010.11.075

Karimnezhad, H., Rajabi, L., Salehi, E., Ashraf, A., Azimi, S., 2014. Novel nanocomposite Kevlar fabric membranes : Fabrication characterization , and performance in oil / water separation. Appl. Surf. Sci. 293, 275–286. https://doi.org/10.1016/j.apsusc.2013.12.149

Karkhanechi, H., Rajabzadeh, S., Di Nicolò, E., Usuda, H., Shaikh, A.R., Matsuyama, H., 2016. Preparation and characterization of ECTFE hollow fiber membranes via thermally induced phase separation (TIPS). Polym. (United Kingdom) 97, 515–524. https://doi.org/10.1016/j.polymer.2016.05.067

Khamforoush, M., Pirouzram, O., Hatami, T., 2015. The evaluation of thin fi lm composite membrane composed of an electrospun polyacrylonitrile nano fibrous mid-layer for separating oil – water mixture. DES 359, 14–21. https://doi.org/10.1016/j.desal.2014.12.016

Khan, I.U., Hafiz, M., Othman, D., Ismail, A.F., Matsuura, T., Hashim, H., Rahman, M.A., Jaafar, J., 2018. Status and improvement of dual-layer hollow fiber membranes via co-extrusion process for gas separation: A review. J. Nat. Gas Sci. Eng. 52, 215–234. https://doi.org/10.1016/j.jngse.2018.01.043.This

Khayet, M., 2003. The effects of air gap length on the internal and external morphology of hollow fiber membranes. Chem. Eng. Sci. 58, 3091–3104. https://doi.org/http://dx.doi.org/10.1016/S0009-2509(03)00186-6

Kim, J., Van der Bruggen, B., 2010. The use of nanoparticles in polymeric and ceramic membrane structures: Review of manufacturing procedures and performance improvement for water treatment. Environ. Pollut. 158, 2335–2349. https://doi.org/https://doi.org/10.1016/j.envpol.2010.03.024

Kinkel, J.N., Unger, K.K., 1984. Role of solvent and base in the silanization reaction of silicas for reversed-phase high-performance liquid chromatography. J. Chromatogr. A 316, 193–200. https://doi.org/https://doi.org/10.1016/S0021-9673(00)96151-X

Kneuer, C., Sameti, M., Haltner, E.G., Schiestel, T., Schirra, H., Schmidt, H., Lehr, C.-M., 2000. Silica nanoparticles modified with aminosilanes as carriers for plasmid DNA. Int. J. Pharm. 196, 257–261. https://doi.org/https://doi.org/10.1016/S0378-5173(99)00435-4

Kochkodan, V., 2013. A review on membrane fabrication : Structure , properties and performance relationship 76–95. https://doi.org/10.1016/j.desal.2013.06.016

Kong, X., Zhou, M.-Y., Lin, C.-E., Wang, J., Zhao, B., Wei, X.-Z., Zhu, B.-K., 2016. Polyamide/PVC based composite hollow fiber nanofiltration membranes: Effect of substrate on properties and performance. J. Memb. Sci. 505, 231–240. https://doi.org/10.1016/j.memsci.2016.01.028

Korminouri, F., Rahbari-Sisakht, M., Matsuura, T., Ismail, A.F., 2015. Surface modification of polysulfone hollow fiber membrane spun under different air-gap lengths for carbon dioxide absorption in membrane contactor system. Chem. Eng. J. 264, 453–461. https://doi.org/10.1016/j.cej.2014.11.110

Kota, A.K., Kwon, G., Choi, W., Mabry, J.M., Tuteja, A., 2012. Hygro-responsive membranes for effective oil–water separation. Nat Commun 3, 1025.

Kourde-hana, Y., Loulergue, P., Szymczyk, A., Bruggen, B. Van Der, Nachtnebel, M., Rabiller-baudry, M., Audic, J., Pölt, P., Baddari, K., 2017. from characterization of membranes with controlled composition 533, 261–269. https://doi.org/10.1016/j.memsci.2017.03.050

Krysztafkiewicz, A., Binkowski, S., Jesionowski, T., 2002. Adsorption of dyes on a silica surface. Appl. Surf. Sci. 199, 31–39. https://doi.org/http://dx.doi.org/10.1016/S0169-4332(02)00248-9

Kumbharkar, S.C., Liu, Y., Li, K., 2011. High performance polybenzimidazole based asymmetric hollow fibre membranes for H 2 / CO 2 separation 375, 231–240. https://doi.org/10.1016/j.memsci.2011.03.049

Laberty-Robert, C., Vallé, K., Pereira, F., Sanchez, C., 2011. Design and properties of functional hybrid organic–inorganic membranes for fuel cells. Chem. Soc. Rev. 40, 961–1005. https://doi.org/10.1039/C0CS00144A

Lazar, R.A., Mandal, I., Slater, N.K.H., 2015. Effect of bore fluid composition on microstructure and performance of a microporous hollow fibre membrane as a cation-exchange substrate. J. Chromatogr. A 1394, 148–153. https://doi.org/10.1016/j.chroma.2015.03.037

Le, N.L., Bettahalli, N.M.S., Nunes, S.P., Chung, T.S., 2016. Outer-selective thin film composite (TFC) hollow fiber membranes for osmotic power generation. J.

Memb. Sci. 505, 157–166. https://doi.org/10.1016/j.memsci.2016.01.027

Le, N.L., Nunes, S.P., 2017. Ethylene glycol as bore fluid for hollow fiber membrane preparation. J. Memb. Sci. 533, 171–178. https://doi.org/10.1016/j.memsci.2017.03.045

Lee, M., Wu, Z., Wang, R., Li, K., 2014. Micro-structured alumina hollow fi bre membranes – Potential applications in wastewater treatment 461, 39–48. https://doi.org/10.1016/j.memsci.2014.02.044

Lee, W.-J., Kim, Y.-J., Jung, M.-O., Kim, D.-H., Cho, D.L., Kaang, S., 2001. Preparation and properties of conducting polypyrrole-sulfonated polycarbonate composites. Synth. Met. 123, 327–333. https://doi.org/10.1016/S0379-6779(01)00302-2

Leong, T.S.H., Wooster, T.J., Kentish, S.E., Ashokkumar, M., 2009. Minimising oil droplet size using ultrasonic emulsification. Ultrason. Sonochem. 16, 721–727. https://doi.org/https://doi.org/10.1016/j.ultsonch.2009.02.008

Li, J.-H., Xu, Y.-Y., Zhu, L.-P., Wang, J.-H., Du, C.-H., 2009. Fabrication and characterization of a novel TiO2 nanoparticle self-assembly membrane with improved fouling resistance. J. Memb. Sci. 326, 659–666. https://doi.org/10.1016/j.memsci.2008.10.049

Li, J.F., Xu, Z.L., Yang, H., Yu, L.Y., Liu, M., 2009. Effect of TiO2 nanoparticles on the surface morphology and performance of microporous PES membrane. Appl. Surf. Sci. 255, 4725–4732. https://doi.org/10.1016/j.apsusc.2008.07.139

Li, Q.F., Rudbeck, H.C., Chromik, A., Jensen, J.O., Pan, C., Steenberg, T., Calverley, M., Bjerrum, N.J., Kerres, J., 2010. Properties, degradation and high temperature fuel cell test of different types of PBI and PBI blend membranes. J. Memb. Sci. 347, 260–270. https://doi.org/10.1016/j.memsci.2009.10.032

Li, X., Zhang, C., Zhang, S., Li, J., He, B., Cui, Z., 2015. Preparation and characterization of positively charged polyamide composite nanofiltration hollow fiber membrane for lithium and magnesium separation. DES 369, 26–36. https://doi.org/10.1016/j.desal.2015.04.027

Li, Y., Cao, B., Li, P., 2017. Fabrication of PMDA-ODA hollow fibers with regular cross-section morphologies and study on the formation mechanism. J. Memb. Sci. 544, 1–11. https://doi.org/10.1016/j.memsci.2017.08.070

Lin, J., Ye, W., Zhong, K., Shen, J., Jullok, N., Sotto, A., Van der Bruggen, B., 2016. Enhancement of polyethersulfone (PES) membrane doped by monodisperse Stober silica for water treatment. Chem. Eng. Process. Process Intensif. 107, 194–205. https://doi.org/10.1016/j.cep.2015.03.011

Lin, Z., Hu, C., Wu, X., Zhong, W., Chen, M., Zhang, Q., Zhu, A., Liu, Q., 2018. Towards improved antifouling ability and separation performance of polyethersulfone ultrafiltration membranes through poly(ethylenimine) grafting. J. Memb. Sci. 554, 125–133. https://doi.org/10.1016/j.memsci.2018.02.065

Lishun, W., Junfen, S., Chunju, H., 2010. Effects of solvent sort, PES and PVP concentration on the properties and morphology of PVDF/PES blend hollow fiber membranes. J. Appl. Polym. Sci. 116, 1566–1573.

https://doi.org/10.1002/app.31573

Liu, M., Li, J., Guo, Z., 2016. Polyaniline coated membranes for effective separation of oil-in-water emulsions. J. Colloid Interface Sci. 467, 261–270. https://doi.org/http://dx.doi.org/10.1016/j.jcis.2016.01.024

Liu, Y., Koops, G.H., Strathmann, H., 2003. Characterization of morphology controlled polyethersulfone hollow fiber membranes by the addition of polyethylene glycol to the dope and bore liquid solution. J. Memb. Sci. 223, 187–199. https://doi.org/https://doi.org/10.1016/S0376-7388(03)00322-3

Liu, Y., Su, Y., Zhao, X., Li, Y., Zhang, R., Jiang, Z., 2015. Improved antifouling properties of polyethersulfone membrane by blending the amphiphilic surface modifier with crosslinked hydrophobic segments. J. Memb. Sci. 486, 195–206. https://doi.org/10.1016/j.memsci.2015.03.045

Liu, Z., Wang, H., Wang, E., Zhang, X., Yuan, R., Zhu, Y., 2016. Superhydrophobic poly (vinylidene fl uoride) membranes with controllable structure and tunable wettability prepared by one-step electrospinning. Polymer (Guildf). 82, 105–113. https://doi.org/10.1016/j.polymer.2015.11.045

Loh, C.H., Wang, R., 2014. Fabrication of PVDF hollow fiber membranes: Effects of low-concentration Pluronic and spinning conditions. J. Memb. Sci. 466, 130–141. https://doi.org/http://dx.doi.org/10.1016/j.memsci.2014.04.021

Low, Z.X., Razmjou, A., Wang, K., Gray, S., Duke, M., Wang, H., 2014. Effect of addition of two-dimensional ZIF-L nanoflakes on the properties of polyethersulfone ultrafiltration membrane. J. Memb. Sci. 460, 9–17. https://doi.org/10.1016/j.memsci.2014.02.026

Lu, K., Zuo, J., Chung, T., 2016. Tri-bore PVDF hollow fi bers with a super-hydrophobic coating for membrane distillation. J. Memb. Sci. 514, 165–175. https://doi.org/10.1016/j.memsci.2016.04.058

Ma, F., Ye, H., Zhang, Y.-Z., Ding, X.-L., Lin, L.-G., Zhao, L., Li, H., 2014. The effect of polymer concentration and additives of cast solution on performance of polyethersulfone/sulfonated polysulfone blend nanofiltration membranes. Desalin. Water Treat. 52, 618–625. https://doi.org/10.1080/19443994.2013.826411

Madaeni, S.S., Badieh, M.M.S., Vatanpour, V., Ghaemi, N., 2012. Effect of Titanium Dioxide Nanoparticles on Polydimethylsiloxane / Polyethersulfone Composite Membranes for Gas Separation. https://doi.org/10.1002/pen

Mahmoud, M.E., Amira, M.F., Zaghloul, A.A., Ibrahim, G.A.A., 2016. Microwave-enforced sorption of heavy metals from aqueous solutions on the surface of magnetic iron oxide-functionalized-3-aminopropyltriethoxysilane. Chem. Eng. J. 293, 200–206. https://doi.org/https://doi.org/10.1016/j.cej.2016.02.056

Mansourizadeh, A., Aslmahdavi, Z., Ismail, A.F., Matsuura, T., 2014. Blend polyvinylidene fluoride/surface modifying macromolecule hollow fiber membrane contactors for CO2absorption. Int. J. Greenh. Gas Control 26, 83–92. https://doi.org/10.1016/j.ijggc.2014.04.027

Martín, A., Arsuaga, J.M., Roldán, N., de Abajo, J., Martínez, A., Sotto, A., 2015.

Enhanced ultrafiltration PES membranes doped with mesostructured functionalized silica particles. Desalination 357, 16–25. https://doi.org/10.1016/j.desal.2014.10.046

Matsuyama, H., Okafuji, H., Maki, T., Teramoto, M., Kubota, N., 2003. Preparation of polyethylene hollow fiber membrane via thermally induced phase separation. J. Memb. Sci. 223, 119–126. https://doi.org/https://doi.org/10.1016/S0376-7388(03)00314-4

Mazzoccoli, J.P., Feke, D.L., Baskaran, H., Pintauro, P.N., 2010. Mechanical and cell viability properties of crosslinked low- and high-molecular weight poly(ethylene glycol) diacrylate blends. J. Biomed. Mater. Res. Part A 93A, 558–566. https://doi.org/10.1002/jbm.a.32563

Mendonza, A.M., Warzywoda, J., Sacco, A., 2006. Investigation of structural order and morphology of MCM-41 mesoporous silica using an experimental design methodology. J. Porous Mater. 13, 37–47. https://doi.org/10.1007/s10934-006-5488-0

Meng, N., Wang, Z., Low, Z.X., Zhang, Y., Wang, H., Zhang, X., 2015. Impact of trace graphene oxide in coagulation bath on morphology and performance of polysulfone ultrafiltration membrane. Sep. Purif. Technol. 147, 364–371. https://doi.org/10.1016/j.seppur.2015.02.043

Miao, W., Zhang, C., Cai, Y., Zhang, Y., Lu, H., 2016. Fast solid-phase extraction of N-linked glycopeptides by amine-functionalized mesoporous silica nanoparticles. Analyst 141, 2435–2440. https://doi.org/10.1039/C6AN00285D

Michaels, A.S., 1980. Analysis and Prediction of Sieving Curves for Ultrafiltration Membranes: A Universal Correlation? Sep. Sci. Technol. 15, 1305–1322. https://doi.org/10.1080/01496398008068507

Miller, D.J., Paul, D.R., Freeman, B.D., 2014. An improved method for surface modification of porous water purification membranes. Polym. (United Kingdom) 55, 1375–1383. https://doi.org/10.1016/j.polymer.2014.01.046

Min, H., Yu, K., Hua, D., Japip, S., Chung, T., 2017. From ultra fi ltration to nano fi ltration : Hydrazine cross-linked polyacrylonitrile hollow fi ber membranes for organic solvent nano fi ltration 542, 289–299. https://doi.org/10.1016/j.memsci.2017.08.024

Mohammadi, T., Kohpeyma, A., Sadrzadeh, M., 2005. Mathematical modeling of flux decline in ultrafiltration. Desalination 184, 367–375. https://doi.org/https://doi.org/10.1016/j.desal.2005.02.060

Mollahosseini, A., Rahimpour, A., Jahamshahi, M., Peyravi, M., Khavarpour, M., 2012. The effect of silver nanoparticle size on performance and antibacteriality of polysulfone ultra fi ltration membrane. DES 306, 41–50. https://doi.org/10.1016/j.desal.2012.08.035

Moslehyani, A., Mobaraki, M., Isloor, A.M., Ismail, A.F., Othman, M.H.D., 2016. Photoreactor-ultrafiltration hybrid system for oily bilge water photooxidation and separation from oil tanker. React. Funct. Polym. 101, 28–38. https://doi.org/http://dx.doi.org/10.1016/j.reactfunctpolym.2016.02.003

Muhamad, M.S., Salim, M.R., Lau, W.-J., 2015a. Preparation and characterization of PES/SiO2 composite ultrafiltration membrane for advanced water treatment. Korean J. Chem. Eng. 32, 2319–2329. https://doi.org/10.1007/s11814-015-0065-3

Muhamad, M.S., Salim, M.R., Lau, W.-J., 2015b. Surface modification of SiO2 nanoparticles and its impact on the properties of PES-based hollow fiber membrane. RSC Adv. 5, 58644–58654. https://doi.org/10.1039/C5RA07527K

Mukherjee, R., De, S., 2016. Novel carbon-nanoparticle polysulfone hollow fiber mixed matrix ultrafiltration membrane : Adsorptive removal of benzene , phenol and toluene from aqueous solution. Sep. Purif. Technol. 157, 229–240. https://doi.org/10.1016/j.seppur.2015.11.015

Naim, R., Ismail, A.F., Cheer, N.B., Abdullah, M.S., 2013. Chemical Engineering Research and Design Polyvinylidene fluoride and polyetherimide hollow fiber membranes for CO 2 stripping in membrane contactor. Chem. Eng. Res. Des. 92, 1391–1398. https://doi.org/10.1016/j.cherd.2013.12.001

Nandanwar, R., Singh, P., Haque, F.Z., 2015. Synthesis and Characterization of SiO2 Nanoparticles by Sol-Gel Process and Its Degradation of Methylene Blue. Am. Chem. Sci. J. 5, 1–10. https://doi.org/10.9734/ACSj/2014/10875

Nasrollahi, N., Vatanpour, V., Aber, S., Mohammad, N., 2018. Separation and Puri fi cation Technology Preparation and characterization of a novel polyethersulfone (PES) ultra fi ltration membrane modi fi ed with a CuO / ZnO nanocomposite to improve permeability and antifouling properties. Sep. Purif. Technol. 192, 369–382. https://doi.org/10.1016/j.seppur.2017.10.034

Ng, C.Y., Mohammad, A.W., Ng, L.Y., Jahim, J.M., 2014. Membrane fouling mechanisms during ultrafiltration of skimmed coconut milk. J. Food Eng. 142, 190–200. https://doi.org/10.1016/j.jfoodeng.2014.06.005

Ngang, H.P., Ahmad, A.L., Low, S.C., Ooi, B.S., 2017. Preparation of thermoresponsive PVDF/SiO2-PNIPAM mixed matrix membrane for saline oil emulsion separation and its cleaning efficiency. Desalination 408, 1–12. https://doi.org/10.1016/j.desal.2017.01.005

Ngang, H.P., Ooi, B.S., Ahmad, A.L., Lai, S.O., 2012. Preparation of PVDF-TiO2 mixed-matrix membrane and its evaluation on dye adsorption and UV-cleaning properties. Chem. Eng. J. 197, 359–367. https://doi.org/10.1016/j.cej.2012.05.050

Norman N. Li, Anthony G. Fane, W. S. Winston Ho, T.M., 2009. Advanced membrane technology and applications. John Wiley & Sons, Inc. https://doi.org/10.1002/9780470276280

Nunes, S.P., Car, A., 2013. From Charge-Mosaic to Micelle Self-Assembly: Block Copolymer Membranes in the Last 40 Years. Ind. Eng. Chem. Res. 52, 993–1003. https://doi.org/10.1021/ie202870y

Obaid, M., Tolba, G.M.K., Motlak, M., Fadali, O.A., Abdelrazek, K., Almajid, A.A., Kim, B., Barakat, N.A.M., 2015. Effective polysulfone-amorphous SiO 2 NPs electrospun nanofiber membrane for high flux oil / water separation. Chem. Eng. J. 279, 631–638. https://doi.org/10.1016/j.cej.2015.05.028

Ong, C.S., Lau, W.J., Goh, P.S., Ng, B.C., Ismail, A.F., 2015. Preparation and characterization of PVDF–PVP–TiO2 composite hollow fiber membranes for oily wastewater treatment using submerged membrane system. Desalin. Water Treat. 53, 1213–1223. https://doi.org/10.1080/19443994.2013.855679

Ostwal, M., Singh, R.P., Dec, S.F., Lusk, M.T., Way, J.D., 2011. 3-Aminopropyltriethoxysilane functionalized inorganic membranes for high temperature CO2/N2 separation. J. Memb. Sci. 369, 139–147. https://doi.org/https://doi.org/10.1016/j.memsci.2010.11.053

Oueiny, C., Berlioz, S., Perrin, F.X., 2014. Carbon nanotube-polyaniline composites. Prog. Polym. Sci. 39, 707–748. https://doi.org/10.1016/j.progpolymsci.2013.08.009

Pal, S., Ambastha, S., Ghosh, T.B., De, S., DasGupta, S., 2008. Optical evaluation of deposition thickness and measurement of permeate flux enhancement of simulated fruit juice in presence of turbulence promoters. J. Memb. Sci. 315, 58–66. https://doi.org/https://doi.org/10.1016/j.memsci.2008.02.029

Pang, R., Li, X., Li, J., Lu, Z., Sun, X., Wang, L., 2014. Preparation and characterization of ZrO 2 / PES hybrid ultra fi ltration membrane with uniform ZrO 2 nanoparticles 332, 60–66. https://doi.org/10.1016/j.desal.2013.10.024

Parida, S.K., Dash, S., Patel, S., Mishra, B.K., 2006. Adsorption of organic molecules on silica surface. Adv. Colloid Interface Sci. 121, 77–110. https://doi.org/http://dx.doi.org/10.1016/j.cis.2006.05.028

Pendergast, M.M., Hoek, E.M. V, 2011. A review of water treatment membrane nanotechnologies. Energy Environ. Sci. 4, 1946–1971. https://doi.org/10.1039/C0EE00541J

Peng, N., Chung, T.S., 2008. The effects of spinneret dimension and hollow fiber dimension on gas separation performance of ultra-thin defect-free Torlon® hollow fiber membranes. J. Memb. Sci. 310, 455–465. https://doi.org/https://doi.org/10.1016/j.memsci.2007.11.018

Peydayesh, M., Mohammadi, T., Bakhtiari, O., 2018. Effective treatment of dye wastewater via positively charged TETA-MWCNT/PES hybrid nanofiltration membranes. Sep. Purif. Technol. 194, 488–502. https://doi.org/10.1016/j.seppur.2017.11.070

Plueddemann, E.P., 1991. Silane Coupling Agents, Second. ed.

Praveen, P., Thi, D., Nguyen, T., Loh, K., 2015. Biodegradation of phenol from saline wastewater using forward osmotic hollow fiber membrane bioreactor coupled chemostat. Biochem. Eng. J. 94, 125–133. https://doi.org/10.1016/j.bej.2014.11.014

Pulido, J.M.O., 2015. A review on the use of membrane technology and fouling control for olive mill wastewater treatment. Sci. Total Environ. https://doi.org/10.1016/j.scitotenv.2015.09.151

Radjabian, M., Koll, J., Buhr, K., Handge, U.A., Abetz, V., 2013. Hollow fiber spinning of block copolymers: Influence of spinning conditions on morphological properties. Polym. (United Kingdom) 54, 1803–1812.

https://doi.org/10.1016/j.polymer.2013.01.033

Raharjo, Y., Wafiroh, S., Nayla, M., Yuliana, V., Fahmi, M.Z., 2017. PRIMARY STUDY OF CELLULOSE ACETATE HOLLOW FIBER AS A GREEN MEMBRANE APPLIED TO HEMODIALYSIS Yanuardi Raharjo , Siti Wafiroh , Mahdya Nayla , Vita Yuliana , Mochamad Zakki Fahmi. J. Chem. Technol. Metall. 52, 1021–1026.

Rahbari-sisakht, M., Ismail, A.F., Matsuura, T., 2012a. Effect of bore fluid composition on structure and performance of asymmetric polysulfone hollow fiber membrane contactor for CO 2 absorption. Sep. Purif. Technol. 88, 99–106. https://doi.org/10.1016/j.seppur.2011.12.012

Rahbari-sisakht, M., Ismail, A.F., Matsuura, T., 2012b. Effect of bore fluid composition on structure and performance of asymmetric polysulfone hollow fiber membrane contactor for CO2 absorption. Sep. Purif. Technol. 88, 99–106. https://doi.org/https://doi.org/10.1016/j.seppur.2011.12.012

Rahimpour, A., Jahanshahi, M., Khalili, S., Mollahosseini, A., Zirepour, A., Rajaeian, B., 2012. Novel functionalized carbon nanotubes for improving the surface properties and performance of polyethersulfone (PES) membrane. Desalination 286, 99–107. https://doi.org/10.1016/j.desal.2011.10.039

Rana, D., Matsuura, T., 2010. Surface Modifications for Antifouling Membranes. Chem. Rev. 110, 2448–2471. https://doi.org/10.1021/cr800208y

Razmjou, A., Mansouri, J., Chen, V., Lim, M., Amal, R., 2011. Titania nanocomposite polyethersulfone ultrafiltration membranes fabricated using a low temperature hydrothermal coating process. J. Memb. Sci. 380, 98–113. https://doi.org/https://doi.org/10.1016/j.memsci.2011.06.035

Razmjou, A., Resosudarmo, A., Holmes, R.L., Li, H., Mansouri, J., Chen, V., 2012. The effect of modified TiO2 nanoparticles on the polyethersulfone ultrafiltration hollow fiber membranes. Desalination 287, 271–280. https://doi.org/http://dx.doi.org/10.1016/j.desal.2011.11.025

Rezaei, H., Ashtiani, F.Z., Fouladitajar, A., 2011. Effects of operating parameters on fouling mechanism and membrane flux in cross-flow microfiltration of whey. Desalination 274, 262–271. https://doi.org/https://doi.org/10.1016/j.desal.2011.02.015

Roh, D.K., Choi, J.K., Koh, J.K., Shul, Y.G., Kim, J.H., 2010. Nanocomposite proton conducting membranes based on amphiphilic PVDF graft copolymer. Macromol. Res. 18, 271–278. https://doi.org/10.1007/s13233-010-0311-9

Roy, I., Ohulchanskyy, T.Y., Bharali, D.J., Pudavar, H.E., Mistretta, R.A., Kaur, N., Prasad, P.N., 2005. Optical tracking of organically modified silica nanoparticles as DNA carriers: A nonviral, nanomedicine approach for gene delivery. Proc. Natl. Acad. Sci. U. S. A. 102, 279 LP-284. https://doi.org/10.1073/pnas.0408039101

Saadati, J., Pakizeh, M., 2017. Separation of oil/water emulsion using a new PSf/pebax/F-MWCNT nanocomposite membrane. J. Taiwan Inst. Chem. Eng. 71, 265–276. https://doi.org/https://doi.org/10.1016/j.jtice.2016.12.024

Sadeghi, I., Aroujalian, A., Raisi, A., Dabir, B., Fathizadeh, M., 2013. Surface modification of polyethersulfone ultrafiltration membranes by corona air plasma for separation of oil / water emulsions. J. Memb. Sci. 430, 24–36. https://doi.org/10.1016/j.memsci.2012.11.051

Saedi, S., Madaeni, S.S., Hassanzadeh, K., Shamsabadi, A.A., Laki, S., 2014. The effect of polyurethane on the structure and performance of PES membrane for separation of carbon dioxide from methane. J. Ind. Eng. Chem. 20, 1916–1929. https://doi.org/10.1016/j.jiec.2013.09.012

Safarpour, M., Vatanpour, V., Khataee, A., Esmaeili, M., 2015. Development of a novel high flux and fouling-resistant thin film composite nanofiltration membrane by embedding reduced graphene oxide/TiO2. Sep. Purif. Technol. 154, 96–107. https://doi.org/http://dx.doi.org/10.1016/j.seppur.2015.09.039

Saghafi, R., Zarrebini, M., Semnani, D., Mahmoudi, M., 2014. The effect of bore fluid type on performance of treated polysulfone hollow-fiber membrane. Text. Res. J. 85, 281–293. https://doi.org/10.1177/0040517514521122

Saleem, M., Alibardi, L., Cossu, R., Lavagnolo, M.C., Spagni, A., 2017. Analysis of fouling development under dynamic membrane filtration operation. Chem. Eng. J. 312, 136–143. https://doi.org/https://doi.org/10.1016/j.cej.2016.11.123

Scott Matteucci, Victor A. Kusuma, Scott D. Kelman, B.D.F., 2008. Gas transport properties of MgO filled poly(1-trimethylsilyl-1-propyne) nanocomposites. Polymer (Guildf). 49, 1659–1675.

Sengur, R., de Lannoy, C.F., Turken, T., Wiesner, M., Koyuncu, I., 2015. Fabrication and characterization of hydroxylated and carboxylated multiwalled carbon nanotube/polyethersulfone (PES) nanocomposite hollow fiber membranes. Desalination 359, 123–140. https://doi.org/10.1016/j.desal.2014.12.040

Setiawan, L., Shi, L., Krantz, W.B., Wang, R., 2012. Explorations of delamination and irregular structure in poly(amide-imide)-polyethersulfone dual layer hollow fiber membranes. J. Memb. Sci. 423–424, 73–84. https://doi.org/http://dx.doi.org/10.1016/j.memsci.2012.07.030

Shao, J., Zhan, Z., Li, J., Wang, Z., Li, K., Yan, Y., 2014. Zeolite NaA membranes supported on alumina hollow fibers: Effect of support resistances on pervaporation performance. J. Memb. Sci. 451, 10–17. https://doi.org/10.1016/j.memsci.2013.09.049

Shen, L., Bian, X., Lu, X., Shi, L., Liu, Z., Chen, L., Hou, Z., Fan, K., 2012a. Preparation and characterization of ZnO/polyethersulfone (PES) hybrid membranes. Desalination 293, 21–29. https://doi.org/10.1016/j.desal.2012.02.019

Shen, L., Bian, X., Lu, X., Shi, L., Liu, Z., Chen, L., Hou, Z., Fan, K., 2012b. Preparation and characterization of ZnO/polyethersulfone (PES) hybrid membranes. Desalination 293, 21–29. https://doi.org/https://doi.org/10.1016/j.desal.2012.02.019

Shen, X., Ding, W., Zhao, Y., Chen, L., 2014. Effect of copolymer concentration on the structure and permeability of temperature-sensitive poly(vinylidene fluoride) hollow fiber membrane. High Perform. Polym. 26, 357–363.

https://doi.org/10.1177/0954008313514252

Shi, Q., Su, Y., Zhu, S., Li, C., Zhao, Y., Jiang, Z., 2007. A facile method for synthesis of pegylated polyethersulfone and its application in fabrication of antifouling ultrafiltration membrane 303, 204–212. https://doi.org/10.1016/j.memsci.2007.07.009

Shieh, J.J., Chung, T.S., 1998. Effect of liquid-liquid demixing on the membrane morphology, gas permeation, thermal and mechanical properties of cellulose acetate hollow fibers. J. Memb. Sci. 140, 67–79. https://doi.org/10.1016/S0376-7388(97)00267-6

Shukla, S., Benes, N.E., Vankelecom, I., Méricq, J.P., Belleville, M.P., Hengl, N., Marcano, J.S., 2015. Sweep gas membrane distillation in a membrane contactor with metallic hollow-fibers. J. Memb. Sci. 493, 167–178. https://doi.org/10.1016/j.memsci.2015.06.040

Simone, S., Figoli, A., Criscuoli, A., Carnevale, M.C., Rosselli, A., Drioli, E., 2010. Preparation of hollow fibre membranes from PVDF / PVP blends and their application in VMD. J. Memb. Sci. 364, 219–232. https://doi.org/10.1016/j.memsci.2010.08.013

Sofian M. Kanan, William T Y Tze, C.P.T., 2002. Method to double the surface concentration and control the orientation of adsorbed (3-aminopropyl)dimethylethoxysilane on silica powders and glass slides. Langmuir 18, 6623–6627.

Son, M., Kim, H., Jung, J., Jo, S., Choi, H., 2017. Chemosphere In fl uence of extreme concentrations of hydrophilic pore-former on reinforced polyethersulfone ultra fi ltration membranes for reduction of humic acid fouling. Chemosphere 179, 194–201. https://doi.org/10.1016/j.chemosphere.2017.03.101

Song, Z.W., Jiang, L.Y., 2013. Optimization of morphology and perf ormance of PVDF hollow fiber for direct contact membrane distillation using experimental design. Chem. Eng. Sci. 101, 130–143. https://doi.org/https://doi.org/10.1016/j.ces.2013.06.006

Sotto, A., Rashed, A., Zhang, R.-X., Martínez, A., Braken, L., Luis, P., Van der Bruggen, B., 2012. Improved membrane structures for seawater desalination by studying the influence of sublayers. Desalination 287, 317–325. https://doi.org/https://doi.org/10.1016/j.desal.2011.09.024

Stack, L.J., Carney, P.A., Malone, H.B., Wessels, T.K., 2005. Factors influencing the ultrasonic separation of oil-in-water emulsions. Ultrason. Sonochem. 12, 153–60. https://doi.org/10.1016/j.ultsonch.2003.10.008

Stępnik, K.E., Malinowska, I., 2013. The use of biopartitioning micellar chromatography and immobilized artificial membrane column for in silico and in vitro determination of blood-brain barrier penetration of phenols. J. Chromatogr. A 1286, 127–36. https://doi.org/10.1016/j.chroma.2013.02.071

Su, Y., Liu, Y., Zhao, X., Li, Y., Jiang, Z., 2015. Preparation of pH-responsive membranes with amphiphilic copolymers by surface segregation method. Chinese J. Chem. Eng. 23, 1283–1290. https://doi.org/10.1016/j.cjche.2015.05.013

Sukitpaneenit, P., Chung, T., 2011. Molecular design of the morphology and pore size of PVDF hollow fiber membranes for ethanol – water separation employing the modified pore-flow concept. J. Memb. Sci. 374, 67–82. https://doi.org/10.1016/j.memsci.2011.03.016

Sun, X., Chen, J.H., Su, Z., Huang, Y., Dong, X., 2016. Highly effective removal of Cu(II) by a novel 3-aminopropyltriethoxysilane functionalized polyethyleneimine/sodium alginate porous membrane adsorbent. Chem. Eng. J. 290, 1–11. https://doi.org/https://doi.org/10.1016/j.cej.2015.12.106

Tan, X., Liu, N., Meng, B., Liu, S., 2011. Morphology control of the perovskite hollow fibre membranes for oxygen separation using different bore fluids. J. Memb. Sci. 378, 308–318. https://doi.org/http://dx.doi.org/10.1016/j.memsci.2011.05.012

Tang, D., Yuan, R., Chai, Y., 2007. Magnetic control of an electrochemical microfluidic device with an arrayed immunosensor for simultaneous multiple immunoassays. Clin. Chem. 53, 1323–1329. https://doi.org/10.1373/clinchem.2006.085126

Tang, Y., Li, N., Liu, A., Ding, S., Yi, C., Liu, H., 2012. Effect of spinning conditions on the structure and performance of hydrophobic PVDF hollow fiber membranes for membrane distillation. Desalination 287, 326–339. https://doi.org/10.1016/j.desal.2011.11.045

Tanudjaja, H.J., Tarabara, V. V, Fane, A.G., Chew, J.W., 2017. Effect of cross-flow velocity, oil concentration and salinity on the critical flux of an oil-in-water emulsion in microfiltration. J. Memb. Sci. 530, 11–19. https://doi.org/https://doi.org/10.1016/j.memsci.2017.02.011

Taylor, P., Zhang, X., Zhang, D., Kong, L., Shao, Z., Lv, Y., Duan, H., 2015. Preparation and characterization of xanthated cotton fiber modified cellulose triacetate ultrafiltration membrane. Desalin. Water Treat. 1–12. https://doi.org/10.1080/19443994.2015.1035679

Thong, Z., Gao, J., Xi, J., Lim, Z., Wang, K., Chung, T., 2018. Separation and Puri fi cation Technology Fabrication of loose outer-selective nano fi ltration (NF) polyethersulfone (PES) hollow fi bers via single-step spinning process for dye removal. Sep. Purif. Technol. 192, 483–490. https://doi.org/10.1016/j.seppur.2017.10.031

Tilahun, M., Wang, J., Zhu, J., Velizarov, S., 2018. Development and characterization of polyethersulfone-based nano fi ltration membrane with stability to hydrogen peroxide. J. Memb. Sci. 550, 462–469. https://doi.org/10.1016/j.memsci.2018.01.022

Todisco, S., Pena, L., Drioli, E., Tallarico, P., 1996. ANALYSIS OF THE FOULING MECHANISM IN MICROFILTRATION OF ORANGE JUICE. J. Food Process. Preserv. 20, 453–466. https://doi.org/10.1111/j.1745-4549.1996.tb00759.x

Tummons, E.N., Tarabara, V. V, Chew, W., Fane, A.G., 2016. Behavior of oil droplets at the membrane surface during crossflow microfiltration of oil-water emulsions. J. Memb. Sci. 500, 211–224.

https://doi.org/10.1016/j.memsci.2015.11.005

Um, M.-J., Yoon, S.-H., Lee, C.-H., Chung, K.-Y., Kim, J.-J., 2001. Flux enhancement with gas injection in crossflow ultrafiltration of oily wastewater. Water Res. 35, 4095–4101. https://doi.org/10.1016/S0043-1354(01)00155-5

Válek, R., Malý, D., Peter, J., Gruart, M., 2017. Effect of the preparation conditions on the properties of polyetherimide hollow fibre membranes for gas separation. Desalin. Water Treat. 75, 300–304. https://doi.org/10.5004/dwt.2017.20747

van den Berg, G.B., Smolders, C.A., 1990. Flux decline in ultrafiltration processes. Desalination 77, 101–133. https://doi.org/https://doi.org/10.1016/0011-9164(90)85023-4

Vatanpour, V., Madaeni, S.S., Moradian, R., Zinadini, S., Astinchap, B., 2012. Novel antibifouling nanofiltration polyethersulfone membrane fabricated from embedding TiO 2 coated multiwalled carbon nanotubes. Sep. Purif. Technol. 90, 69–82. https://doi.org/10.1016/j.seppur.2012.02.014

Vatanpour, V., Madaeni, S.S., Moradian, R., Zinadini, S., Astinchap, B., 2011. Fabrication and characterization of novel antifouling nanofiltration membrane prepared from oxidized multiwalled carbon nanotube/polyethersulfone nanocomposite. J. Memb. Sci. 375, 284–294. https://doi.org/10.1016/j.memsci.2011.03.055

Vatsha, B., Ngila, J.C., Moutloali, R.M., 2014. Preparation of antifouling polyvinylpyrrolidone (PVP 40K) modified polyethersulfone (PES) ultrafiltration (UF) membrane for water purification. Phys. Chem. Earth 67–69, 125–131. https://doi.org/10.1016/j.pce.2013.09.021

Viguié, J., Savart, T., Duru, P., Rouch, J.C., Remigy, J.C., 2013. Characterisation of 3D porous macrostructure of hollow fibre membranes using X-ray tomography-Effects of some spinning process conditions. J. Memb. Sci. 435, 11–20. https://doi.org/10.1016/j.memsci.2013.01.062

Vincent Vela, M.C., Álvarez Blanco, S., Lora García, J., Bergantiños Rodríguez, E., 2009. Analysis of membrane pore blocking models adapted to crossflow ultrafiltration in the ultrafiltration of PEG. Chem. Eng. J. 149, 232–241. https://doi.org/https://doi.org/10.1016/j.cej.2008.10.027

Wang, F., Zhang, H., Zhu, H., Guo, Y., 2014. Ultra-hydrophobic modification of TiO2 nanoparticles via thermal decomposition of polytetrafluoroethylene. Powder Technol. 253, 548–552. https://doi.org/10.1016/j.powtec.2013.12.010

Wang, H., Yang, L., Zhao, X., Yu, T., Du, Q., 2009. Improvement of Hydrophilicity and Blood Compatibility on Polyethersulfone Membrane by Blending Sulfonated Polyethersulfone. Chinese J. Chem. Eng. 17, 324–329. https://doi.org/10.1016/S1004-9541(08)60211-6

Wang, H., Zhao, X., He, C., 2016. Innovative permeation and antifouling properties of PVDF ultrafiltration membrane with stepped hollow SiO2 microspheres in membrane matrix. Mater. Lett. 182, 376–379. https://doi.org/10.1016/j.matlet.2016.06.075

Wang, K.Y., Fei Li, D., Chung, T.-S., Bor Chen, S., 2004. The observation of

elongation dependent macrovoid evolution in single- and dual-layer asymmetric hollow fiber membranes. Chem. Eng. Sci. 59, 4657–4660. https://doi.org/https://doi.org/10.1016/j.ces.2004.06.035

Wang, L., Li, Z., Ren, J., Li, S.-G., Jiang, C., 2006. Preliminary studies on the gelation time of poly(ether sulfones) membrane-forming system with an elongation method. J. Memb. Sci. 275, 46–51. https://doi.org/https://doi.org/10.1016/j.memsci.2005.08.019

Wang, L., Ye, Y., Lu, X., Wen, Z., Li, Z., Hou, H., Song, Y., 2013. Hierarchical Nanocomposites of Polyaniline Nanowire Arrays on Reduced Graphene Oxide Sheets for Supercapacitors. Sci. Rep. 3, 3568.

Wang, W., Zhu, L., Shan, B., Xie, C., Liu, C., Cui, F., Li, G., 2018. Preparation and characterization of SLS-CNT/PES ultrafiltration membrane with antifouling and antibacterial properties. J. Memb. Sci. 548, 459–469. https://doi.org/10.1016/j.memsci.2017.11.046

Wang, X., Shi, Y., Graff, R.W., Lee, D., Gao, H., 2015. Developing recyclable pH-responsive magnetic nanoparticles for oil e water separation. Polymer (Guildf). 72, 361–367. https://doi.org/10.1016/j.polymer.2014.12.056

Wang, X., Zhang, L., Sun, D., An, Q., Chen, H., 2008. Effect of coagulation bath temperature on formation mechanism of poly(vinylidene fluoride) membrane. J. Appl. Polym. Sci. 110, 1656–1663. https://doi.org/10.1002/app.28169

Wei, Y., Chu, H.-Q., Dong, B.-Z., Li, X., Xia, S.-J., Qiang, Z.-M., 2011. Effect of TiO2 nanowire addition on PVDF ultrafiltration membrane performance. Desalination 272, 90–97. https://doi.org/10.1016/j.desal.2011.01.013

Wienk, I.M., Olde Scholtenhuis, F.H.A., van den Boomgaard, T., Smolders, C.A., 1995. Spinning of hollow fiber ultrafiltration membranes from a polymer blend. J. Memb. Sci. 106, 233–243. https://doi.org/https://doi.org/10.1016/0376-7388(95)00088-T

Woo, K.T., Lee, J., Dong, G., Kim, J.S., Do, Y.S., Hung, W.S., Lee, K.R., Barbieri, G., Drioli, E., Lee, Y.M., 2015. Fabrication of thermally rearranged (TR) polybenzoxazole hollow fiber membranes with superior CO2/N2 separation performance. J. Memb. Sci. 490, 129–138. https://doi.org/10.1016/j.memsci.2015.04.059

Wu, C., Huang, X., Wang, G., Lv, L., Chen, G., Li, G., Jiang, P., 2013. Highly Conductive Nanocomposites with Three-Dimensional, Compactly Interconnected Graphene Networks via a Self-Assembly Process. Adv. Funct. Mater. 23, 506–513. https://doi.org/10.1002/adfm.201201231

Wu, H., Tang, B., Wu, P., 2014. Development of novel SiO2–GO nanohybrid/polysulfone membrane with enhanced performance. J. Memb. Sci. 451, 94–102. https://doi.org/10.1016/j.memsci.2013.09.018

Xiang, Y., Wang, Y., Lin, H., Wang, Y., Xiong, Z., Liu, F., 2015. Ef fi cient separation of O / W and W / O micro-emulsion by thermally responsive superantiwetting PVDF membrane. REACT 97, 86–95. https://doi.org/10.1016/j.reactfunctpolym.2015.10.013

Xu, A., Yang, A., Young, S., DeMontigny, D., Tontiwachwuthikul, P., 2008. Effect of internal coagulant on effectiveness of polyvinylidene fluoride membrane for carbon dioxide separation and absorption. J. Memb. Sci. 311, 153–158. https://doi.org/10.1016/j.memsci.2007.12.008

Xu, G.-R., Wang, J.-N., Li, C.-J., 2013. Strategies for improving the performance of the polyamide thin film composite (PA-TFC) reverse osmosis (RO) membranes: Surface modifications and nanoparticles incorporations. Desalination 328, 83–100. https://doi.org/http://dx.doi.org/10.1016/j.desal.2013.08.022

Xu, L., Zhang, C., Rungta, M., Qiu, W., Liu, J., Koros, W.J., 2014. Formation of defect-free 6FDA-DAM asymmetric hollow fiber membranes for gas separations. J. Memb. Sci. 459, 223–232. https://doi.org/10.1016/j.memsci.2014.02.023

Yakun, G., Meiying, W., Hongqi, Z., Guodong, L., Liqun, Z., Xiongwei, Q., 2007. The surface modification of nanosilica, preparation of nanosilica/acrylic core-shell composite latex, and its application in toughening PVC matrix. J. Appl. Polym. Sci. 107, 2671–2680. https://doi.org/10.1002/app.27310

Yan, J., Lau, W.W.Y., 1998. Effect of Internal Coagulant on Morphology of Polysulfone Hollow Fiber Membranes. I. Sep. Sci. Technol. 33, 33–55. https://doi.org/10.1080/01496399808544754

Yan, L., Hong, S., Li, M., Shui, Y., 2009. Application of the Al 2 O 3 – PVDF nanocomposite tubular ultrafiltration (UF) membrane for oily wastewater treatment and its antifouling research 66, 347–352. https://doi.org/10.1016/j.seppur.2008.12.015

Yang, Q., Chung, T.-S., Santoso, Y.E., 2007. Tailoring pore size and pore size distribution of kidney dialysis hollow fiber membranes via dual-bath coagulation approach. J. Memb. Sci. 290, 153–163. https://doi.org/http://dx.doi.org/10.1016/j.memsci.2006.12.036

Yang, X., Zhu, L., Chen, Y., Bao, B., Xu, J., Zhou, W., 2015. Preparation and characterization of hydrophilic silicon dioxide film on acrylate polyurethane coatings with self-cleaning ability. Appl. Surf. Sci. 349, 916–923. https://doi.org/http://dx.doi.org/10.1016/j.apsusc.2015.05.007

Yang, Y., Zhang, H., Wang, P., Zheng, Q., Li, J., 2007. The influence of nano-sized TiO2 fillers on the morphologies and properties of PSF UF membrane. J. Memb. Sci. 288, 231–238. https://doi.org/http://dx.doi.org/10.1016/j.memsci.2006.11.019

Yano, S., Iwata, K., Kurita, K., 1998. Physical properties and structure of organic-inorganic hybrid materials produced by sol-gel process. Mater. Sci. Eng. C 6, 75–90. https://doi.org/https://doi.org/10.1016/S0928-4931(98)00043-5

Yi, X.S., Yu, S.L., Shi, W.X., Sun, N., Jin, L.M., Wang, S., Zhang, B., Ma, C., Sun, L.P., 2011. The influence of important factors on ultrafiltration of oil/water emulsion using PVDF membrane modified by nano-sized TiO2/Al2O3. Desalination 281, 179–184. https://doi.org/10.1016/j.desal.2011.07.056

Yi, X.S., Yu, S.L., Shi, W.X., Wang, S., Jin, L.M., Sun, N., Ma, C., Sun, L.P., 2012. Separation of oil/water emulsion using nano-particle (TiO(2)/Al(2)O(3))

modified PVDF ultrafiltration membranes and evaluation of fouling mechanism. Water Sci. Technol. 67, 477 LP-484.

Yin, J., Deng, B., 2015. Polymer-matrix nanocomposite membranes for water treatment. J. Memb. Sci. 479, 256–275. https://doi.org/10.1016/j.memsci.2014.11.019

Yin, J., Kim, E.S., Yang, J., Deng, B., 2012. Fabrication of a novel thin-film nanocomposite (TFN) membrane containing MCM-41 silica nanoparticles (NPs) for water purification. J. Memb. Sci. 423–424, 238–246. https://doi.org/10.1016/j.memsci.2012.08.020

Yip, N.Y., Tiraferri, A., Phillip, W.A., Schiffman, J.D., Elimelech, M., 2010. High Performance Thin-Film Composite Forward Osmosis Membrane. Environ. Sci. Technol. 44, 3812–3818. https://doi.org/10.1021/es1002555

Yu, L.-Y., Shen, H.-M., Xu, Z.-L., 2009. PVDF–TiO2 composite hollow fiber ultrafiltration membranes prepared by TiO2 sol–gel method and blending method. J. Appl. Polym. Sci. 113, 1763–1772. https://doi.org/10.1002/app.29886

Yu, L., Zhang, Y., Wang, Y., Zhang, H., Liu, J., 2015. High flux, positively charged loose nanofiltration membrane by blending with poly (ionic liquid) brushes grafted silica spheres. J. Hazard. Mater. 287, 373–383. https://doi.org/https://doi.org/10.1016/j.jhazmat.2015.01.057

Yuliwati, E., Ismail, A.F., 2011. Effect of additives concentration on the surface properties and performance of PVDF ultra fi ltration membranes for re fi nery produced wastewater treatment. DES 273, 226–234. https://doi.org/10.1016/j.desal.2010.11.023

Yuliwati, E., Ismail, A.F., Lau, W.J., Ng, B.C., Mataram, A., Kassim, M.A., 2012. Effects of process conditions in submerged ultrafiltration for refinery wastewater treatment: Optimization of operating process by response surface methodology. Desalination 287, 350–361. https://doi.org/10.1016/j.desal.2011.08.051

Yuliwati, E., Ismail, A.F., Matsuura, T., Kassim, M.A., Abdullah, M.S., 2011. Characterization of surface-modified porous PVDF hollow fibers for refinery wastewater treatment using microscopic observation. Desalination 283, 206–213. https://doi.org/https://doi.org/10.1016/j.desal.2011.02.037

Yusoff, A., Murray, B.S., 2011. Modified starch granules as particle-stabilizers of oil-in-water emulsions. Food Hydrocoll. 25, 42–55. https://doi.org/10.1016/j.foodhyd.2010.05.004

Zaviska, F., Drogui, P., Grasmick, A., Azais, A., Héran, M., 2013. Nanofiltration membrane bioreactor for removing pharmaceutical compounds. J. Memb. Sci. 429, 121–129. https://doi.org/10.1016/j.memsci.2012.11.022

Zhang, D., Karkooti, A., Liu, L., Sadrzadeh, M., Thundat, T., Liu, Y., Narain, R., 2018. Fabrication of antifouling and antibacterial polyethersulfone (PES)/cellulose nanocrystals (CNC) nanocomposite membranes. J. Memb. Sci. 549, 350–356. https://doi.org/10.1016/j.memsci.2017.12.034

Zhang, H., Li, B., Sun, D., Miao, X., Gu, Y., 2018. SiO2-PDMS-PVDF hollow fiber membrane with high flux for vacuum membrane distillation. Desalination 429, 33–43. https://doi.org/10.1016/j.desal.2017.12.004

Zhang, P., Wang, Y., Xu, Z., Yang, H., 2011. Preparation of poly (vinyl butyral) hollow fi ber ultra fi ltration membrane via wet-spinning method using PVP as additive. DES 278, 186–193. https://doi.org/10.1016/j.desal.2011.05.026

Zhang, S., Wang, R., Zhang, S., Li, G., Zhang, Y., 2014. Treatment of wastewater containing oil using phosphorylated silica nanotubes (PSNTs)/ polyvinylidene fluoride (PVDF) composite membrane. DES 332, 109–116. https://doi.org/10.1016/j.desal.2013.11.008

Zhang, S., Wang, R., Zhang, S., Li, G., Zhang, Y., 2013. Development of phosphorylated silica nanotubes (PSNTs)/ polyvinylidene fluoride (PVDF) composite membranes for wastewater treatment. Chem. Eng. J. 230, 260–271. https://doi.org/10.1016/j.cej.2013.06.098

Zhang, X., Hu, J., Chang, Q., Wang, Y., Zhou, J., Zhao, T., 2015. Influences of internal coagulant composition on microstructure and properties of porous YSZ hollow fibre membranes for water treatment. Sep. Purif. Technol. 147, 337–345. https://doi.org/10.1016/j.seppur.2015.01.027

Zhang, Y., Liu, F., Lu, Y., Zhao, L., Song, L., 2013. Investigation of phosphorylated TiO2–SiO2 particles/polysulfone composite membrane for wastewater treatment. Desalination 324, 118–126. https://doi.org/10.1016/j.desal.2013.06.007

Zhang, Y., Wan, Y., Pan, G., Shi, H., Yan, H., Xu, J., Guo, M., Wang, Z., Liu, Y., 2017. Surface modification of polyamide reverse osmosis membrane with sulfonated polyvinyl alcohol for antifouling. Appl. Surf. Sci. 419, 177–187. https://doi.org/10.1016/j.apsusc.2017.05.047

Zhang, Y., Wang, L., Xu, Y., 2015. ZrO2 solid superacid porous shell/void/TiO2 core particles (ZVT)/polyvinylidene fluoride (PVDF) composite membranes with anti-fouling performance for sewage treatment. Chem. Eng. J. 260, 258–268. https://doi.org/10.1016/j.cej.2014.08.083

Zhang, Y., Wang, R., 2014. Novel method for incorporating hydrophobic silica nanoparticles on polyetherimide hollow fiber membranes for CO2 absorption in a gas–liquid membrane contactor. J. Memb. Sci. 452, 379–389. https://doi.org/http://dx.doi.org/10.1016/j.memsci.2013.10.011

Zhao, G., Chen, W., 2015. Enhanced PVDF membrane performance via surface modi fi cation by functional polymer poly (N-isopropylacrylamide) to control protein adsorption and bacterial adhesion. REACT 97, 19–29. https://doi.org/10.1016/j.reactfunctpolym.2015.10.001

Zhao, S., Yan, W., Shi, M., Wang, Z., Wang, J., Wang, S., 2015. Improving permeability and antifouling performance of polyethersulfone ultrafiltration membrane by incorporation of ZnO-DMF dispersion containing nano-ZnO and polyvinylpyrrolidone. J. Memb. Sci. 478, 105–116. https://doi.org/10.1016/j.memsci.2014.12.050

Zhao, X., Chen, W., Su, Y., Zhu, W., Peng, J., Jiang, Z., Kong, L., Li, Y., Liu, J.,

2013. Hierarchically engineered membrane surfaces with superior antifouling and self-cleaning properties. J. Memb. Sci. 441, 93–101. https://doi.org/https://doi.org/10.1016/j.memsci.2013.04.012

Zhao, Y.F., Zhang, P. Bin, Sun, J., Liu, C.J., Zhu, L.P., Xu, Y.Y., 2016. Electrolyte-responsive polyethersulfone membranes with zwitterionic polyethersulfone-based copolymers as additive. J. Memb. Sci. 510, 306–313. https://doi.org/10.1016/j.memsci.2016.03.006

Zheng, L., Wu, Z., Zhang, Y., Wei, Y., Wang, J., 2016. Effect of non-solvent additives on the morphology, pore structure, and direct contact membrane distillation performance of PVDF-CTFE hydrophobic membranes. J. Environ. Sci. 1–12. https://doi.org/10.1016/j.jes.2015.09.023

Zhu, H., Jie, X., Cao, Y., 2017. Fabrication of Functionalized MOFs Incorporated Mixed Matrix Hollow Fiber Membrane for Gas Separation. J. Chem. 2017. https://doi.org/10.1155/2017/2548957

Zhu, L.J., Zhu, L.P., Zhang, P. Bin, Zhu, B.K., Xu, Y.Y., 2016. Surface zwitterionicalization of poly(vinylidene fluoride) membranes from the entrapped reactive core-shell silica nanoparticles. J. Colloid Interface Sci. 468, 110–119. https://doi.org/10.1016/j.jcis.2016.01.043

Zhu, M., Lerum, M.Z., Chen, W., 2012. How to prepare reproducible, homogeneous, and hydrolytically stable aminosilane-derived layers on silica. Langmuir 28, 416–423. https://doi.org/10.1021/la203638g

Zhu, X., Dudchenko, A., Gu, X., Jassby, D., 2017. Surfactant-stabilized oil separation from water using ultrafiltration and nanofiltration. J. Memb. Sci. 529, 159–169. https://doi.org/https://doi.org/10.1016/j.memsci.2017.02.004

Zhu, X., Tu, W., Wee, K., Bai, R., 2014. Effective and low fouling oil / water separation by a novel hollow fi ber membrane with both hydrophilic and oleophobic surface properties. J. Memb. Sci. 466, 36–44. https://doi.org/10.1016/j.memsci.2014.04.038

Zhu, Y., Wang, D., Jiang, L., Jin, J., 2014. Recent progress in developing advanced membranes for emulsified oil/water separation. NPG Asia Mater. 6, e101. https://doi.org/10.1038/am.2014.23

Zhu, Y., Xie, W., Li, J., Xing, T., Jin, J., 2015. pH-Induced non-fouling membrane for effective separation of oil-in-water emulsion. J. Memb. Sci. 477, 131–138. https://doi.org/10.1016/j.memsci.2014.12.026

Zinadini, S., Zinatizadeh, A.A., Rahimi, M., Vatanpour, V., Zangeneh, H., 2014. Preparation of a novel antifouling mixed matrix PES membrane by embedding graphene oxide nanoplates. J. Memb. Sci. 453, 292–301. https://doi.org/10.1016/j.memsci.2013.10.070

Zulhairun, A.K., Ng, B.C., Ismail, A.F., Surya Murali, R., Abdullah, M.S., 2014. Production of mixed matrix hollow fiber membrane for CO2/CH4separation. Sep. Purif. Technol. 137, 1–12. https://doi.org/10.1016/j.seppur.2014.09.014

Zuo, G., Wang, R., 2013. Novel membrane surface modi fi cation to enhance anti-oil fouling property for membrane distillation application. J. Memb. Sci. 447, 26–

35. https://doi.org/10.1016/j.memsci.2013.06.053

Zuo, J., Chung, T., Brien, G.S.O., Kosar, W., 2017. distillation crossmark. J. Memb. Sci. 523, 103–110. https://doi.org/10.1016/j.memsci.2016.09.030

Zydney, A.L., Ho, C.-C., 2002. Scale-up of microfiltration systems: fouling phenomena and Vmax analysis. Desalination 146, 75–81. https://doi.org/https://doi.org/10.1016/S0011-9164(02)00492-7

APPENDICES

Appendix A: Calculations of APTES-SiO_2 particle concentration and weight percentage of dope solution (at 17.25 wt.% PES, 3.6 wt.% APTES-SiO_2, 3.72 wt.% PEG and 75.43 wt.% DMAc)

Appendix A1: Calculating the amount of synthesized APTEs-SiO_2 particles

Volume of suspension added = 25 ml

Mass of dried glass petri-dish = 33.2683 g

Mass of dried particle in petri-dish = 38.6743 g

APTES particle concentration = $\frac{38.6743-33.2683\ g}{25\ ml} = \frac{0.406\ g}{25\ ml} = \frac{0.01624\ g}{ml}$

Appendix A2: Weight percent (wt.%) of dope solution (at 17.25 wt.% PES, 3.6 wt.% APTES-SiO_2, 3.72 wt.% PEG and 75.43 wt.% DMAc) of a total mass of 120 grams.

Mass of PES = 20.7 g

Mass of PEG = 4.464 g

Mass of APTES-SiO_2 = 4.344 g

Mass of DMAc = 90.516 g

PES (wt.%) = $\frac{20.7}{120}\ X\ 100$ = 17.25 wt.%

PEG (wt.%) = $\frac{4.464}{120}\ X\ 100$ = 3.72 wt.%

APTES-SiO_2 (wt.%) $= \frac{4.344}{120} X\ 100$ = 3.6 wt.%

DMAc (wt.%) $= \frac{90.516}{120} X\ 100$ = 75.43 wt.%

Appendix B: Characterization of Oil Emulsion

Appendix B1: Oil Emulsion Absorbance Spectrum and Calibration Curve

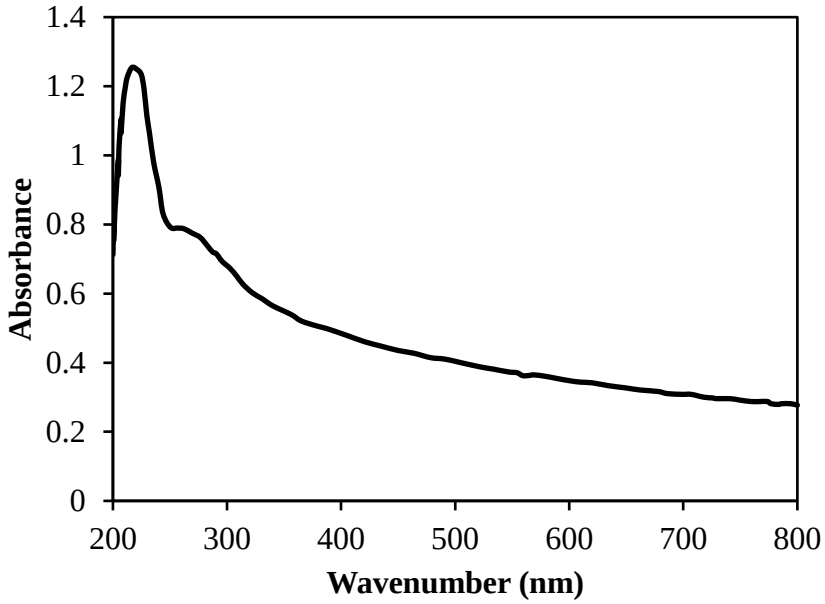

Figure B1.1: Oil Emulsion Absorbance Spectrum

Table B1.2: Calibration curve data of oil concentration versus absorbance.

Oil concentration (mg/L)	Absorbance
0	0
1	0.0242
5	0.1215
10	0.2343
15	0.3512
20	0.4815
30	0.7214
40	0.9713
50	1.1912
100	2.343

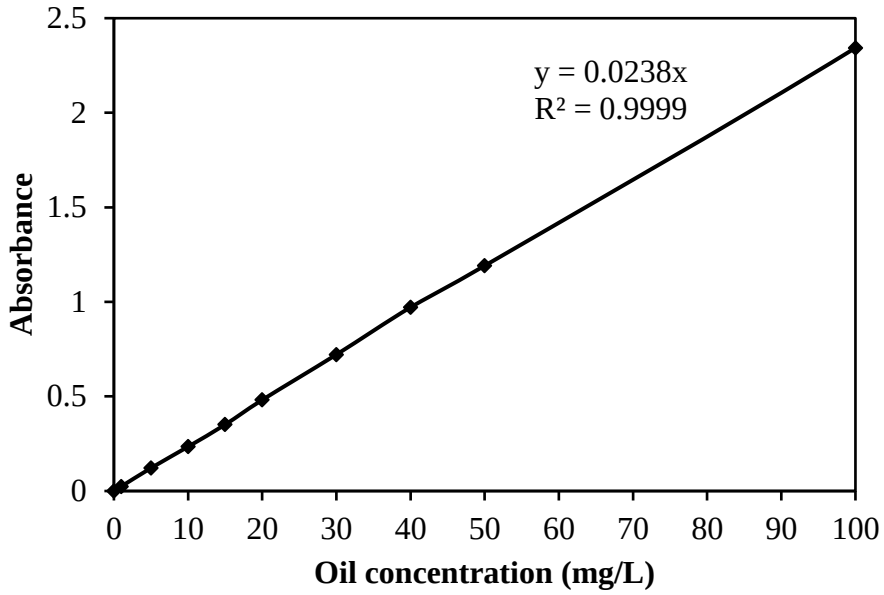

Figure B1.3: Calibration curve of absorbance versus oil concentration at wavelength of 225 nm.

Appendix B2: Droplet size of oil Emulsion

The hydro-dynamic diameter (Dh) of the synthesized oil-in-water emulsion was determined according to the Brownian motion of the droplet of oil (Ong et al., 2015) using DLS. The intensity according to the Dh distribution of droplet of oil is presented in Figure B2.1. The mean droplet of oil at 250 mg/L oil content shows an average diameter of 761 ± 3.12 nm.

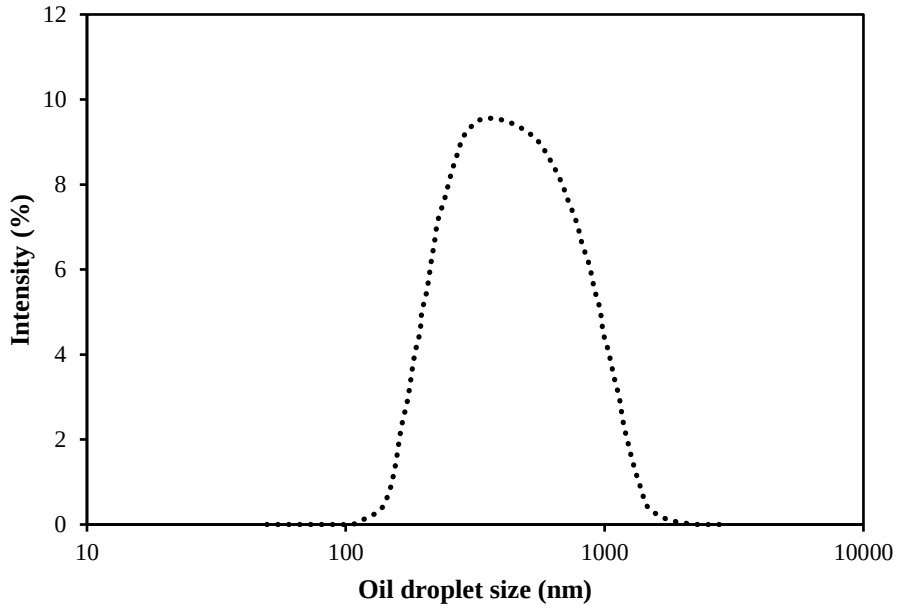

Figure B2.1: Hydrodynamic diameter distribution of synthetic oil-in-water emulsion (250 mg/L of oil concentration).

The oil droplet diameter at different oil concentrations was determined and are displayed in Figure B2.2. As observed, the oil droplet size increased with the increased of oil concentrations. Furthermore, a relatively narrow size distribution was observed at lower oil content. The average oil droplet size was 375 ± 2.74 nm, 761 ± 3.12 nm and 1081 ± 4.75 nm and for oil content of 100 mg/L, 250 mg/L and 500 mg/L, respectively. The increase in average oil droplet upon increase in oil content can be associated due to higher oil droplet collisions frequency which promoted a higher chance for oil droplet to aggregate (Leong et al., 2009).

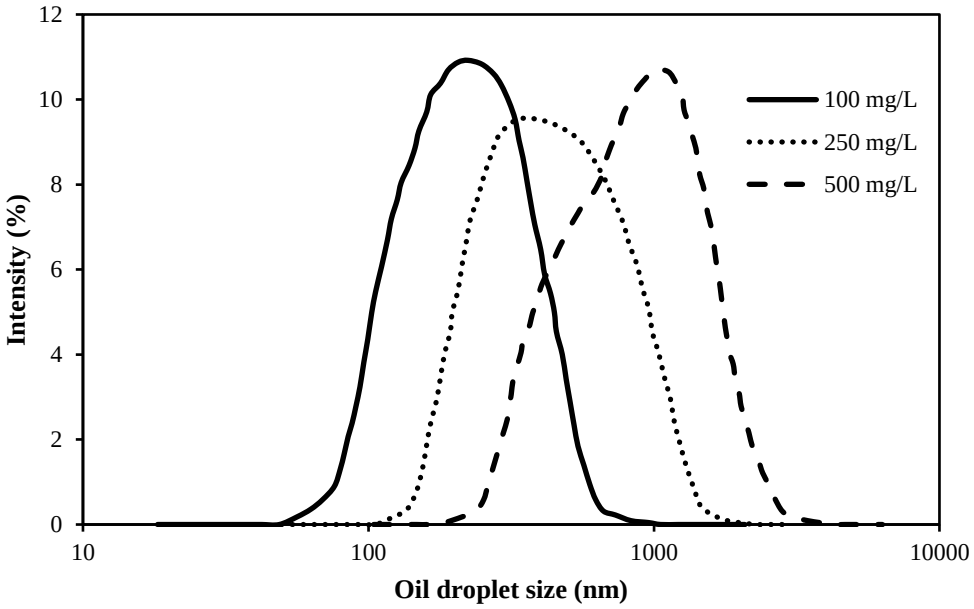

Figure B2.2: Hydro-dynamic diameter distribution of oil emulsion at different oil concentration.

Appendix B3: Oil Emulsion Stability

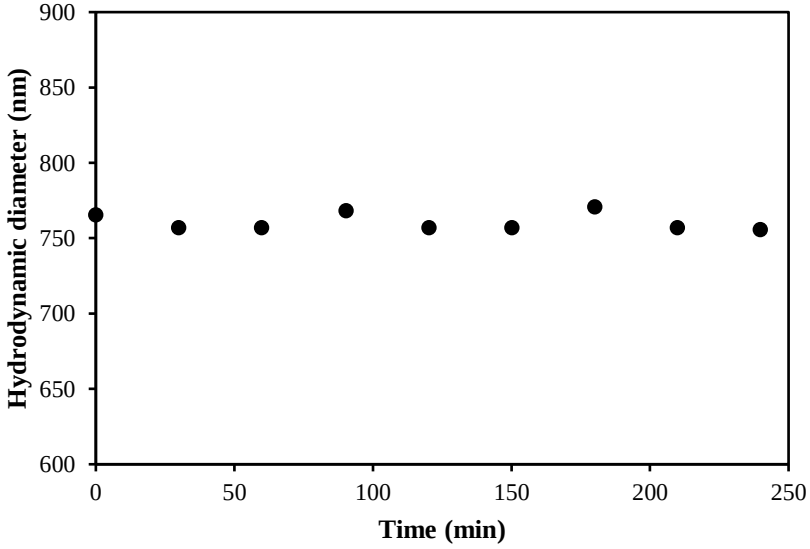

Figure B3.1: Stability of the synthetic oil-in-water emulsion for duration of 4 h (250 mg/L of oil concentration).

Appendix C: Permeation system

Appendix C1.1: Cross-flow filtration setup for hollow fiber and flat sheet membrane

Appendix D: Hollow fiber module preparation

Hollow fiber module connects the filtration system and the hollow fibers and plays a major role the permeation testing. The following gives a brief steps in the module preparation:

- Eight HF with length ranging from 49-50 cm were chosen.
- The fibers were inserted in the male connection, while leaving about 1-2 cm of the fiber out of the connector.
- The male connector was filled with epoxy and subsequently kept vertically for 10 min.
- The other ends of the fibers were sealed with epoxy.
- The module was left to dry at room temperature for about 12 h. Thereafter, the edge near to the connector was cut with a knife in order to open the lumens of the fibers.
- Finally, the module were immersed in ethanol for 3 hrs, followed by immersion in distilled water for 24 h.

Appendix E: Analysis of variance of all responses

Table E1: ANOVA table of PWF response

Source	Sum of squares	df	Mean square	F Value	p-value Prob > F	
Model	3.566E+005	4	89146.85	23.72	< 0.0001	significant
A	85448.63	1	85448.63	22.74	< 0.0001 *	
B	6171.23	1	6171.23	1.64	0.2118	
C	2.494E+005	1	2.494E+005	66.37	< 0.0001 *	
AB	15518.31	1	15518.31	4.13	0.0214 *	
Residual	93957.29	25	3758.29			
Lack of fit	87122.06	20	4356.10	3.19	0.1012	not significant
Pure Error	6835.23	5	1367.05			
Cor Total	4.505E+005	29				

* Significant < 0.05

Table E2: ANOVA table of OPF response

Source	Sum of squares	df	Mean square	F Value	p-value Prob > F	
Model	87825.64	2	43912.82	36.20	< 0.0001	significant
A	27704.98	1	27704.98	22.84	< 0.0001 *	
C	60120.66	1	60120.66	49.56	< 0.0001 *	
Residual	32751.28	27	1213.01			
Lack of fit	30394.71	22	1381.58	2.93	0.1176	not significant
Pure Error	2356.56	5	471.31			
Cor Total	1.206E+005	29				

* Significant < 0.05

Table E3: ANOVA table of OR response

Source	Sum of squares	df	Mean square	F Value	p-value Prob > F	
Model	97.53	9	10.84	5.49	0.0007	significant
A	0.28	1	0.28	0.14	0.7117	
B	10.80	1	10.80	5.47	0.0298 *	
C	5.76	1	5.76	2.92	0.1029	
D	0.018	1	0.018	9.199E-003	0.9245	
AC	13.43	1	13.43	6.81	0.0168 *	
A^2	9.72	1	9.72	4.92	0.0382 *	
B^2	19.69	1	19.69	9.98	0.0049 *	
C^2	5.32	1	5.32	2.69	0.1164	
D^2	26.69	1	26.69	13.53	0.0015 *	
Residual	39.46	20	1.97			
Lack of fit	34.52	15	2.30	2.33	0.1790	not significant
Pure Error	4.94	5	0.99			
Cor Total	136.99	29				

* Significant < 0.05

Appendix F: Calculations for membrane testing

F1: Membrane effective area, $A = \pi \mathrm{DLN}$

Diameter, D = $0.95\ mm = 0.00095\ m$

Length, L = $46.5\ cm = 0.465\ m$

Number of fibers, N = 8

$$A = \pi(0.00095\ X\ 0.465\ X\ 8)\ m^2$$

$$A = 0.011103826\ m^2$$

$$A = 111.03826\ cm^2$$

F2: Membrane permeation flux

Collected volume, V = 5,323 mL

= 5.323 L

= 5.323 kg

Time required for permeate collected, t = 10,800 s

$$= \frac{10800\ s}{60\ s * 60\ min}$$

$$= \frac{10800\ s}{3600\ s.h}$$

= 3 h

To determine the membrane permeate flux associated with the volume of water collected at the permeate side at 3 h interval, equation (3,3) may be used accordingly.

Membrane permeate flux, J_s =

$$\frac{volume\ of\ water\ collected, V}{(membrane\ effective\ area, A) * (time\ required\ for\ water\ collection, t)}$$

$$= \frac{5.323\ kg}{(0.011103826\ m^2) * (3\ h)}$$

= 159.793 kg/m^2 h

= 159.8 kg/m^2 h

F3: Oil rejection

The oil rejection was solved using equation (3.11) in previous section 3.9.2. UV absorbance for permeate solution and feed solution were measured using UV spectrophotometer (UV mini-1240, Shimadzu) in order to obtain its concentration from the calibration curve of oil concentration versus UV absorbance as displayed in Appendix B1.3.

UV absorbance of feed solution = 1.463

UV absorbance on permeate solution = 0.011

By referring to the oil concentration data from the calibration curve,

Feed solution concentration, C_{fd} = 61.47 mg/L

Permeate solution concentration, C_{pmt} = 0.472 mg/L

Membrane rejection, R (%) $= 1 - \frac{C_{pmt}}{C_{fd}} * 100$

$$= 1 - \frac{0.472\ mg/L}{61.47\ mg/L} * 100$$

= 99.232 %

F4: Flux recovery ratio

The flux recovery ratio was solved using equation (3.12) in previous section 3.9.3

Initial pure water flux, J_{wf1} = 235.20 kg/m^2 h

Pure water flux after physical cleaning, J_{wf2} = 212.76 kg/m^2 h

Flux recovery ratio, FRR $= \left(\frac{J_{wf2}}{J_{wf1}}\right) X100$

$$= \left(\frac{212.76}{235.20}\right) X100$$

= 90.46%

F5: Relative flux reduction

The relative flux reduction was solved using equation (3.13) in previous section 3.9.3

Initial pure water flux, J_{wf1} = 235.20 kg/m^2 h

Permeate flux, J_s = 159.80 kg/m^2 h

Relative flux reduction, RFR $= \left(1 - \frac{J_s}{J_{wf1}}\right) X100$

$$= \left(1 - \frac{159.80}{235.20}\right) X100$$

= 32.06%

F6: Irreversible resistance

The irreversible resistance was solved using equation (3.16) in previous section 3.9.3

Initial pure water flux, J_{wf1} = 235.20 kg/m^2 h

Pure water flux after physical cleaning, J_{wf2} = 212.76 kg/m^2 h

Irreversible resistance, Rir $= \left(\frac{J_{wf1} - J_{wf2}}{J_{wf1}}\right) X100$

$$= \left(\frac{235.20 - 212.76}{235.20}\right) X100$$

= 9.54%

F7: Reversible resistance

The reversible resistance was solved using equation (3.15) in previous section 3.9.3

Initial pure water flux, J_{wf1} = 235.20 kg/m^2 h

Pure water flux after physical cleaning, J_{wf2} = 212.76 kg/m^2 h

Permeate flux, J_s = 159.80 kg/m^2 h

Reversible resistance, Rr $= \left(\frac{J_{wf2} - J_s}{J_{wf1}}\right) X100$

$$= \left(\frac{212.76 - 159.8}{235.20}\right) X100$$

= 22.52%

F8: Total resistance

The total resistance was solved using equation (3.14) in previous section 3.9.3

Initial pure water flux, J_{wf1} = 235.20 kg/m^2 h

Permeate flux, J_s = 159.80 kg/m^2 h

Total resistance, Rt $= \left(\frac{J_{wf1} - J_s}{J_{wf1}}\right) X100$

$$= \left(\frac{235.20 - 159.8}{235.20}\right) X100$$

= 32.06%

Appendix G: Dynamic Fouling Modelling of E4-2.5 Membrane Permeate Flux

G1 Origin Curve Fitting Tool Results

G1.1 Cake Filtration Model (n=0)

Nonlinear Curve fit (January 16, 2019 22:17:07)

Iteration Algorithm: Levenberg Marquardt

Equation: $J = J_o/\sqrt{1 + (2K_c{J_o}^2 t)}$

Iterations Performed = 2

Total Iterations in Session = 36

STATISTICS:

	Flux
Number of points	59
Degrees of freedom	58
Reduced Chi-Sqr	53.295
Residual Sum of Squares	3091.14657
Adj. R-Square	0.96928
Fit Status	Succeeded (100)

Fit Status Code :

100: Fit converged. Chi-Sqr tolerance value of 1E-9 was reached.

SUMMARY

	Jo		**Kc**		**Statistics**	
	Value	**Standard Error**	**Value**	**Standard Error**	**Reduced Chi-Sqr**	**Adj. R-Square**
Flux	281	0	1.04777E-5	2.00717E-7	53.29563	0.96928

ANOVA

		DF	Sum of Squares	Mean Square	F Value	Prob>F
Flux	**Regression**	1	1.60566E6	1.60566E6	30127.36192	1
	Residual	58	3091.14657	53.29563		
	Uncorrected Total	59	1.60875E6			
	Corrected Total	58	100612.64462			

G1.2 Intermediate Pore Blocking Model (n=1)

Nonlinear Curve fit (January 16, 2019 23:26:50)

Iteration Algorithm: Levenberg Marquardt

Equation: $J = J_o/(1 + K_i J_o t)$

Iterations Performed = 2

Total Iterations in Session = 24

STATISTICS:

	Flux
Number of points	59
Degrees of freedom	58
Reduced Chi-Sqr	46.04726
Residual Sum of Squares	2670.7411
Adj. R-Square	0.97346
Fit Status	Succeeded (100)

Fit Status Code :

100: Fit converged. Chi-Sqr tolerance value of 1E-9 was reached.

SUMMARY

	Jo		Kc		Statistics	
	Value	**Standard Error**	**Value**	**Standard Error**	**Reduced Chi-Sqr**	**Adj. R-Square**
Flux	273	0	0.00194	2.81707E-5	46.04726	0.97346

ANOVA

		DF	**Sum of Squares**	**Mean Square**	**F Value**	**Prob>F**
Flux	**Regression**	1	1.60608E6	1.60608E6	34878.88623	1
	Residual	58	2670.7411	46.04726		
	Uncorrected Total	59	1.60875E6			
	Corrected Total	58	100612.64462			

G1.3 Standard Pore Blocking Model (n=1.5)

Nonlinear Curve fit (January 16, 2019 23:15:08)

Iteration Algorithm: Levenberg Marquardt

Equation: $J = J_o/(1 + \frac{K_s J_o^{\frac{1}{2}}}{2}\ t)^2$

Iterations Performed = 3

Total Iterations in Session = 22

STATISTICS:

	Flux
Number of points	59
Degrees of freedom	58
Reduced Chi-Sqr	76.37283
Residual Sum of Squares	4429.62439
Adj. R-Square	0.95597
Fit Status	Succeeded (100)

Fit Status Code :

100: Fit converged. Chi-Sqr tolerance value of 1E-9 was reached.

SUMMARY

	Jo		Kc		Statistics	
	Value	**Standard Error**	**Value**	**Standard Error**	**Reduced Chi-Sqr**	**Adj. R-Square**
Flux	271	0	0.02635	4.35287E-4	76.37283	0.95597

ANOVA

		DF	**Sum of Squares**	**Mean Square**	**F Value**	**Prob>F**
Flux	**Regression**	1	1.60432E6	1.60432E6	21006.39954	1
	Residual	58	4429.62439	76.37283		
	Uncorrected Total	59	1.60875E6			
	Corrected Total	58	100612.64462			

G1.4 Complete Pore Blocking Model (n=2)

Nonlinear Curve fit (January 16, 2019 23:36:22)

Iteration Algorithm: Levenberg Marquardt

Equation: $J = J_o \exp(-K_b t)$

Iterations Performed = 2

Total Iterations in Session = 2

STATISTICS:

	Flux
Number of points	59
Degrees of freedom	58
Reduced Chi-Sqr	135.4419
Residual Sum of Squares	7855.63004
Adj. R-Square	0.92192
Fit Status	Succeeded (100)

Fit Status Code :

100: Fit converged. Chi-Sqr tolerance value of 1E-9 was reached.

SUMMARY

	Jo		Kc		Statistics	
	Value	**Standard Error**	**Value**	**Standard Error**	**Reduced Chi-Sqr**	**Adj. R-Square**
Flux	268	0	0.35285	0.00679	135.4419	0.92192

ANOVA

		DF	**Sum of Squares**	**Mean Square**	**F Value**	**Prob>F**
Flux	**Regression**	1	1.60089E6	1.60089E6	11819.77141	1
	Residual	58	7855.63004	135.4419		
	Uncorrected Total	59	1.60875E6			
	Corrected Total	58	100612.64462			

LIST OF PUBLICATIONS

T.A. Otitoju, A.L. Ahmad, B.S. Ooi, Synthesis of 3-aminopropyltriethoxysilane-silica modified polyethersulfone hollow fiber membrane for oil-in-water emulsion separation, React. Funct. Polym. 136 (2019) 107–121. doi:10.1016/j.reactfunctpolym.2018.12.018.

A.L. Ahmad, **T.A. Otitoju**, B.S. Ooi, Hollow fiber (HF) membrane fabrication: A review on the effects of solution spinning conditions on morphology and performance, Journal of Industrial and Engineering Chemistry, 70 (2019) 35-50.

A.L. Ahmad, **T.A. Otitoju**, B.S. Ooi, Optimization of a high performance 3-aminopropyltriethoxysilane-silica impregnated polyethersulfone membrane using response surface methodology for ultrafiltration of synthetic oil-water emulsion, Journal of the Taiwan Institute of Chemical Engineers, 93 (2018) 461–476.

T.A. Otitoju, A.L. Ahmad, B.S. Ooi, Recent Advances in hydrophilic modification and performance of polyethersulfone (PES) membrane via additive blending, RSC Advances 8 (2018) 22710–22728.

T.A. Otitoju, A.L. Ahmad, B.S. Ooi, Polyethersulfone composite hollow-fiber membrane prepared by in-situ growth of silica with highly improved oily wastewater separation performance, Journal of Polymer Research 24 (2017) 1–11.

T.A. Otitoju, A.L. Ahmad, B.S. Ooi, Influence of ethanol as bore fluid component on the morphological structure and performance of PES hollow fiber membrane for oil in water separation, Korean Journal Chemical Engineering 34 (2017) 1–7.

T.A. Otitoju, A.L. Ahmad, B.S. Ooi, Superhydrophilic (superwetting) surfaces: A review on fabrication and application, Journal of Industrial and Engineering Chemistry 47 (2017) 19–40.

T.A. Otitoju, A.L. Ahmad, B.S. Ooi, Polyvinylidene fluoride (PVDF) membrane for oil rejection from oily wastewater: A performance review, Journal of Water Process Engineering 14 (2016) 41-59.

Conference proceedings

A.L. Ahmad, **T.A. Otitoju**, B.S. Ooi, Application of PES-SiO_2 hollow fiber membrane for wastewater treatment and its anti-fouling ability, 10th International Conference on Challenges in Environmental Science Engineering (CESE) – Kunming, China 11 – 15th November, 2017.